AD NUMBER

AD817527

NEW LIMITATION CHANGE

TO

Approved for public release, distribution unlimited

FROM

Distribution authorized to U.S. Gov't. agencies and their contractors; Administrative/Operational use; May 1967. Other requests shall be referred to Air Force Flight Dynamics Lab, Wright-Patterson AFB OH 45433-0000.

AUTHORITY

AFFDL ltr, 27 Sep 1971

AFFDL-TR-67-32

AIR CUSHION LANDING GEAR FEASIBILITY STUDY

T. DESMOND EARL

BELL AEROSYSTEMS COMPANY

TECHNICAL REPORT AFFDL-TR-67-32

MAY 1967

AIR FORCE FLIGHT DYNAMICS LABORATORY
RESEARCH AND TECHNOLOGY DIVISION
AIR FORCE SYSTEMS COMMAND
WRIGHT-PATTERSON AIR FORCE BASE, OHIO

NOTICES

When Government drawings, specifications, or other data are used for any purpose other than in connection with a definitely related Government procurement operation, the United States Government thereby incurs no responsibility nor any obligation whatsoever; and the fact that the Government may have formulated, furnished, or in any way supplied the said drawings, specifications, or other data, is not be be regarded by implication or otherwise as in any manner licensing the holder or any other person or corporation, or conveying any rights or permission to manufacture, use, or sell any patented invention that may in any way be related thereto.

Copies of this report should not be returned to the Research and Technology Division unless return is required by security considerations, contractual obligations, or notice on a specific document.

200 - June 1967 - CO192 - 87-926

AFFDL-TR-67-32

AIR CUSHION LANDING GEAR FEASIBILITY STUDY

T. DESMOND EARL

FOREWORD

The Air Cushion Landing Gear Feasibility Study reported herein was performed under United States Air Force Contract No. AF 33(615)3296 from February 1966 to March 1967. The contract was initiated under Project No. 1369 Task No. 136907.

The work was carried through by Bell Aerosystems Company, P.O. Box 1, Buffalo, N.Y. 14240 (managed by T.D. Earl - Project Manager, Air Cushion Landing Gear). The project was directed by the Air Force Flight Dynamics Laboratory (Aivars Petersons, Head, Landing Gear Group AFFDL and David J. Perez, Project Engineer, Landing Gear Group AFFDL).

The project was initiated by an unsolicited proposal from Bell Aerosystems Company (Report No. D7233-953001) and the present report carries the Bell Aerosystems designation D7233-945001.

A 16 mm sound and color movie film of tests included in the work was produced.

Manuscript released by the author 15 March 1967 for publication as an RTD Technical Report.

This technical report has been reviewed and is approved.

Aivars Petersons
Acting Branch Chief.
Mechanical Branch
Air Force Flight Dynamics Laboratory

ABSTRACT

The system concept is described. It is a scheme to replace aircraft wheel gear with an annular jet air cushion. It embodies a large pneumatic bag or bags surrounding and beneath the fuselage. A continuous air feed from an on-board power source maintains the bag inflated while producing a distributed jet flow at its base. The escaping jets create a pressure beneath the aircraft whenever it is close to the takeoff or landing surface, and eliminate friction. Air clearance beneath the bags is minimal, surface irregularities being tolerated by the resilience of the flexible material itself.

The objective is to provide an improved tolerance to the takeoff and landing maneuver and environment with no compromise of flight performance.

The study considers application to a C-119 twin boom flying boxcar - selected as a suitable development aircraft. Alternative configurations are analyzed, a single main cushion of 560 ft^2 area being preferred.

The work included tests of a 1/3 scale partial length model and a 1/12 scale quasi-static wind tunnel model. The 1/3 scale partial model was tested on an hydraulically powered whirling arm rig to develop satisfactory retraction and determine obstacle performance, energy absorption and damping. Neat retraction was achieved using specially developed one way stretch elastic material. With representative powering, the model was able to traverse a 10 inch full scale wall at 10 mph and up, and cross a series of mounds up to 22 inches. Drop tests indicated the estimated design vertical sink rate of over 20 ft/sec without wing lift would be achieved in the flat attitude with critical damping.

The wind tunnel was tested over the moving ground at the NASA Langley Research Center and successfully simulated landing and takeoff maneuvers in response to elevator control. The model was free in pitch and heave. Free air drag of the inflated bag was found to be the same as that of the extended wheel gear.

It is concluded that the landing and takeoff maneuver presents no special problems to takeoff rotation elevator power and that superior energy absorption and damping are available. The retraction method using elastic material appears to be most promising. To the extent that this research covers the expected problem areas the system feasibility is established.

CONTENTS

CONTENTS (CONT)

ILLUSTRATIONS

ILLUSTRATIONS (CONT)

ILLUSTRATIONS (CONT)

LIST OF SYMBOLS

AR	Aspect ratio
b	Radius of torus; cushion width; span, ft
bhp	brake horsepower
C_D	Discharge coefficient; drag coefficient
C_{D_i}	Induced drag coefficient
C_{D_o}	Parasite drag coefficient
C_L	Lift coefficient
c.p.	Center of pressure
C_T	Thrust coefficient
C_W	Wave drag coefficient
C_X	Axial force coefficient
C_Y	Side force coefficient
c	Cushion perimeter at ground tangent; chord; damping force
c_p	Specific heat at constant pressure
D	Diameter, ft, Drag, lb
D_p	Propeller diameter, ft
D_W	Wave drag, lb
d_{R1}	Outer radius center distance out from side
e	Oswald efficiency factor
g	Nozzle gap dimension; acceleration due to gravity, ft/sec^2
g_o	Total nozzle gap
H	Water head, ft
hp_j	Jet horsepower
hp_M	Main cushion horsepower
hp_N	Nose cushion horsepower
h, h_j	Jet height or air clearance
h_{R1}	Outer radius center height below base
h_{TH}	Theoretical jet height
h_t	Base height

J	Joule's equivalent 778 ft-lb/BTU
k	Stiffness, lb/ft
L	Lift, lb
L_M	Main wheel or cushion lift, lb
L_N	Nose wheel or cushion lift, lb
l	Cushion length, ft; trunk cross section length, ft
$l_{1, 2, 3}$	Partial trunk cross section lengths
m	Mass flow (slug/sec)
N	rpm
N_θ	Hoop tension
N_ϕ	Meridional tension
N_S	Stretch direction tension
P_F	Fan pressure rise, lb/ft^2
P_j	Trunk pressure, lb/ft^2
P_1	Total pressure Station 1 lb/ft^2 abs
P_2	Total pressure Station 2 lb/ft^2 abs
p	Pressure lb/ft^2
p_c	Cushion pressure, lb/ft^2
p_{c_m}	Main cushion pressure, lb/ft^2
p_{c_n}	Nose cushion pressure, lb/ft^2
Q	Volume flow, ft^3/sec
Q_N	Nose cushion volume flow, ft^3/sec
q	Dynamic Pressure, lb/ft^2
R	Jet radius dimension; Reaction, lb
R_o	Jet outer edge radius
R_1	Outer trunk radius
R_2	Inner trunk radius
r_o	Radius to point on torus shell
S	Area
S_c	Cushion area
S_j	Jet area

S_N	Nozzle area
s_1	Ground roll distance, ft
s_2	Transition distance, ft
s_3	Initial climb distance, ft
T	Trunk tension, lb/in.; thrust, lb; torque lb-ft
T_c	Thrust coefficient
T_R	Reverse thrust
T_1	Initial total temperature °R
t	Jet thickness dimension
t_o	Total ground jet thickness
ΔT	Total temperature rise, °F
U	Nozzle velocity; fan blade tangential velocity, ft/sec
U_R	Blade root tangential velocity, ft/sec
U_T	Blade tip tangential velocity, ft/sec
V_o	Free stream velocity, ft/sec
V_2	Initial climb speed, ft/sec
V_a	Axial velocity, ft/sec
V_G	Ground speed, ft/sec
V_h	Hump speed, ft/sec
V_j	Jet exhaust velocity, ft/sec
V_{SI}	Stalling speed, takeoff configuration, ft/sec
V_{SO}	Stalling speed, landing configuration, ft/sec
V_W	Wind speed, ft/sec
ΔV_u	Change of whirl velocity, ft/sec
W	Weight, lb
w	Contact width
X	Axial body force
x	Buttock line distance
Y	Side force, lb
α_{TL}	Thrust line angle of attack, degrees
γ	Angle of tangent to trunk; ratio of specific heats; angle of climb, degrees

δ_e	Elevator angle, degrees
η	Adiabatic efficiency
μ	Coefficient of friction
θ	Meridional section heading; inward jet angle; air deflection angle, degrees; pitch angle, degrees
ϕ	Roll angle, degrees
ψ	Meridional section tangent to ground; preassure rise coefficient; angle of yaw, degrees
ρ	Density of air, slug/ft^3
ρ_w	Density of water, lb/ft^3
σ	Trunk tension, lb/in.; fan solidity

I. INTRODUCTION

A. SYSTEM CONCEPT

The Air Cushion Landing Gear is a scheme to replace, or in certain cases load relieve aircraft wheel gear with an annular jet air cushion. As illustrated in Figure 1, it embodies a pneumatic bag or bags mounted beneath and surrounding the fuselage. A continuous air feed from an on-board power source maintains the bag inflated while producing a distributed jet flow at its base. The escaping jets create a pressure in the cavity contained by the bag beneath the aircraft whenever it is close to the takeoff or landing surface. Air clearance beneath the bags is minimal, surface irregularities being tolerated by the resilience of the flexible material itself. The inflation pressure is very low (330 lb/ft^2). The bags are retractable and the entire system is expected to be competitive with wheel gear in terms of weight and drag.

The objective is to provide an improved tolerance to the takeoff and landing maneuver and environment with no compromise of performance and enable aircraft to operate from any surface consistency, including water. It is in fact a soft landing system with footprint pressure in the region of 1 to 3 $lb/in.^2$.

While offering significant other advantages associated with takeoff and landing such as cross-wind capability, kneeling, distributed load, fast retraction, high energy absorption and damping, and improved overland braking, the system is also expected to result in improved operating economy. This is because it will tend to allow a longer takeoff and landing run to be used in any given situation, due to the less stringent field requirement and the forgiving nature of the system. Given equivalence of weight and drag, this will result in improved payload/gross weight.

The crucial effect of this factor is well known and it can be shown that a 10% increase in takeoff speed is likely to provide an economic impact as great as a 20% improvement in load factor. It is believed that this improved economy will be combined with increased capability and, therefore, indicates a large potential, both military and civilian, for the developed system.

B. TEST AIRCRAFT

The present study considers the application of the system to a C-119. This aircraft was selected as a suitable test bed for the following reasons:

(a) It is a suitable size, large enough so that prototype application to a front line logistic aircraft can follow directly.
(b) It is ideally configured. The wheel arrangement (retracting into twin booms) is such that no alteration is necessary for test purposes. The fuselage is straight sided, flat bottomed, roomy and structurally convenient, with a minimum of services and equipment beneath the floor. Equipment relocation is thus minimal.

Figure 1. Artist's Impression of the Air Cushion Landing Gear

A number of alternative configurations for the air cushion were considered, and three quite radically different arrangements were tested in the wind tunnel. The best of these for the C-119 application is considered to be the single main cushion using the elastic bag type trunk shown in Figure 2. Advantages and disadvantages of the alternatives are discussed in Section II. The effects of varying the detail geometry for the single main cushion with the reasons for selecting that illustrated are also analyzed.

The power system is considered purely as a test bed aircraft installation. In an operational application a compact auxiliary power package will be required such as that illustrated in Figure 3 which represents a C-130 as a typical operational application. In this case, for the C-119 test aircraft, test convenience is the only criterion and no effort was made to design a compact power package. However, alternative powerplants were considered using different engines and different types of fans and these installations give an idea of the tradeoff between system weight and size with cushion performance. The best system for the test aircraft is considered to be as shown in Figure 4, which uses twin T58-10 gas turbines driving backward-curved centrifugal fans. This constitutes overpowering the system in terms of a probable operational installation, which is a desirable feature for the test aircraft, enabling the effect of power on system performance to be determined fully. However, except for general dependability, selection of a particular powerplant and fan is not critical to the development program.

C. WIND TUNNEL MODEL

Tests were conducted on a 1/12 scale quasi-dynamic model of the C-119 fitted with air cushion landing gear. Figure 5 shows the model in the low speed section of the NASA Langley 7 ft x 10 ft tunnel where the tests were run, using the moving ground (a continuous belt) as the takeoff and landing surface. The tests consisted of performing actual takeoffs and landings with the model, into which air for the air cushion was piped along the sting from an external source. The model was pitched by its own remotely controlled elevator. It was also free to slide some eight inches up the vertical mounting post, clear of the ground, but it was fixed in yaw, roll and in the side to side and fore and aft directions. Thus, the technique was to start with model resting to the ground; inflate the air cushion, bringing the model up to about 30 inches full scale height in hover and friction free on the surface; bring the ground belt and tunnel velocity up to the takeoff speed in a level attitude; and operate the elevator in small increments to raise the nose, when the model would take off smoothly and leave the ground in a simulated takeoff. For landing, tunnel and belt speeds were reduced with the model at a suitably high angle of attack until the model sank back to the ground on the rear of the air bag and the nose was then lowered by elevator control in a simulated landing.

Measurements of lift, drag, elevator angle, pitch attitude, height and pressures were made and are analyzed in a subsequent section. The tests were successful, and provide proof that the normal takeoff and landing maneuver will not be compromised by the air cushion despite some deficiencies in model characteristics. Takeoffs and

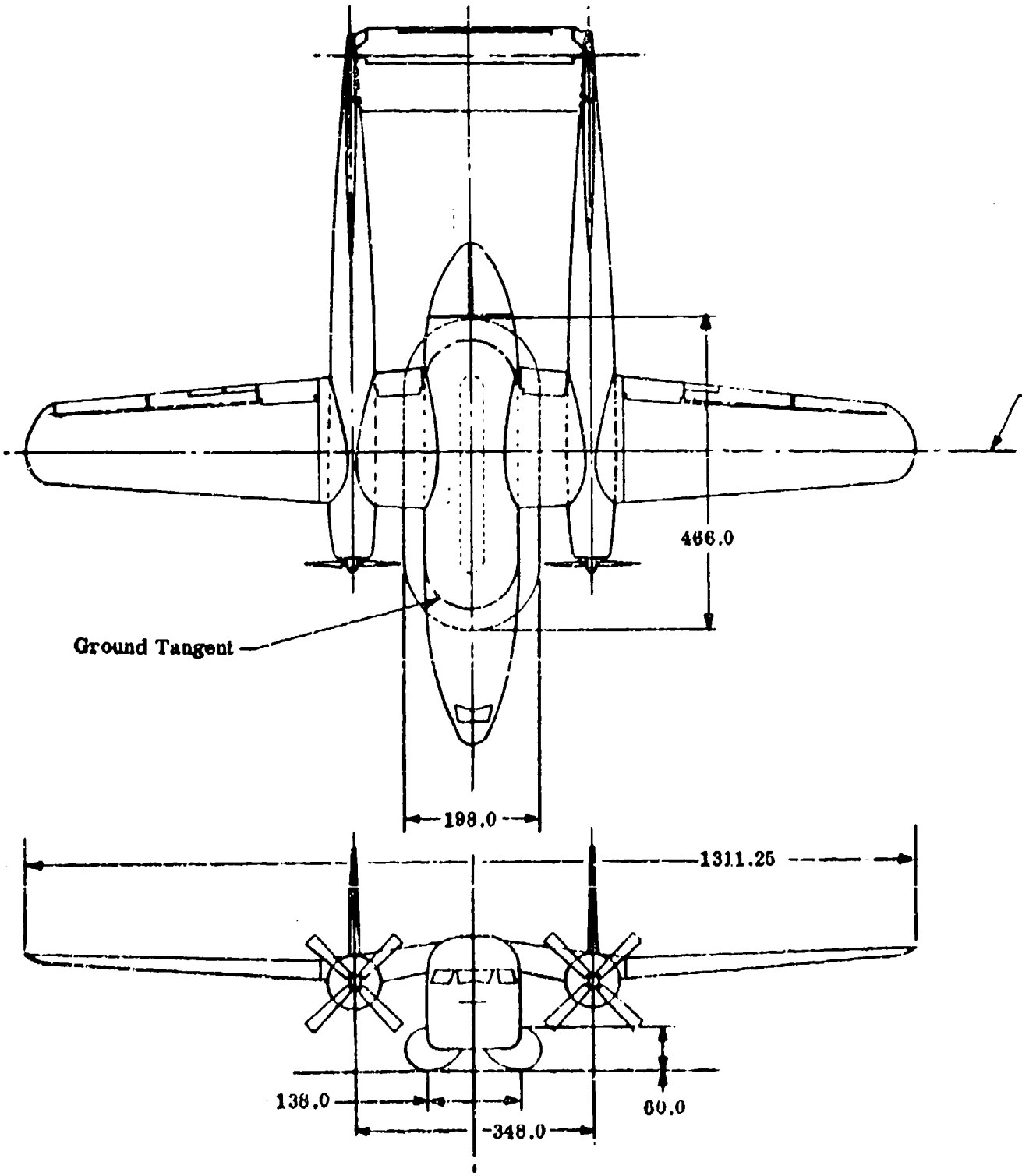

Figure 2. C-110 Basic Configuration Three-View

Air Cushion Data	
Main Cushion Area	360.5 Ft^2
Perimeter	80.7 Ft.

40% Chord Line

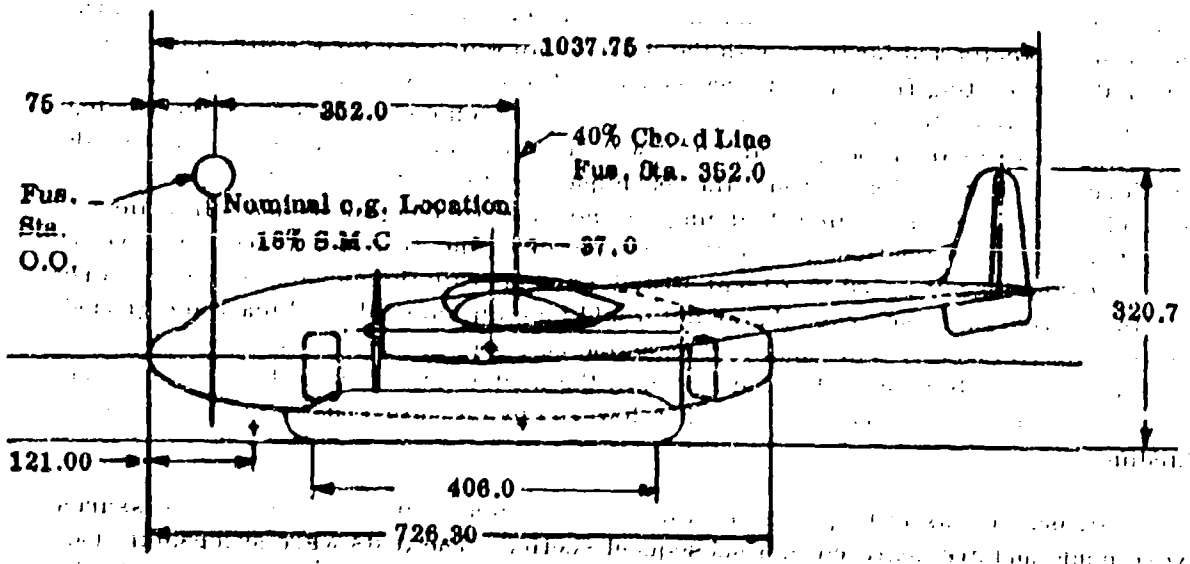

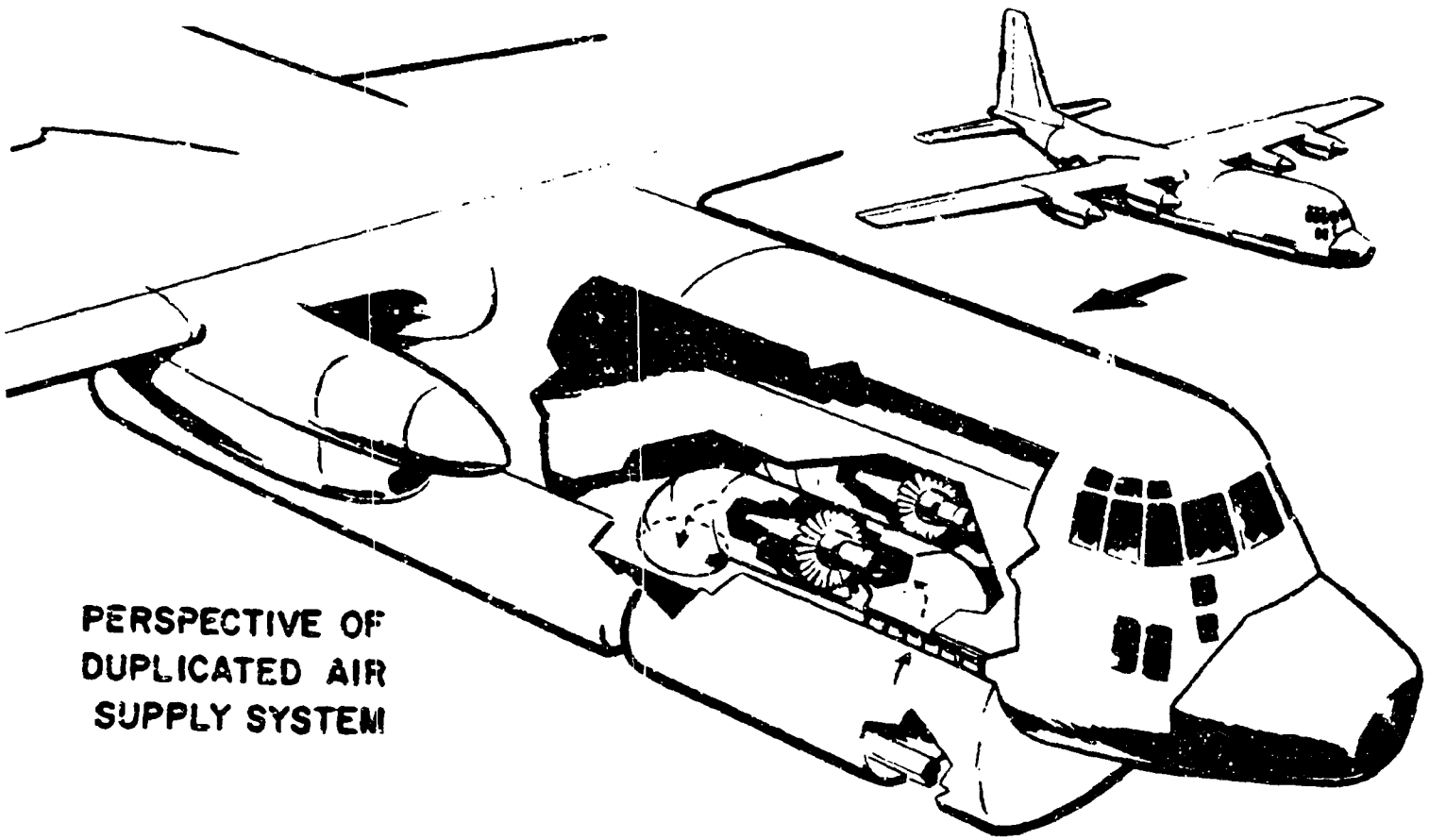

Figure 3. Operational Aircraft Auxiliary Power System

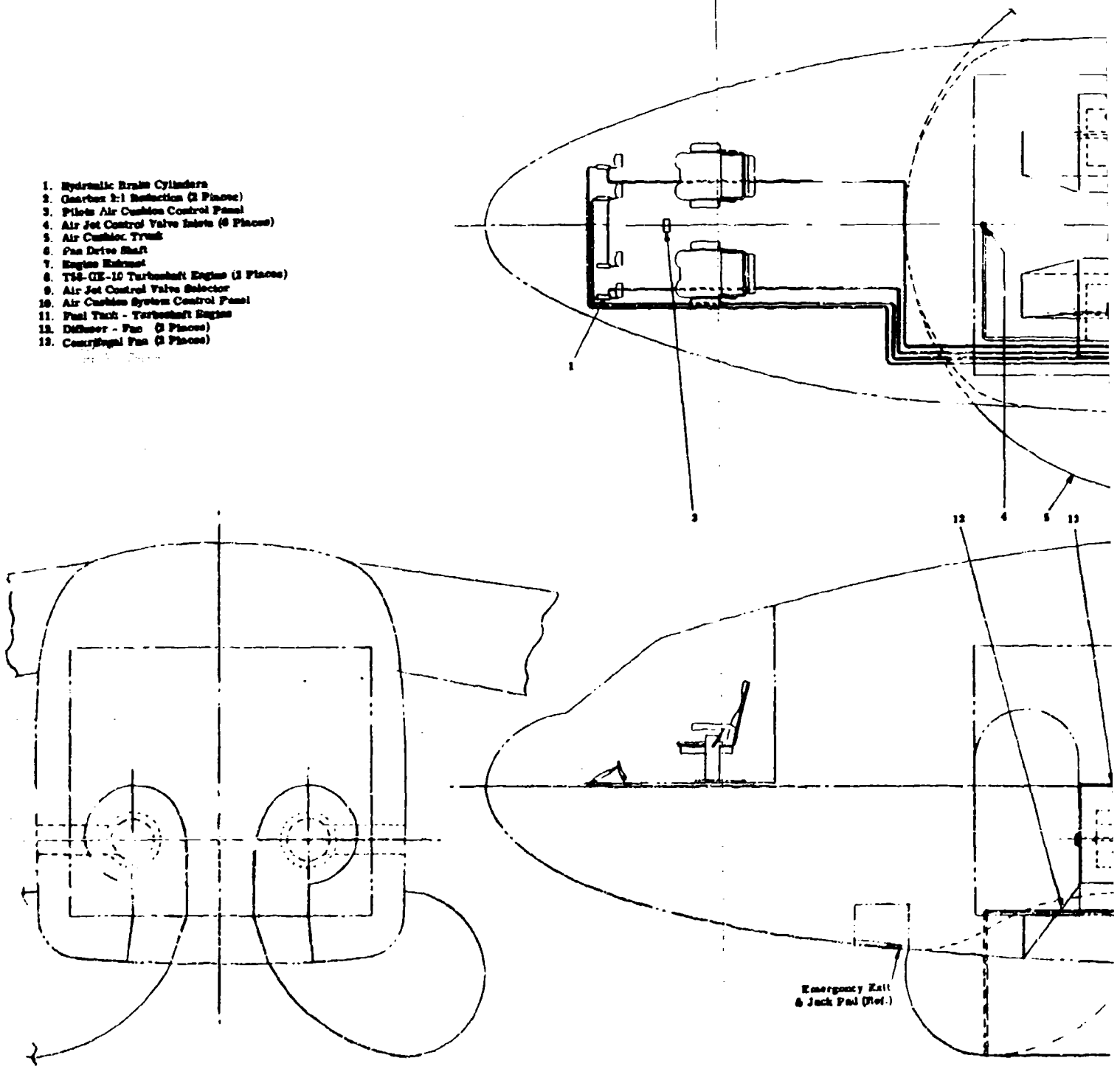

Figure 4. Inboard Profile With T58-10 Engines.

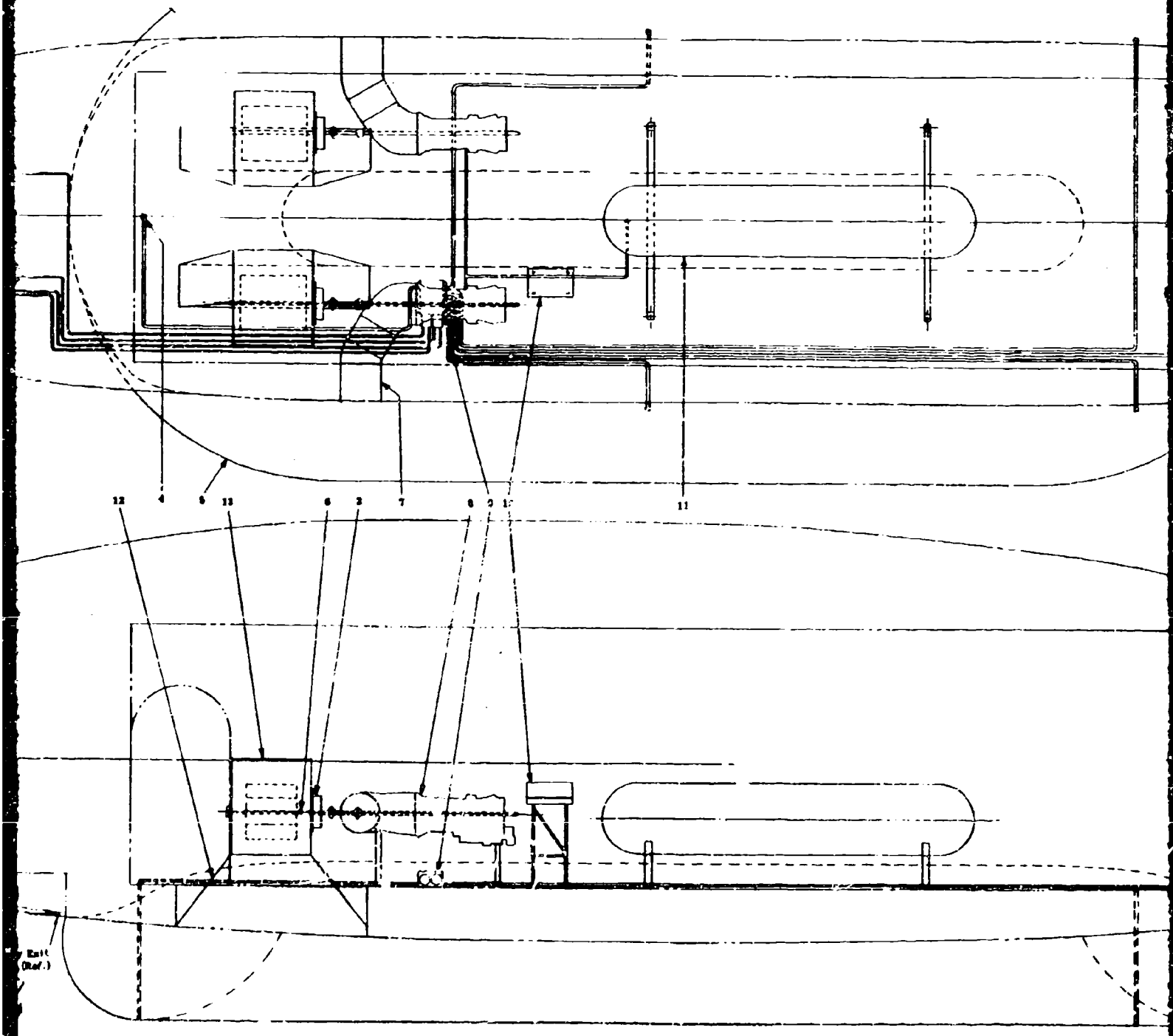
12
4
9
13
6
3
7
8
2
11
Exit
(Ref.)

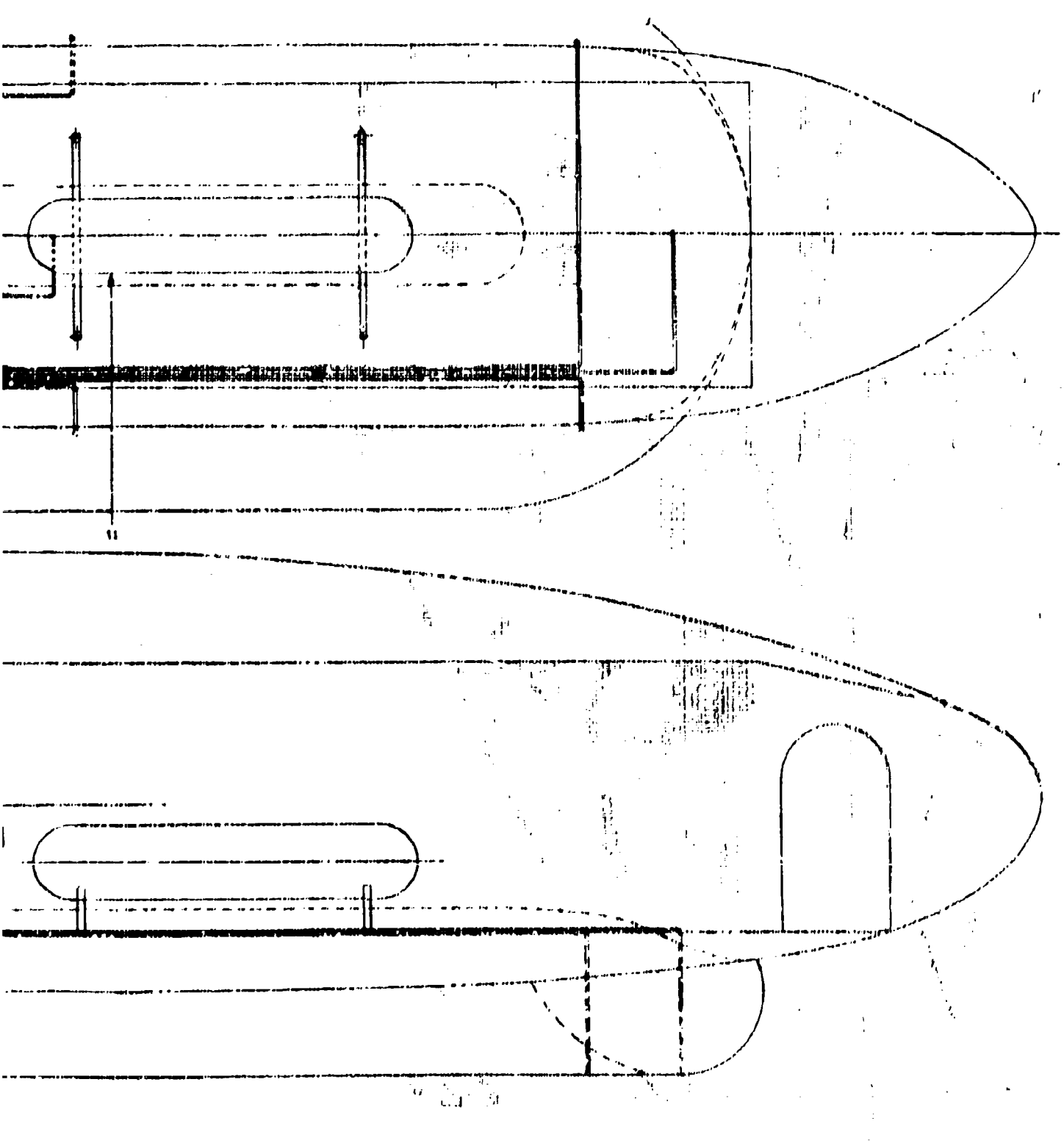

Figure 5. 1/12 Scale Quasi Dynamic Model in Wind Tunnel

landings were made down to approximately 1.05 times the power-off stalling speed. The in-flight drag of the inflated bag was found to be similar to that of the extended wheels. However, the total of profile and momentum drags is larger, resulting in a reduced climb angle with the bag inflated. This is offset by the fast retraction available with the bag system, plus the extra thrust available from diverting the air cushion flow.

D. WHIRLING ARM MODEL

The objectives of the whirling arm model tests were to develop satisfactory retraction, determine behavior in crossing selected obstacles and evaluate energy absorption and damping. The model is shown in Figure 6 mounted on the whirling arm, with the trunks inflated, while Figure 7 is a general view of the whirling arm and obstacles showing the model resting on the ground with the trunks deflated.

The model represents a wingtip float suitable for C-119 installation, and also represents approximately a 4/10 length main air cushion at 1/3 scale. Air for the cushion is provided by a special hydraulically driven centrifugal fan, hydraulic power being provided through swivel joints at the hub of the rotating arm. The model is mounted on parallel links to be free to rise and fall but is otherwise restrained. The arm is rotated by a small hydraulic motor driving a pneumatic tire in contact with the ground.

Prior to whirl testing, measurements of cushion pressure, trunk pressure, and fan rpm were made and the model performance was related to these and to the model weight. For drop tests, measurements included a continuous record of height, cushion pressure and vertical acceleration versus time.

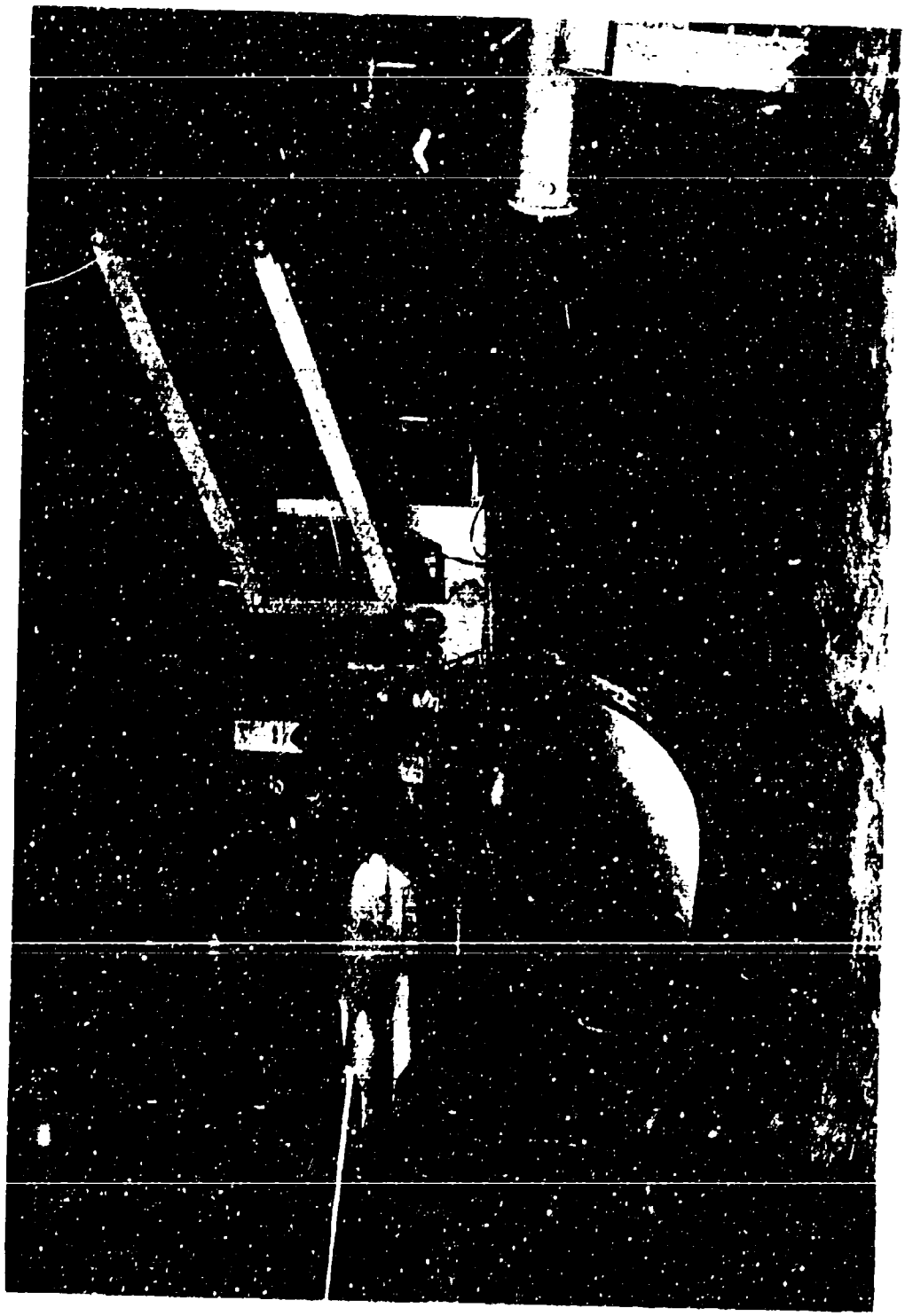

Figure 6. 1/3 Scale Model, Elastic Trunk Inflated

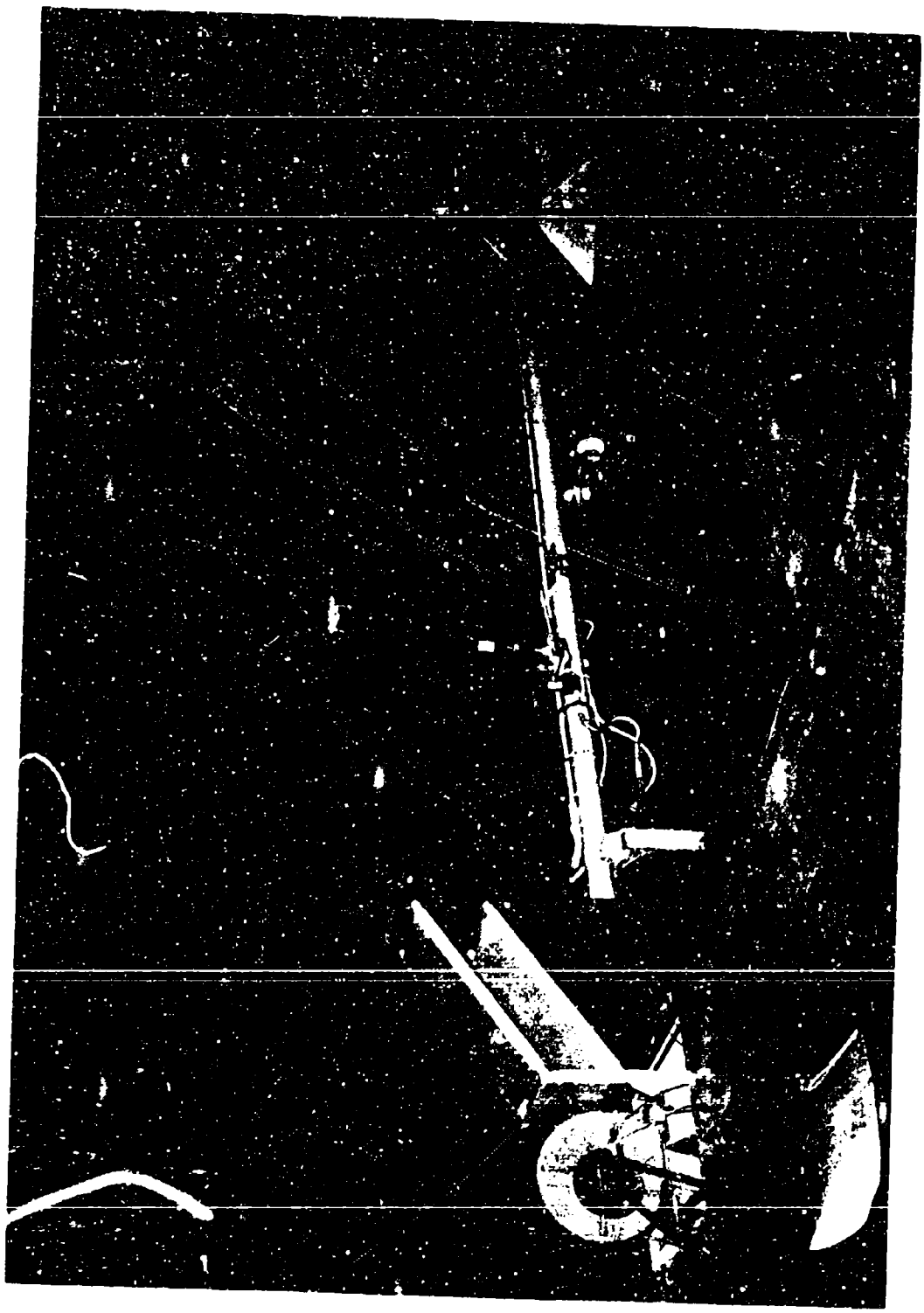

Figure 7. Whirling Arm with 1/3 Scale Model

II. SYSTEM DESIGN AND ANALYSIS

A. AIR CUSHION CONFIGURATION

A wide range of air cushion landing gear configurations is possible. For the C-119, which to some extent was chosen for this reason, they are confined to arrangements beneath the fuselage, which is considered best because then the system hardly interferes with the aircraft aerodynamics.

The area available beneath the fuselage limits the maximum area of air cushion. There are two excellent reasons why the maximum possible area should be used:

(a) Cushion pressure will be minimized and jet height (to which terrain performance is related for a given type of air cushion) will be maximized for given power. Jet height will be shown to vary as cushion pressure to the power of 1.5 so that loading has a strong effect on jet height.

(b) Over water wave drag is inversely proportional to area times length. Since increasing cushion length also increases area, for given width drag is proportional to length squared, which is again a very strong effect. It is desirable to be able to show an overwater capability for the C-119 not so much from the viewpoint of actual overwater testing as that it should, as a test aircraft, represent a typical operational application. For an operational aircraft, an amphibious capability, if not accompanied by the usual weight and drag penalty, will almost certainly be required.

Properties required of the air cushion trunk are as follows:

Retractability
Durability
Ease of Braking
Minimum weight
Flexibility (for performance)
Simplicity (for low cost)
Stability

Consideration of the above factors has led to the selection of the single maximum area bag type trunk, using one way stretch elastic retraction as the preferred configuration. The present study has shown this configuration to be feasible. However, other configurations having significant advantage have been studied. A comparison is made in Table I.

TABLE I

CUSHION CONFIGURATIONS

CONFIGURATION	GROSS AREA	EST. WAVE DRAG/WT	PRINCIPAL ADVANTAGES	PRINCIPAL DISADVANTAGES	REMARKS
1. Single main cushion (elastic retraction)	360	0.15	Simplicity, Stability, Energy Absorption	None	Single Air Feed
2. Maximum area Main and Nose Cushion (elastic Retraction)	359	0.13	Pitch Stiffness, Ease of Rotation	Heavy - Complex	Smaller Area Than No. 1
3. Small Main Bag and Nose Plenum	187.1	1.02	Low Weight, Ease of Rotation	Low Performance (none over water), Internal Ducting	Nose Plenum retraction not studied. May Not be Needed.
4. As No. 1 or 2 with Tip Floats	360	0.13 0.15	Tip Floats May be Found Necessary Over Water	Additional Tip Float System	Retractable conventional Tip Floats Are Possible
5. Double Main Plenum Plus Nose Plenum	141	1.0	Plenum Has Best Basic Simplicity	Low Performance, Unstable in roll, No Braking, Internal Ducting, Low Energy Absorption	Retraction Not Studied
6. Mechanical Retraction of Configuration 1.	360	0.13	Possible Ease of Assembly	Heavy, Complex and Costly	Methods Not Studied in Detail

Three-view drawings were made of the first four configurations, drawing numbers D7233-099004, D7233-099005 and D7233-099006, reproduced in this report as Figures 2, 8, and 9. Figure 61 illustrates configuration 5. Configurations 1, 3 and 5 were tested in the wind tunnel.

It will be seen from these drawings that all the bag trunk configurations are parallel sided with toroidal ends and have the same cross section under 1 g load, this cross section being maintained through any plan radius at the ends. The detail design of the trunk is discussed in the next section. The trunk design is a new one, of a type not previously tried. It is, however, derived from the typical annular jet bag trunk which itself replaced the earlier complex ribbed trunk in air cushion vehicles. These different approaches are compared in Figure 10.

The cross-section shape of the bag trunk at 1 g load is determined by the selected cushion pressure/jet pressure ratio and by the length and center position of the outer radius. The way these variations affect the cross-section shape is shown in Figure 11. The recommended design cross-section is the top figure in each block. In this case the fuselage is supported at the same ground clearance and attitude as it is on the wheels. The variations shown are all practical. Comments are as follows:

In the case of increasing R_1 the increased trunk depth provides a longer stroke for energy absorption without excessive g (i.e. a softer system) at the expense of material weight. The inflated/deflated ratio tends to reduce slightly with increasing depth until the trunk inner attachments coincide in the middle when it starts to increase sharply. (Figure 11 (a)).

Increasing trunk pressure (P_j) increases static roll stability and energy absorption but reduces terrain capability. Below $P_c/P_j = 0.4$ stretch increases markedly (Figure 11 (b)).

Raising the aircraft out of the trunk as shown in Figure 11 (c) increases trunk depth in the best way and spreading the trunk as shown in Figure 11 (d) is effective in increasing roll stiffness and cushion area and reducing wave drag. In the former case if the upper attach point starts around the radius the inflated/deflated ratio increases very rapidly.

Analysis and tests discussed in the following sections indicate that the selected design point is the most suitable compromise for the test installation.

B. TRUNK DESIGN AND ELASTIC ANALYSIS

1. Description

The detail trunk design is illustrated on drawing No. D7233-188001 (Figure 12). This cross-section is maintained around the entire bag circumference. The elastic material specified is a four-ply sheet of one way stretch. It consists of four

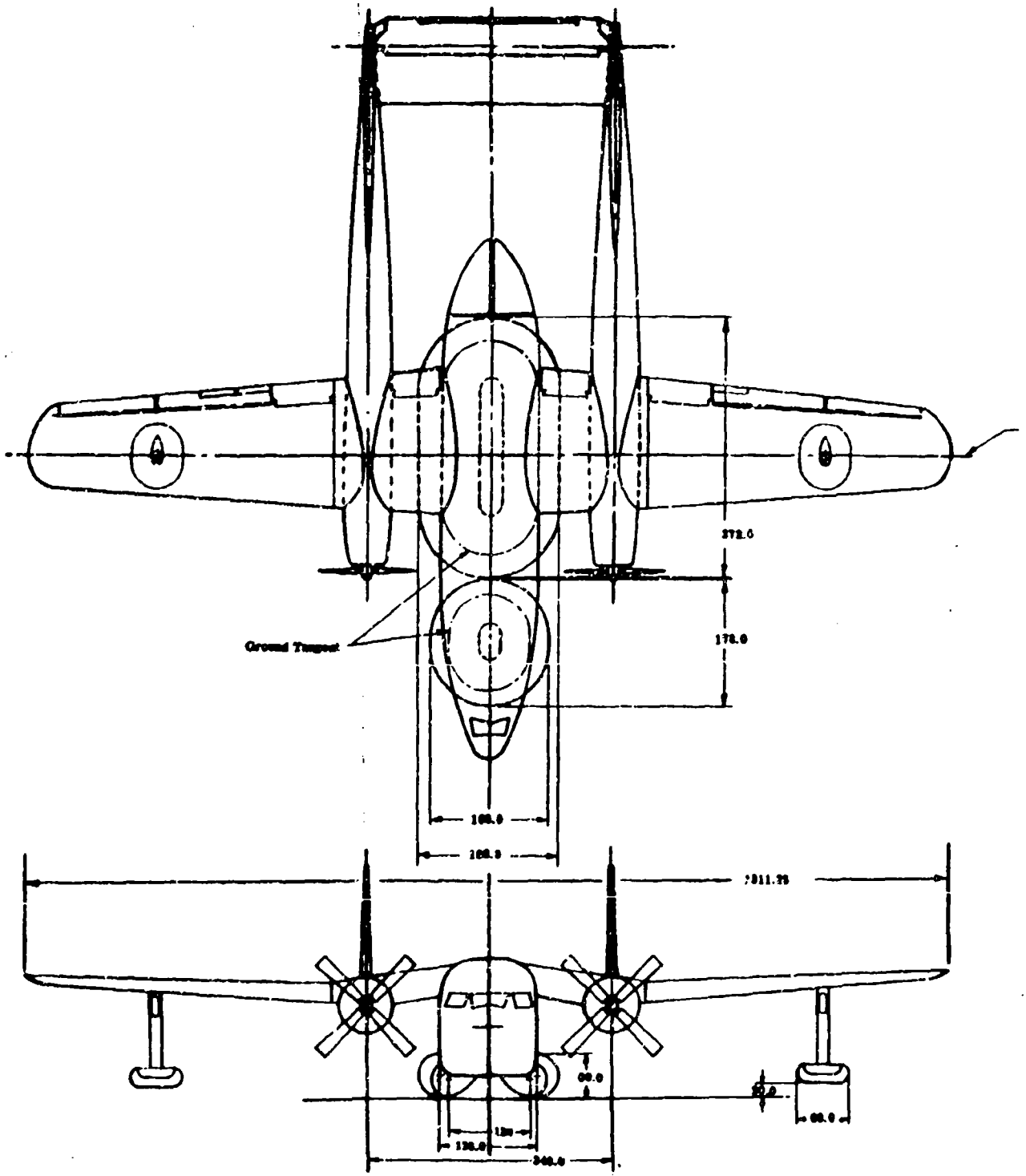

Figure 8. Three-View of Dual Cushion with Tip Floats

Air Cushion Data	
Main Cushion Area	370.0 Ft^2
Perimeter	61.6 Ft
Nose Cushion Area	60.0 Ft^2
Perimeter	23.1 Ft
Tip Float Area	16.6 Ft^2
Perimeter	14.7 Ft

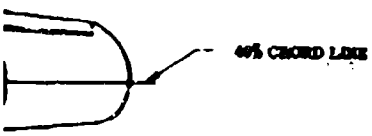

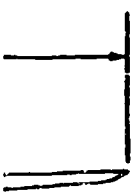

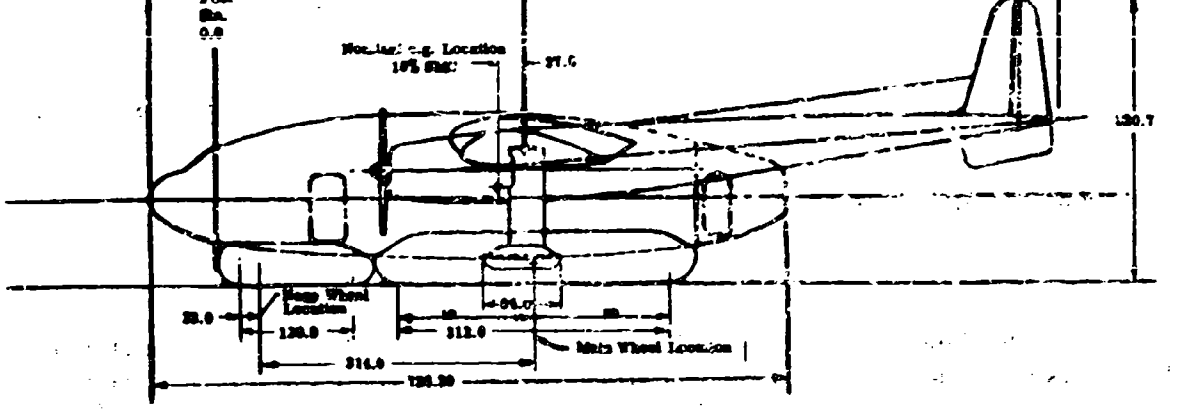

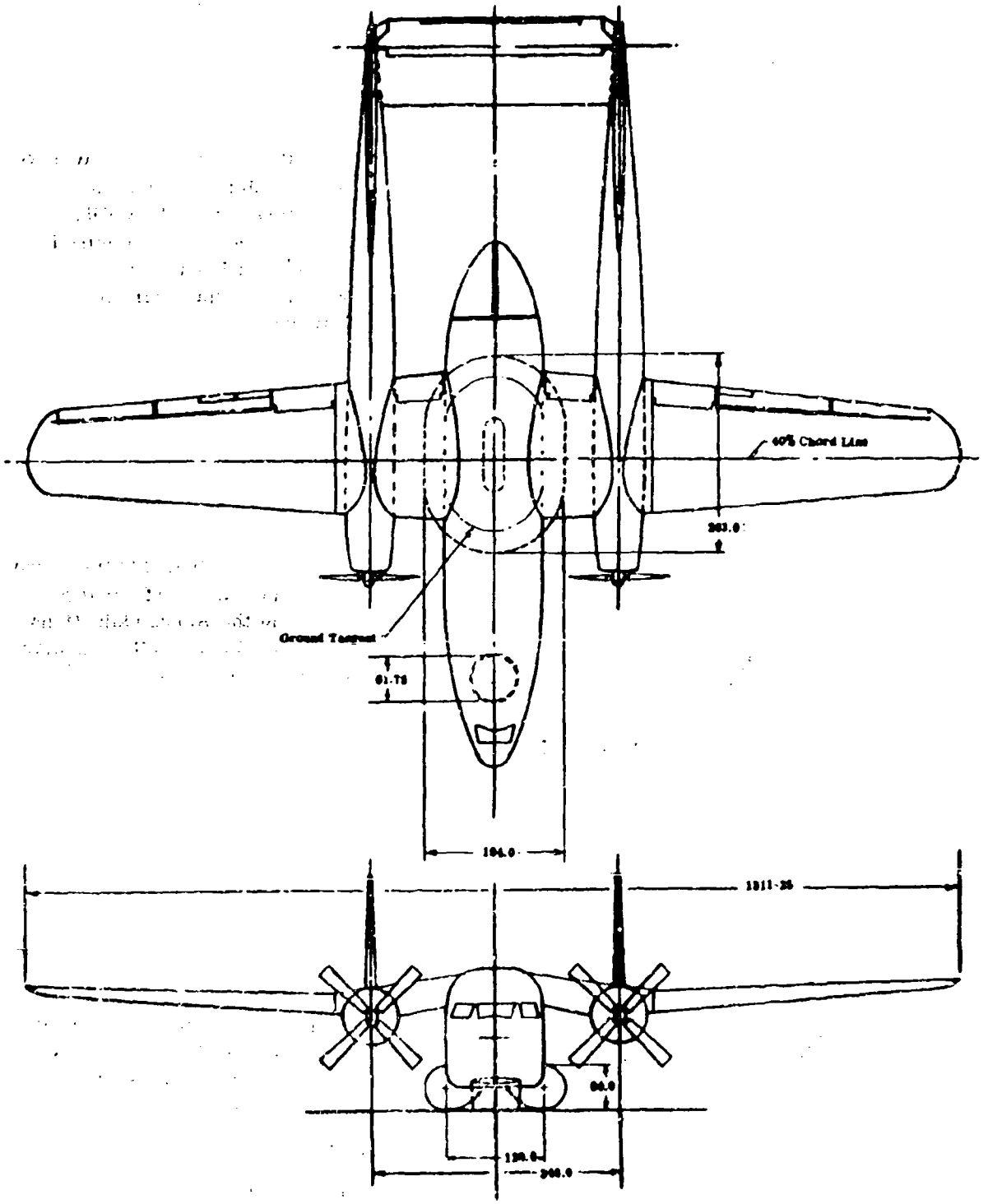
40% Chord Line
Ground Tangent
104.0
1311.25
66.0
120.0
240.0

Air Cushion - Data	
Main Cushion Area	163.3 ft^2
Perimeter	48.9 ft
Nose Cushion Area	80.[illegible] ft^2
Perimeter	16.3 ft

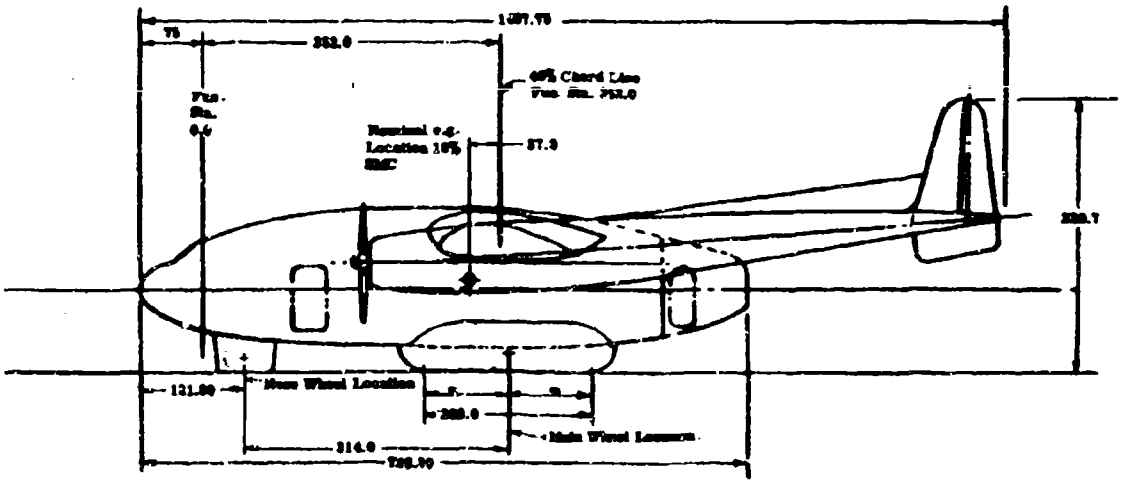

Figure 9. Three-View of 1/2 Length Main Cushion with Nose Plenum

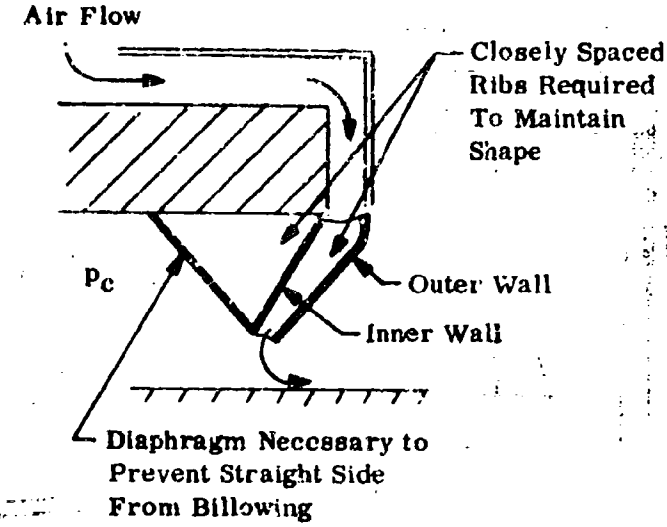

This Design Provided a Well Directed Annular Jet in a Flexible Structure. The Many Ribs And Bonded Joints Required Introduced Local Stiffness With Resultant Wear and Damage

(a) Original USN SKMR-1 Trunk

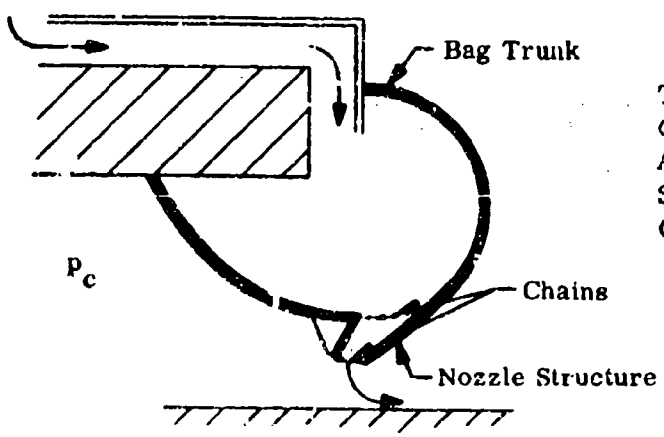

This Design Provided Improved Clearance and Performance Avoiding the Above Objections. Separate Bags and Rectangular Corners Were Used.

(b) Developed SKMR-1 Design

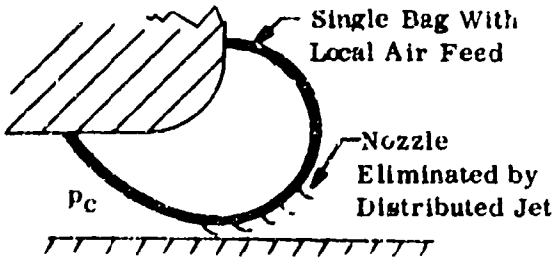

The C-119 Air Cushion Landing Gear Design Avoids a Nozzle Structure But Has Lower Jet Height. The Ends are Toroidal and Local Stiffness Corners Are Eliminated. It is Cleanly Retractable

(c) C-119 Air Cushion Trunk

Figure 10. Comparison of Trunk Designs

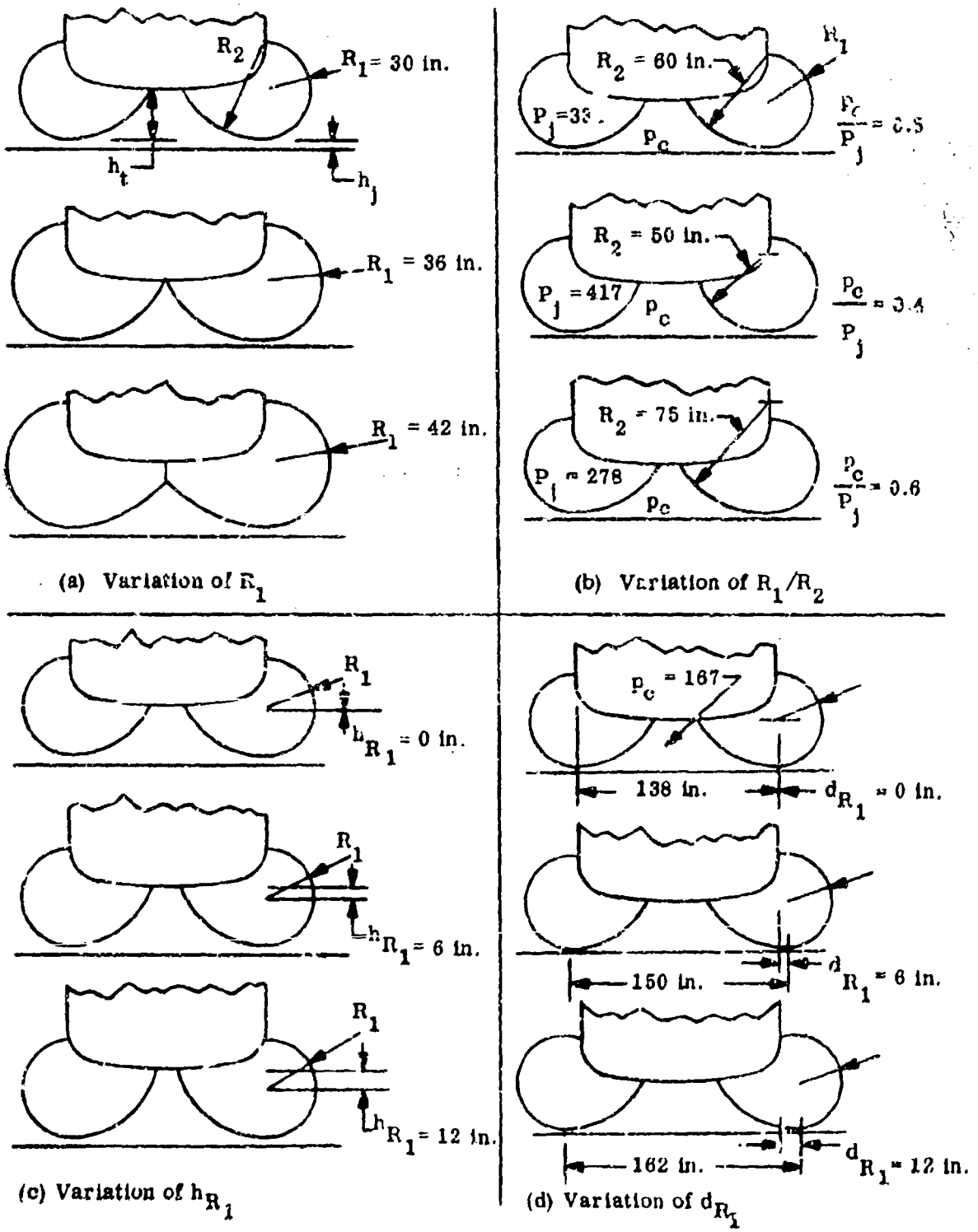

Figure 11. Section Geometry Variations

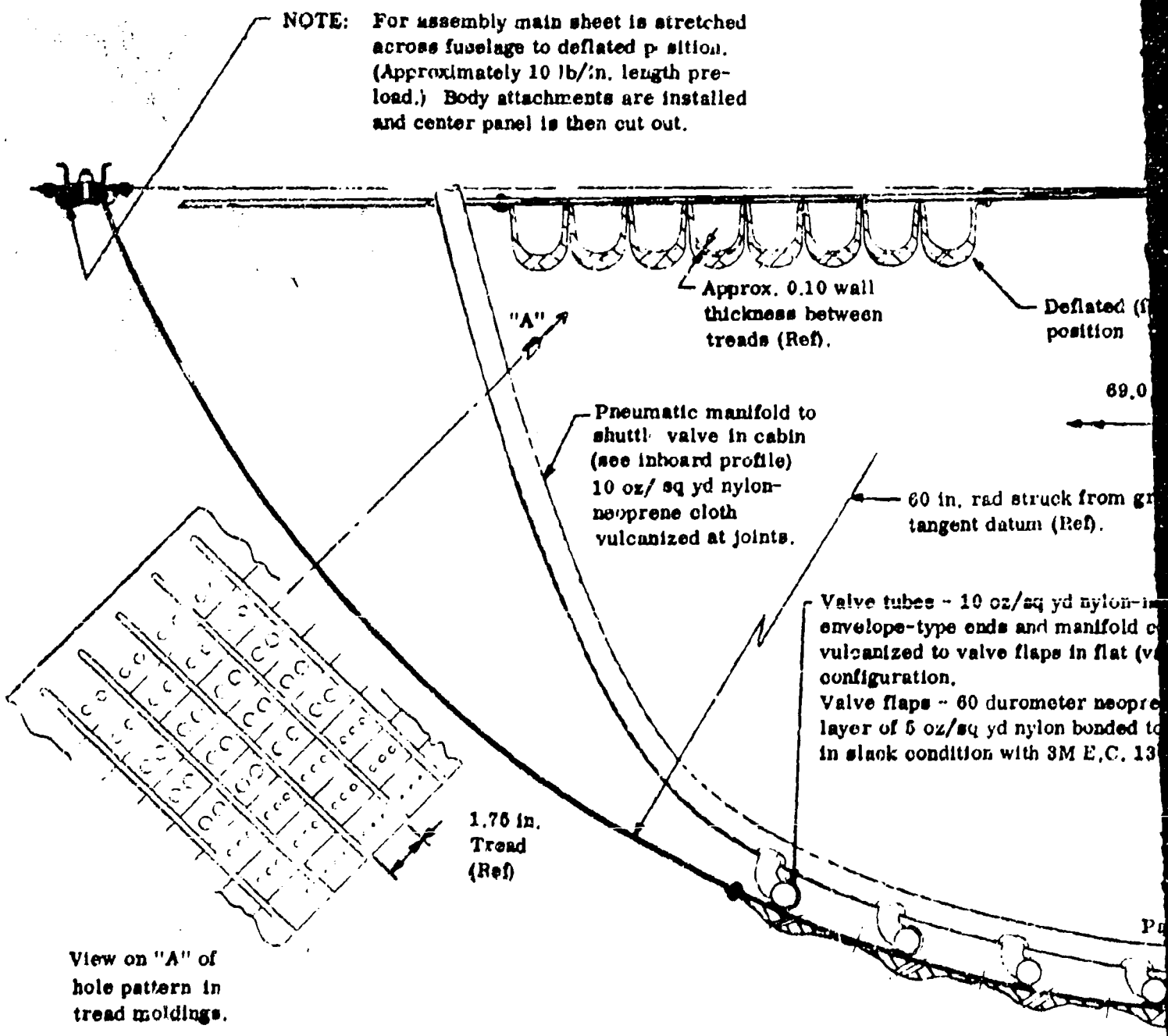

Figure 12. Cross Section of C-119 Air Cushion Design

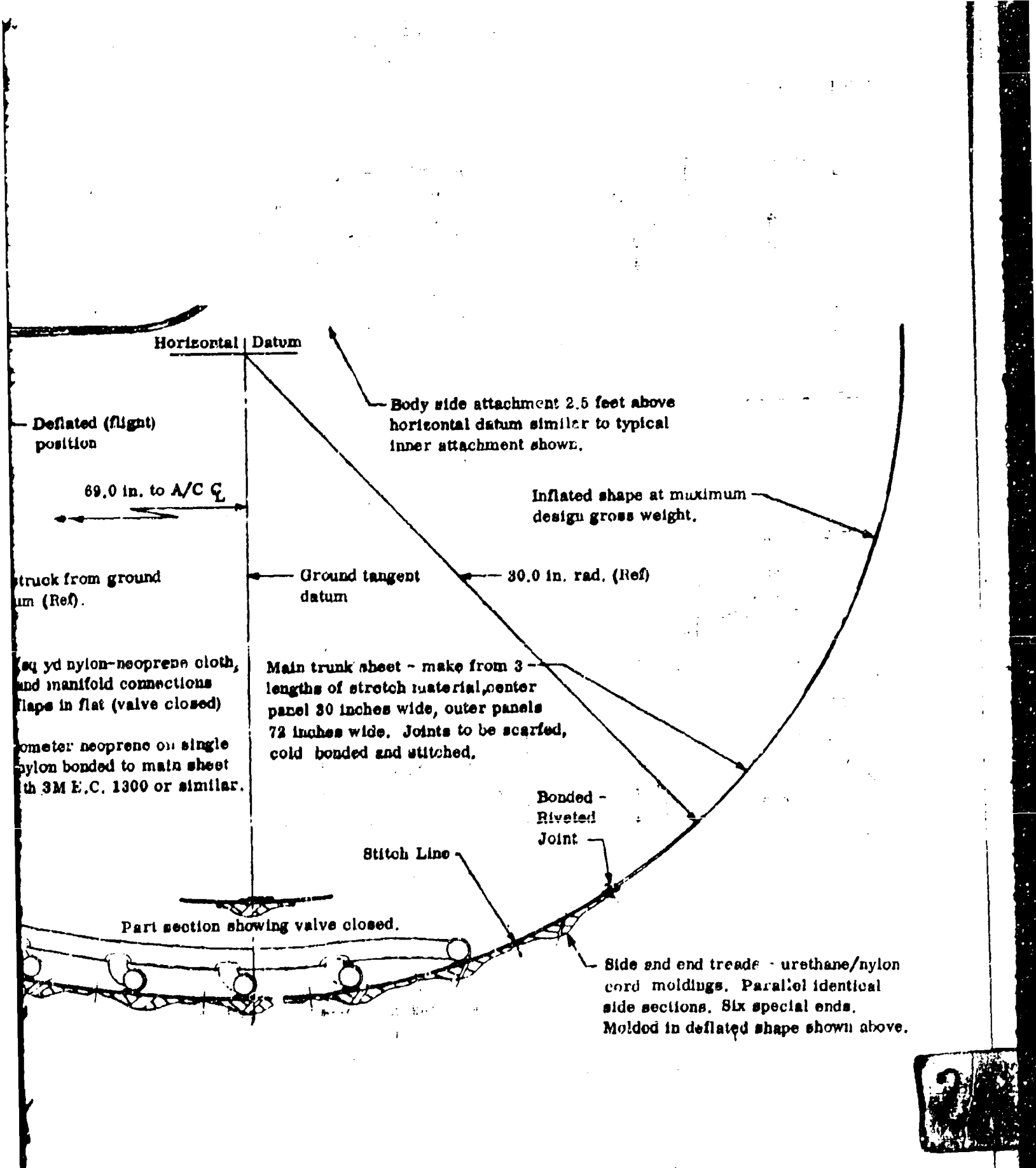
Horizontal Datum
Body side attachment 2.5 feet above horizontal datum similar to typical inner attachment shown.
Deflated (flight) position
69.0 in. to A/C ℄
Inflated shape at maximum design gross weight.
truck from ground
um (Ref).
Ground tangent datum
30.0 in. rad. (Ref)
sq yd nylon-neoprene cloth,
and manifold connections
flaps in flat (valve closed)
Main trunk sheet - make from 3 lengths of stretch material, center panel 30 inches wide, outer panels 72 inches wide. Joints to be scarfed, cold bonded and stitched.
ometer neoprene on single
nylon bonded to main sheet
th 3M E.C. 1300 or similar.
Bonded - Riveted Joint
Stitch Line
Part section showing valve closed.
Side and end treads - urethane/nylon cord moldings. Parallel identical side sections. Six special ends. Molded in deflated shape shown above.

sheets of nylon fabric (Stern and Stern type A5063) with natural rubber layers sandwiched between each sheet. The outside is coated with Neoprene. The purpose of this construction is to combine the characteristics of the individual components for an ideal composite. Thus:

(a) The nylon is woven with coiled fill threads and has an elongation of approximately 300% (4 : 1) before the threads are straightened. It stretches very easily to this point (a mechanical extension) after which it has considerable ultimate load capacity. Load capacity at full stretch and tear resistance are the properties provided.

(b) The natural rubber provides the best possible elastic behavior. Numerous synthetics have been considered but comparable elasticity is very hard to find.

(c) The neoprene provides environmental protection for the natural rubber and being more plastic is better as an outside coat. The natural rubber has more tendency to develop local high stress and break into holes. Random breakdown inside the sheet is not objectionable. In normal stretch both rubber and neoprene will easily elongate 700%.

The material specified is not considered ideal. It is believed that substantial improvements in tear strength and strength/weight ratio will be made. However, it is available and suitable for the test aircraft. Its elastic characteristic and ultimate strength are shown in Figure 13. The working point is also indicated. This is found from

$$T = P_j R_1$$

$$= \frac{333}{144} \times 30 = 69.3 \text{ lb/in.}$$

The trunk sheet is made from two pieces of 72 inch wide material and one piece 30 inches wide. The complete single sheet is a rectangle measuring 14.5 x 45 ft. before assembly. The 72 inch wide material is the coated width. Procurement of 14.5 ft. wide material is not possible. The nylon material is only available 12 inches wide. (It is woven wide and contracts after being removed from the loom). Thus each nylon ply in the 6 foot material is made from 6 widths stitched at the selvedges. The total cost of the basic trunk sheet is estimated to be in the order of $5000.

The elastic material is not designed to withstand wear. To provide durability a tread section is attached to the sheet. This extends from the ground tangent inwards and outwards to protect the area where the bag may contact the ground. This is a urethane accordion molding made in sections and stitched through the trunk sheet. The stitch lines lie along the warp of the basic trunk including at the ends; the accordion folds being aligned with the stretch direction at all times. Each hoop of the molding incorporates a slant orifice so that a distributed inward facing jet pattern is established over a wide area. These orifices register with holes in the trunk sheet

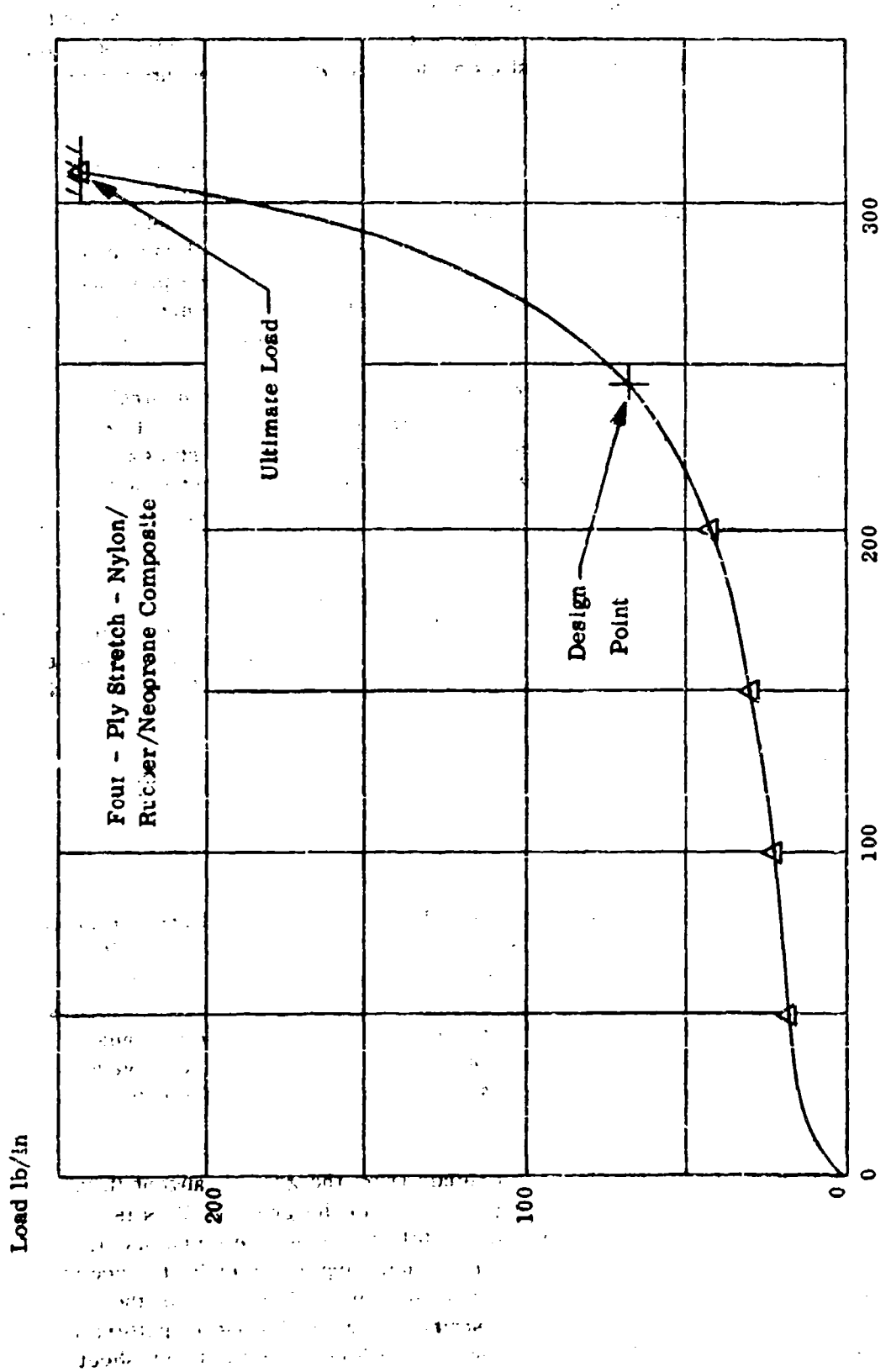

Figure 13. Material Stretch Characteristics

on inflation. At the edges of the molding a strong riveted and bonded joint is made.

The reasons for this jet pattern are as follows:

(a) Discrete holes are used to avoid the need for bridging a slot with ties. It is not possible to achieve equivalent flexibility with slots whose edges must be stiffened to take bending load. Furthermore, at the ends, the slots (which must lie in the stretch direction) would not be peripheral. It is feasible to consider a built-up nozzle structure on the outside of the bag but this is complex, causes retracted drag and interferes with retraction. Additionally it must be backed by large holes in the basic sheet is excessive pressure drop is to be avoided.

(b) Rather than a single line of discrete holes at the ground tangent the jets are spread inwards for two reasons: first to provide optimum air lubrication; second to avoid local suction forces leading to dynamic instability and ground resonance.

If the aircraft pitch or roll attitude is changed without alteration of cushion pressure such as will deflect the cushion outwardly and maintain an air clearance, then the trunk will flatten in ground contact. It has been found from tests that this contact area can be reliably "air lubricated", to avoid friction drag. The trunk pressure is realized on the outside between the sheet and the ground, abrupt pressure drop occurring at the flattened edges; to the inside to cushion pressure and to the outside to atmosphere. The membrane is not pressed onto the surface. The most effective "air-lubrication" is obtained with a distributed jet.

In the second place dynamic instability is reliably inhibited by having the jet pattern dispersed away from the ground tangent. The reason for this is further discussed in Section II.F.

For braking, cushion pressure is destroyed and the weight transferred by direct contact of the tread with the ground over a wide area. At gross weight the contact area is approximately 140 ft^2 giving an average contact width of about 20 inches, half the tread width in the inflated condition. To eliminate cushion pressure and maintain the bag inflated the nozzles must be closed. This is accomplished by the pneumatic valve system shown. Each row of nozzle holes is blanketed by a long peripheral strip, bonded to the inside wall. These are made of natural rubber. On the inside face of each strip thin-walled tubes of coated material are bonded across the width of the strip. These tubes are suitably manifolded to a moderate pressure air supply - in this case engine bleed air and when inflated, lift the flaps to open the nozzles and form the air cushion.

2. Assembly Method

The complete nozzle and tread system is attached to the trunk sheet before assembly. To accomplish assembly the outer edges of the trunk sheet at the sides are attached to heavy rails which are jacked close to either side of the aircraft. This provides the required prestretch, which is 10 lb/in. The total lift on each rail is approximately 5000 pounds. The side and inner attachments (illustrated in Figure 12) are then made. The inner attachment line lies outside the center panel of the trunk sheet along the sides. Thus the side portions of the trunk are effectively of one piece construction. After assembly the center panel inside the attachment is cut out and discarded. Seams joining the panels only appear at the ends as shown in the following sketch of the trunk sheet.

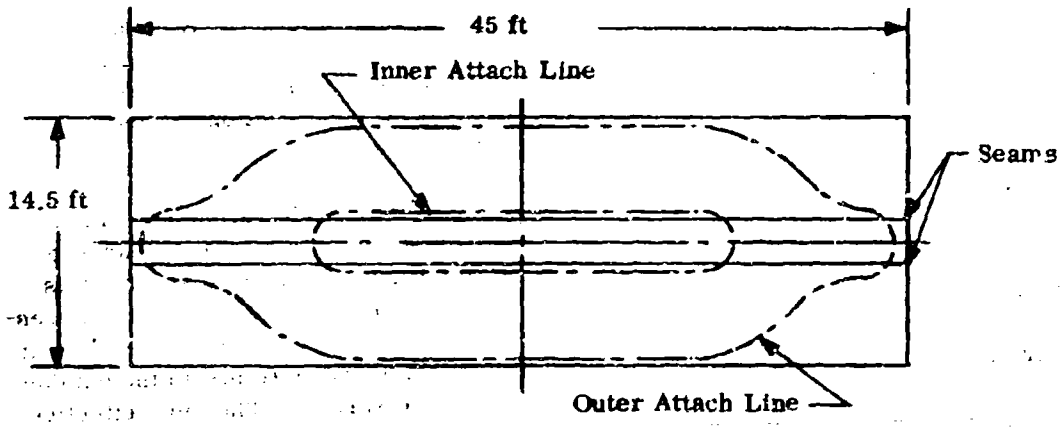

Trunk Sheet

Because the material does not stretch in the fore and aft direction, it must be pulled towards the center at the ends to provide spare material, before making the attachment. This is accomplished by wrinkling the sheet laterally before prestretch and fixing local clamps on the wrinkles on the outside. The required longitudinal contraction is accomplished by block and tackle connecting the end clamp and the end attachments are then made. This contraction causes the material to lie in a few tight lateral folds at the ends outside the tread section when deflated. The effect can be seen on the 1/12 scale model photograph of Figure 14. This shows the C-119 lower fuselage shell with an elastic sheet attached to it adjusted to give a regular inflated shape.

Good progress towards the development of the tread and elastic material at C-119 scale has been made by Bell Aerosystems in an Independent Research and Development program. A small portion of this type of molding roughly bonded to a four-ply piece is shown in Figure 15 slack and in Figure 16 stretched to a load of 70 lb/in. Satisfactory performance from the type of nozzle valve incorporated in the design has also been obtained in tests.

Figure 14. C-119 1/12 Scale Model With Elastic Trunk

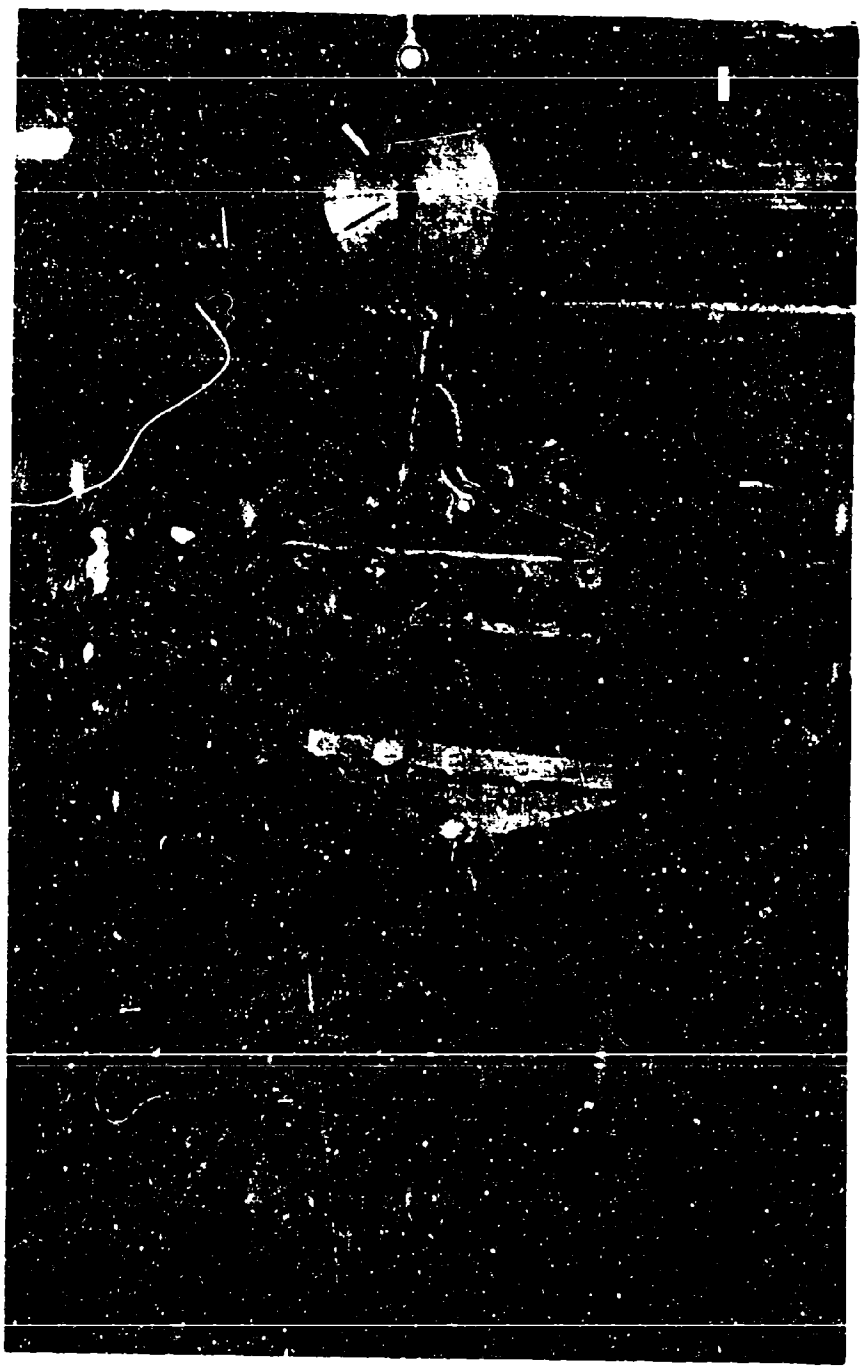

Figure 15. Tread Specimen Contracted

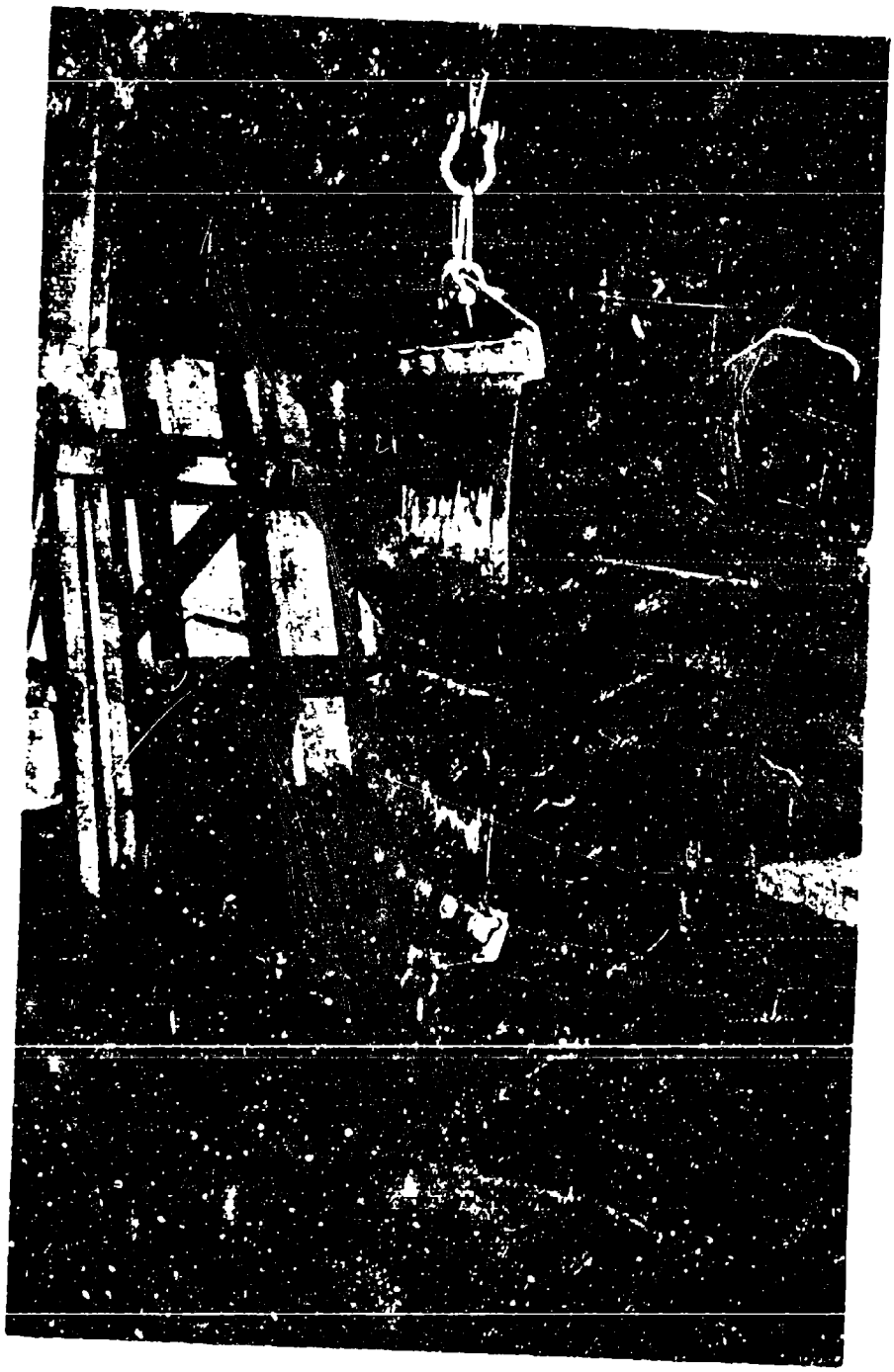

Figure 16. Tread Specimen at Design Stretch

It is seen from Figure 13 that the ultimate strength of the material is greater than the two-dimensional design tension by a factor of 3.5. This is satisfactory, however three-dimensionally the tension is not constant, due to the effect of hoop stress at the ends. An analysis of local stress in the material leading to a method of integrating material stretch at all points to find slack shape is given in the following paragraphs.

3. Stress Analysis

The tension at a point P anywhere on the surface of a thin toroidal shell (Figure 17) is considered in two parts; that due to hoop stress which acts in the horizontal plane and that due to meridional stress which acts in the vertical plane passing through the axis of the torus.

Because of the cushion pressure the resulting toroidal end is lop-sided, the inner radius being double the outer radius. However, the abrupt change in meridional section radius is caused by an abrupt change in pressure differential across the membrane so that there is no discontinuity in tension at the ground tangent.

The hoop and meridianal tensions have been developed in Reference 1. By considering an element of the membrane it is shown that hoop tension

$$N_\theta = \frac{p R_1}{2} \tag{1}$$

Where R_1 is the meridional radius, in this case the outer radius is used so that p is the trunk pressure above ambient.

Meridional tension is variable, being modified by the hoop tension

$$N_\phi = p \frac{R_1 (r_o + b)}{2 r_o} \tag{2}$$

Note that this expression becomes pR_1 (the two-dimensional value), when $r_o = b$.

The two tensions both have a component in the lateral direction and can be resolved and summed to find the total lateral tension at p as follows (see Figure 18).

$$S = \frac{p R_1}{2} \left(\cos\theta \cos\gamma + \frac{r_o + b}{r_o} \sin\theta \cos\left[\gamma - \Psi\right] \right) \tag{3}$$

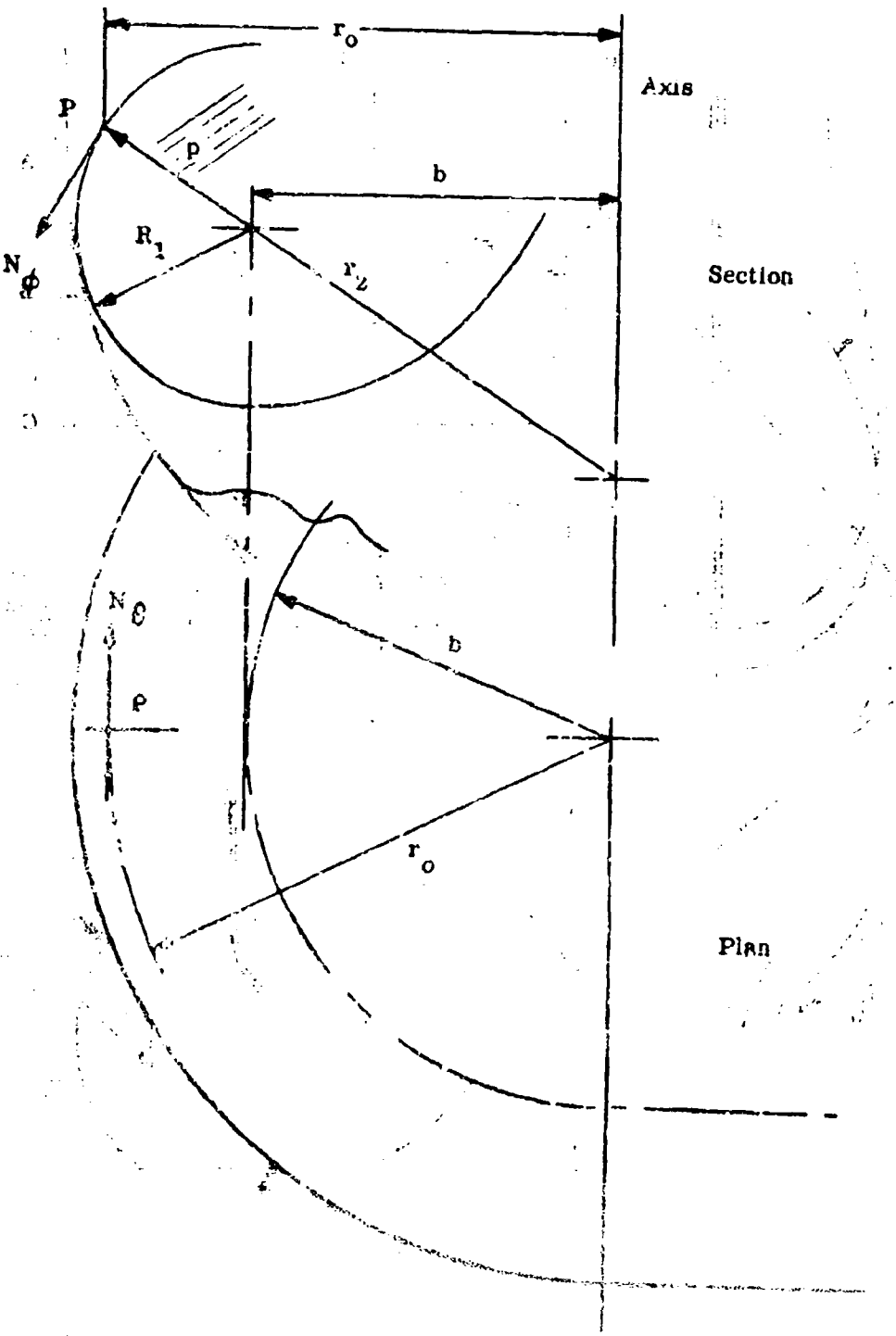

Figure 17. Torus Geometry and Notation

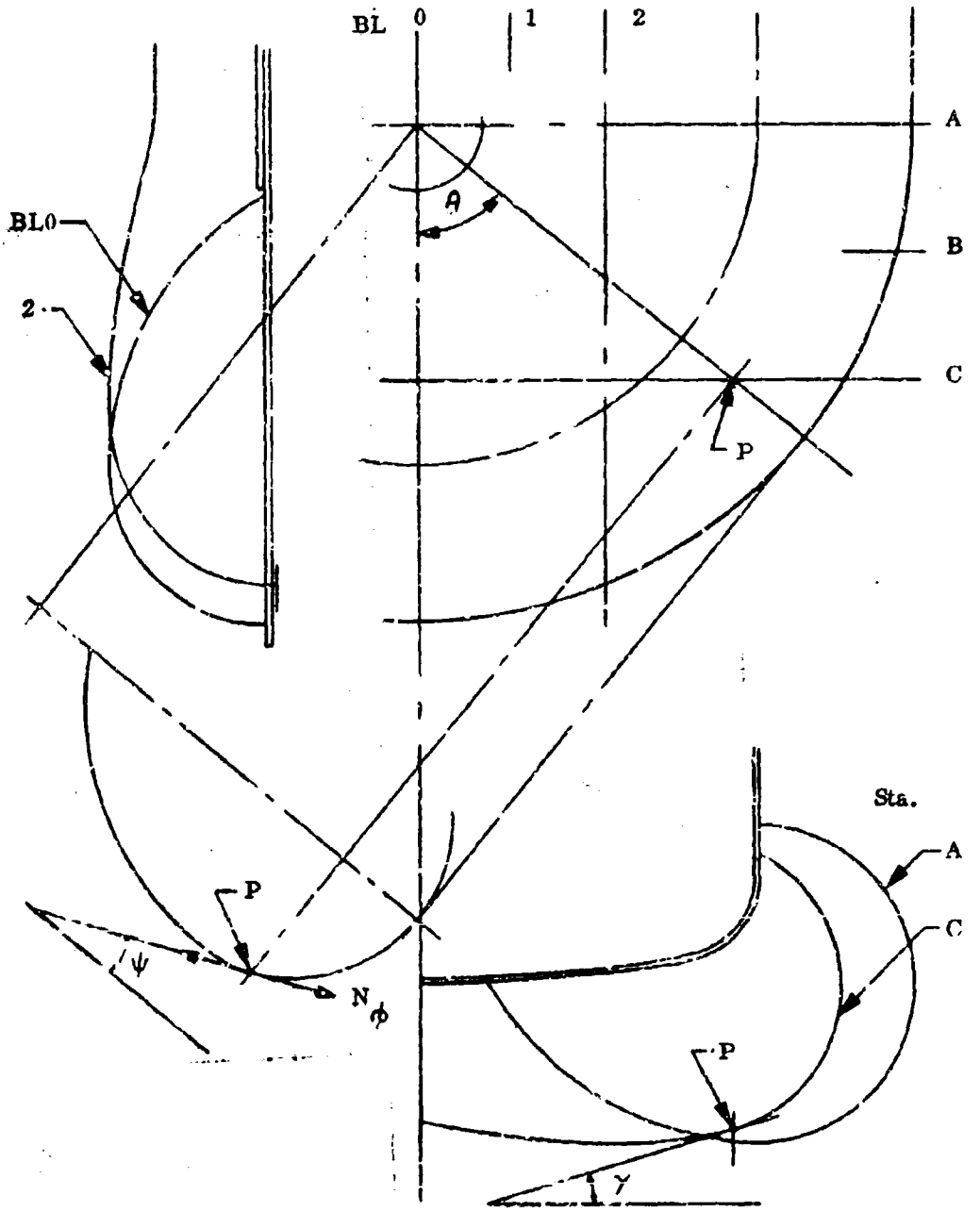

Figure 18. Skeleton Trunk Lines

Maximum stress is found to occur on the inner attachment line at the ends and is equal to 1.4 times the two-dimensional value. Thus the ultimate load factor for the present material is reduced to 2.5 at this local point. Minimum stress occurs at the outer attachment point at the ends, and is approximately half the two-dimensional value.

4. Determination of Slack Shape

The two-dimensional geometry having been determined (Station A) a series of lateral sections (Station B, C, D etc.) are drawn, the section at any radius being the same as A or part of A if interrupted by the body (Figure 18). Because of the symmetry these station lines are also buttock lines save where the body limits them differently. For convenience buttock sections may also be drawn in the side elevation. The stations lie generally in the stretch direction. For a series of points on each station, both r_c and the angles θ, γ and ψ can be measured; b is constant. Thus the tension at any point can be calculated. Using the material characteristic (conveniently shown in the form of Figure 19)*, the slack/stretched ratio at any point is then found and plotted versus the inflated station length around the contour, (Figure 20). The area under this curve is a first approximation of station length.

Similarly by partial integration the slack length to any chosen position on the approximate inflated length can be drawn for each station (Figure 21).

The inflated station lines will not retract as straight lines at the same longitudinal position on the slack sheet. However, the slack buttock lines, which lie plumb in the non-stretch direction as straight threads and may be assumed not to change in length can now be drawn on the inflated shape and their junction line with th fuselage so determined. For convenience, the inflated length along any station is plotted against the buttock distance x (inflated). Figure 22.

Suitable slack buttock lines are laid on Figure 21 and the inflated length is used to enter Figure 22 and find the inflated buttock distance x The slack buttock line lengths are determined by measurement of the surface distance on a three dimensional mold of the inflated shape. The total length of these lines from station A fore or aft now enables an approximate slack shape to be determined. (Figure 23). Also the position of each point can be registered with its corresponding point on the body.

Since the slack buttock lines are assumed not to stretch, the position of particular stretch threads or slack station lines can now be drawn more accurately at chosen intervals from station A along these lines. It will be seen that an iterative procedure has now been developed since the tension along the stretch thread can now be recalculated to reposition the slack buttock lines, etc.

---

* This is a two-ply material characteristic. Two-ply was used for the whirling arm model which is 1/3 scale to the C-119.

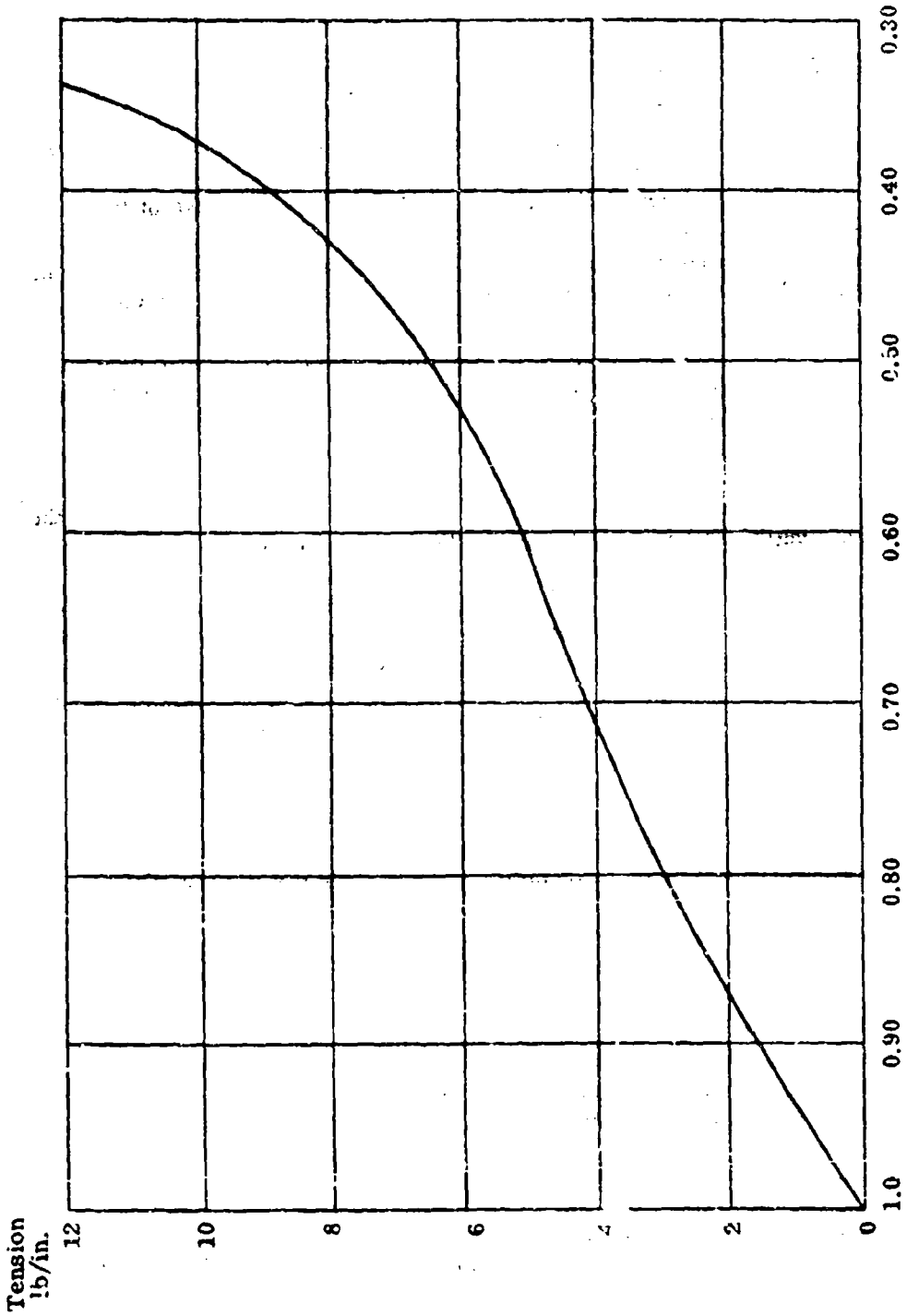

Figure 19. Two-Ply Stretch Characteristics

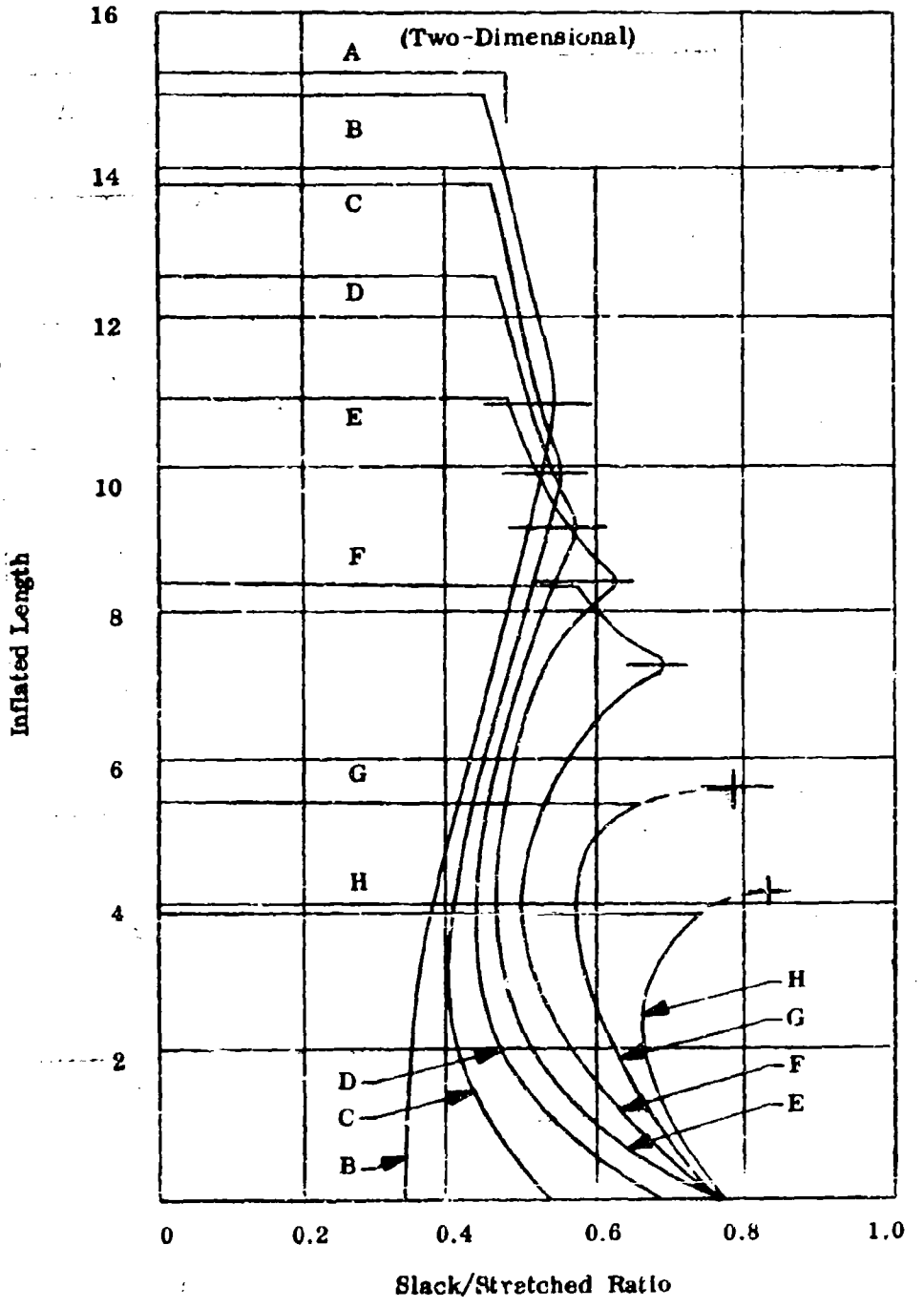

Figure 20. Slack/Inflated Ratio versus Inflated Length

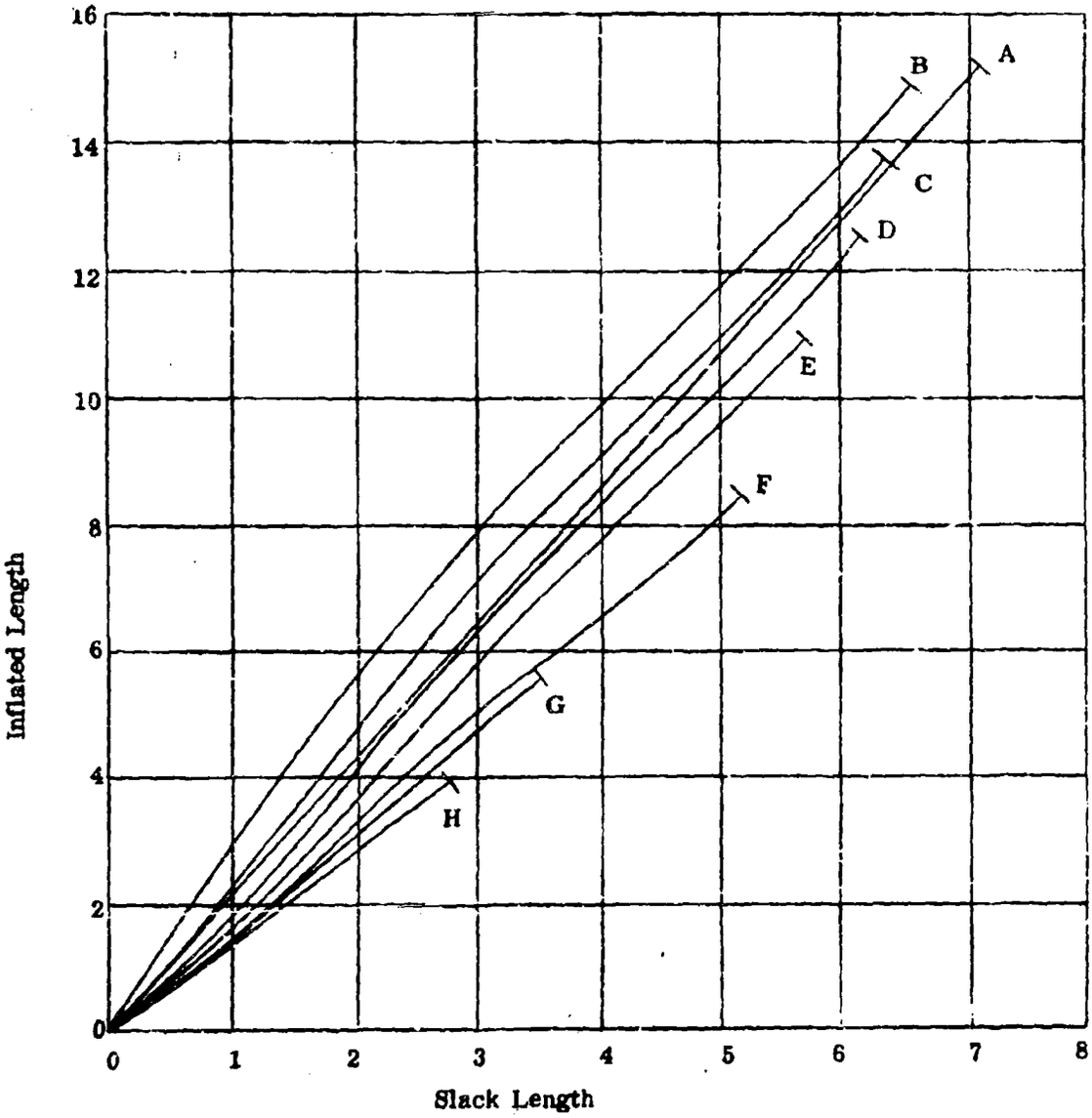

Figure 21. Slack Length versus Inflated Length

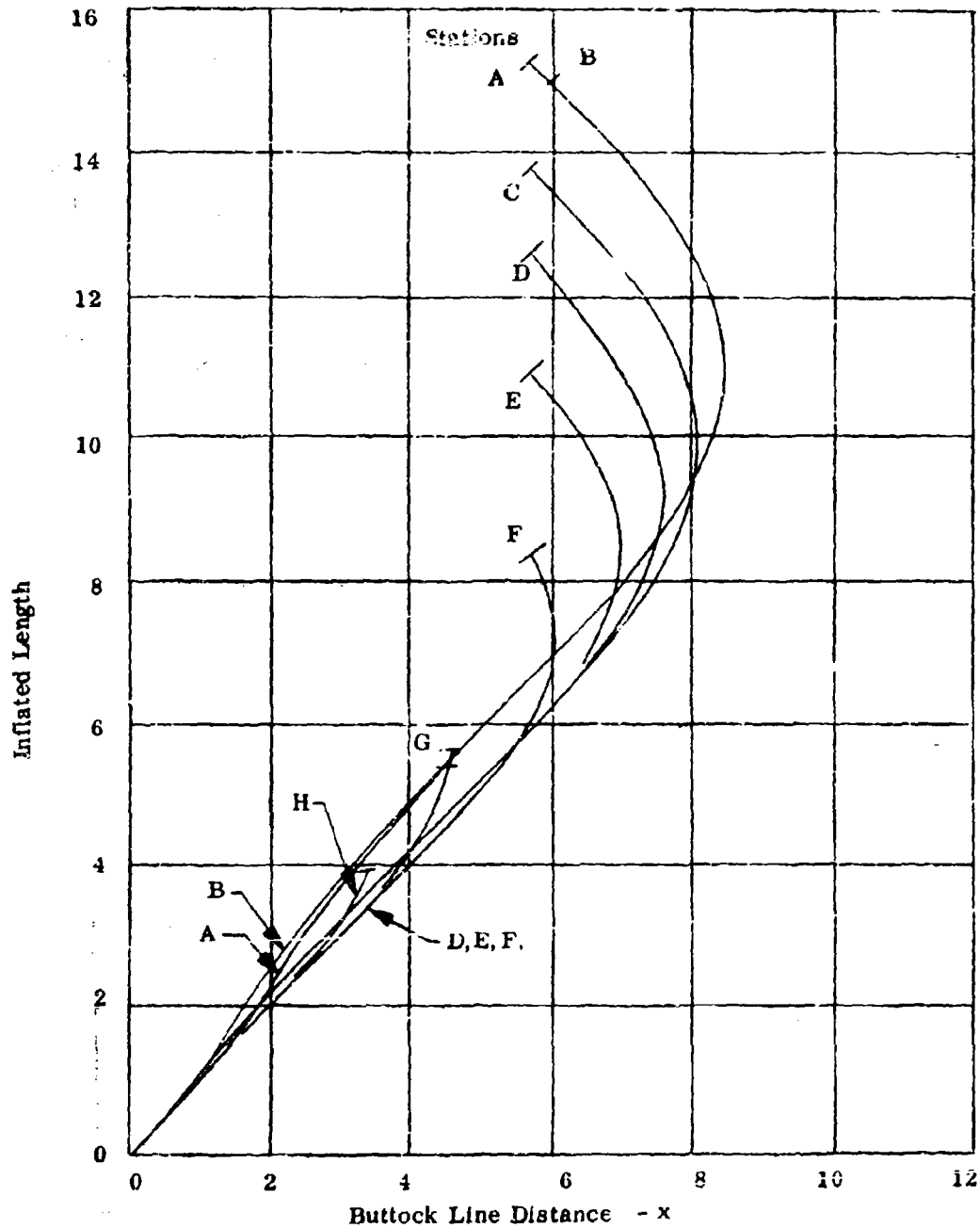

Figure 22. Buttock Line Distances

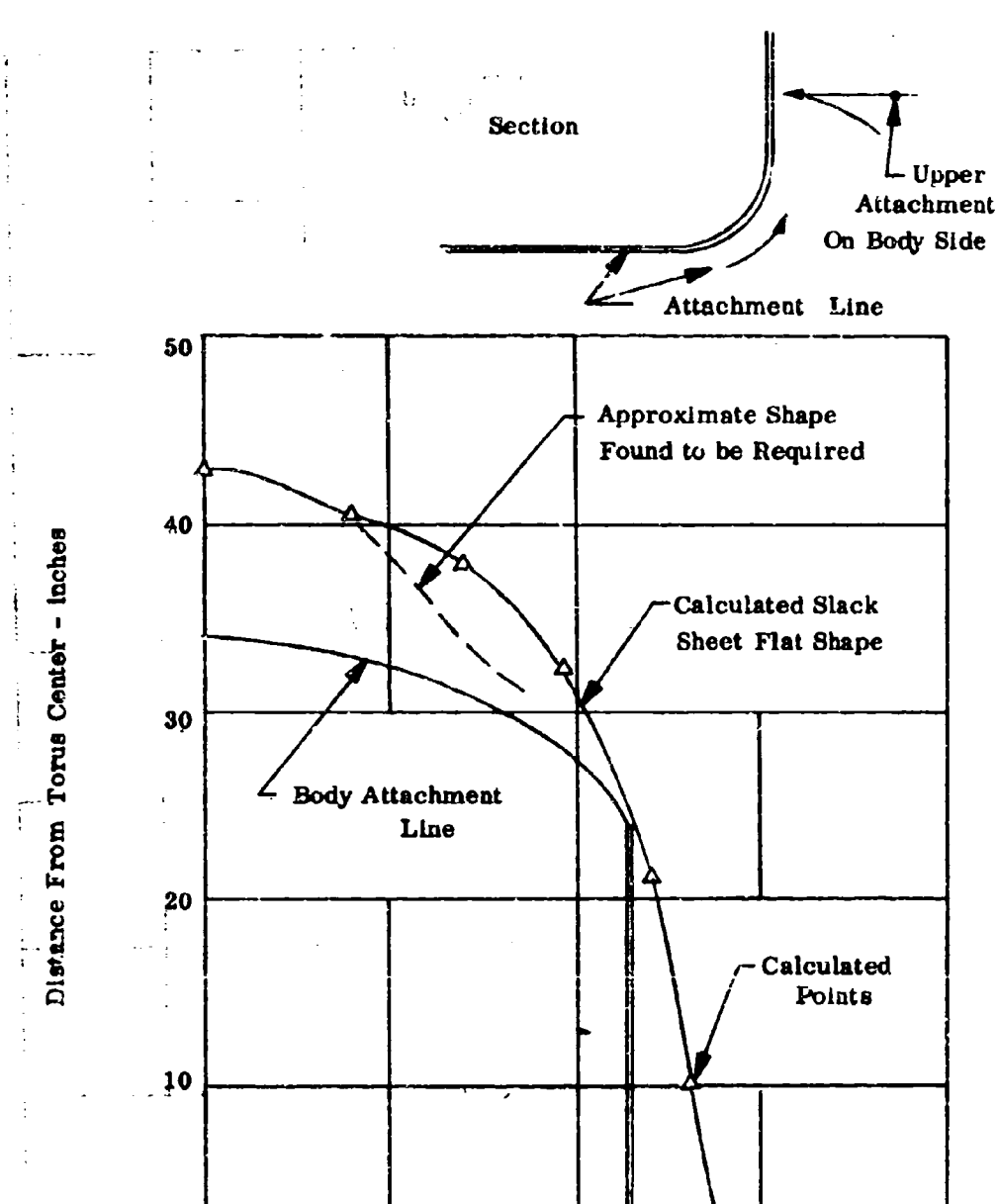

Figure 23. Calculated Flat Slack Shape

The first approximation of this method was applied to fabricate the 1/3 scale model trunk. It was found to provide excess material in the diagonal corners of the sheets as indicated on Figure 23. Further analysis including the effect of hoop tension carried along the parallel sides, which has an influence on stretch not considered here, is considered to be valuable. An accurate method of shape prediction is strongly needed. Such analysis also provides considerable understanding of the elastic retraction mechanism.

C. POWERING, AIRFLOW AND JET HEIGHT

1. General

In Air Cushion Vehicles experience it is found that the capability of a particular design employing a given trunk design is related to the "air clearance" or "jet height".

General observation of comparative vehicle behavior also indicates that cushion systems having poor basic jet height efficiency (high cushion exhaust discharge coefficient) lose performance less rapidly over rough surfaces. Such a case is the plain plenum chamber configuration. It may be said that as roughness increases so that large local irregular venting passages are formed beneath the bottom of the skirt or trunk, all configurations tend to behave like the plenum chamber.

On these grounds it is reasonable to assume that if a theoretical jet height similar to those currently in use on ACV's is provided, in this case, satisfactory performance will be achieved. The design jet height to be chosen will be the minimum at which tolerable performance to moderate speed has been achieved on ACV's - two to three inches. In the case of the air cushion landing gear the jet height will increase markedly with speed because wing lift will reduce cushion pressure upon which jet height depends strongly.

A method for calculating jet height will first be presented after which the performance of alternative configurations will be analyzed.

2. Cushion Flow and Powering at Low Jet Height

At moderate jet height, i.e., where the jet height is at least twice the annular nozzle gap it has commonly been sufficient to assume that nozzle jet velocity from which mass flow is computed is average between the inside and outside of the jet. Thus flow is given by

$$Q = \sqrt{\frac{2}{\rho} \times (P_j - \frac{P_c}{2})} \times S_N$$

Where Q is the volume flow, P_j, p_c are jet and cushion pressure and S_N is the nozzle area.

At low jet height the assumption breaks down because it is based on a constant jet width, which is not realistic. For example at zero jet height where the flow is cut off altogether and $p_c = P_j$ the above formula gives a flow

$$Q = \sqrt{\frac{2}{\rho} \times \frac{p_c}{2}} \times S_N$$

For low jet height calculations it is necessary to have a more realistic performance method. In the present analysis a simple flow model is assumed which provides a rational method of calculating flow down to the cut off point. New derivations of cushion pressure recovery as well as flow and power parameters are made. The alternative formula for cushion pressure recovery agrees exactly with the previous method at 45° jet angle, but a satisfactory approximation to flow and horsepower at low jet height is not combined with it.

A geometry which allows for the thickness of the jet escaping along the ground to be a decreasing fraction of the nozzle gap is used. This is defined and compared with the previous assumption in the two dimensional cross sections shown in Figure 24.

The following assumptions are made:

$$\frac{t}{t_o} = \frac{g}{g_o} \quad , \quad \frac{V}{V_j} = \frac{R_o}{R}$$

The ground jet has uniform velocity V_j.

From the geometry:

$$h = h_o + g \sin\theta$$

$$= R(1 + \sin\theta) + t_o - t$$

Whence, $$R = \frac{h_o + g\sin\theta - t_o + t}{1 + \sin\theta}$$

Also, $$R_o = \frac{h_o - t_o}{1 + \sin\theta}$$

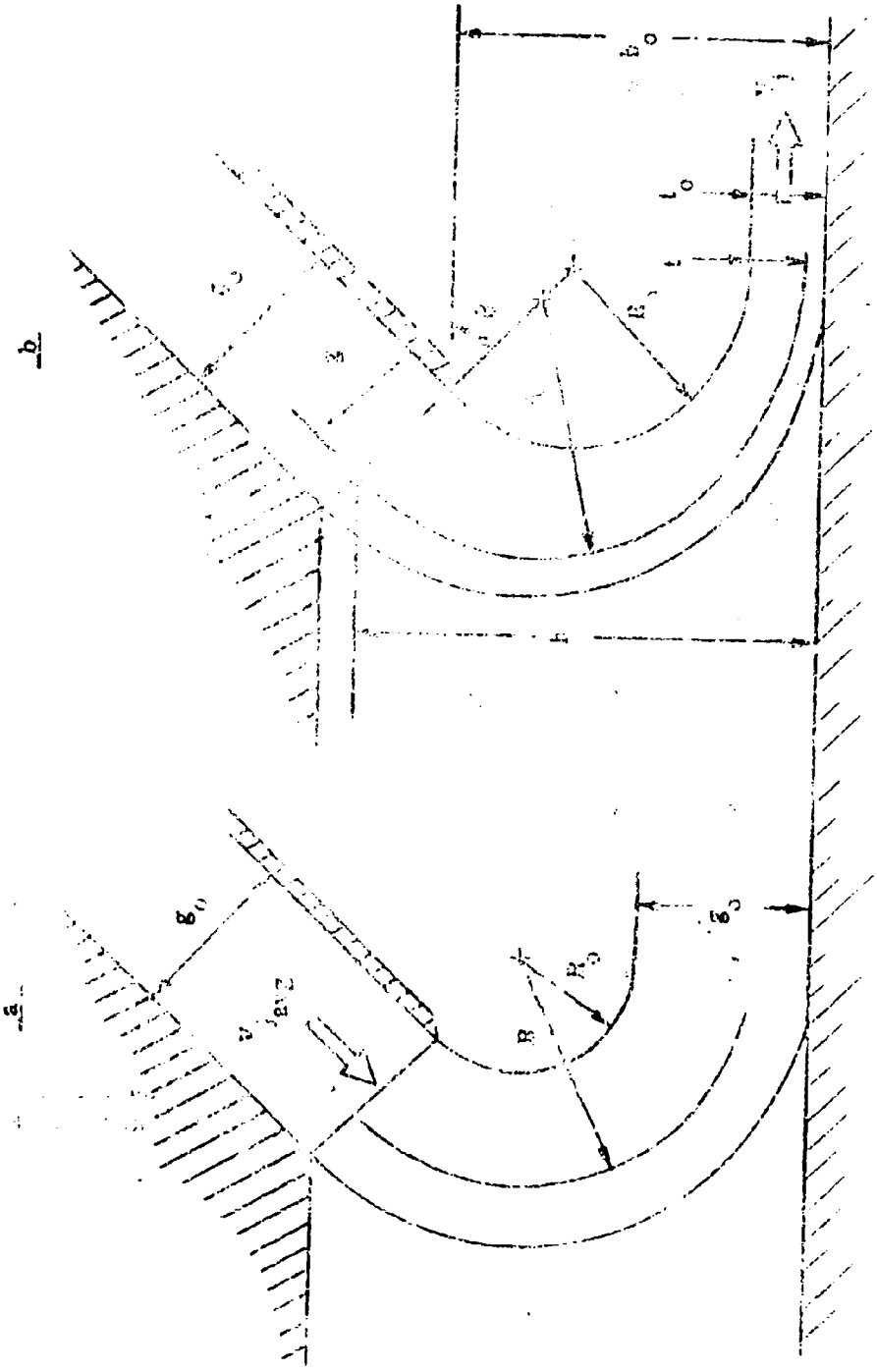

Figure 24. Alternative Jet Geometries

$$\frac{R_o}{R} = \frac{h_o - t_o}{h_o + g \sin\theta + t - t_o}$$

$$= \frac{1}{1 + g\left(\dfrac{t_o/g_o + \sin\theta}{h_o - t_o}\right)}$$

Flow Determination

From continuity

$$t_o V_j = \int_o^{g_o} V \, dg$$

$$t_o = \int_o^{g_o} \frac{V}{V_j} \, dg = \int_o^{g_o} \frac{R_o}{R} \, dg$$

$$t_o = \int_o^{g_o} \frac{dg}{1 + g\left(\dfrac{t_o/g_o + \sin\theta}{h_o - t_o}\right)}$$

$$= \frac{h_o - t_o}{t_o/g_o + \sin\theta} \log_e \left(1 + \frac{t_o + g_o \sin\theta}{h_o - t_o}\right)$$

$$\frac{t_o}{g_o} = \frac{h_o/g_o - t_o/g_o}{t_o/g_o + \sin\theta} \log_e \left(1 + \frac{t_o/g_o + \sin\theta}{h_o/g_o - t_o/}\right)$$

. . . . . (4)

This expression relates the thickness of the jet along the ground t to the nozzle width g and is solved for $\theta = 45°$ to produce the variation shown in Figure 25. Flow may now be determined from

$$Q = \sqrt{\frac{2 P_j}{\rho}} \times t_o \times c$$

(c is the perimeter)

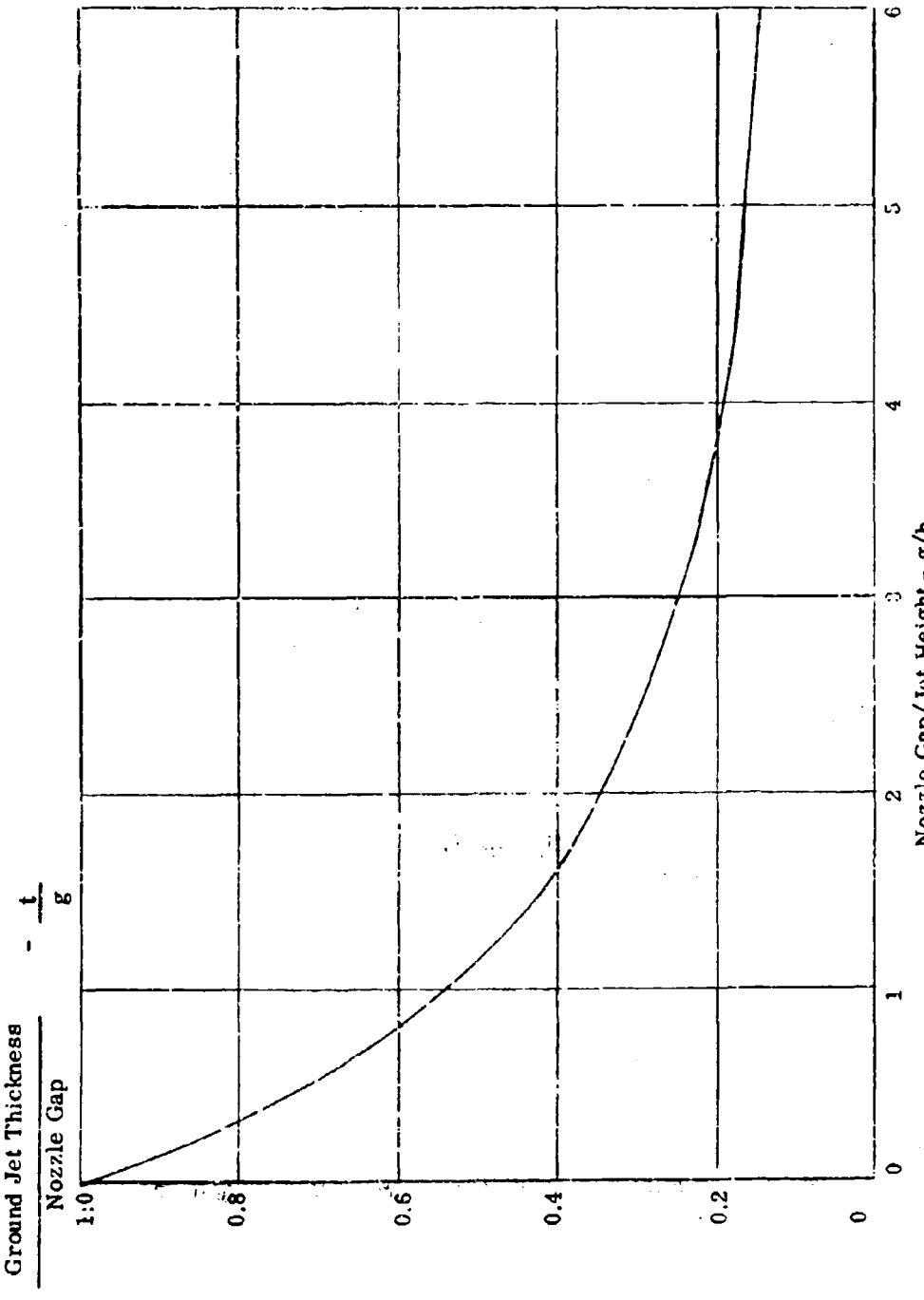

Figure 25. Variation of Ground Jet Thickness with Jet Height

Alternatively a nondimensional flow parameter may be used

$$\frac{Q}{c \times g} \times \sqrt{\frac{\rho}{2p_c}} = \frac{P_j}{p_c} \times \frac{t}{g}$$

Since p_c/P_j is a function of h/g, and t/g is given in Figure 25 the RHS of this equation is known. Using the following evaluation it is plotted versus h/g in Figure 26.

The flow curve which results from the average assumption $Q = \sqrt{\frac{2}{\rho}} \times (P_j - \frac{p_c}{2}) \times S_N$ is also shown for comparison.

Cushion Pressure Recovery

$$\frac{dp}{dg} = -\frac{\rho U^2}{R} = \frac{-2(P_j - p)}{R}$$

$$= \frac{-2(P_j - p)\ (1 + \sin\theta\ )}{h_o + g \sin\theta\ - t_o + t}$$

Whence,

$$\int_o^{p_c} \frac{1}{P_j - p}\, dp = \int_o^{g_o} \frac{-2\ (1 + \sin\theta\ )}{(h_o - t_o) + g\ (\ t_o/g_o + \sin\theta\ )}\, dg$$

$$\log_e \left(1 - \frac{p_c}{P_j}\right) = \frac{-2(1 + \sin\theta\ )}{t_o/g_o + \sin\theta}\ \log_e \left(1 + \frac{t_o + g_o \sin\theta}{h_o - t_o}\right)$$

and therefore

$$1 - \frac{p_c}{P_j} = \left(1 + \frac{t_o/g_o + \sin\theta}{h_o/g_o - t_o/g_o}\right)^{\frac{-2\ (1 + \sin\theta)}{t_o/g_o + \sin\theta}} \qquad \ldots\ldots\ldots (5)$$

which may be compared with the standard expression:

$$1 - \frac{p_c}{P_j} = e^{-2\ g/h\ (1\ +\ \sin\theta\ )}$$

and is found to give a nearly identical result for $\theta = 45°$ when the t/g relationship from Figure 25 is used. Equation (5) is also plotted for $\theta = 45°$ in Figure 26.

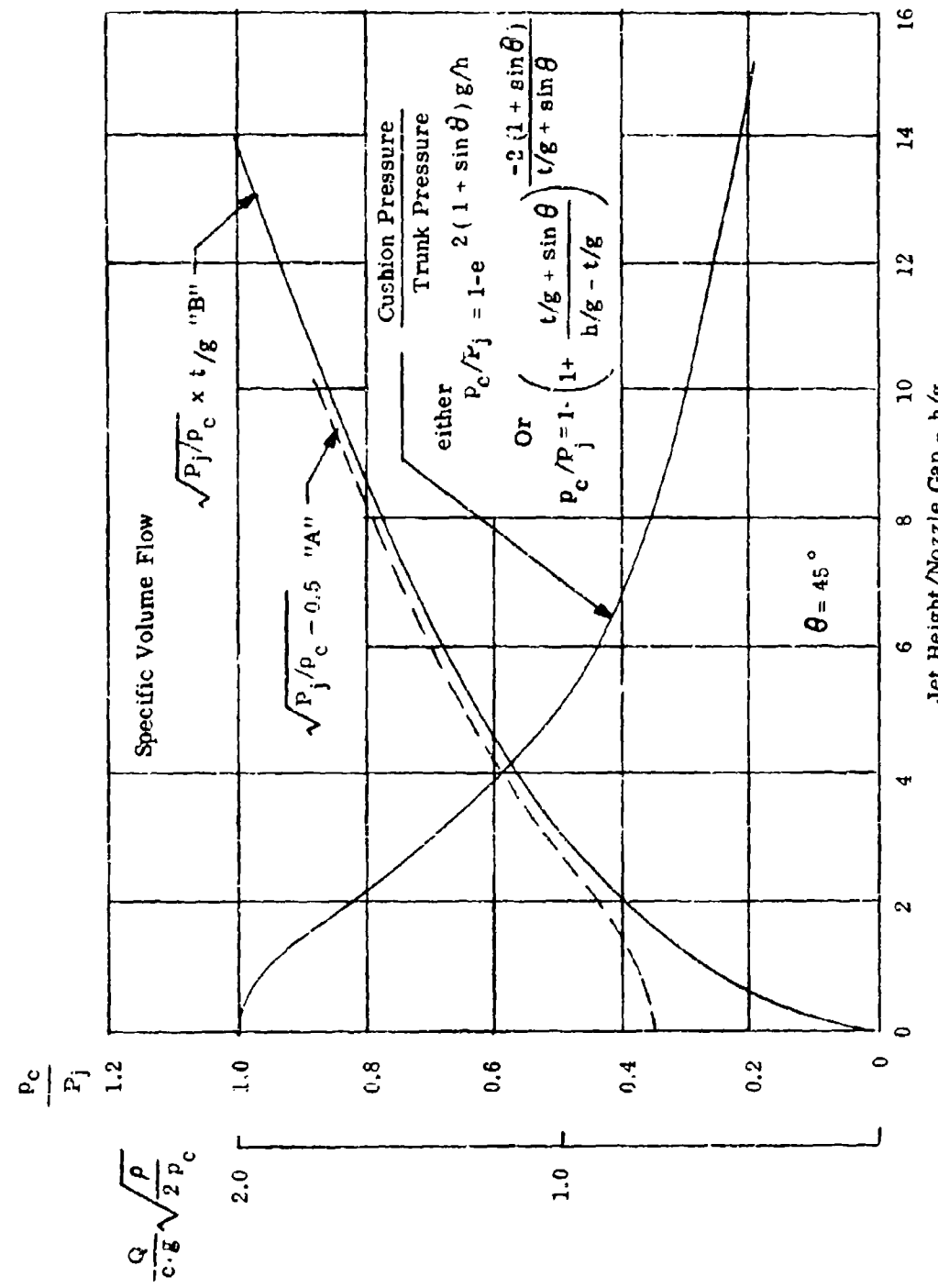

Figure 26. Variations of Pressure and Flow with Jet Height

Jet Horsepower

Neglecting compressibility, jet horsepower is given by

$$hp_j = \frac{Q \cdot P_j}{550}$$

To show the variation of power with jet height a nondimensional power parameter is used.

$$\frac{550\ hp_j}{c.g.p_c^{3/2}} \sqrt{\frac{\rho}{2}} = f\ (h/g)$$

This is plotted in Figure 27. The variation is nearly linear in the range h/g = 3 to 8. Below and above these heights more horsepower is required for an equivalent jet height. This effect is better illustrated by plotting the variation of the horsepower to jet height ratio:

$$\frac{550\ hp_j}{c.h.p_c^{3/2}} \times \sqrt{\frac{\rho}{2}} = f\ (h/g) \qquad \ldots\ldots\ldots\ (6)$$

Also since the cushion pressure ratio is the more fundamental design criterion particularly for bag trunks where the basic ratio chosen so strongly affects trunk shape, stability, energy absorption, etc., the above horsepower jet height nondimensional ratio is preferrably shown versus cushion pressure ratio as in Figure 28.

3. Basic Configuration Jet Height Analysis

For the basic configuration, the following parameters apply (See Figure 2).

W = 60,000 lb $\qquad S_c = 360.5\ ft^2$

$\qquad c = 80.8\ ft^2$

60,000 lb represents a maximum gross weight condition. A minimum test weight of approximately 47,500 pounds is feasible. The system will be designed for 60,000 pounds but to determine static performance at lighter weight and to show the effect of wing lift on jet height, this will be evaluated over the complete weight range. The design point case is treated first:

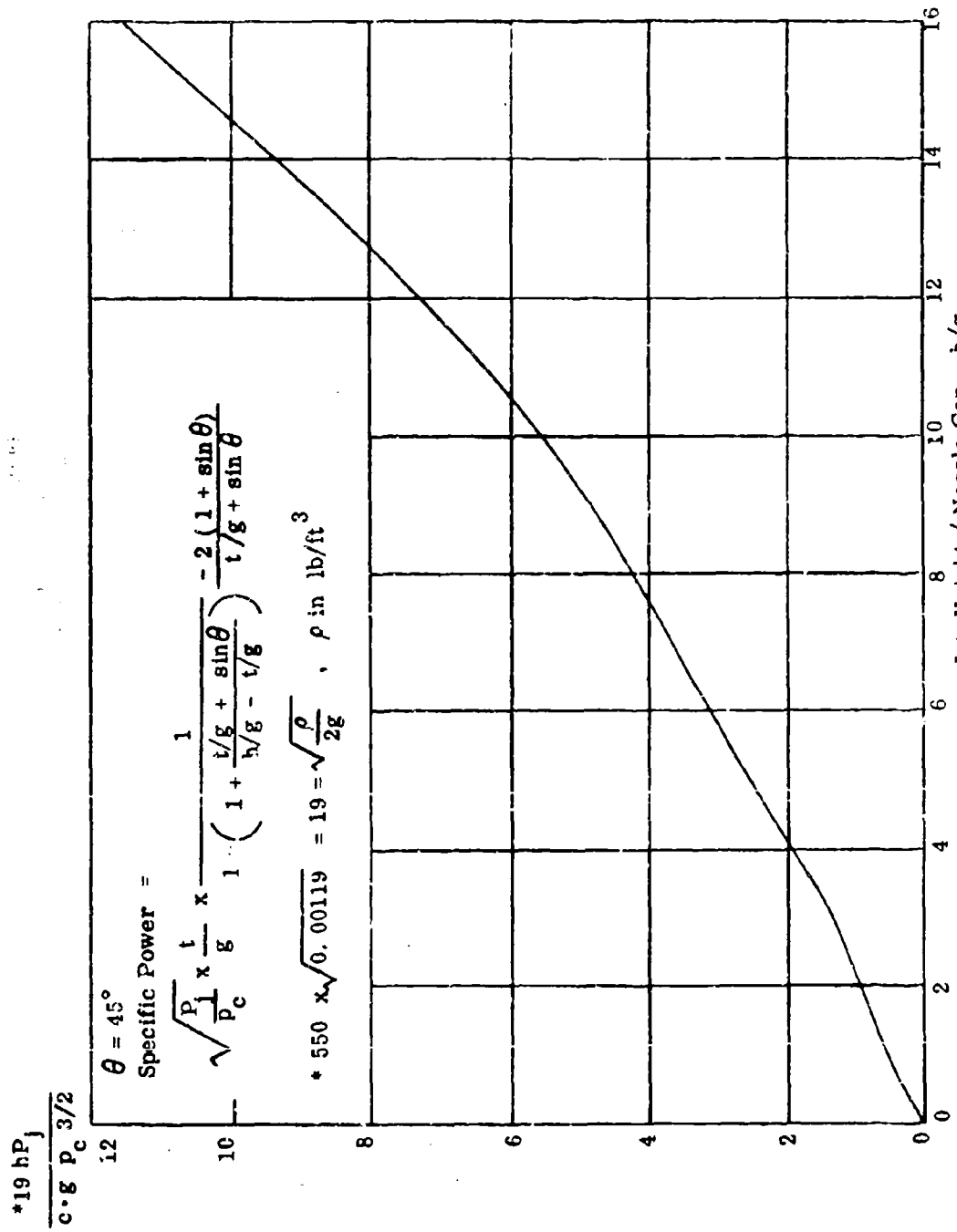

Figure 27. Variation of Horsepower with Jet Height

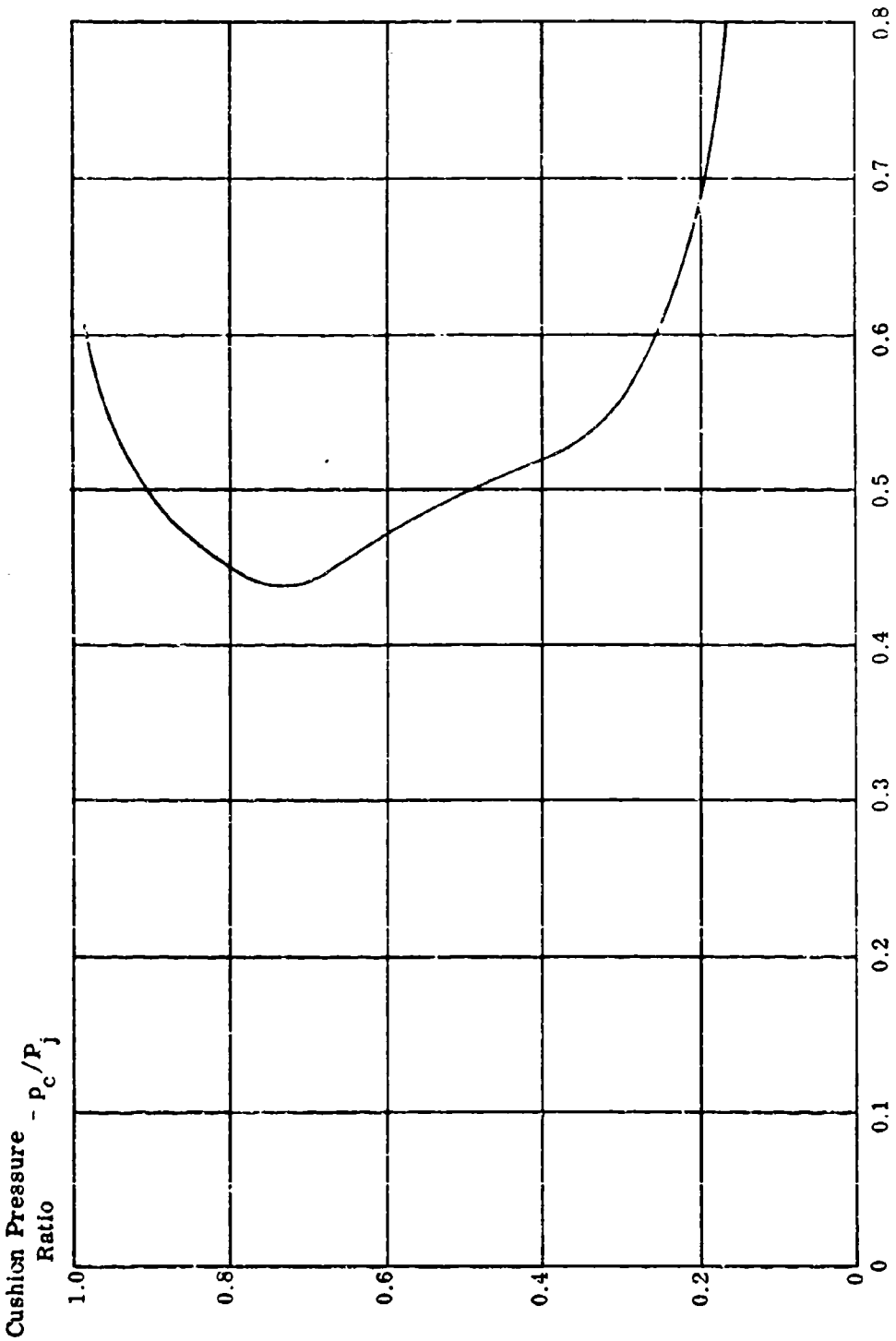

Figure 28. Variation of Horsepower/Jet Height with p_c/P_j Parameter with Cushion Pressure Ratio

p_c, lb/ft^2		166.5
p_c/P_j		0.5
P_j, lb/ft^2		333
19 $hp_j/hcp_c^{3/2}$	(Figure 28)	0.5
hp_j/h, hp/ft		4560
$(Q\sqrt{\rho/2})/(c.g.\sqrt{p_c}$	(Figure 26)	1.22
Q/g		37,200
h/g	(Figure 26)	5.0
Q/h, ft^3/sec/ft		7450

Two power units have been considered. One is based on the use of one T-67 of 1540 bhp and the other on two T-58/10 of 1400 hp each. In both cases an overall efficiency of 0.7 to convert brake horsepower is assumed. This factor accounts for fan adiabatic efficiency, fan entry and diffuser loss and trunk entry port loss.

Jet height is plotted against horsepower and flow in Figure 29. This is the theoretical annular jet daylight clearance (an alternative term) with 45° inward facing jet slot. In practice the true annular jet with 45° inward facing jet achieves about 85% jet height efficiency. The present trunk design with distributed jets is not expected to achieve more than 50% jet height efficiency. These three jet heights of interest are tabulated as follows for the two alternative power systems, together with flow and equivalent annular nozzle gap and flow area.

	One T-67	Two T-58/10
Theoretical annular h_j	2.85 in.	5.20 in.
Practical annular jet h_j	2.42 in.	4.42 in.
Estimated distributed jet h_j	1.425 in.	2.60 in.
Flow, ft^3/sec	1780	3250
Equivalent gap,	0.57 in.	1.04 in.
Net nozzle area, ft^2	3.84	7.0

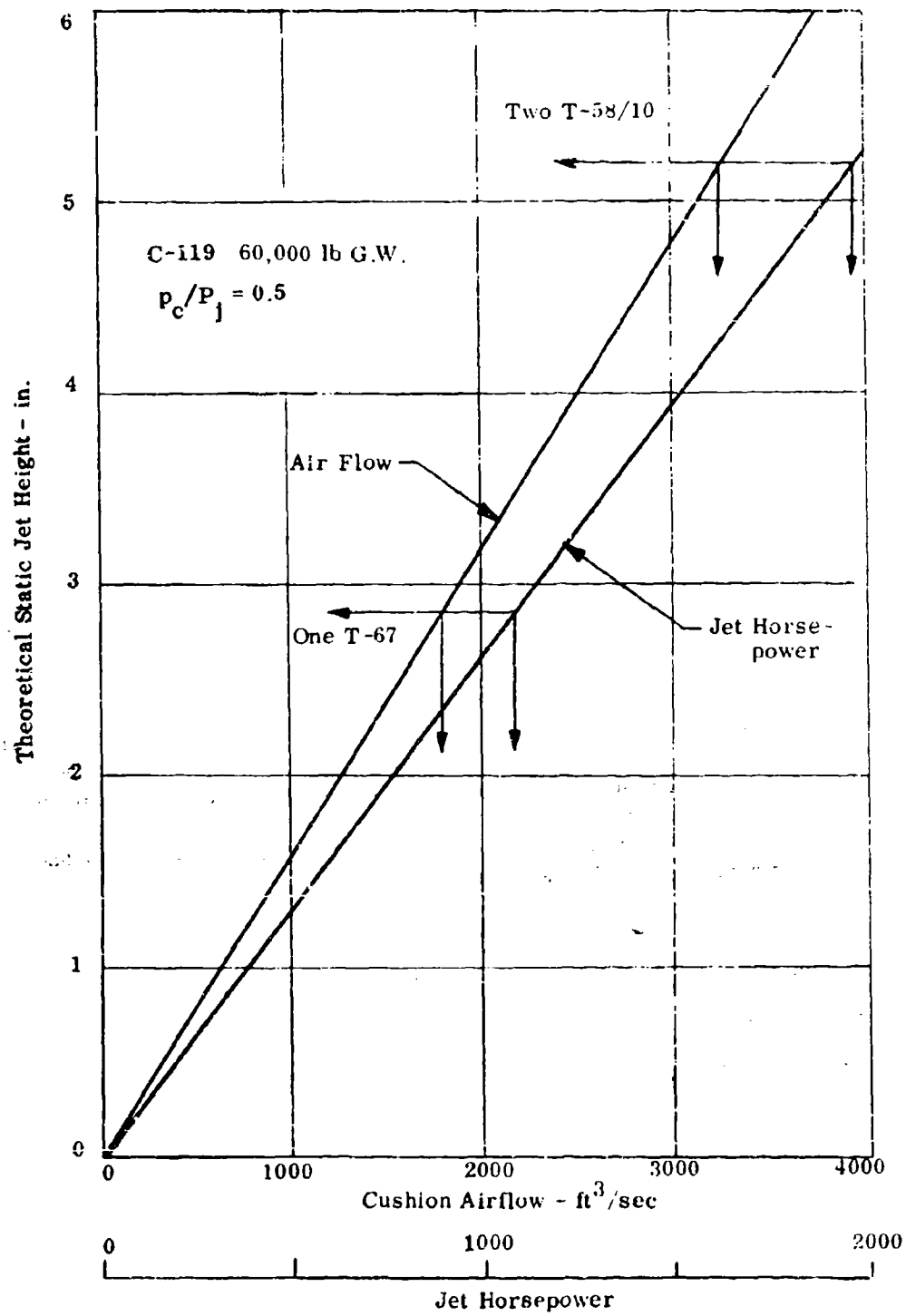

Figure 29. C-119 Horsepower, Flow and Jet Height

The practical annular jet height of 2.42 inches is considered adequate. However, for test purposes the ample power provided by the T-58 engines is attractive. It is considered that these two power systems effectively illustrate alternative possibilities. However, use of obsolescent turbines or even piston engines is not ruled out.

The variation of jet height with weight will be illustrated at the lower power level. Strictly the variation at constant engine throttle setting is required but for simplicity constant jet horsepower will be used. The reduction in cushion pressure with weight is modified by the change in bag shape which occurs as p_c/P_j changes so that iteration for cushion area is required. The bag also changes shape slightly because the material tension increases and alters the length. These are minor effects but are accounted for in the following mid-weight calculation.

W lb	30,000
W/S_c (at 60,000 lb) lb/ft^2	83
p_c, lb/ft^2	90
P_j	321
p_c/P_j	0.28
R_1/R_2	0.72
Δp_j	1,080
Q ft^3/sec	1,845
h/g	10.6

Nozzle area remains unchanged at 3.64 ft^2. Cushion area (S_c) is assumed to be reduced in proportion to the inward movement of the ground tangent at the sides. The two cross sections are compared in Figure 30. Notice that tension increase is 10% resulting in a 6% extension. (See Figure 13.) Also as jet height increases there is a slight increase in cushion flow and reduction of pressure at constant jet horsepower.

Jet height is plotted over cushion lift in Figure 31.

4. Alternate Configurations

a. Dual Cushion with Tip Floats

The purpose of the dual cushion arrangement is to increase pitch stiffness and ease takeoff rotation, the two cushions effectively performing the functions of the aircraft's main and nose gear. Since it is found from test that the single cushion has adequate stiffness and does not appear to have a rotation problem, the simpler single cushion is preferred. As is seen from Figure 8, the total cushion area is 271 + 87 -- almost the same as the basic version. Jet height performance will be very similar and requires no separate evaluation.

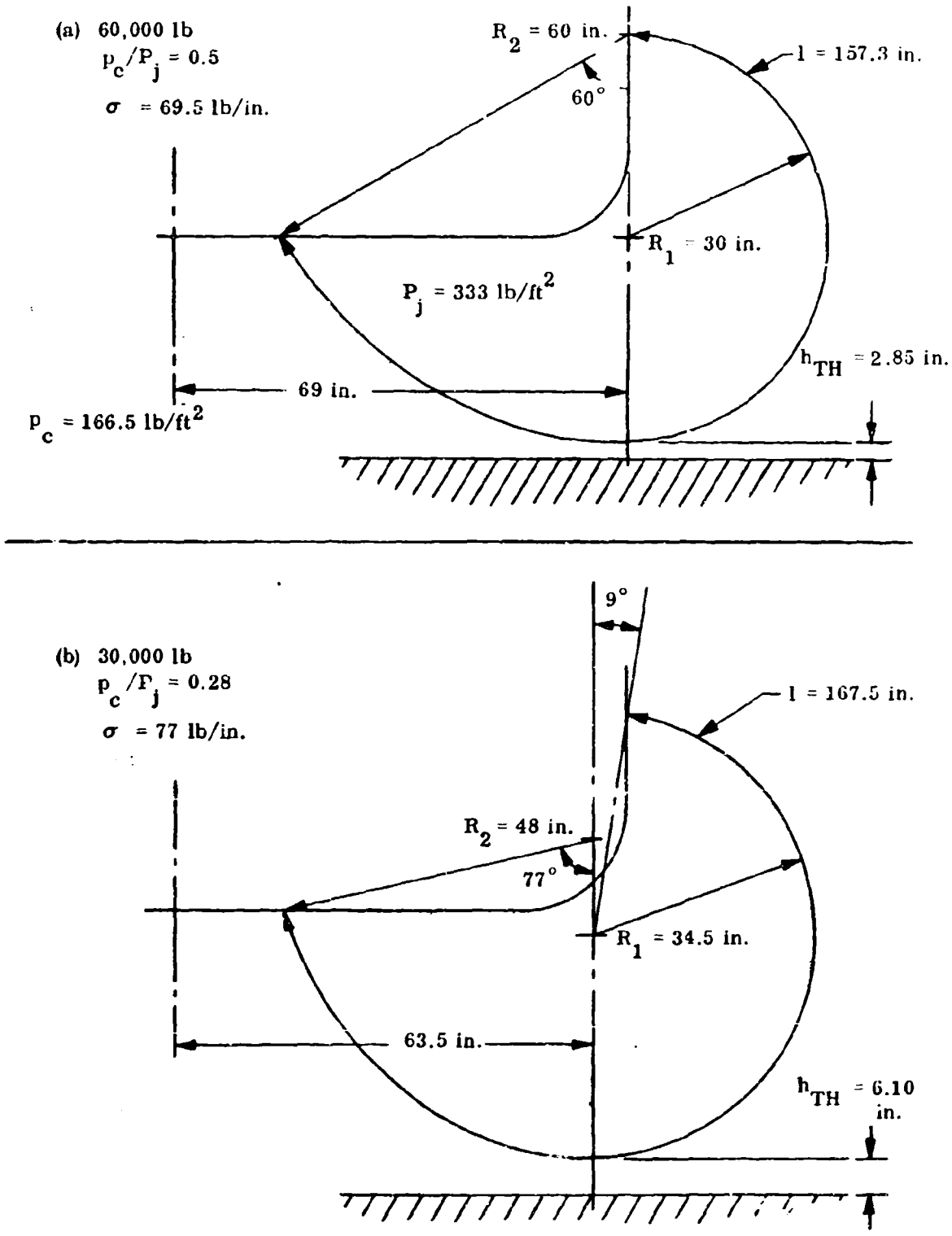

Figure 30. C-119 Basic Trunk Sections

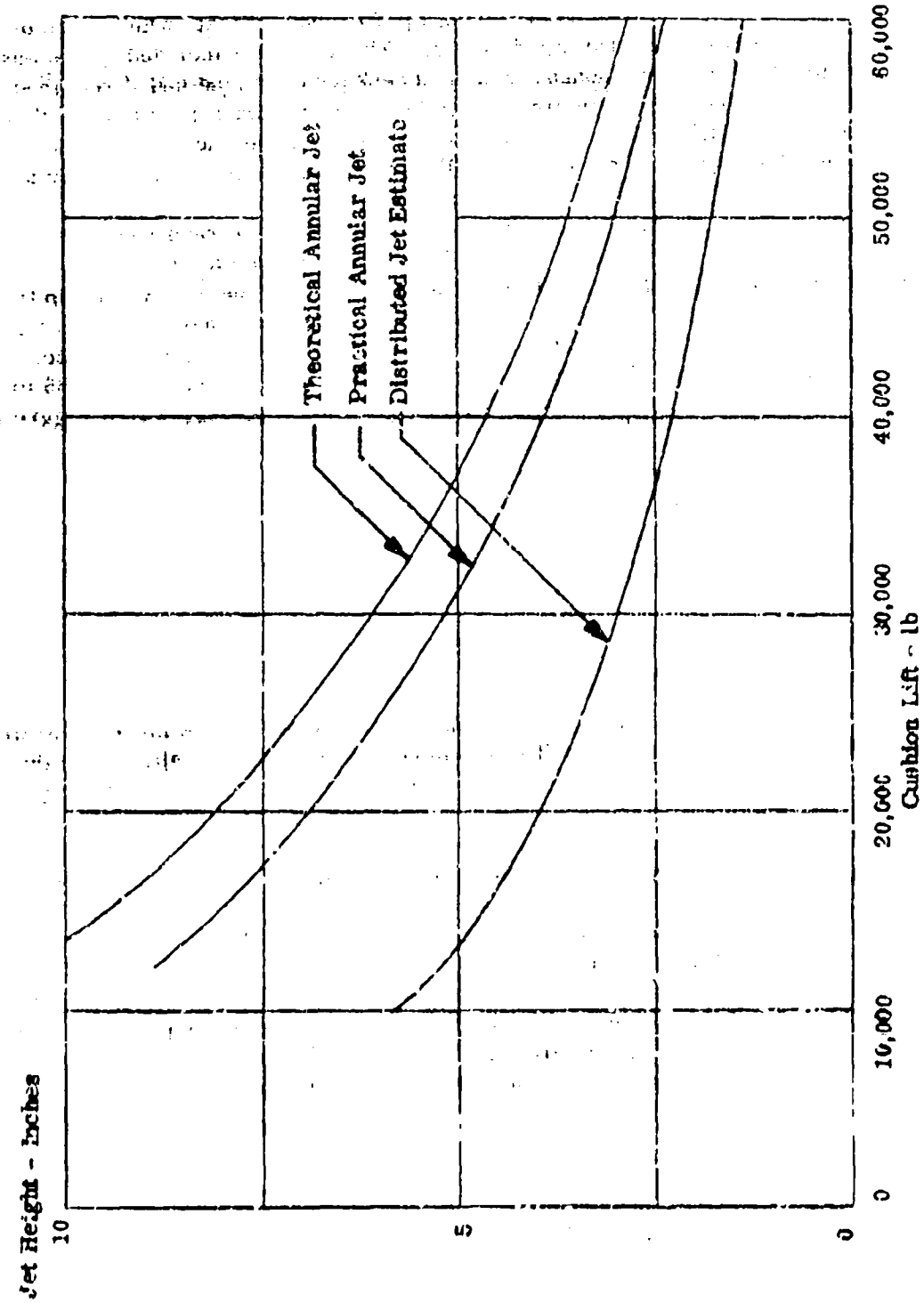

Figure 31. Variation of Jet Height With Lift

This version includes the wing tip air cushion floats which were one of the bases for the whirling arm model design. These are not included on the basic version because they are now thought to be unnecessary over land and if required for overwater do not need to be in air cushion form. If required, it is thought they should be powered to achieve the same type of performance as the main cushion at a load equivalent to a maximum side gust rolling moment. Rolling moment for a side gust is estimated subsequently(in Section II.E.1 (c.f.)), to be 42,500 lb/ft. The floats are positioned 38.8 ft from the center line. Thus, the required load = 42,500/38.8 = 1090 lb. The tip float area is 16.6 ft^2 and perimeter is 14.7 ft (Figure 8). Cushion pressure is 1090/16.6 = 65.8 lb/ft^2. In the case of the tip float there is no requirement for roll stiffness and little advantage in having high energy absorption. On the other hand a soft bag will give the best terrain performance. Since a soft bag can be used the jet height will be arbitrarily reduced from 2.85 to 2.0 inches. A p_c/P_j for optimum power to jet height can be chosen. From Figure 28 at $p_c/P_j = 0.73$

$$19\ hp_j/Lc\ p_c^{3/2} = 0.44$$

$$\frac{hp_j}{h} = \frac{0.44 \times 14.7 \times 540}{19 \times 12}$$

$$= 15.3\ hp_j/inch$$

For 2.0 inch h_j, bhp = 40.6 assuming an overall efficiency of 0.75. A higher overall efficiency is taken in this case since it is assumed the fan will be positioned in the float with an ideal diffuser. A hydraulic drive is visualized with a special pump on each main power unit.

b. Half Length Main Cushion with Nose Plenum

This configuration (Figure 9) is compared with the basic version first to find the power required for equivalent performance and jet height. The main cushion is centered at the main wheel location and for the relatively minor support required at the nose wheel location a simple plenum -- independently powered -- is used. For load distribution the forward c.g. case is considered (20% BMC, c.g. positions 1 and 3, see Reference 2 p. 178). Then taking moments about the c.g. (Figure 9).

$$L_M + L_N = 60{,}000$$

$$L_M \times 33.3 = L_N \times 272.4$$

Thus $$L_N = 0.123\ (60{,}000 - L_N)$$

$$L_N = 6850 \quad L_M = 53{,}150$$

We also have S_c = 166.3 (main)

c = 46.9 (main)

S_c = 20.8 (nose)

c = 16.2 (nose)

The same cushion trunk pressure ratio will be used.

p_{c_m} lb/ft^2 = 321

P_j lb/ft^2 = 642

hp_j/h = 6160

For the nose plenum the fan outlet pressure will be taken to be 1.20 times plenum pressure. Fan sizing will not be considered.

p_{c_N} lb/ft^2 = 314

P_F lb/ft^2 = 377

V_j ft/sec = 513 $\left(\sqrt{2\, p_c / \rho} \right)$

V_j is based on the plenum pressure. Flow is related to jet height.

$$Q = \delta_j V_j = C_D h\ c\ V_j \qquad (7)$$

Where C_D is a discharge coefficient for the air exhaust beneath the bottom of the skirt. This is a single-sided sharp edged orifice and an average value between that applicable to a three-dimensional sharp-edged orifice and 1.0 is used. The annular jet may also be considered to have an effective discharge coefficient, variable with p_c/P_j. The above equation connecting Q and C_D may be written

$$C_D = \frac{Q}{h.c.} \sqrt{\frac{\rho}{2\, p_c}}$$

From Figure 26 the function $\frac{Q}{cg} \sqrt{\frac{\rho}{2\, p_c}}$ which is plotted over h/g may be divided by h/g to obtain an equivalent discharge coefficient for the annular jet, and expressed as a function of p_c/P_j.

Figure 32 then represents a comparison of plenum chamber and annular jet on a discharge coefficient basis and it is seen that for the case in point

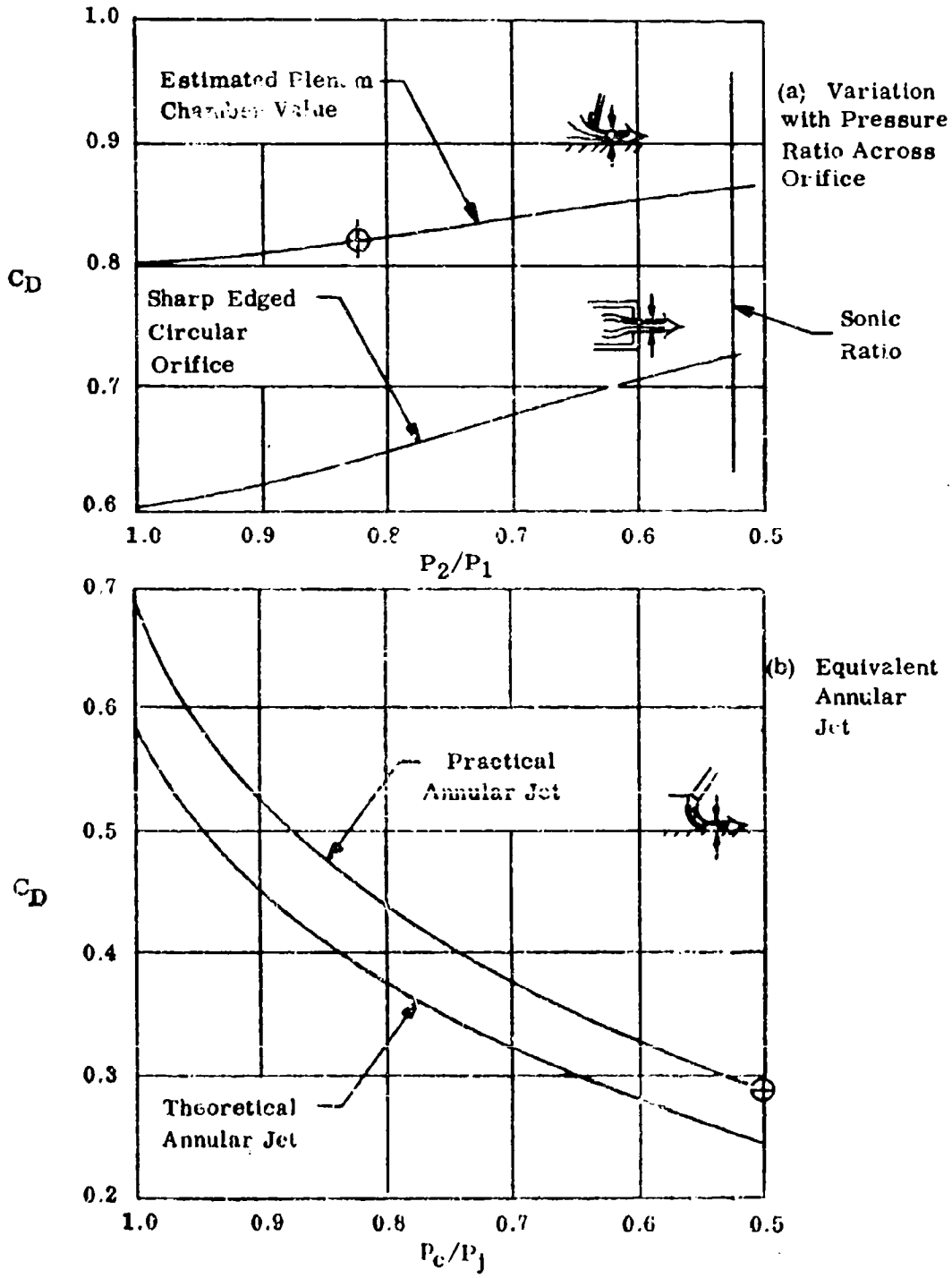

Figure 32. Coefficients of Discharge

the flexible structure ground clearance of the plenum chamber is 35% of the annular jet at the same value of flow to perimeter. However, it was pointed out earlier that over uneven surfaces the annular jet tends to deteriorate to plenum conditions. Therefore, a jet height of 35% of the annular jet will be required for the plenum, using annular jet performance as the reference datum.

Actual plenum jet height to provide equivalent performance to the basic configuration with 1540 bhp will be 0.35 x 2.85 = 1.0 in. Comparative power is calculated as follows:

$$Q_N = 0.82 \times 16.2 \times 513 \times 0.0833$$

$$= 567 \text{ ft}^3/\text{sec}$$

$$hp_N = \frac{567 \times 377}{550 \times 0.82} \quad \text{(0.82 is the assumed fan efficiency)}$$

$$= 474$$

$$hp_M = \frac{6160}{0.7} \times \frac{2.85}{12} \quad \text{(0.70 is the overall efficiency)}$$

$$= 2096$$

Total hp 2570

Thus 2/3 more power is required for the same performance with this configuration.

c. Three Plenum Chamber Configuration

The gross cushion area for this configuration is less than half that of the basic configuration. Its performance will therefore be very poor and it has no overwater capability, and other road-block disadvantages. It was included in tests from the viewpoint of basic feasibility but the jet height and powering is not considered worth detail examination.

D. POWER SYSTEM PERFORMANCE AND PRELIMINARY FAN DESIGN

1. Description of Systems

Two alternative power systems applicable to the basic configuration are shown on the inboard profile drawings D7233-099003 and D7235-099001 reproduced in this report as Figures 4 and 33. Additionally, a cushion fan flow diverter scheme designed to match the first power installation is shown in Figure 34. This is a desirable option, which is recommended for either configuration.

In Figure 34 a single T67 driving an axial flow fan is used. The fan is centered over the existing floor cut-out in the forward fuselage and the cargo drop doors removed. These are replaced with permanent structure incorporating two trunk entry ports symmetrically placed about the longitudinal centerline.. Fan air is diffused in the outlet annulus to a depth of 18 inches below the second stator, feeding into a plenum box mounted from the floor around the door cut-out. The fan unit is of welded aluminum construction. The inner shroud carrying the bearings and reduction gearbox is connected to the outer shroud through the stator blades. The unit is mounted to the floor by tubular struts. A fiberglass bellmouth and center fairing are incorporated above the fan, which draws air from within the fuselage. To allow the fan to breathe freely the rear paradrop doors will be opened when the system is in operation.

Figure 4 shows the alternative power plant using two T58/10 engines. The engines are similarly located and in this case are exampled each driving a backward curved centrifugal fan of the squirrel cage type. This configuration evidently has better reliability because of the twin engine feature. It is clear that alternative combinations are also feasible, for example, the T67 can drive a similar centrifugal blower or the T58 engines can be coupled to drive an axial fan. The choice of fan type is not critical. It is probable that the centrifugal has a somewhat milder stall characteristic and is more rugged. However, the axial fan is probably lighter and has a higher design point efficiency. In both cases the engines are mounted from the floor using typical welded strut supports which land on channels attached to existing tie-down points (of which there are many) on the cabin floor.

Engine controls and instruments are routed to the cockpit for direct operation by, and display to, the crew. An observer/engineer station is visualized, adjacent to the engine location.

For fuel an existing C-119 LR tank is used. This is designed for tie-down on the cabin floor and incorporates a booster pump. The capacity is much larger than is needed but for the test installation this is of no consequence. Use of JP2 is desirable because of its low flash point.

1. Hydraulic Brake Cylinders
2. Inlet & Ducting Assy (Cushion Air)
3. Duct Support Brackets
4. Air Cushion Trunks
6. Fan Gear Box
7. Fan Drive Shaft
8. Inlet
9. Cushion Fan
10. Stator Vanes
11. Engine Supports
12. YT 67-T-1 Continental Twin Turboshaft Engine
13. Air Jet Control Valve Selector
14. Air Cushion System Control Panel
15. Engine Exhaust
16. Air Cushion Engine Fuel Tank (C-119 LR Tank)
17. Pilots Air Cushion Control Panel

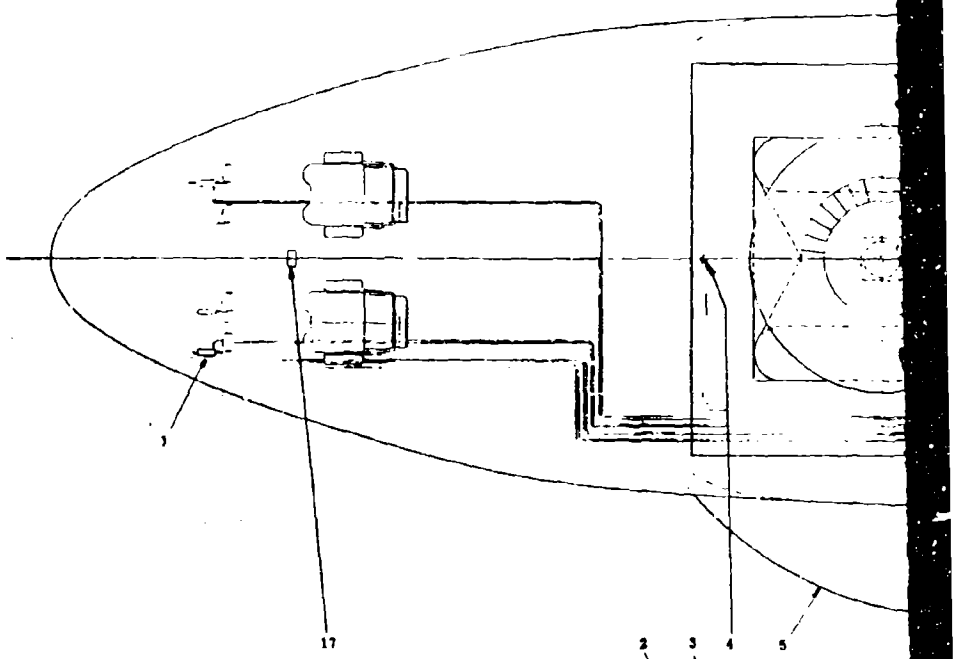

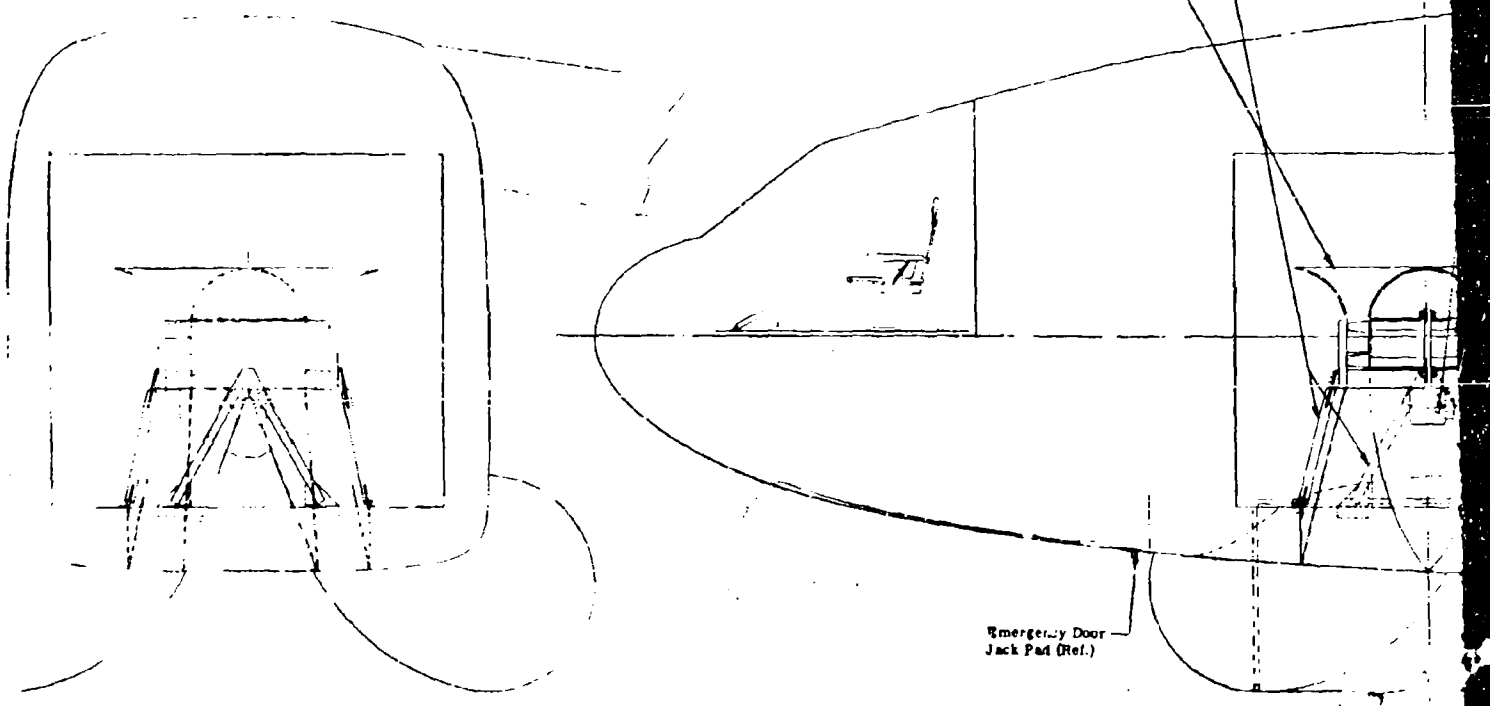

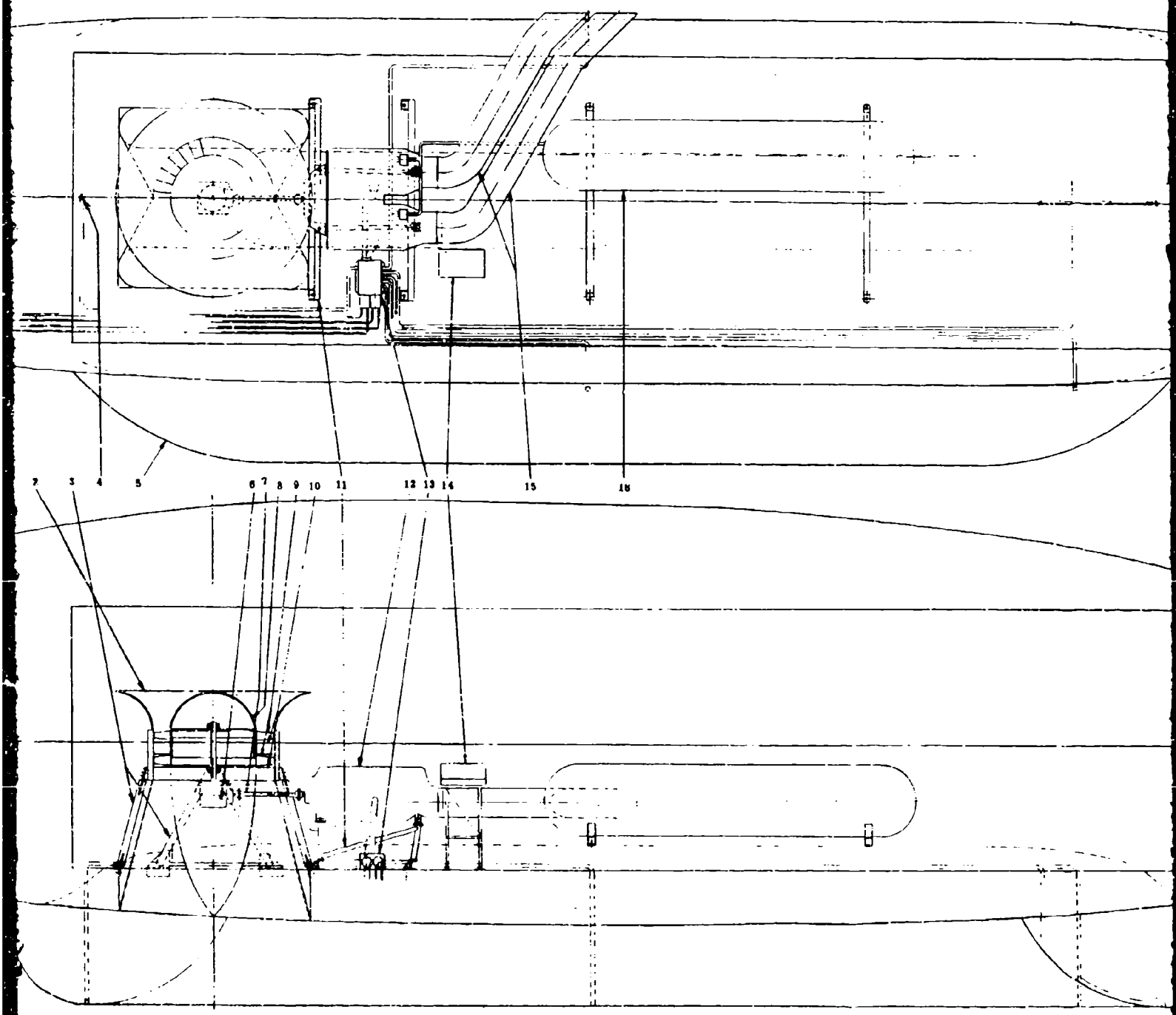

Figure 33.

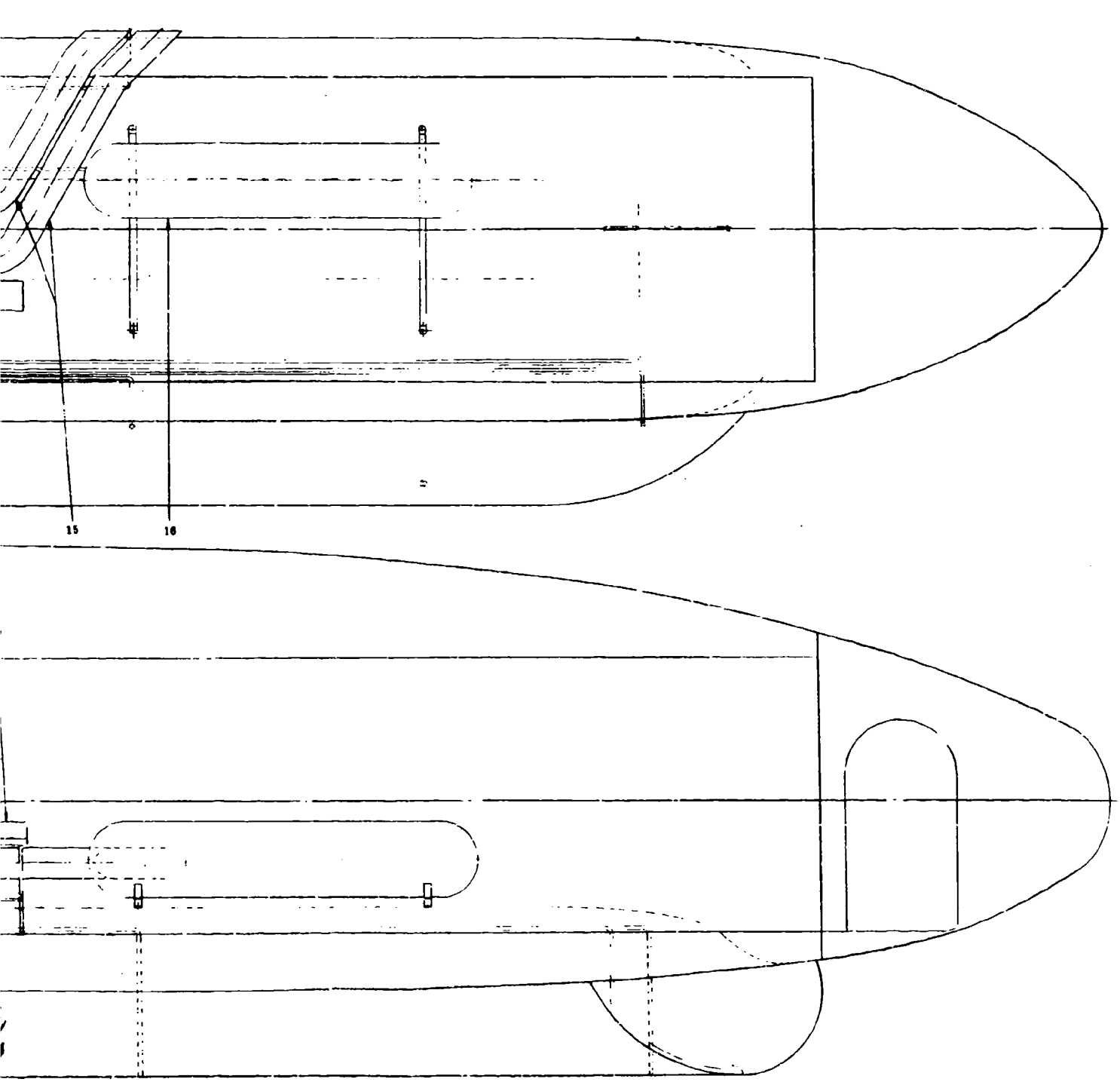

Figure 33. Inboard Profile with T-67 Engine

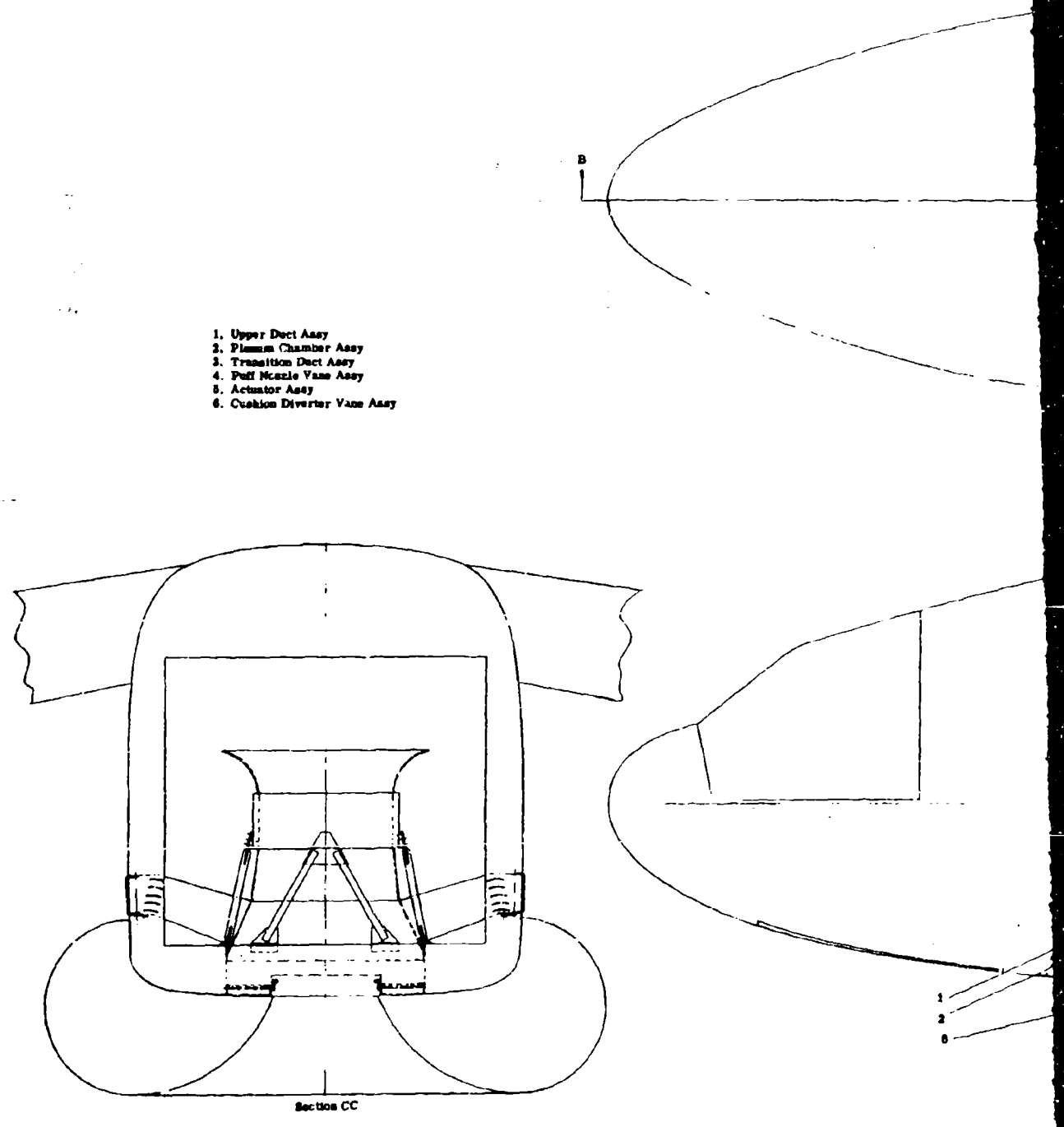

Figure 34. Cushion Fan Flow Diverter

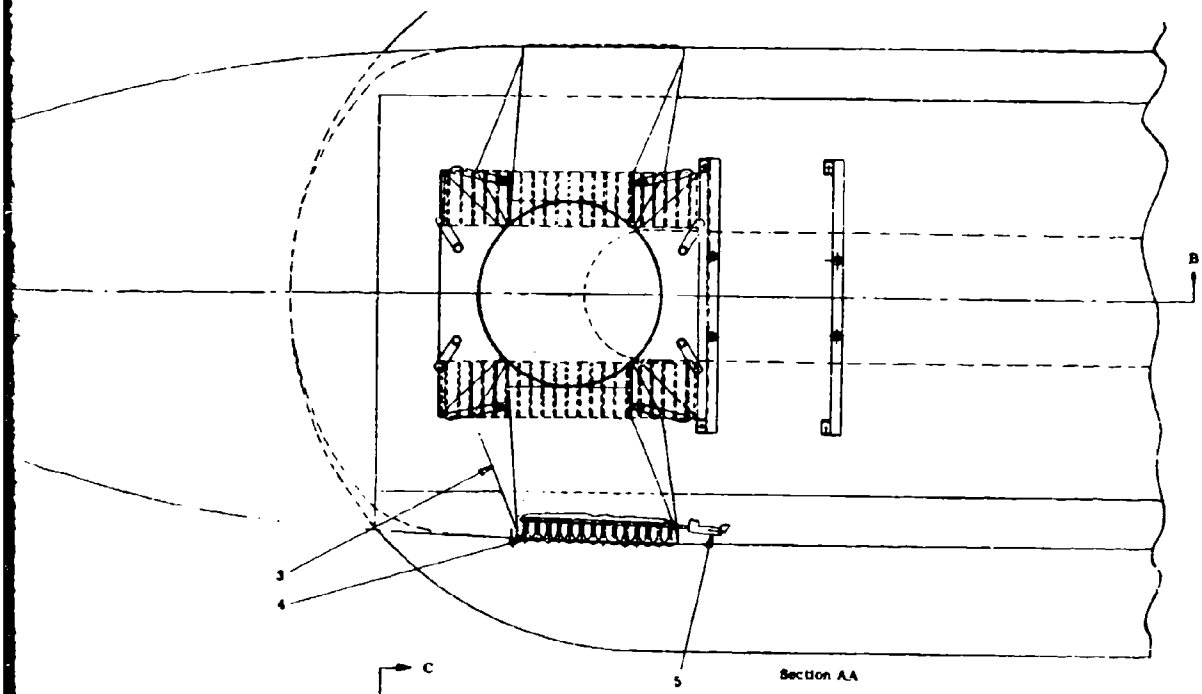

Section AA

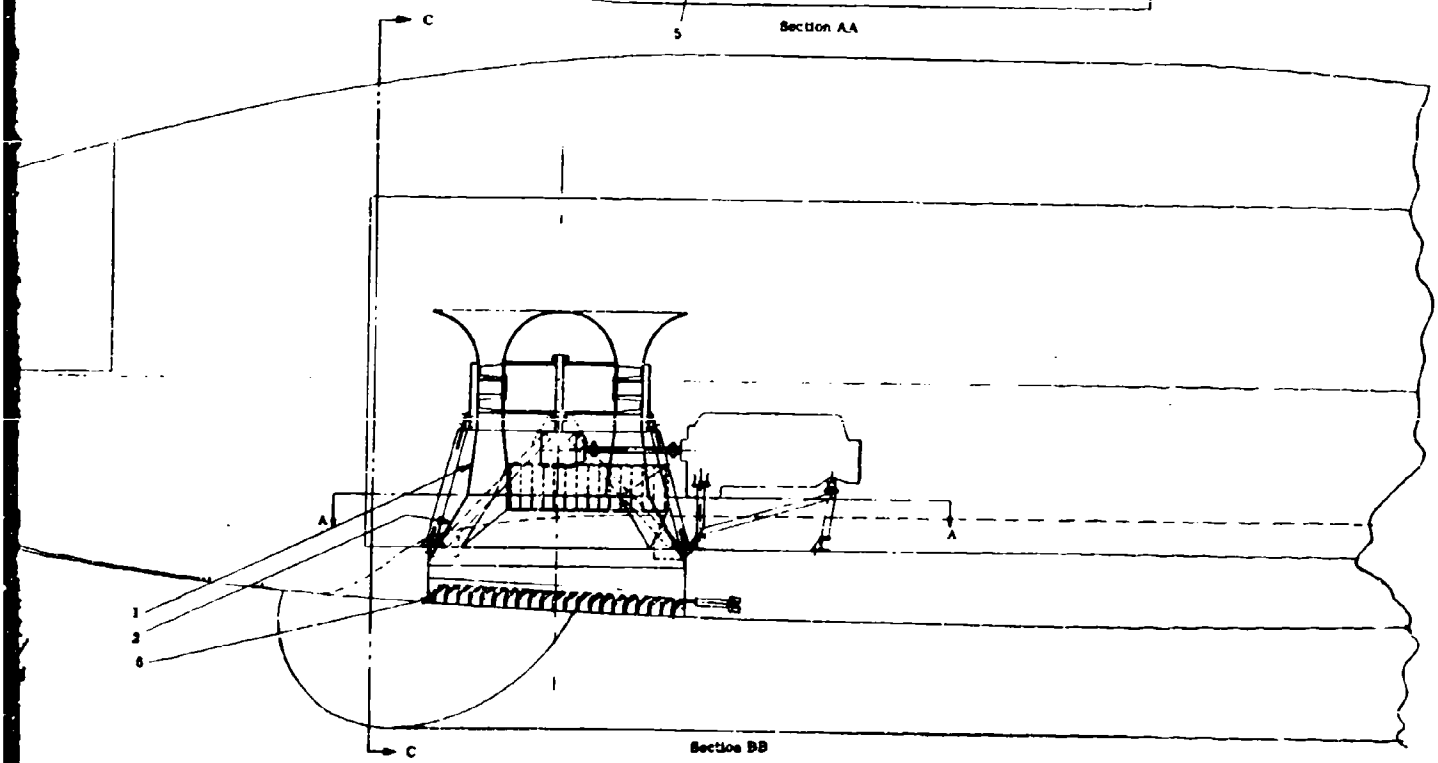

Section BB

To control the nozzle valving, auxiliary engine bleed air will be used. As drawn the layout illustrates a selector controlling pressure into six manifolds collectively or differentially. The selector is operated hydraulically in parallel with the wheel brakes by the pilot's toe pedals.

The flow diverter arrangement, Figure 34, incorporates a set of vanes in the trunk entry ports operated by a hydraulic actuator in parallel with two sets of cascade vanes in the fuselage sides to which air is ducted through tee ducts from the plenum. The diversion is accomplished in response to an inflate/deflate lever in the cockpit and provides for immediate trunk retraction and thrust boost on the initial climb. The vanes in the diverter exit also provide additional reverse thrust, braking and yaw control at low speeds as further described in Section II.5.

2. Preliminary Fan Design

a. Axial Flow Fan

(1) Fan Sizing

The design point flow and pressure are taken as the one g static case at maximum gross weight as follows.

Q = 1780 ft^3/sec (4.24 slug/sec)
bhp = 1540 (1570 - 2% transmission loss)

In the previous subsection on jet height, horsepower was considered to be given by volume flow Q multiplied by total pressure P (psig). This neglects compressibility which is a minor correction but will be accounted for in fan design.

$$\text{Fan work input} = mg\,J c_p \Delta T, \tag{8}$$

Where m is the mass flow and ΔT is the fan temperature rise, related to the pressure rise by

$$P_2/P_1 = \left(1 + \eta \frac{\Delta T}{T_1}\right)^{\frac{\gamma}{\gamma-1}} \tag{9}$$

η being the fan adiabatic efficiency and T_1 the inlet total temperature.

From (8) with 1540 bhp

$$\Delta T = \frac{1540 \times 550}{4.24 \times 32.2 \times 778 \times 0.2401} = 33.2^\circ F$$

From (9) assuming a fan efficiency of 0.85 and a 60°F day, $\gamma = 1.4$

$$\frac{P_2}{P_1} = \left(1 + \frac{0.85 \times 33.2}{519}\right)^{3.5} = 1.204$$

he area of the paradrop doors is approximately 36 ft^2. An inlet depression equal to the dynamic head of the air at the velocity induced through 80% of this area will be assumed.

$$\frac{1780}{36 \times 0.8} = 62.2 \text{ ft/sec}$$

$$0.00119 \times 62.2^2 = 4.6 \text{ lb/ft}^2 \quad (0.00119 = \rho/2)$$

In sea level standard conditions therefore $P_1 = 2111$ lb/ft^2. Hence ΔP, the fan pressure rise:

$$\Delta P = 0.204 \times 2111 = 430^* \text{ lb/ft}^2$$

A fan having a mild stall and good cutoff characteristics is required. These will be obtained with high hub/tip ratio and using flat impulse type blading. A hub/tip ratio of 0.70 will be used, and a tip air inlet angle $\beta = 25°$.

It is also desirable for the design point to lie well to the high flow side of the maximum efficiency point so that when flow is cut down or cut off the fan will transiently respond with much higher pressure, as in a hard landing. This implies lightly loaded blades and high solidity.

Finally, it is an object to keep the fan outlet velocity low to minimize system loss particularly because the air is discharged through the trunk entry port with complete loss of dynamic head.

(*) For comparison if the fan pressure rise is calculated by dividing the work output by the volume flow,

$$\Delta P = \frac{1540 \times 550 \times 0.85}{1780} = 405 \text{ lb/ft}^2$$

The required pressure ratio of 1.204 is commonly achieved by a single stage in axial flow compressors. However, this requires high tip speed and through flow velocity. For this reason and considering the other desirable characteristics a two stage design is preferred. The pressure rise per stage is then 215 lb/ft^2.

Rotational speed will be set by choosing a pressure rise coefficient (ψ) of 0.80 at the blade root:

$$1/2 \ \rho \ U_R^2 = 215/0.80 \ lb/ft^2$$

$$U_R = 475 \text{ and } U_T = 679 \text{ ft/sec}$$

$$V_a = U_T \times \tan \beta = 679 \tan 25^\circ = 317 \text{ ft/sec}$$

$$\text{Annulus area} = 1780/317 = 5.62 \text{ ft}^2$$

$$\text{Therefore tip diameter} = 45.0 \text{ in.}$$

$$\text{and root diameter} = 31.5 \text{ in.}$$

(2) Gearing

Engine output rpm is 6600. Fan rpm is found to be

$$N = \frac{675 \times 60 \times 12}{\pi \times 45} = 3440$$

The required reduction ratio is 1.92:10. However, for simplicity a ratio of 2:1 can probably be used with minor adjustment of the design.

(3) Fan blading

$$\Delta P/\text{stage} = \rho \ U \ \Delta V_u = 215 \ lb/ft^2$$

$$U \ \Delta V_u = 90{,}200 \ ft^2/sec^2$$

	Root	Tip
Diameter, ft	2.625	3.75
V_a, ft/sec	317	317
U, ft/sec	475	679
ΔV_u, ft/sec	190	133
$U - \Delta V_u/2$, ft/sec	380	612.5
$\tan \beta$ mean $= (U - \Delta V_u/2)/V_a$	1.20	1.93

	Root	Tip
β mean	50° 12'	62° 36'
$\cos\beta$ mean	0.640	0.460
$V_{mean} = V_a/\cos\beta$ mean	495	689
$C_L\sigma = 2\Delta V_u/V_m$	0.768	0.386
σ	1.5	1.0
C_L	0.512	0.386
Circumference, ft	8.25	11.8
cn $= \sigma\pi D$	12.38	11.8
Chord c, ft	0.425	0.407
No. of blades,	29	29

Reference 3 presents complete data on the lift characteristics of a suitable airfoil in cascade. This data is used to determine a choice of camber and angle of attack which will give the required C_L with adequate margin from the stall. See the reference for the following:

Deflection angle θ	$14\frac{0}{19}$° 18'	$5\frac{0}{7}$° 10'
Aerofoil	65 - 810	65 - 810
Camber (% chord)	8%	4%
Angle of Attack	10° 40'	4° 30'

The first stage triangles and blading can now be drawn (Figure 35).

The second stage will be very similar, probably using identical blades and does not require detail analysis for the present purpose. The estimated characteristic is shown in Figure 36.

b. Centrifugal Fans

The centrifugal fans are doubled sided and of the type in which the case width is greater than that of the wheel. Size is determined by scaling an existing design. Design point flow and pressure are.

$Q = 3225\ ft^3/sec = 7.74\ slug/sec$

$P = 430\ lb/ft^2$

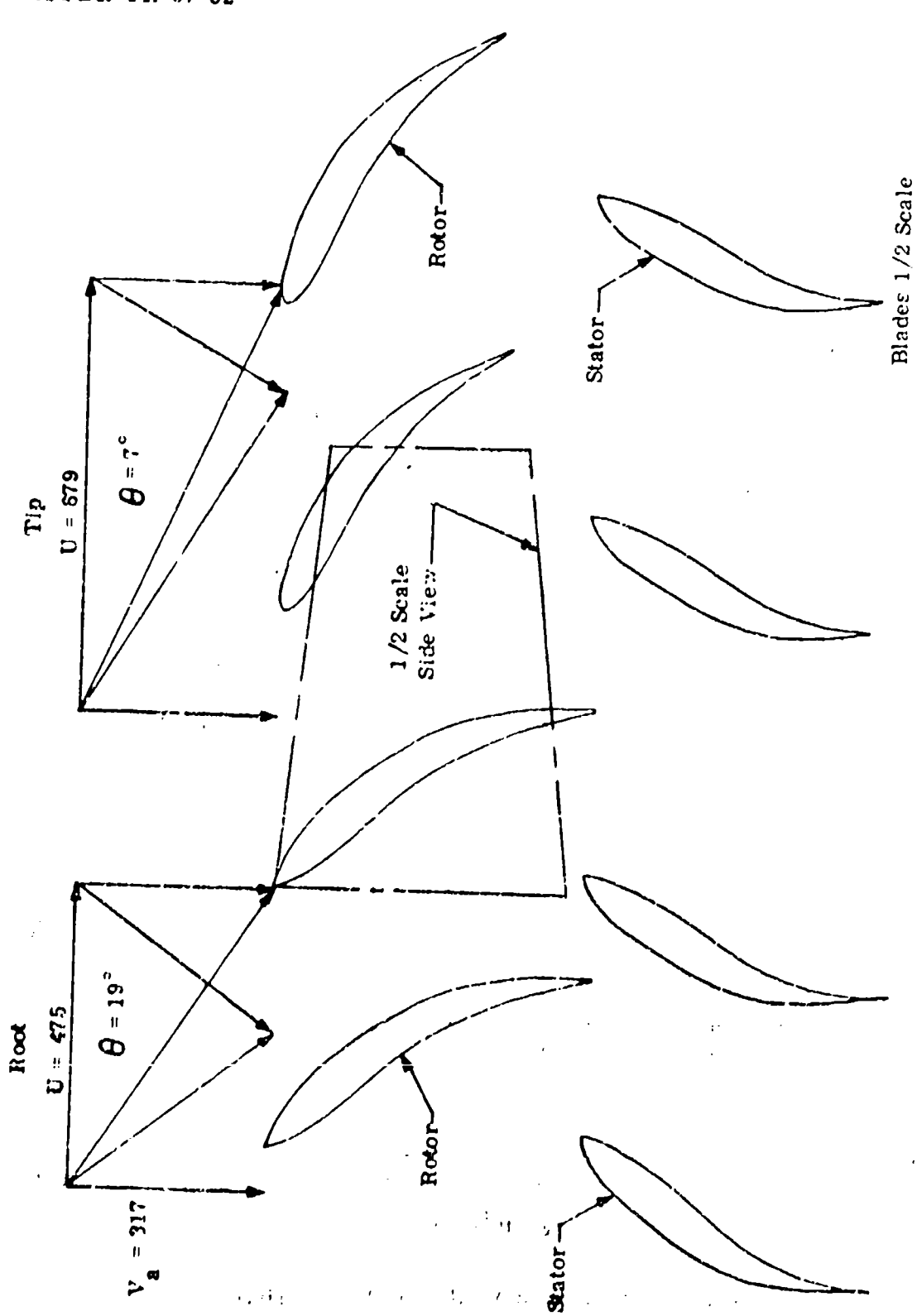

Figure 35. First Stage Blading: Axial Fans

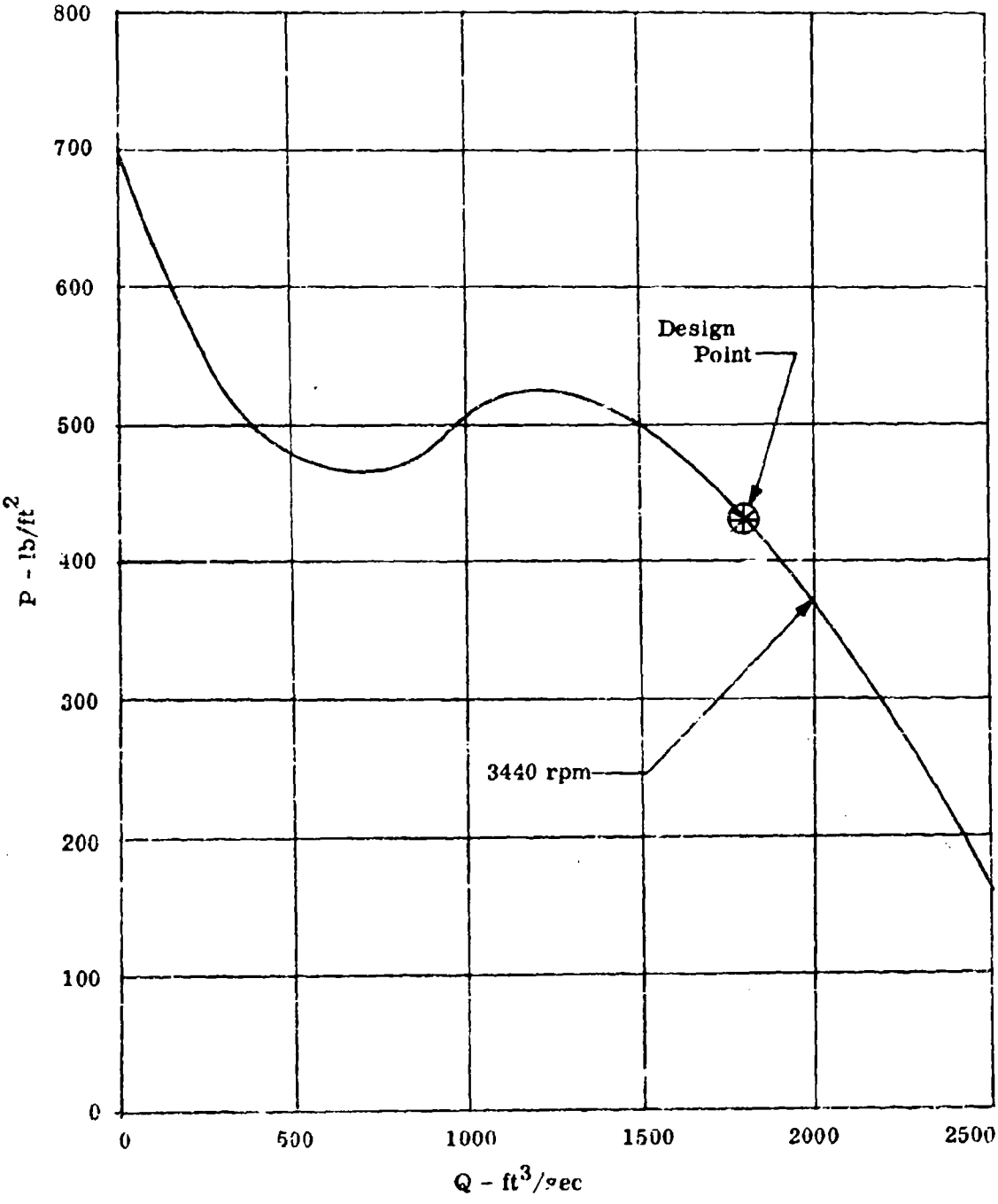

Figure 36. Estimated Axial Fan Characteristic

Essential characteristics of the known design are

$Q = 4000\ ft^3/min$
$P = 6$ in. water head
$rpm = 5000$

Where diameter = 10 inches

A twin fan installation is proposed

$$Q/fan = \frac{3225}{2} \times 60 = 97{,}000\ ft^3/min$$

$$P = 430/5.2 = 82.8 \text{ in. water}$$

For scaling:

At constant rpm: $Q \propto D^3$
$P \propto D^2$

At given size: $Q \propto rpm$
$P \propto rpm^2$

Using suffix 0 for known conditions:

$$\frac{Q}{Q_o} = \left(\frac{D}{D_o}\right)^3 \times \frac{rpm}{rpm_o} \; ; \; \frac{P}{P_o} = \left(\frac{D}{D_o}\right)^2 \left(\frac{rpm}{rpm_o}\right)^2$$

$$\frac{Q}{Q_o} = \frac{97000}{4000} = 24.2 \qquad \frac{P}{P_o} = \frac{82.8}{6} = 13.8$$

$$\frac{rpm}{rpm_o} = \sqrt{\frac{P}{P_o}} \times \frac{D_o}{D} = 3.72\ \frac{D_o}{D}$$

$$\left(\frac{D}{D_o}\right)^3 \times \frac{D_o}{D} \times 3.72 = 24.2$$

$$\frac{D}{D_o} = 2.54; \qquad \frac{rpm}{rpm_o} = 1.46$$

Hence a 25.4 inch wheel is required rotating at 7350 rpm. This implies a tip speed of 810 ft/sec, which is very high for a squirrel cage wheel and may introduce difficult structural design problems. In the alternative design of the axial fan no such problems are anticipated

3. Pressure Loss

Pressure loss upstream of the fan is estimated at 5 lb/ft^2 (page 58).

The axial fan annulus hydraulic diameter is 2.7 ft, and the distance from fan outlet vertically downward to the end of the diffuser is 1.5 ft. The flow diffuses at a maximum effective angle of 14° so that the hydraulic diameter at diffuser exit is 3.07 ft and the area is 7.4 ft^2. The loss will be the dynamic head at this point which is 69 lb/ft^2. The area of the trunk entry ports is 6.75 ft^2 each and the dynamic head at this point will also be lost, a further 21 lb/ft^2. Summarizing,

Inlet	5.0
Plenum	69.0
Trunk Entry	21.0
Total	95.0

Thus the trunk pressure is 335 lb/ft^2 approximately corresponding to the 0.7 overall efficiency assumed in the preceding work. In practice it is found that for systems of this type (e.g. in ACVs) this efficiency is seldom bettered.

Similar considerations apply to the alternative power system for which the same overall efficiency has been assumed.

4. Diverter Thrust

Exhaust area equivalent to the trunk nozzle area is provided, in order to keep the fan operating at its design point. Total head at the diverter nozzle will evidently be 356 lb/ft^2 since there is no trunk entry port loss. The flow exhausts through port and starboard louvers at 30° to the fuselage side. Net thrust, both forward and reverse is calculated as a function of speed as follows:

V ft/sec	0	100	200
T67 Engines			
Q = 1780 ft^3/sec			
m V_j cos 30°, lb	2050	2050	2050
m V_j, lb	0	424	848
Net forward thrust, lb	2050	1626	1202
Net Reverse thrust, lb	2050	2474	2898
T58 Engines			
Q = 3225 ft^3/sec			
m V_j cos 30°, lb	4200	4200	4200
m V_j, lb	0	770	1640
Net forward thrust, lb	4200	3430	2060
Net Reverse thrust, lb	4200	4970	5740

These forward and reverse thrusts are plotted in Figure 37.

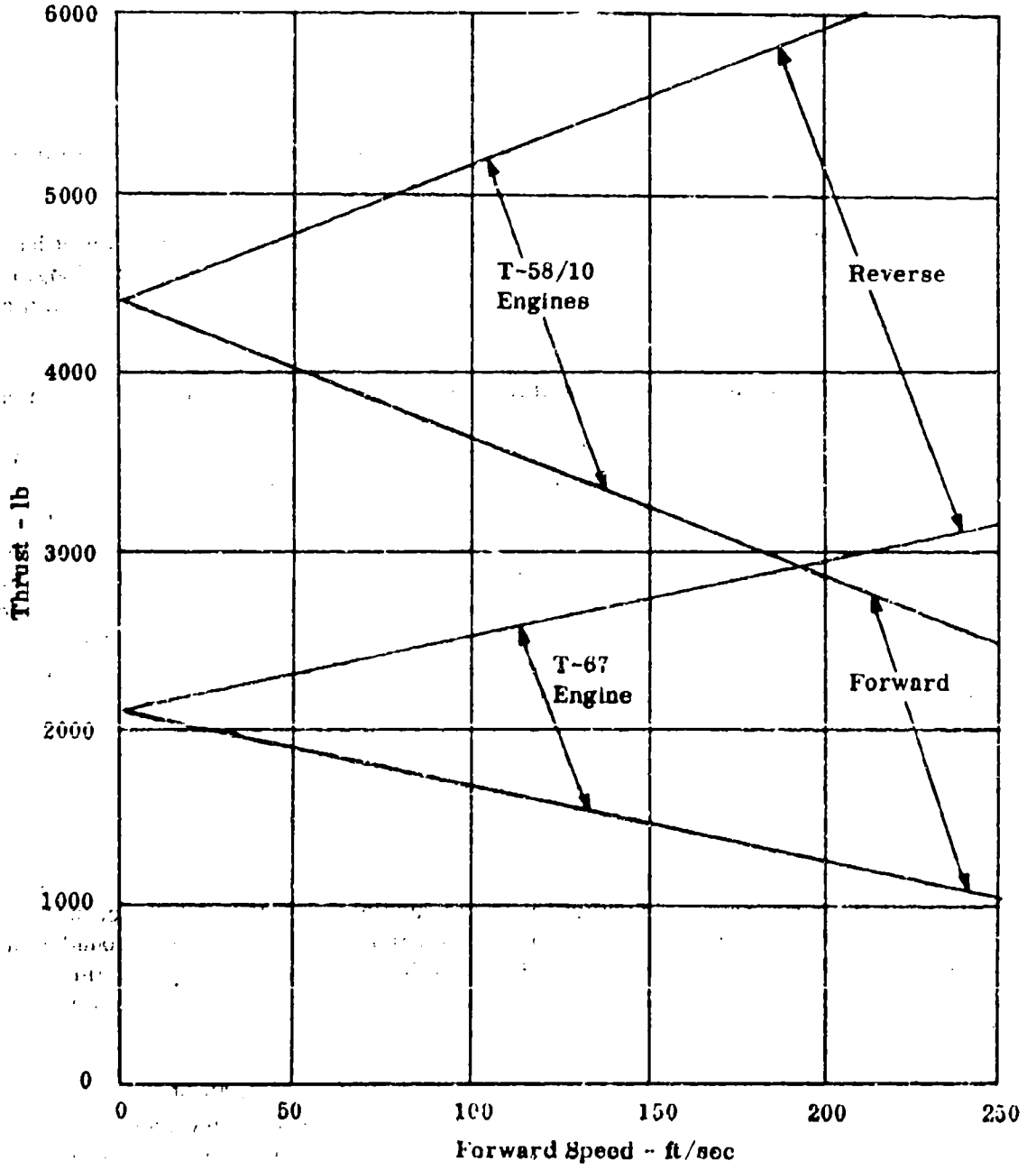

Figure 37. Diverter Thrusts

E. CUSHION STABILITY AND CONTROL

1. Static Stiffness

a. General

The bag trunk with distributed jets as designed for theC-119 exhibits very good pitch and roll stiffness and strong heave stability.

In ACV's, including ACV's with bag trunks and annular nozzles it has been the practice to incorporate static stability jets, usually in the form of a longitudinal keel trunk, with or without jet flow from its base and a similar lateral trunk, the two forming a cross beneath the vehicle.

The purpose of these stability trunks is to inhibit the cross flow which is easily seen to create an unstable condition (Figure 38, a, b). Clearly as soon as the trunk flattens against the ground a large restoring moment will be initiated. Therefore, considering roll, it would be expected that without the keel trunk there would be a small unstable range near $\phi = 0$ and that the normal equilibrium would be with a slight list in either direction. No keel trunk is incorporated in the present design but no such central instability has been encountered in model tests (see Section III). The wind tunnel model was tested with sufficient jet nozzle area and cushion flow to achieve an appropriate and fairly uniform jet height at all parts of the trunk. This prevented a lack of roll stiffness from being masked either by local bag contact; or by the lower jet height available with the model jet angle at the scaled flow.

The reason for this satisfactory behavior is believed to be that a different pressure distribution on the walls of the cushion cavity - principally consisting of the inner trunk radius - is induced by the radically different geometry (Figure 38 c).

The stiffness provided by the trunk itself is usable because, as described in Section II.B above, when in "contact" it is air-lubricated by the distributed jets. The trunk lift (area in contact times trunk pressure) acts directly on the ground without pressing the bag material on to it. Low drag results. Closing the nozzle in this condition restores the drag since the trunk pressure now forces the material into the surface.

Because of the cushion aspect ratio (length to breadth of the basic configuration is 2.95 to 1.0) pitch stiffness is expected to be adequate and indeed a problem in take-off rotation was anticipated. However, provision of sufficient roll stiffness may be a critical factor. The major contribution due to trunk contact can be calculated if the contact area is determined as a function of the appropriate parameters.

b. Analysis of Ground Contact

The theoretical ground contact moment can be developed graphically fairly simply using a trial and error method as follows:

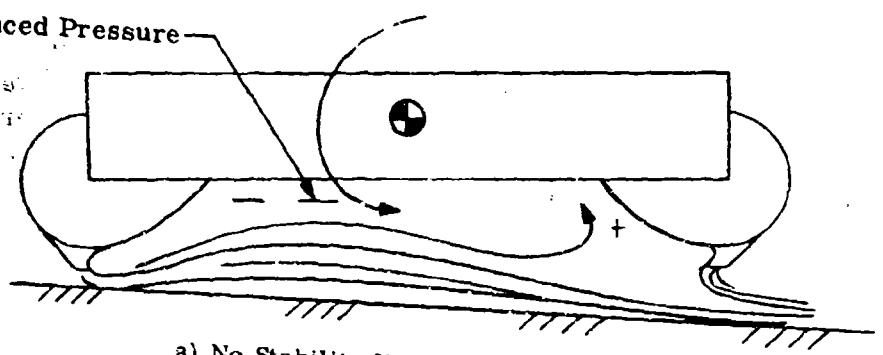

a) No Stability Keel

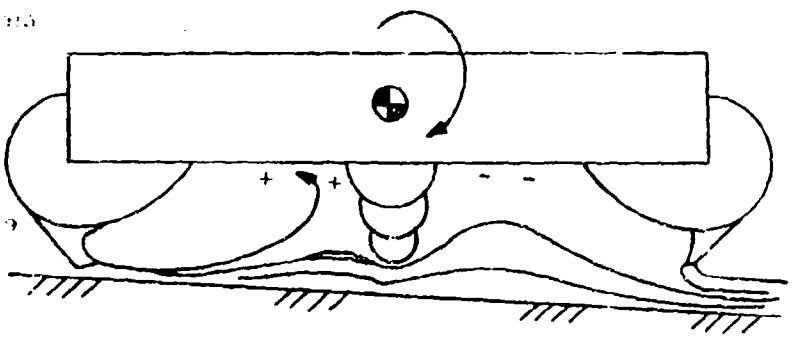

b) With Stability Keel

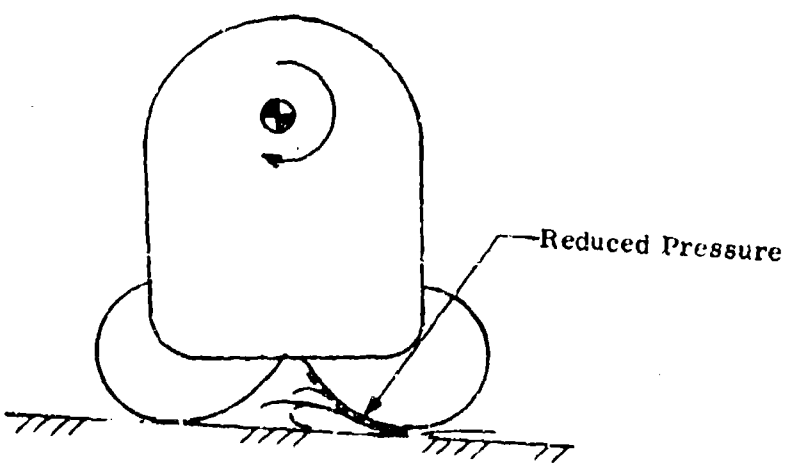

c) Narrow Body and No Nozzle

Figure 38. Static Stiffness Mechanism

(1) For a given roll angle (ϕ) assume a value of p_c/P_j. This will be below p_c/P_j for $\phi = 0$ because the trunk lift will carry some of the weight. Determine R_1 and R_2 on the high side to give the correct value of l, the material cross section length. In the design case l = 157 in. The ratio $R_1/R_2 = 1 - p_c/P_j$. This is obtained from the continuity of trunk tension at the ground tangent.

$$T = P_j R_1 = (P_j - p_c) R_2$$

Dividing by $R_2 P_j$

$$R_1/R_2 = 1 - p_c/P_j$$

(2) Draw the ground line at the given ϕ at distance h_j from the trunk tangent at this angle.

(3) Determine R_1 and R_2 on the low side which will give the correct l (sum of l_1 l_2 and l_3, the last being the contact length).

(4) Find the sum of trunk lift (contact width times effective length times trunk pressure) and the cushion lift (cushion width times effective length times cushion pressure). The effective length must be assumed.

(5) Compare the total lift with the weight. Iterate p_c/P_j until the total lift equals the weight.

For example, at $\phi = 5°$:

Assume $p_c/P_j = 0.44$
Then $R_1/R_2 = 0.56$
$l = 157$ in.

On high side choose $R_1 = 31.4$ in.
Then $R_2 = 56.1$

With $R_1 = 31.4$ θ_1 is found to be 180°
θ_2 is found to be 59.5°

$R_1 \theta_1 = 98.7$

$R_2 \theta_2 = 58.3$

$l = 157.0$

Draw the ground line at estimated high side $h_j = 0.95 \times 2h_{lo} = 1.9 \times 1.426 = 2.71$ in.

On low side choose R_1 = 26.0 in.

R_2 = 46.5 in.

With R_1 = 26.0 in. θ_1 is found to be 193°

With R_2 = 46.5 in. θ_2 is found to be 63.5°

$R_1 \quad \theta_1$ = 87.5 in.

$R_2 \quad \theta_2$ = 51.5 in.

l_3 is scaled = 16.0 in.

l = 157.0 in.

Trunk Lift = $P_j \times l_3 \times$ effective length

= 333 x 1.33 x 31.3 = 13900

Cushion Lift = $p_c \times b \times$ effective length

= 146.5 x 10.1 x 31.3 = 46100

Total Lift = 60000

The sum of cushion and trunk lift produces the vector shown on Figure 39.

This was carried through for two roll angles and the resulting cross sections and total lift vectors are shown in Figure 39. The righting moment increases with angle. Righting moment about cg 3 and 4 is shown in Figure 40. To this must be added the cushion basic stability contribution due to suction on the inner trunk radius on the high side. Also the exhausting cushion flow causes a side force and rolling moment. If the nozzles are closed on the contact side this is reacted at the ground. To estimate this contribution in the alternative case jet velocity is calculated from cushion pressure.

$$V_j = 29 \sqrt{166.7} = 375 \text{ ft/sec}$$

An arbitrary factor varying linearly from 0.4 at 0.6° (initial contact) to 0.95 at 5° will also be applied. This is intended to allow for the fore and aft components of flow at the ends. Evidently at initial contact along one side a large proportion of the cushion momentum will escape in fore and aft directions. As roll angle increases the contact point will move around the ends until at large roll angle the majority of the cushion momentum will exhaust laterally on the high side. The above arbitrary factor is introduced to account for this effect.

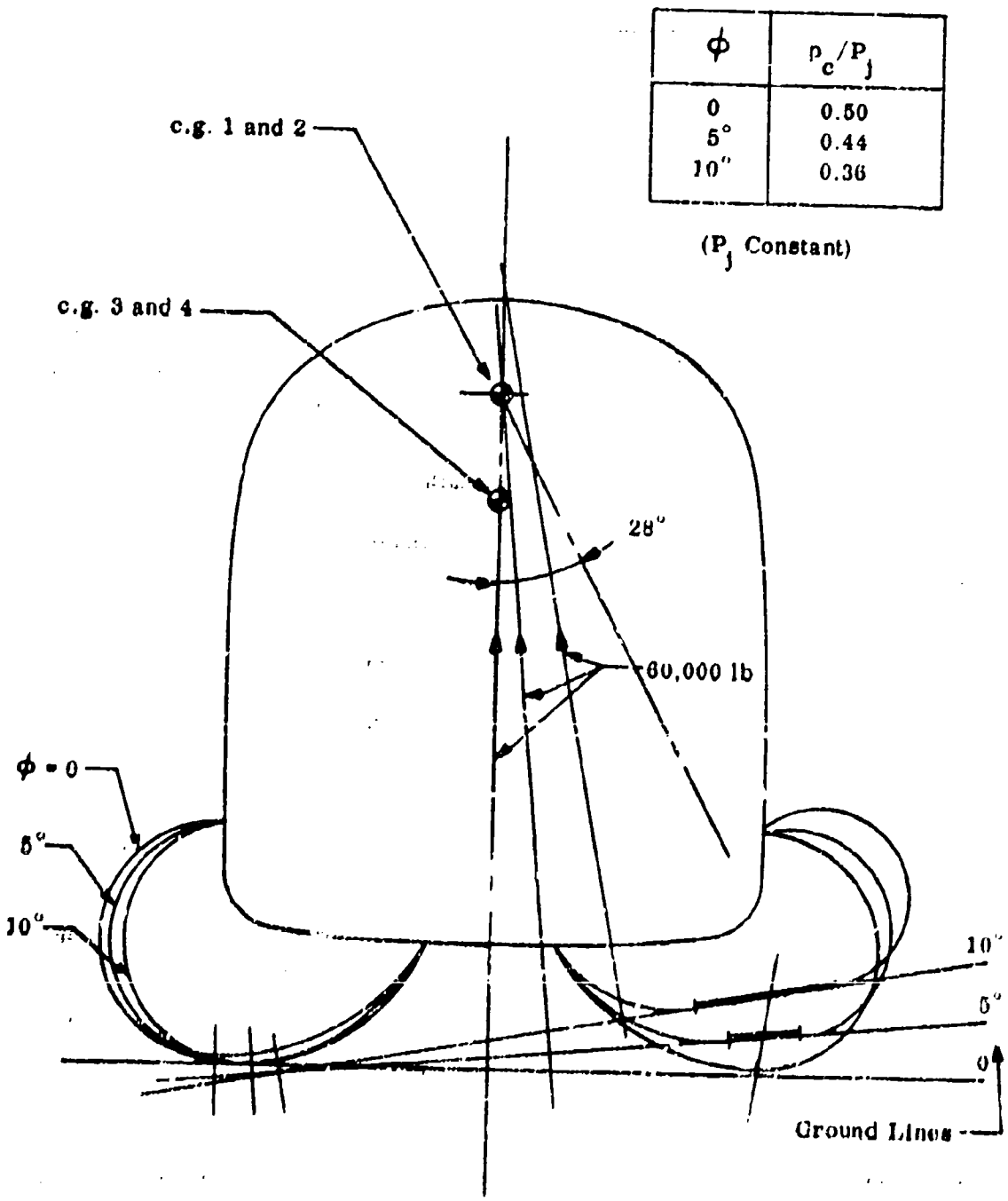

Figure 39. Trunk Distortions in Roll

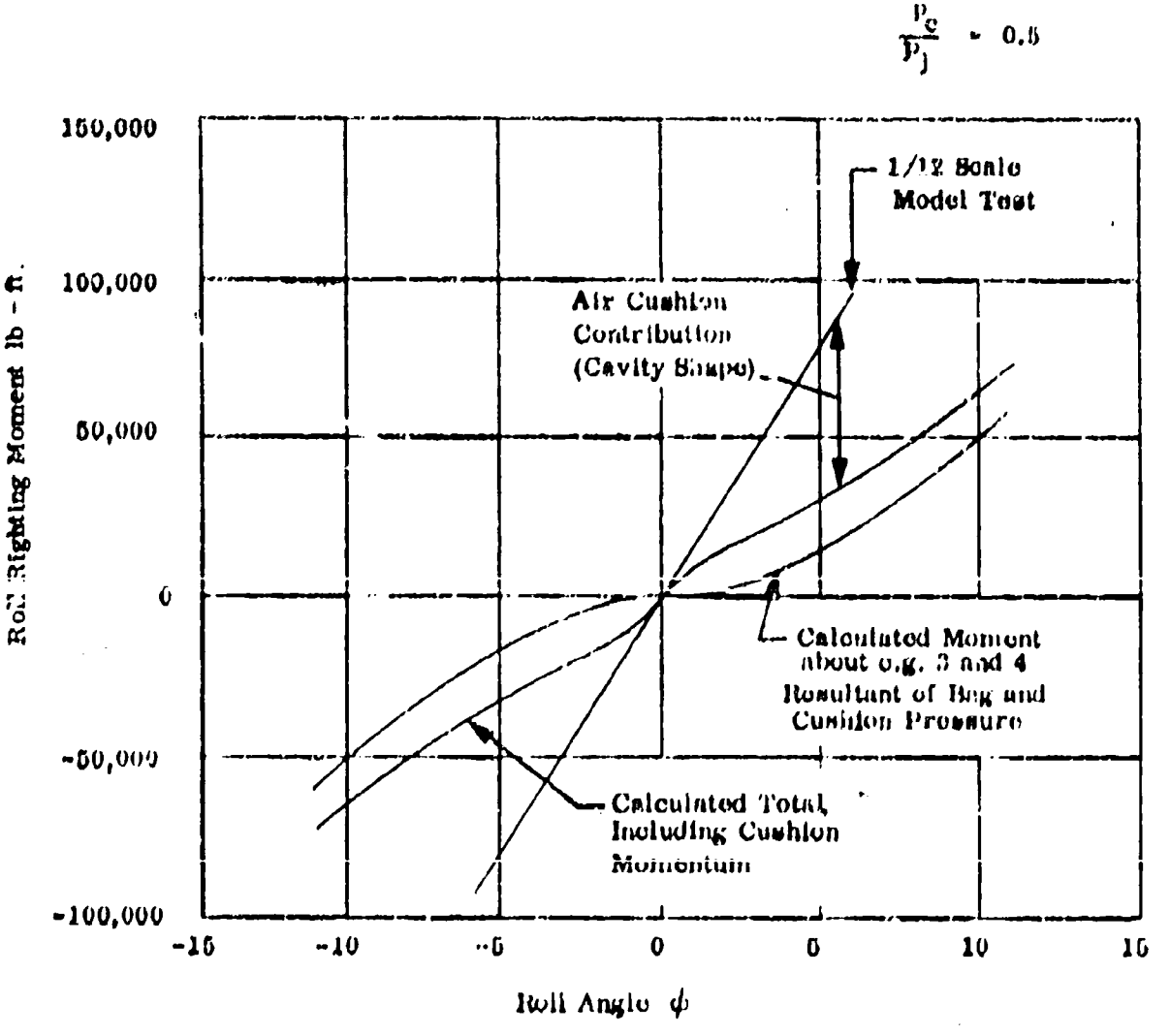

Figure 40. Static Roll Stiffness

$$m V_j = 4.24 \times 375 = 1590 \text{ lb}$$

ϕ	0.6	2	5	10
Y, lb	640	920	1510	1510
l, ft	12.0	11.95	11.7	11.16
Moment, ft/lb	7500	10950	17700	16900

Measured righting moment from 1/12 scale model test is also shown on this figure for comparison. It appears that a substantial stabilizing moment is provided by the air cushion. This stiffness at the design p_c/P_j appears to be quite satisfactory. Stiffness varies with p_c/P_j and measurements over a range of this parameter were made on the wind tunnel model (See Section III). The results are shown in Figure 41 as a plot of cp ϕ/ degree against cushion pressure ratio. It is shown that at 10° roll the cushion cp has moved nearly a quarter of the beam of 11.5 ft or 2-3/4 ft e.g.,

$$cp_\phi = 0.0235/\text{deg at } p_c/P_j = 0.5$$

$$\Delta cp = 0.235 \times b \text{ at } 10^\circ \text{ roll angle}$$

$$= 0.235 \times 11.5 = 2.71 \text{ ft}$$

c. Roll Stiffness Criteria

Required roll stiffness may be considered in relation to engine torque, side wind gust, or sideslip.

(1) Engine Torque

$$\text{Torque} = \frac{\text{Brake horsepower} \times 33{,}000}{2\pi \times \text{rpm}}$$

Considering max power at the start of the take-off run:

$$T = \frac{5300 \times 6250}{2651} = 10{,}000 \text{ lb/ft}$$

(2) Side Gust

A rolling moment due to body, fins and wing will be considered.

Body, $C_D = 1.0$

Side Area = 477 ft^2

1/12 Scale Model Measurements

$$c.p._{\phi} \quad \frac{\text{Rolling Moment/Degree}}{\text{Lift x Cushion Width}}$$

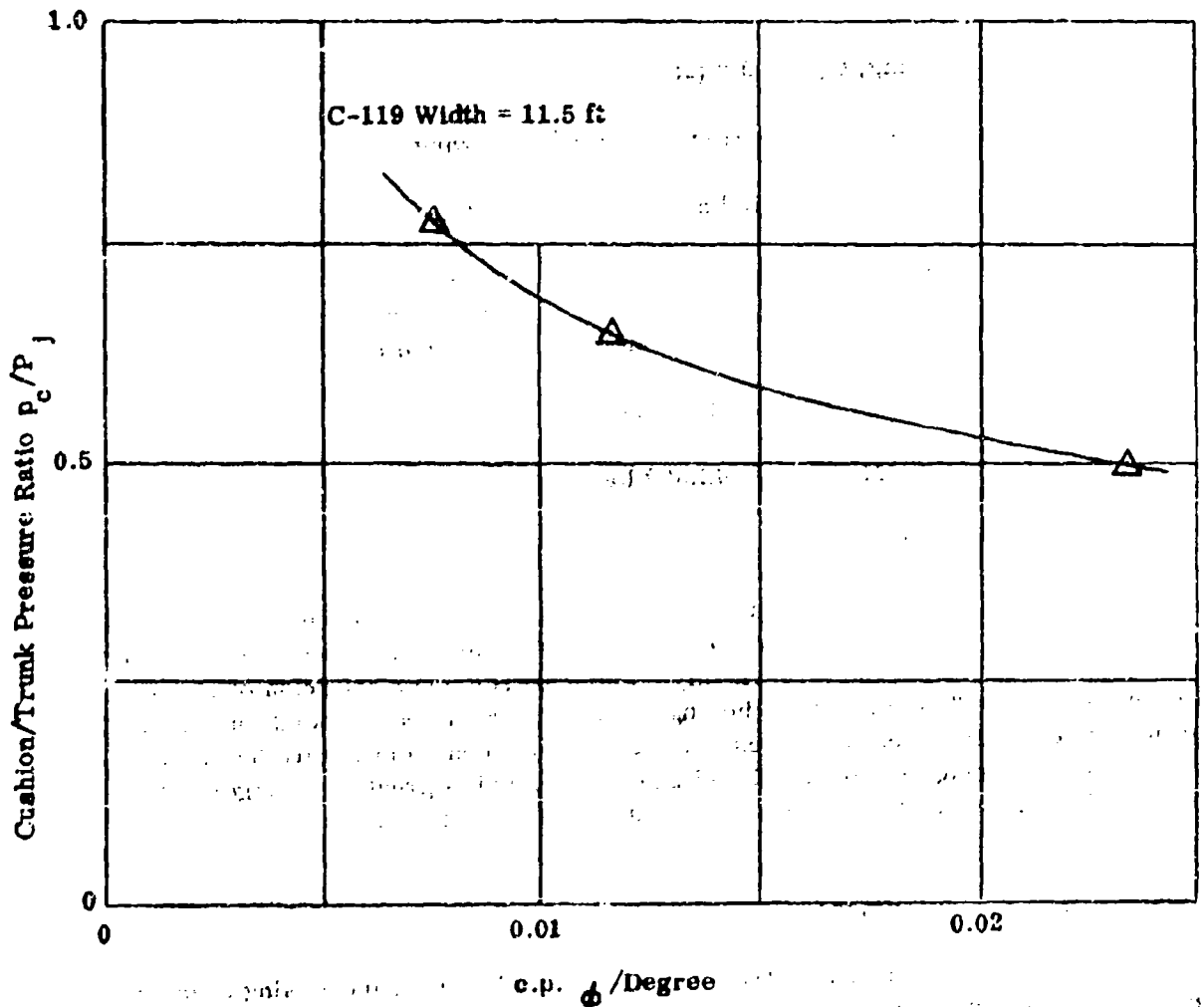

Figure 41. Roll Stiffness Variation with Bag Pressure

cp above ground = 9.5 ft

Moment = 1.0 x 470 x 3.5 x q = 4460 q lb/ft

Fins, C_D = 1.2

Side area = 75 x 2 = 150 ft^2

cp above ground = 22 ft

Moment = 1.2 x 150 x 22 x q = 6600 q lb/ft

Wing, C_L = 0.2 (at $\alpha = 10°$)

Plan area = 700 ft^2 (1/2 wing)

cp from longitudinal center line = 20 ft

Moment = 0.2 x 700 x 20 x q = 2800 q lb/ft

Total Moment 13860 q lb/ft

For a side gust of 30 knots q = 3.06 lb/ft^2

Moment = 42,500 lb/ft

(3) Sideslip

The sideslip case with the air cushion is different to the normal case with wheels since the former does not react sideforce, and may be sideslipped intentionally. However, the (presumably empirical) roll-over criterion of Reference 4 is in fact met. This states that the angle between wheel contact point and aircraft cg in front elevation must not be less than 25°. It is seen from Figure 39 that a 10° roll this is 25° using the high cg (1 and 2 positions) and is greater at larger roll angles. Actual roll righting moment is considerably greater than shown in this figure, as evidenced by Figure 40.

d. Heave Stiffness

As load increases from the design condition the increasing cushion pressure causes the trunk to move up and out. Theoretically at the bottom of the stroke $p_c/P_j = 1.0$, the inner trunk radius is infinite (a straight line) and the static g is a maximum. Evidently the maximum g depends on the design p_c/P_j. For example at initial $p_c/P_j = 1.0$ and constant P_j the maximum cushion pressure would be twice the dosign condition.

Factors which modify the static heave stiffness are (1) the change in cushion area due to trunk deflection, (2) the increase in P_j provided by the fan. The latter may be considered at constant power or at constant rpm. The latter is probably the more valuable since transient response will be at essentially constant rpm.

It is valuable to determine theoretical two-dimensional heave stiffness in order to predict its variation with design p_c/P_j. A brief analysis is made in the following and values obtained from 1/3 scale model tests are compared with the results.

For simplicity constant material length is used. Using an iterative procedure similar to that described in subsection 1.(b) above, two-dimensional trunk shape is calculated to provide the geometry variations shown in Figure 42. Stiffness at constant rpm is obtained from the fan characteristic of Figure 36. For the calculation, flow coefficient and jet height for a range of p_c/P_j are taken from Figure 26:

p_c/P_j	0.3	0.5	0.7	0.9
h/g	9.8	5.0	2.95	1.5
$(Q/cg)\sqrt{\rho/2p_c}$	1.675	1.22	0.95	0.68

since nozzle area is constant,

$(Q/\sqrt{p_c})_0/(Q/\sqrt{p_c})$	0.729	1.0	1.283	1.795
h_{jo}/h_j	1.96	1.0	0.59	0.3

p_c may be found by iterating with the fan characteristic, assuming that duct loss varies as Q^2.

Q/p_c	189.5	138	107.5	77
$Q, ft^3/sec$	1830	1780	1710	1500
$p_c, lb/ft^2$	93	166.5	252	379
$P_j, lb/ft^2$	310	333	360	421
$\Delta P, lb/ft^2$	102	97	90	78
P_{Fan}	412	430	450	499
h_j in.	2.8	1.425	0.84	0.43

It will be noticed that although the cushion pressure has more than doubled the fan is still not stalled. These variations of p_c and h_j are also shown on Figure 42. An estimated stiffness can now be found from

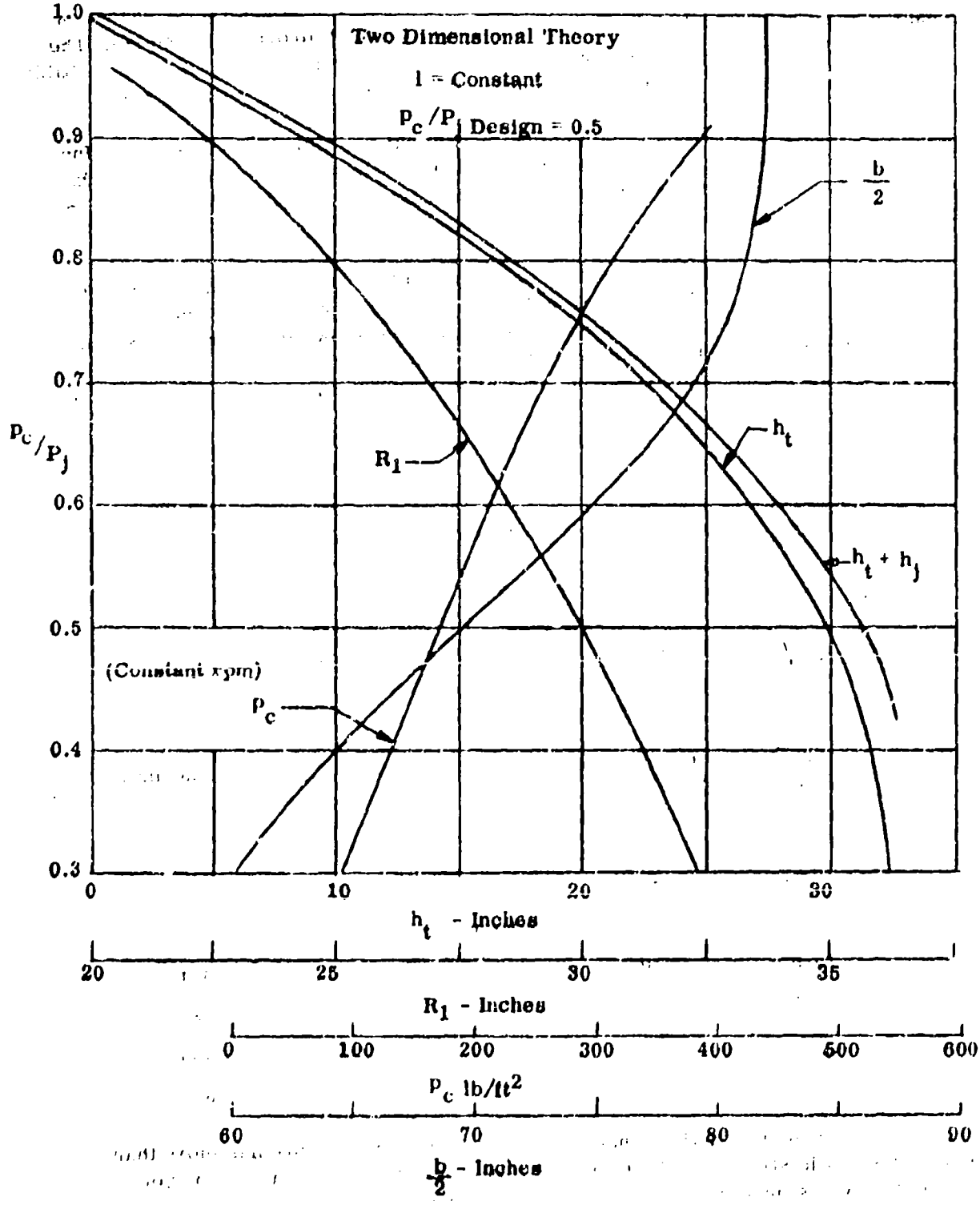

Figure 42. Trunk Geometry Variations

$$\frac{L}{L_o} = \frac{p_c}{p_{c_o}} \times \frac{b}{b_o}$$

The ratio b/b_o represents the two dimensional increase in cushion width at the ground tangent. Due to the low aspect ratio it is considered an acceptable factor for accounting for the cushion area increase. The area increases because of increased trunk distortion as cushion pressure increases. b/b_o is calculated by iterating to find the trunk shape as described in subsection 1 (b).

L/L_o is plotted against $h_t + h_j$ in Figure 43.

e. Pitch Stiffness

Prediction of pitch stiffness is unduly complex because of the imponderable bag contact area at the three dimensional ends. Pitch stiffness measurements were made on the 1/12 scale model (see Section III) and reliance is placed on these for the rotation analysis in Section III.F.

2. Dynamic Stability

a. Ground Resonance

The plain air bag (without a built up nozzle structure such as is indicated in Figure 38 (a) and (b) is subject to ground resonance. Violently divergent ground resonance was encountered during the development of the 1/12 scale model and some oscillation was also found in the early development stage on the 1/3 scale model.

The mechanism appears to be simple and is not much affected either by the trunk material elasticity or the air cushion characteristics. This is evidenced by the fact that at extreme roll angle (beyond wing tip to ground contact) the resonance can be induced and it can be induced as readily with an inelastic as an elastic trunk. (Both were fitted to the 1/12 scale model.) It appears to be reliably inhibited by the distributed jet which is why the extreme roll angle is required to induce it. The edge of the jet pattern is then on the ground tangent. What is thought to happen is shown in Figure 44. From an equilibrium position (a) with the escaping jet concentrated at the ground tangent the edge of the material is sucked down by the escaping air, the body falls, the contact pressure causes the lift to exceed the weight, the body rises, overshoots upwardly and proceeds into a divergent oscillation. Alternatively as in (b) the suction force on the material can be prevented by distributing the jet flow and no oscillation occurs.

b. Trunk Stability

Trunk vibration has also been experienced in the test models. The dynamics of trunk vibration are not clearly understood. This phenomena is annoying

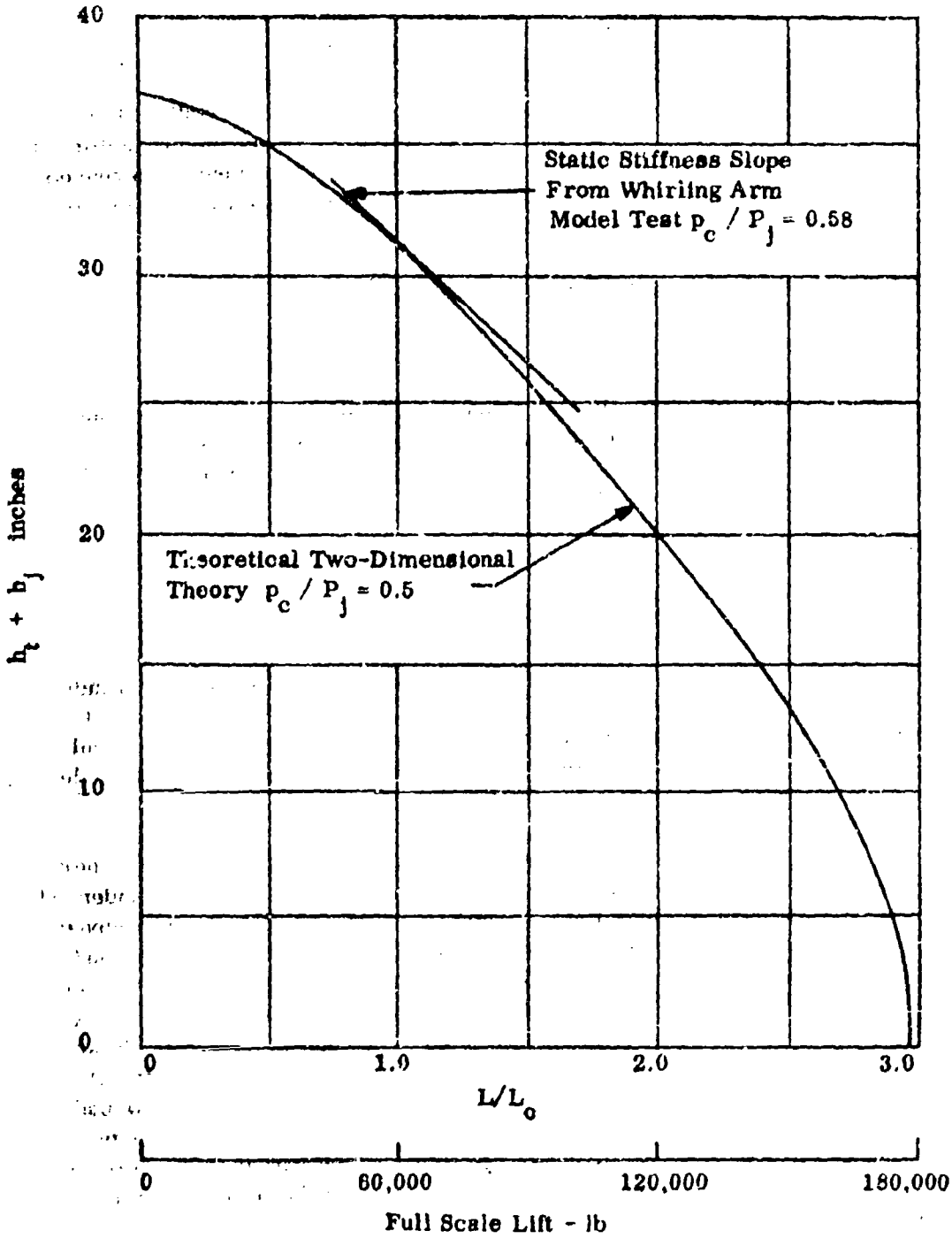

Figure 43. Static Heave Stiffness

(a) Unstable Configuration

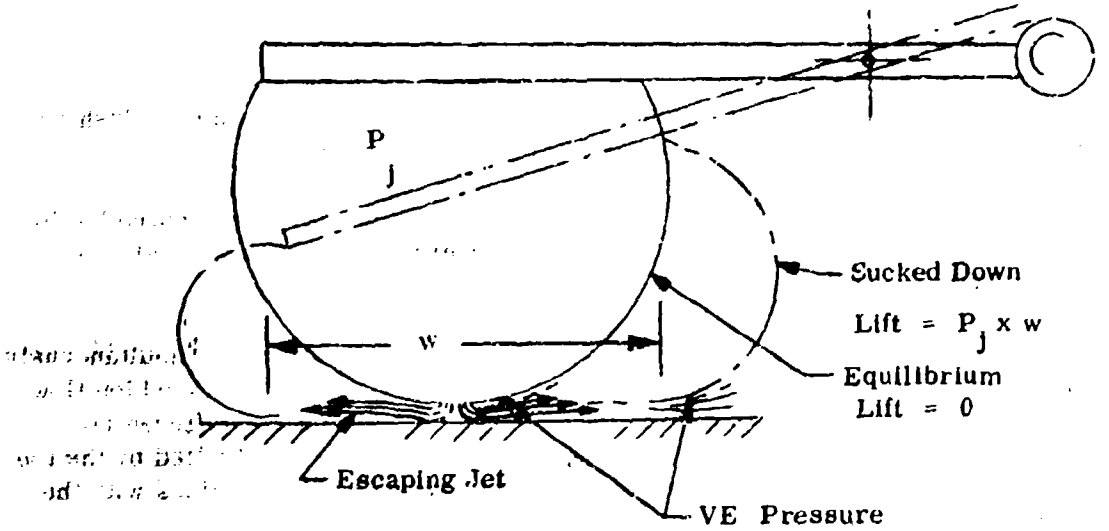

(b) Stable Configuration

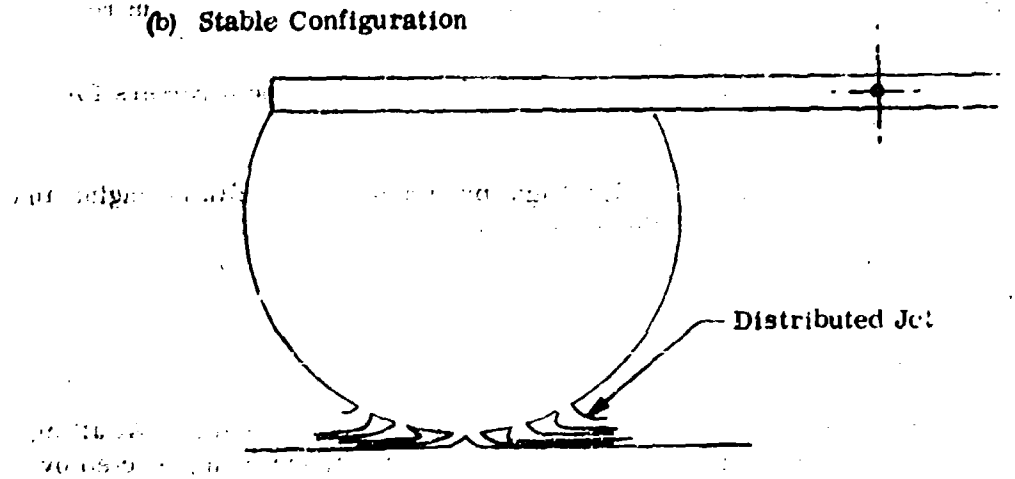

Height loss does not decrease pressure

Figure 44. Ground Resonance Mechanism

and noisy but otherwise apparently unobjectionable. In most cases a small amount of damping, such as by placing the palm of the hand on the bag on the whirling arm model, will stop the vibration. Addition of a small mass at the outer tangent to the bag is effective in reducing it.

3. Control

Normal flight controls are not compromised by the air cushion. Cushion controls are brakes, flow diverter and auxiliary engine controls.

The nozzle valving will be operated by engine bleed air, and controlled by the pilots toe pedals in parallel with the brakes. Operation of the nozzle valve is described in Section II.B.

The diverter valves in the fuselage side operate collectively simultaneously with the vanes in the trunk entry ports (Figure 34). The interchange of cushion flow is controlled by an inflate/deflate lever in the cockpit. Additionally, differential reverse control of the diverter valves is superimposed and also controlled by the toe pedals. This provides additional control in the ground run and harmonizes with the braking valves as follows:

(1) Lever at inflate, trunk port vanes open, diverter valves closed ready for landing.

(2) Right brake closes RHS nozzles, opens RHS diverter valves in reverse; and vice versa.

(3) Full brake on both closes all jets and opens both side diverters for reverse thrust.

The diverter vanes are closed in flight by stopping the auxiliary engine and selecting inflate, ready for landing. Figure 45 is a system schematic.

4. Trim

a. Ground Trim

The cushion center of pressure is placed at the forward cg. At aft cg there will be a small change in ground attitude, the weight moment being reacted by the air cushion pitch stiffness. Forward cg is at 20% MAC and aft cg is at 30% MAC. The weight moment is then

$$0.10 \times \frac{168.28}{12} \times 60{,}000 = 84{,}200 \text{ lb/ft}$$

(neglecting the change in ground angle.)

This is conveniently expressed as a change in air cushion center of pressure. Using an effective cushion length of 31.4 ft

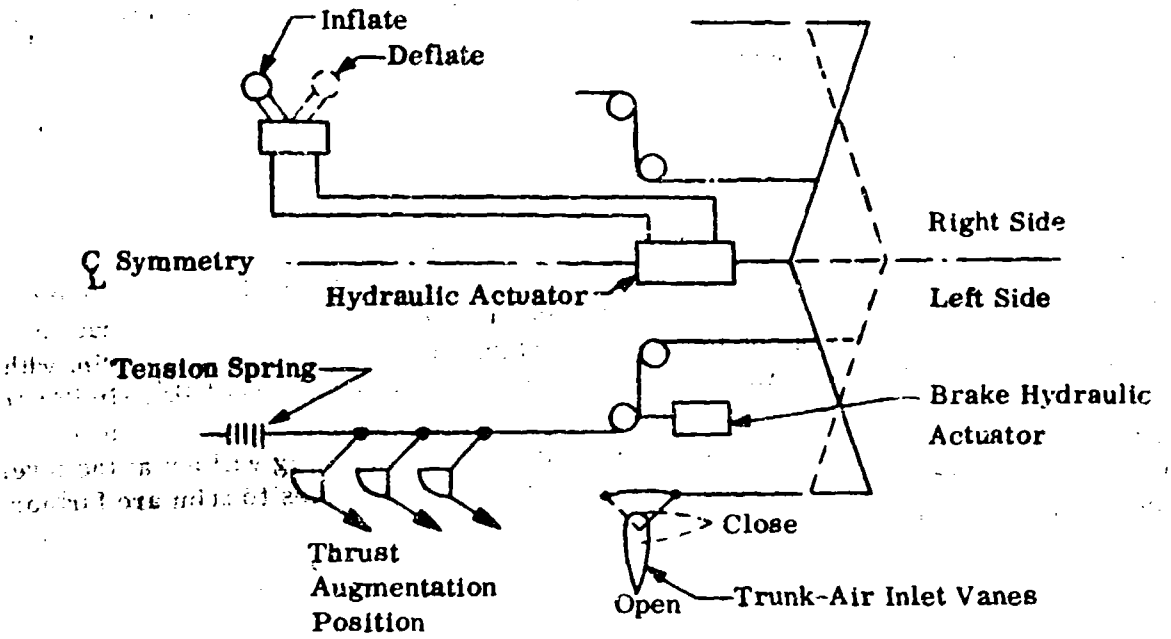

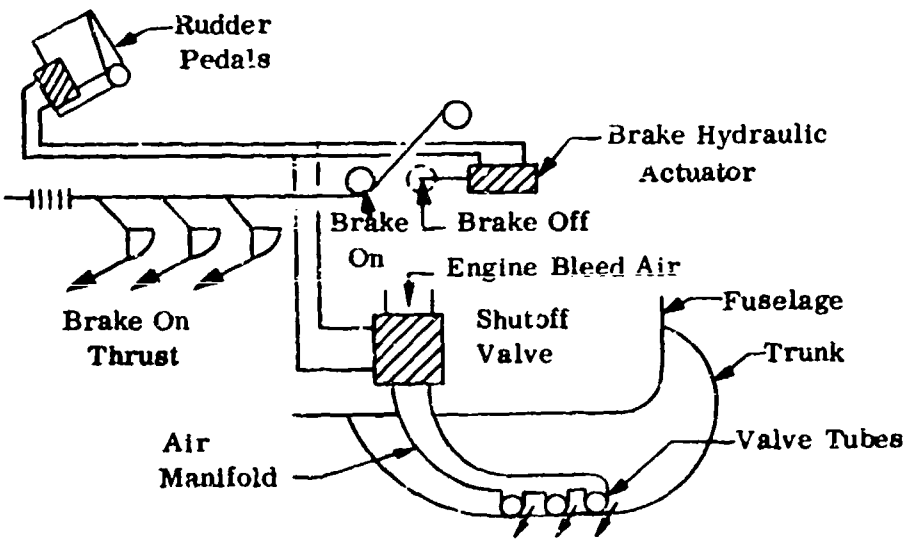

Figure 45. Control System Schematic

$$cp = \frac{84,200}{60,000 \times 31.4} = 0.046$$

Cushion pitch stiffness was obtained from 1/12 scale model test (Section III).

$$cp_{\theta} = 0.059/deg$$

Hence the attitude change is approximately 3/4°.

b. Flight Trim

A major object of the wind tunnel test was to determine change in elevator angle to trim through the take-off and landing maneuver. It was found that the existing elevator was capable of accomplishing take-off rotation. Change of trim with the air bag in comparison to wheels is small - the drag of the air bag being similar to that of the extended wheels. Momentum drag was not simulated in the wind tunnel. However, this is not expected to cause any change, since this drag will act at the level of the air entry which is close to the vertical cg. Elevator angles to trim are further discussed in Section III.

F. TAKEOFF ROTATION ANALYSIS

1. General

The purpose of the wind tunnel test was to confirm the feasibility of the takeoff and landing from and to the air cushion using the existing aerodynamic controls, with measurement of drag.

Because of the large length/breadth of the fuselage mounted air cushion and the small jet height only a small rotation angle is possible before the rear of the bag is in ground contact. It was feared that a large moment due to this contact might develop before sufficient aerodynamic lift was realized which would be beyond the power of the elevator to control. Also it was thought that bag contact over a large area might cause considerable drag.

In fact neither of these fears were realized, and the wind tunnel tests showed no real problem exists. This assurance is amplified by the following comparative analysis:

2. Takeoff Speed and Angle-of-Attack

Figure 46 shows the relevant dimensions. The worst case is evidently c.g. 3, for which the thrust moment is negative and the weight moment a maximum.

Takeoff speed is assumed to be 1.2 V_{SI} where V_{SI} is the stalling speed in the takeoff configuration. $C_{L\,max}$ (T-O) is determined from Reference 2 from which Figure 47 has been plotted. A value of 2.14 at $T_C = 0.64$ is indicated.

At 60,000 lb G.W.

$W/b\ C_L = 60,000/1447 \times 2.14 = 19.4$

q at $1.2\ V_{SI} = 1.44 \times 18.1 = 28$

$V_{SI} = 153$ ft/sec $= 90.5$ knots

Thrust at 90.5 Kt. $= 8250$ lb/engine

$$T_C = \frac{T}{\rho V^2 D_p^2} \qquad \text{(Reference 2 Figure 106 and P. 254)}$$

$$= \frac{250}{0.00238 \times 153^2 \times 15.09^2} = 0.66$$

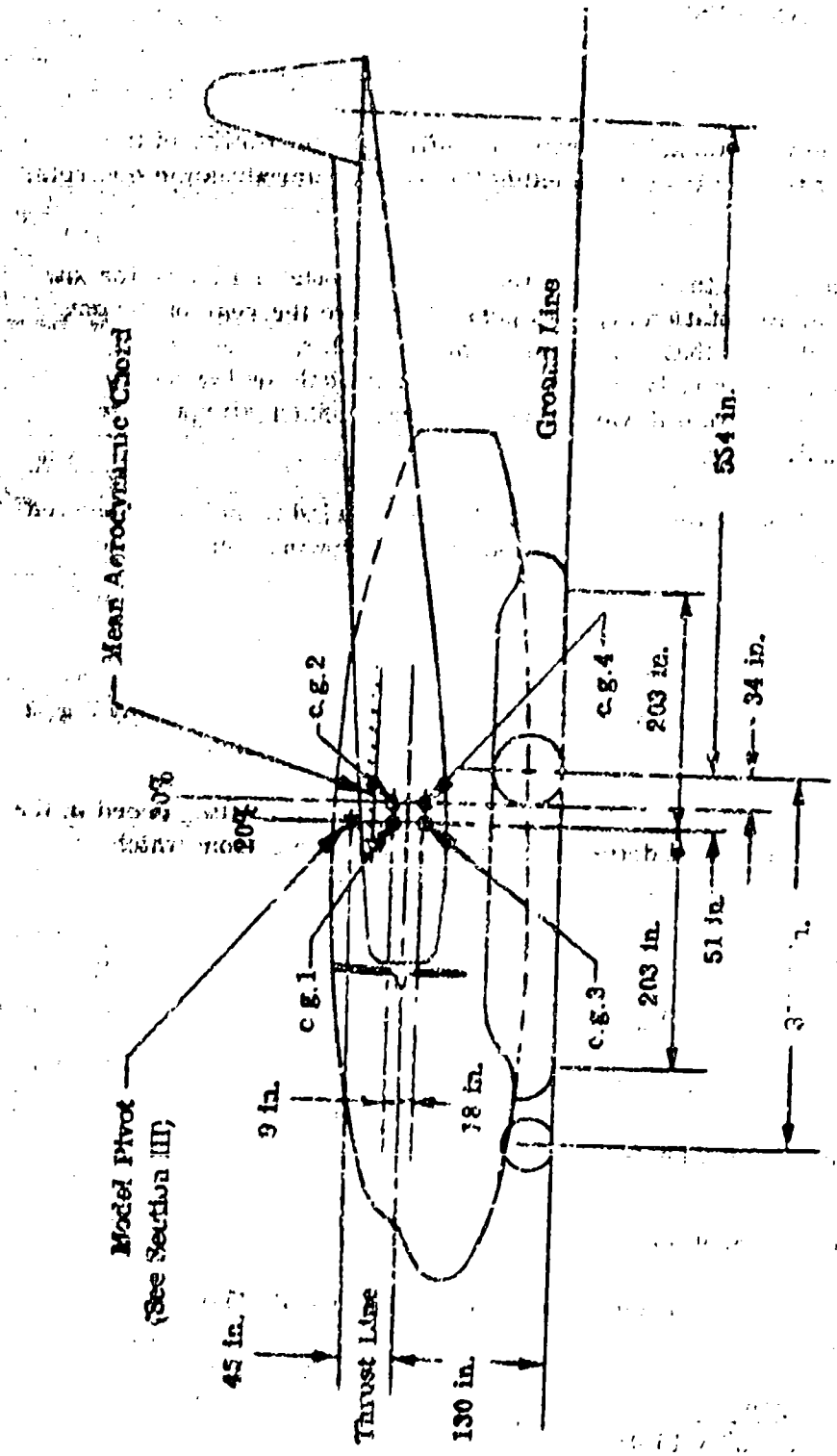

Figure 46. C-119 Air Cushion, C of G, Wheel and Tail Locations

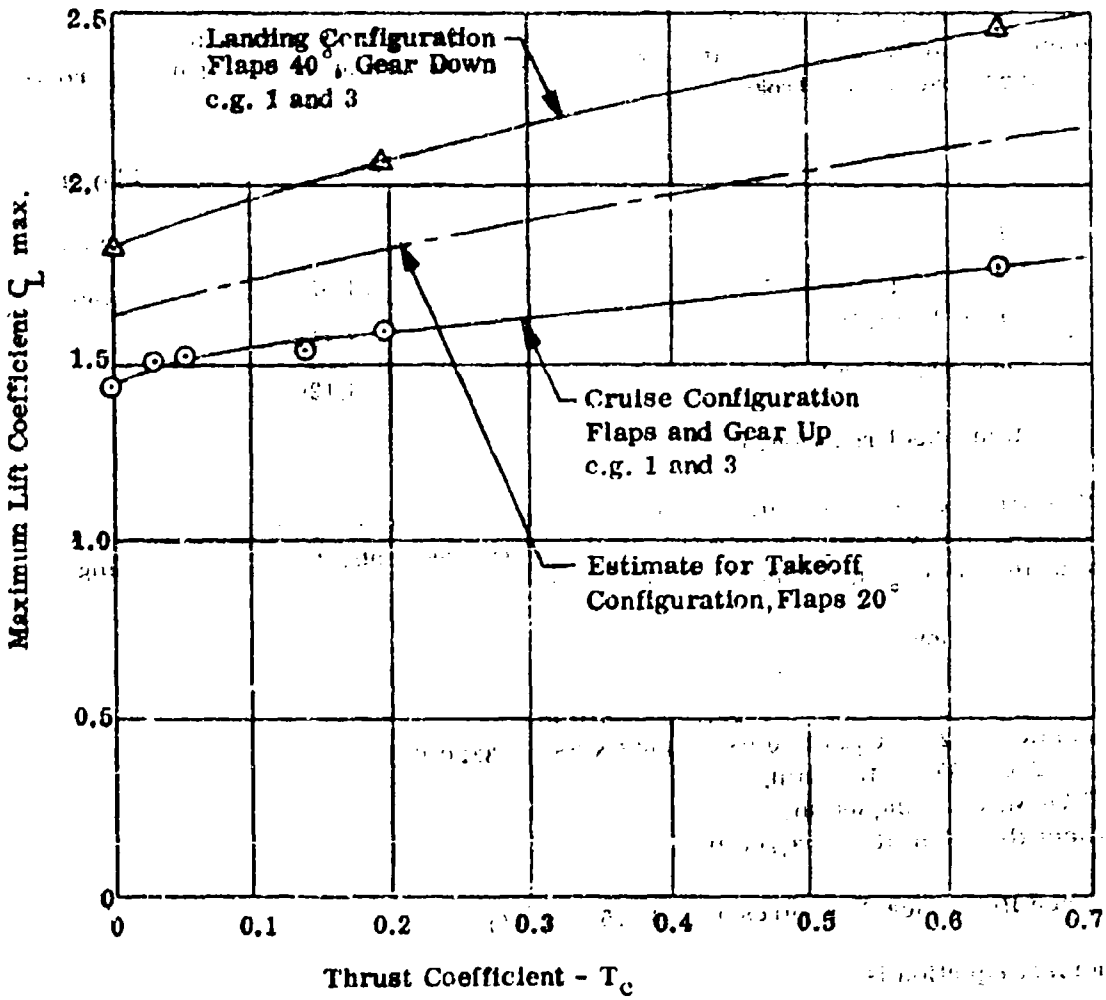

Figure 47. C-119 Maximum Lift Coefficients

$C_{L_{max}}$ = 2.1 will be assumed.

$C_{L_{T-O}}$ = 2.1/1.44 = 1.46

α_{TL} = 6.8° in ground effect (Reference 2 Figures 1, 3, 82)

3. Takeoff Rotation on Wheels

Maximum elevator will be required when the main gear reaction is a maximum. It will be assumed that nose wheel liftoff occurs at α_{TL} = 1.0° (Approximately 6 inch nose wheel stroke.)

	α_{TL} = 0	α_{TL} = 1.0°
C_L	0.54	0.65
Lift = C_L x 1447 x 28, lb.	21,850	26,300
Wheel Load, lb.	38,150	33,700
Nose wheel load (Figure 46), lb.	6,120	0
Main wheel reaction, R, lb.	32,030	33,700

Conventionally moments are often taken about the wheel contact point. However for better comparison with the air cushion, moments are taken about the c.g., omitting the virtual inertia (T-D), for an identical result.

Forces are as follows:

Rolling friction = μR = 0.025 x 33,700 = 840 lb.
Aerodynamic Drag = $C_D Sq$ = 0.082 x 1447 x 28 = 3320 lb.
Thrust = 2 x 8250 = 16,500 lb.
Lift at 0.26 MAC = 26,300 lb.
Main Wheel Reaction, R = 33,700 lb.

(For C_D see Reference 2, Figures 12, 14, 15, and 16)

The moment equation is:

$$585\ L_T = 840 \times 112 - 3320 \times 6 + 16{,}500 \times 18 + 26{,}300 \times 10.1 + 33{,}700 \times 53$$

$\therefore L_T$ = 4100 lb.

Note that ΔL_T to balance wheel reaction and rolling friction = 3100 lb.

4. Takeoff Rotation on Air Cushion

On the air cushion it is not clear what will be the angle of attack requiring maximum elevator angle. Therefore, moments must be evaluated for the angle of attack range up to the takeoff α_{TL} of 6.8°. The appropriate trimmed lift curve from Reference 2 is shown in Figure 48.

α_{TL}	0	2	4	5	6
C_L	0.54	0.8	1.07	1.20	1.34
Wing Lift = $C_L Sq$	21,900	32,400	43,300	48,500	54,200
Cushion Lift	38,100	27,600	16,700	11,560	5,800

Cushion lift will be the sum of cushion pressure times cushion area and bag contact area times bag pressure if there is any contact. The variation of estimated jet height with lift is given in Figure 31. Two effects modify this curve in the present instance:

(1) The variation of jet height with angle at constant lift.
(2) The effect of forward speed on jet height at given angle of attack.

Experience has shown that the former is small. However, it is unfavorable. The latter is imponderable, but favorable. For present purposes they may be assumed to cancel. Alternatively the variation of cushion moment with lift at constant angle may be found directly from model tests and the favorable effect of forward speed neglected, which is conservative.

Using the latter approach; the 1/12 scale model pitch stiffness was obtained for a range of weight. Moment per degree is plotted against weight in Figure 49.

α_{TL}	0	2	4	5	6
Cushion Moment ft/lb.	0	110,000	132,000	115,000	69,000
ΔL_T lb.	0	2,250	2,700	2,360	1,410

The maximum tail load is less than it is with wheel gear. Tail loads to trim are compared in Figure 50.

G. ENERGY ABSORPTION ANALYSIS

Drop tests were carried through on the whirling arm model to determine energy absorption capability. The model was dropped in the flat attitude and a large capacity

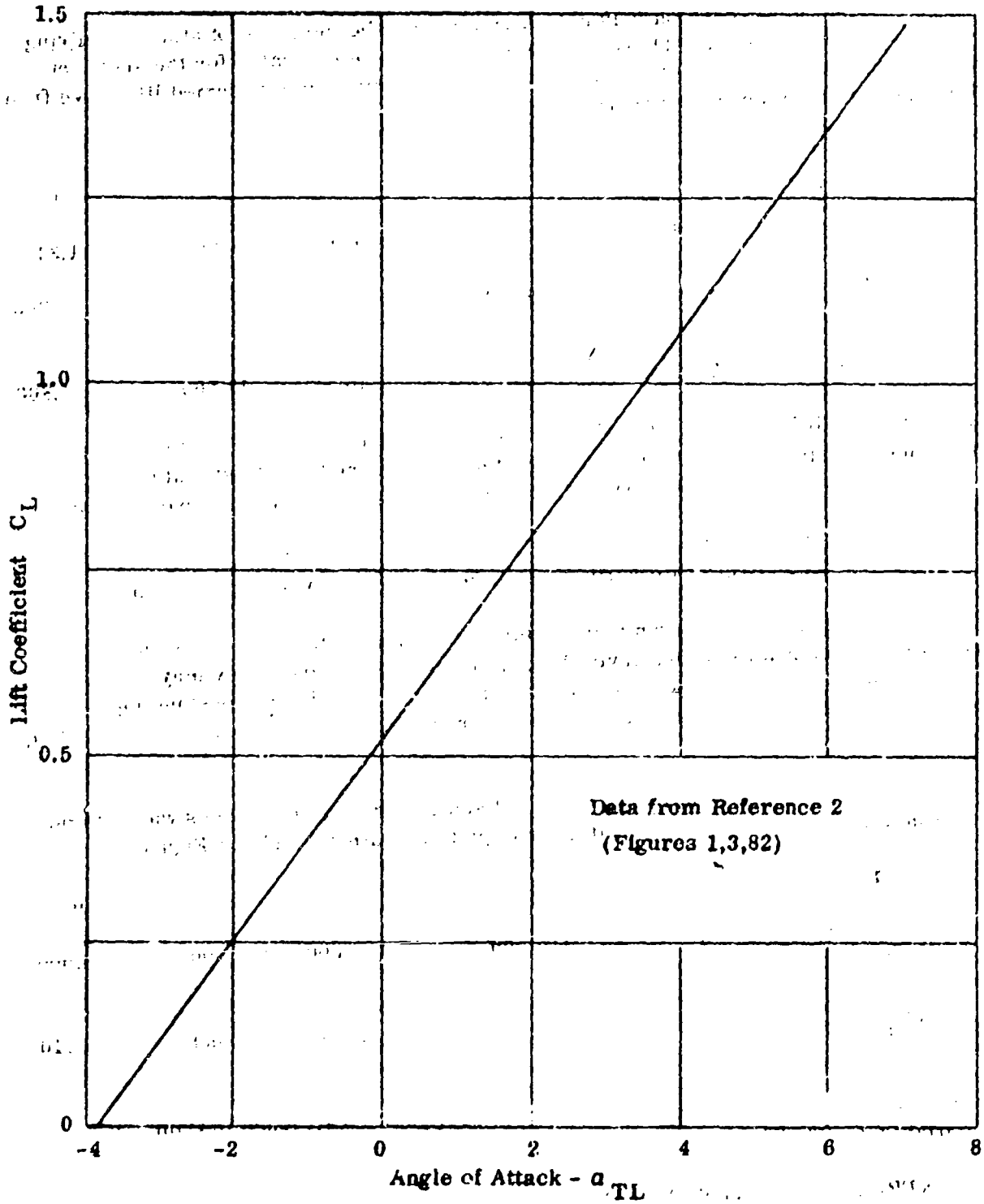

Figure 48. Takeoff Configuration Lift Curve in Ground Effect

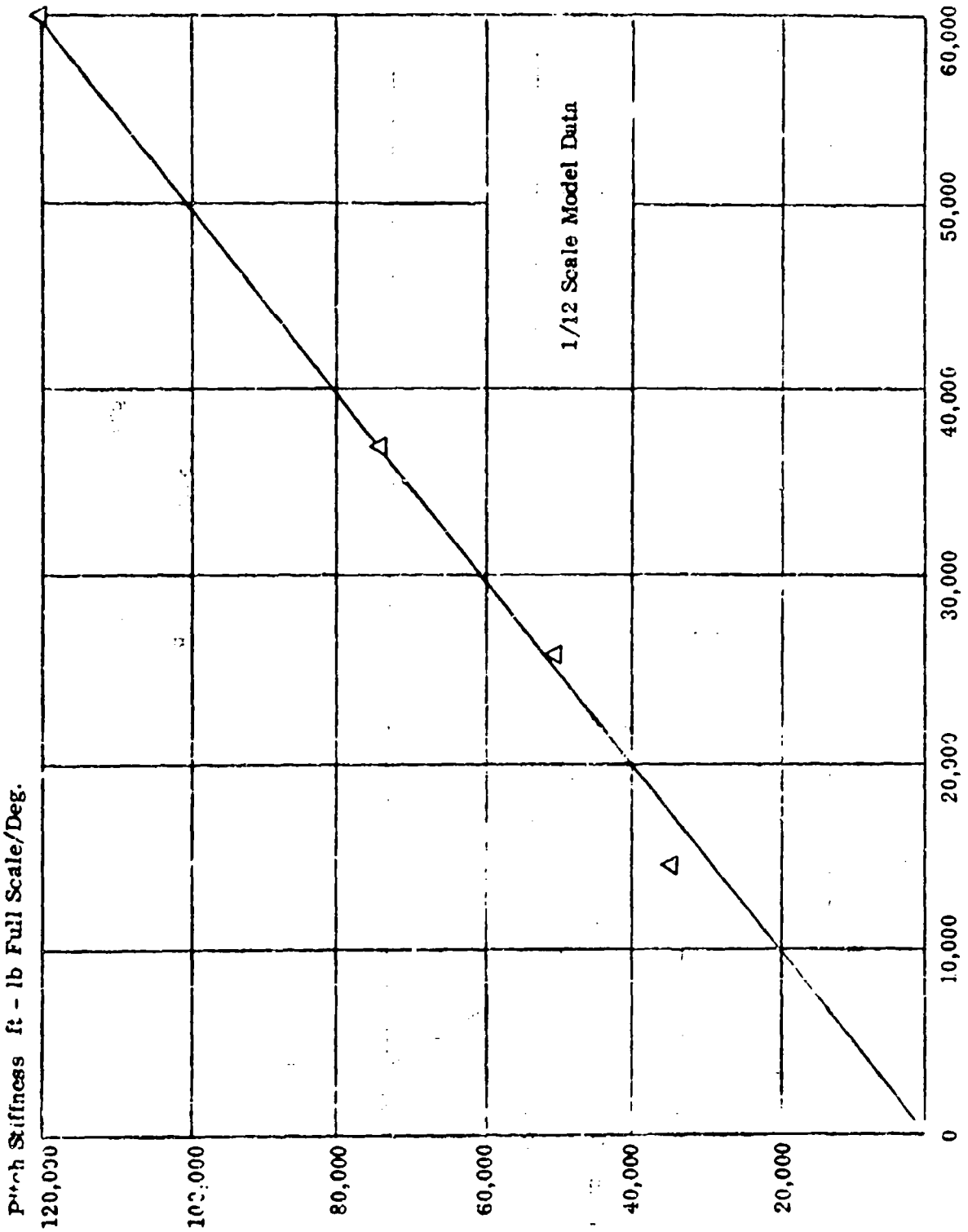

Figure 49. Variation of Pitch Stiffness with Lift

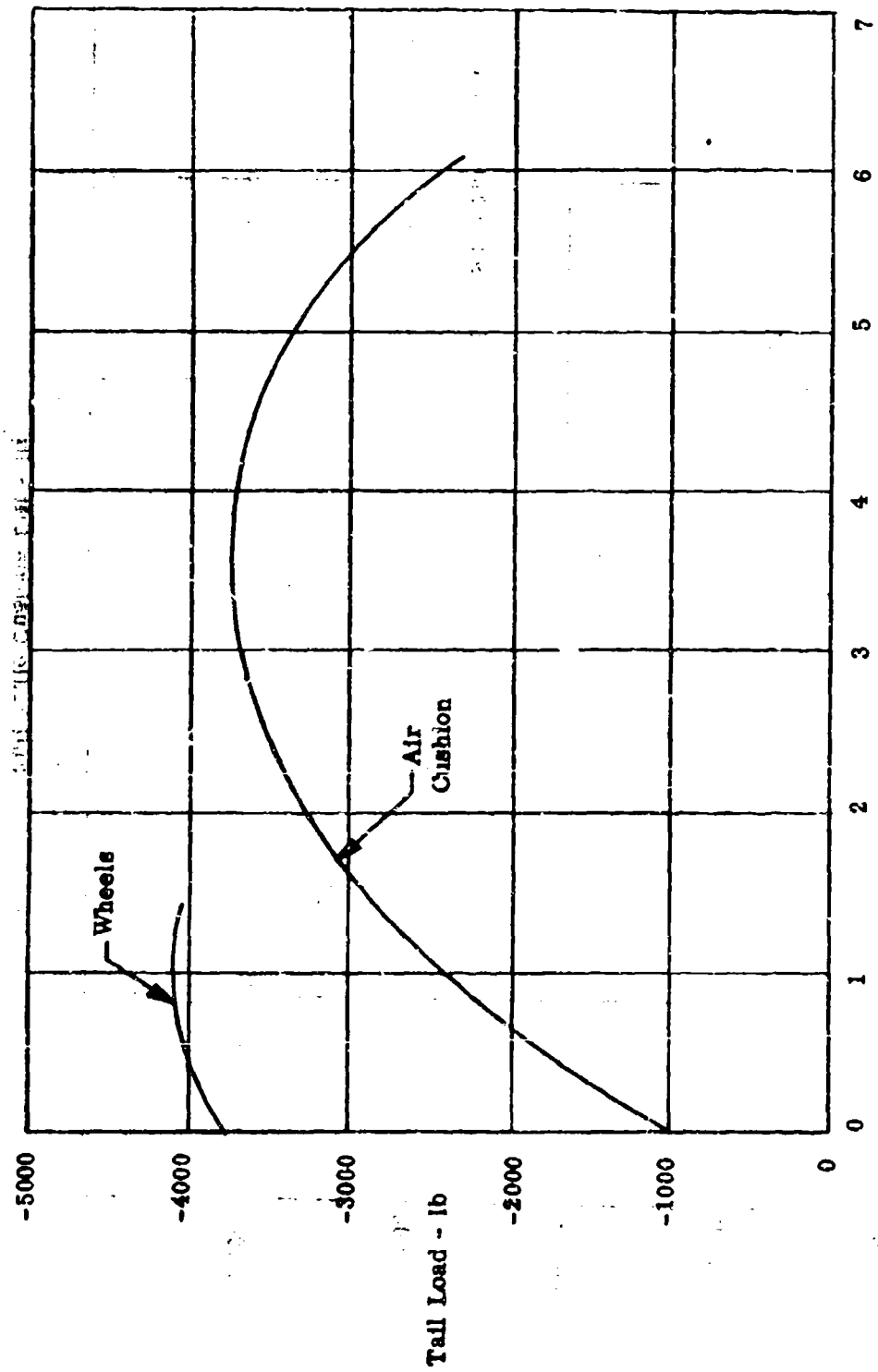

Figure 50. Tail Loads Required to Trim

to absorb vertical sink was demonstrated. This was combined with excellent damping. In this section the mechanism of energy absorption by the air cushion is examined and estimates of sink rate are made and compared with test data.

Energy absorption capacity is provided by the static stiffness of the air cushion and by the transient increase of pressure in the cushion cavity and trunk system. Deflection of the air bag under load is such that a considerable increase in cushion area results, and the duct pressure is backed up by the fan. The fan will transiently respond at constant rpm with increase of pressure as the flow is throttled.

Estimation of the transient response of the air cushion system is complex and unreliable. Furthermore the tests show that this transient response makes a major contribution to energy absorption. For the total response, therefore, dependence is placed on the drop test data. However, the static stiffness contribution at constant fan rpm gives the minimum condition and is worth considering by itself.

The energy absorption capacity in ft-lb due to static stiffness (at constant rpm) is represented by the area beneath the heave stiffness curve, Figure 43. For the design case of $p_c/P_j = 0.5$ this is found to be 365,000 ft-lb. Without wing lift this is equal to the kinetic energy of the aircraft at its sink rate.

$$\frac{WV^2}{2g} = 365{,}000$$

$$V = 19.8 \text{ ft/sec}$$

This sink rate can theoretically be achieved therefore without the transient response but using the full stroke in the flat attitude. It is notable that the maximum g is below 3.0. A more practical limit is represented by moving 2/3 of this stroke in which case

$$V = 15.5 \text{ ft/sec}$$

The static stiffness on which this is based may now be compared with the dynamic stiffness determined from drop tests on the 1/2 scale whirling arm model. In these tests a direct record of g versus height was obtained. Figure 51 shows the stiffness comparison. The total response (again using 2/3 of the stroke) gives a sink rate

$$V = 20.8 \text{ ft/sec}$$

In order to determine the variation of sink rate with p_c/P_j the theoretical static stiffness was evaluated for a range of one g trunk pressures, similar to the calculations shown in Section II.E.1 (d). It may be assumed that the transient contribution due to compressing the air in the cushion cavity varies with trunk pressure. The cavity volume is essentially unaltered. On this basis the total sink rate capacity versus p_c/P_j is shown in Figure 52.

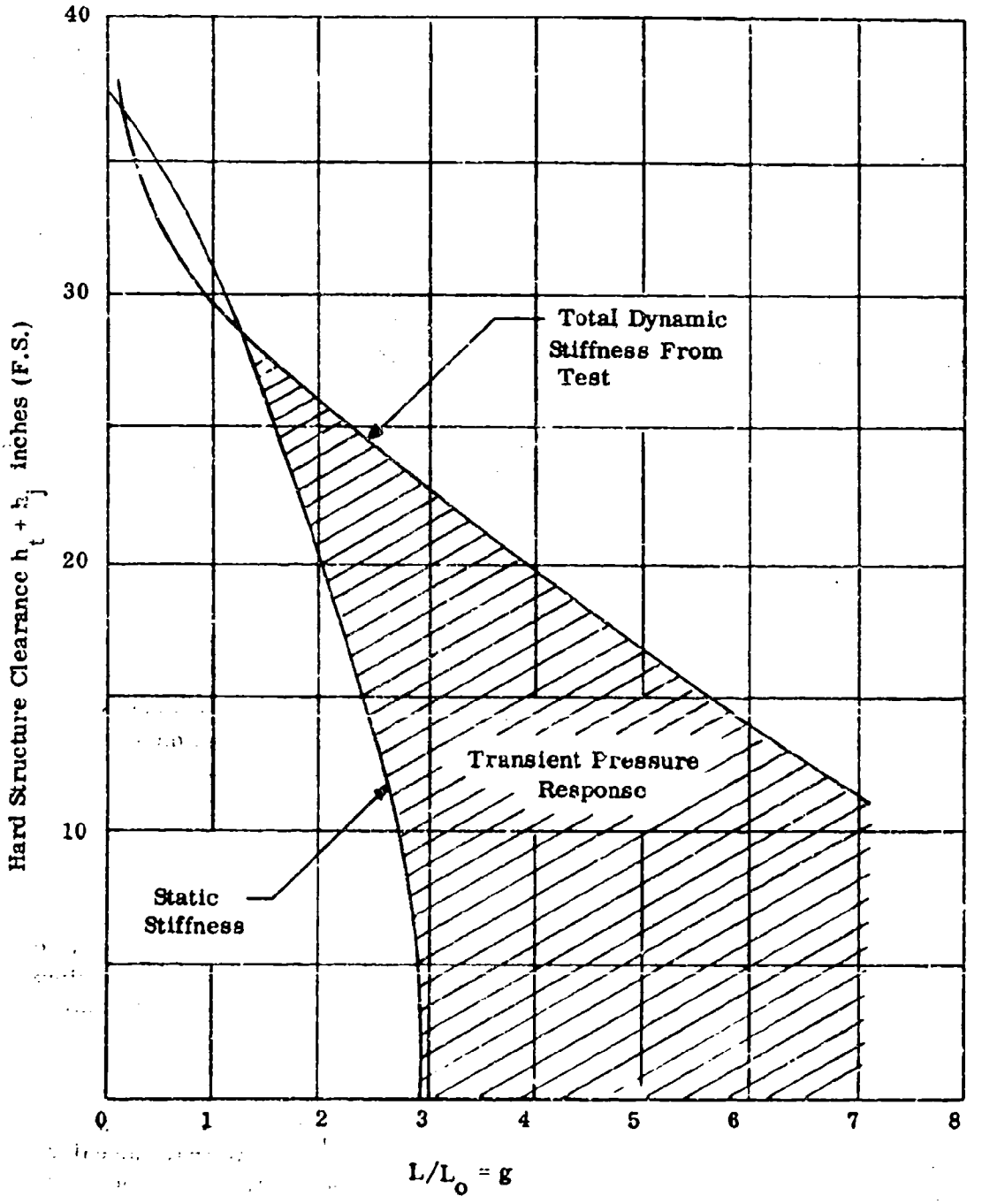

Figure 51. Energy Absorption

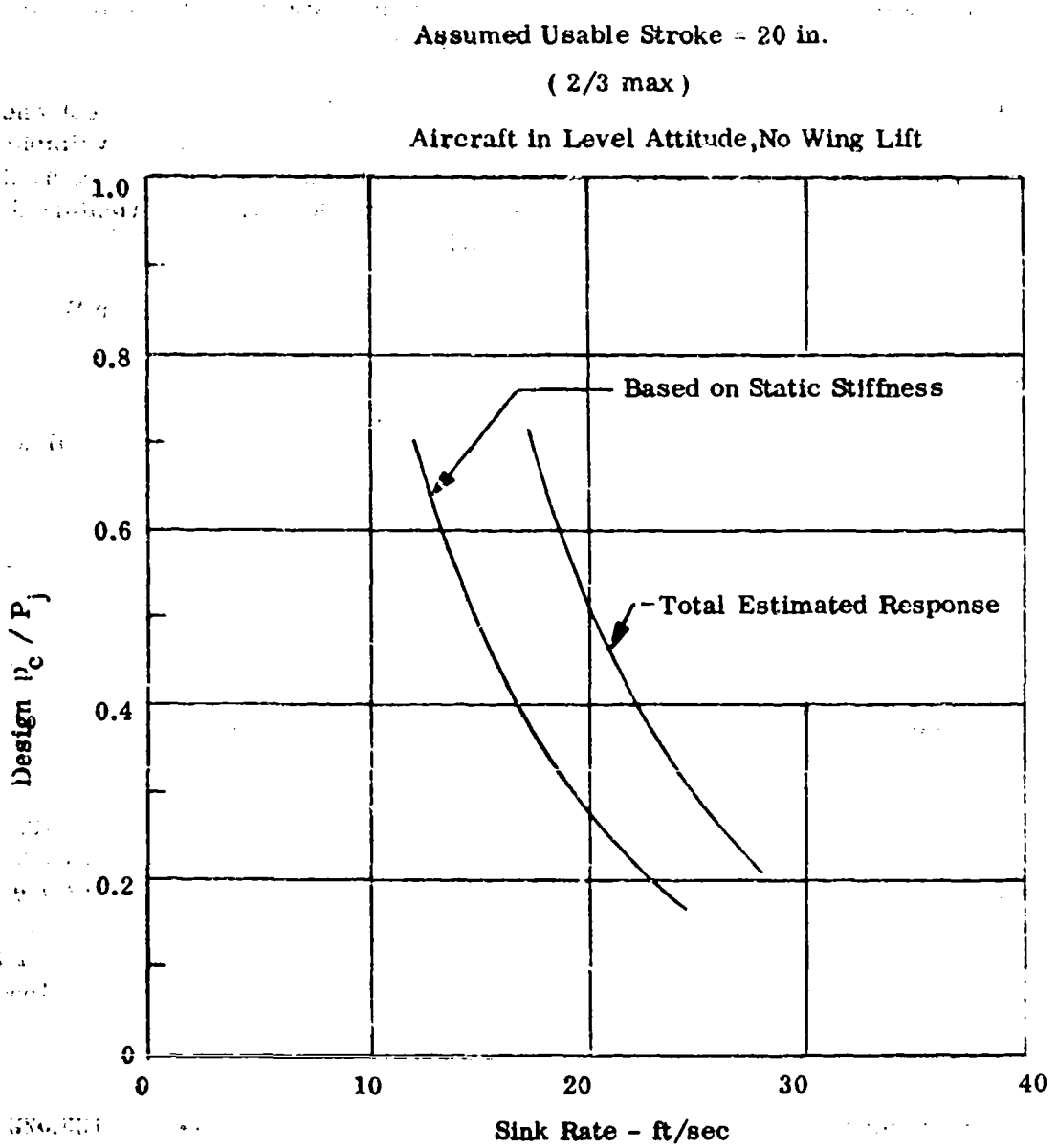

Figure 52. Energy Absorption Variation with P_j

The air cushion is a soft landing system in that it essentially incorporates a long stroke. Thus the sink rate per g tends to be high. The g load is transferred through cushion pressure and trunk attachments to the fuselage. Stress analysis to verify structure is beyond the scope of the present program.

Clearly absorption capacity (in the flat attitude) well beyond the present wheel gear capability is available. It seems probable that adequate reserve is available to tolerate heavy landings at angles of pitch and roll. This may quite simply be handled with equations of motion in two and three degrees of freedom with confirmatory drop tests but is beyond the scope of the present work.

The heave damping provided by the air cushion is analyzed in Section IV.

H. WEIGHT AND BALANCE

The detail weight and balance estimate for the T-67 installation is as follows:

1. Weights and Moment T-67 Engine .

	Weight	c.g. F.S.	Moment
Engine Installation	933		
T-67-T-1 Contin. Twin T/Shaft Eng.	680	218	126,440
Resid. Grease, Oil	6	218	1.308
Gearbox Oil	30		6,030
Engine Oil	30	[illegible]	6,540
Engine Mts.	31	219.1	6,792.1
Engine Exhausts	136	274.8	37,372
Starting System	60	201	12,060
Lubrication System	10	218	2,180
Controls - Engine (Throttle)	25	31.3	782.5
Instruments - Eng. (Incl. Panel)	25	46.6	1,165
Fuel System	386		
Tanks & Supports	356	355.44	126,522
Plumbing, Fill Sys, Venting, Pump	30	355.44	10.662
Fan Installation	646		
Drive Shaft	35	180.84	6.328
Gearbox	113	159.60	18,035
Fan	83	159.60	13,768
Fan Str. Struc-Center, Spinner, Supts.	187	168.00	31,441
Outer, Supts.	202	155.00	38,095
Valves - Inlet, Shutter	18	159.60	2,873

		Weight	c.g. F.S.	Moment
Air Jet Controls		127		
Hyd. aulics	22		58.7	1.291.4
Air Control Valve & Bleed	25		219.84	5,495
Air Control Pneumatic Plumbing	30		363.6	10.908
Control Panels & Wiring	50		214.8	10.740
Trunks		1.291		
Attach to C-119C	323		315.6	101,939
Trunk Fabric	398		315.8	125,609
Boot (Tread)	570		315.6	179,892
Flow Diverter, Cushion Fan		375	157.2	59,000
Total, Air Cushion Landing Sys. Dry		3,758	249.5	936,572

2. Aircraft Balance

Condition	c.g. % MAC	Weight	c.g. F.S.	Moment
Gross Wt.	25	60,000	327.0	19.620.000
Less Cargo	27.4	- 3,537	331.0	- 1.170.000
Less Fuel	41.8	-15.600	355.4	- 5.545.000
Orig. Operating Wt. Empty	18.6	40,863	316.3	12,905.000
Air Cush. L/G		3,758	249.5	937.000
Revised Operating Wt. Empty	14.6	44.621	309.5	13.842.000
Fuel	41.8	15.374	355.4	5.475,000
Revised Gr. Wt.	22.3	60.000	322.5	19.317.000

The c.g. is moved forward by approximately 3% by the addition of the air cushion system. For test purposes it may be assumed that crew is equivalent to normal crew. However, it will be preferable to hold this c.g. to 18% MAC at a minimum flying weight with 2000 lb. fuel. (Ref. 2 P. 178) Ballast is then required in the rear fuselage as follows:

	c.g. % MAC	Weight	c.g. F.S.	Moment
Fuel	41.8	2000	355.4	711.000
Ballast	-	500	500	250.000
Min. Flying Wt.	18.0	47,121	315.3	14.802.000

3. Weights, 2 x T-58 Engines.

	Weight	
Eng. Instl.		988.4
T-58-GE 10 Eng. (2 req'd.)	682	
Resid. Grease Oil	5.4	
Gearbox Oil	15.0	
Eng. Oil	30.0	
Eng. Mts.	40.0	
Eng. Exhausts	56.0	
Starting System	75.0	
Lubrication System	20.0	
Controls - Eng. (Throttle)	35.0	
Instruments - Eng. (Incl. Panel)	30.0	
Fuel Sys.		406
Tank & Supports	356	
Plumbing, Fill Sys, Vent, Pump	50	
Fan Installation		894
Drive Shafts	24	
Gearboxes	190	
Fans	200	
Fan Structure		
Fan Exhausts	180	
Outer Supts.	200	
Inlets	100	

	Weight	
Air Jet Controls		127
Hydraulics	22	
Air Control Valve & Bleed	25	
Pneumatic Plumbing	30	
Control Panels & Wiring	50	
Trunks		1291
Attach to C-119C	323	
Trunk Fabric	398	
Boot (Tread)	570	
Total, Air Cushion Landing Sys., Dry		3706

4. Comparison

Major groups are compared as follows:

	T-67	2 x T58
Engine Installation	933	988
Fuel System	386	386
Fan Installation	646	894
Air Jet Controls	127	127
Trunks	1291	1291
Flow Diverter	375	-
Total	2758	3706

5. Weight Tradeoff

These weights are for the test installations proposed. In an operational installation it is probable that weight can be somewhat reduced. For example the fuel system weight is based on the use of existing long range tanks. Allowing 10 minutes fuel, this weight would be reduced to approximately 200 pounds for the T-67 installation, for a total weight of approximately 3500 pounds (wet).

The weights not proportional to the installed power are the jet controls, trunks and flow diverter which account for 46.5% of the gross system weight. To examine the tradeoff of system weight with jet height; rather than compare these alternative installations in which the fan types and engine specific weights are different, it will be assumed that the remaining 53.5% varies with power. A fixed overall efficiency of 0.7 is combined with the hp_j/h figure derived in Section II.C. to produce the tradeoff shown in Figure 53.

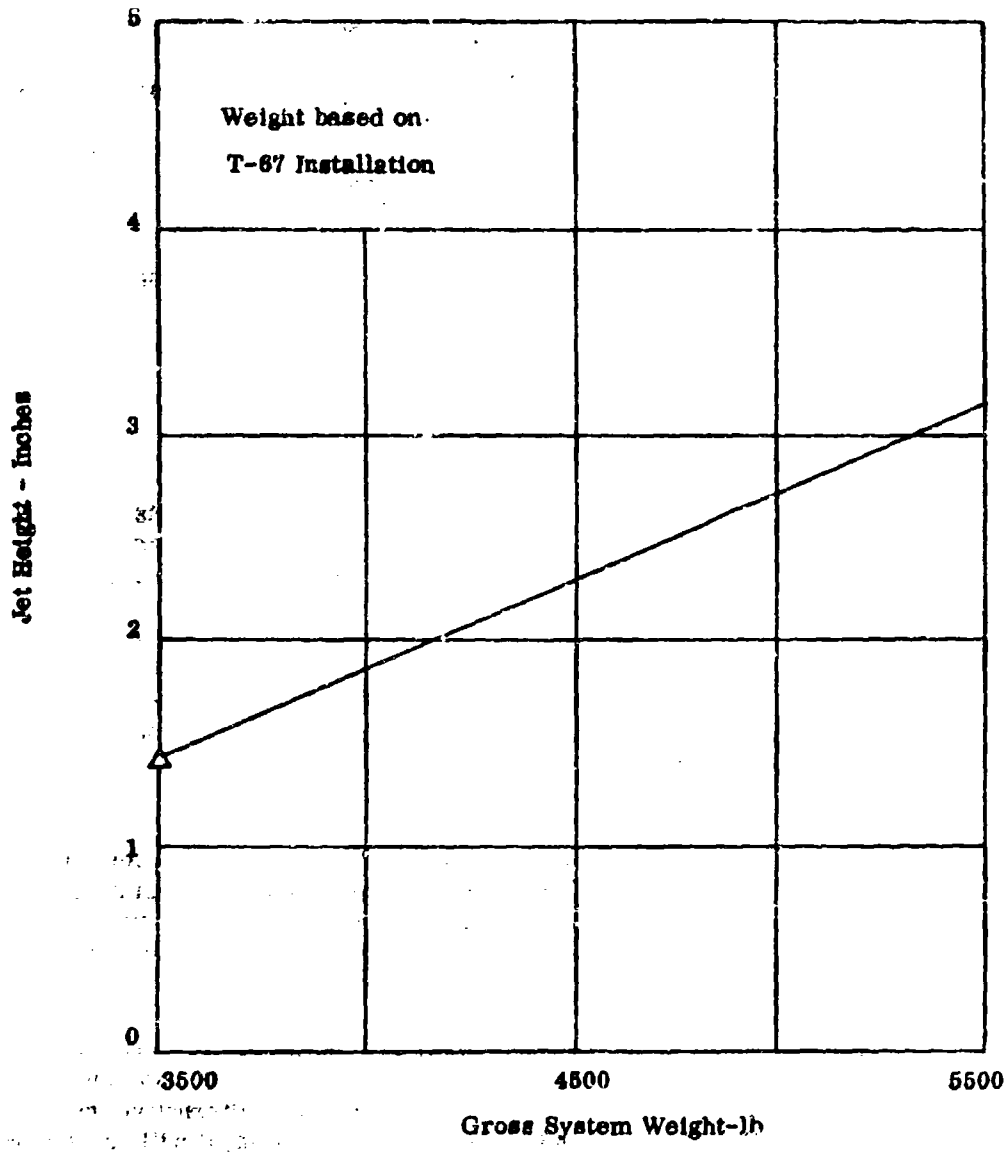

Figure 53. Jet Height and System Weight Tradeoff

I. TAKEOFF AND LANDING PERFORMANCE

1. Comparative Takeoff Distances.

Unstick speed of 1.2 V_{SI} will be used, and also average forces at 0.7 x unstick speed (Reference 5).

Ground roll distance is calculated from

$$s_1 = \frac{W}{2g} \times \frac{V_{SI}^2}{T-D}$$

V_{SI} = 153 ft/sec (See Section II.F.2.)

$0.7\ V_{SI}$ = 107 ft/sec

Thrust and drag forces are plotted against speed in Figure 54. Thrust is obtained directly from Reference 2 and induced drag Oswald efficiency factor is found from Figure 12 of Reference 2 as follows. Other drag and thrust factors are as used in Section II. F. 3 and II. D.4., except for overwater wave drag which is derived in paragraph d. of this section.

$$C_{D_i} = C_L^2/\pi \times AR \times e$$

At C_L = 1.0 C_D = 0.081

C_{D_o} = 0.025

C_{D_i} = 0.056

$$\text{Aspect ratio} = \frac{109.25^2}{1447} = 8.25$$

$$e = \frac{1.0}{0.056 \times \pi \times 8.25} = 0.69$$

$C_{L_{\text{ground run}}}$ = 0.65 , $C_{D_{i\ \text{ground run}}}$ = 0.024

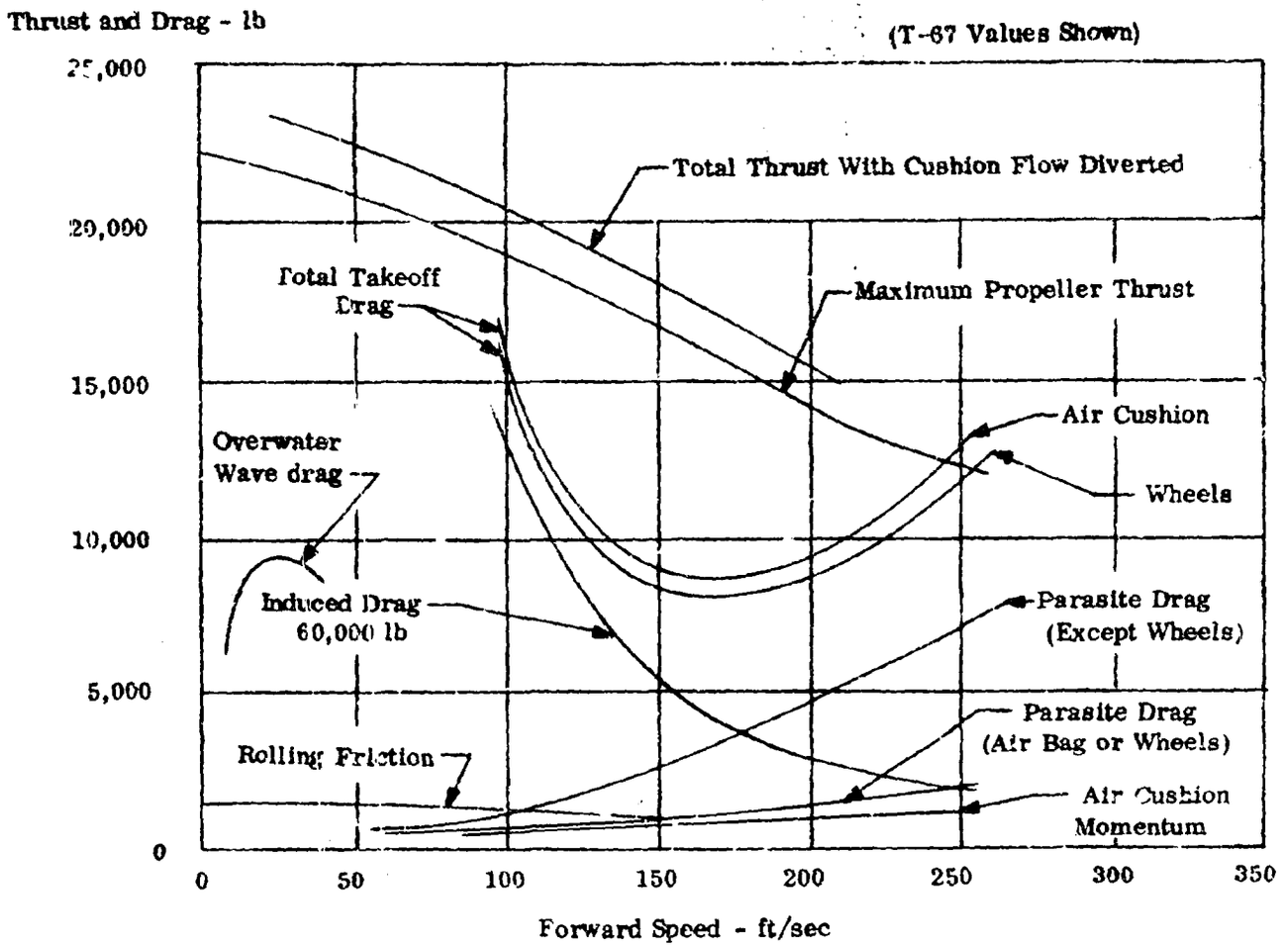

Figure 54. C-119 Thrust and Drag

	Wheels		Air Cushion	
Thrust		18,800		18,800
Parasite Drag	1620		1600	
Induced Drag	473		473	
Rolling friction	1180		0	
Air Momentum	0		450	
		3273		2523
		15,527		16,277
Ground roll distance s_1, ft.		1404		1340

Transition distance is the curved flight path between the unstick point and the position above the intersection of the climb-out flight path with the ground plane. (See Reference 5.) Acceleration to climb-out speed V_2 takes place. V_2 is the optimum climb speed in the takeoff configuration. The distance is given by

$$s_2 = \frac{W}{2g} \times \frac{(V_2^2 - V_{SI}^2)}{T-D}$$

V_2 ft/sec	160		160	
T-D, lb	8350		7800	
Transition distance s_2, ft.		245		262

Initial climb is at V_2. Initial climb to 50 ft. distance is obtained from angle of climb.

$$s_3 = \frac{50}{\tan\gamma} \quad \text{where} \quad \sin\gamma = \frac{T-D}{W}$$

T-D lb.	8200		7650	
γ, degrees	7.85		7.31	
Climb distance s_3, ft		362		389
Time, sec	2.28		2.45	
Climb, rate, ft/min.	1315		1220	
Total $s_1 + s_2 + s_3$, ft	2017		1991	

It is seen that the elimination of rolling friction on the ground roll gives the air cushion a slight advantage. At the higher power level with increased momentum drag the difference will be negligible.

2. Use of Cushion Flow Diverter

It is expected that the cushion flow diverter will allow very fast retraction. Flow to the cushion is completely cut off as soon as "deflate" is selected, the elastic material snaps back immediately and the volume of air to be exhausted from the air cushion trunk is small compared with the inflated flow rate, e.g.

Approx. trunk volume = 1250 ft^3
Normal volume flow rate = 1900 ft^3/sec
Time to empty at max flow rate = 0.66 secs

In fact a logarithmic decay will occur. It will be arbitrarily assumed that the trunk is effectively deflated in one second. Thus, if the trunk is retracted on the initial climb at 160 ft/sec., thrust is increased to 17,600 lb. (Figure 54). Drag is reduced by the momentum drag (included in the net thrust increment) and bag drag, to 7100 lb.

T-D = 10,500 lb.
= 9.9 deg.
Climb rate = 1,650 ft/min.

This would reduce the initial climb distance by about 70 to 320 feet. However, in the case of engine failure at the critical point in takeoff, the advantage is very significant. Inspection of the thrust-drag plot shows this aircraft has no climb rate in the takeoff configuration on one engine, even omitting the drag of a windmilling propeller, and the associated asymmetric trim drag.

With cushion flow diverted:

T	= 17,600	- 8100	= 9500 lb
D, bag inflated	= 8050		
Deduct bag drag	- 770		
Add windmilling	+ 835		
Add trim drag	+ 175		
Total drag			8290 lb
T-D			1210 lb

Windmilling and trim drags are found in Reference 2 Figures 127 and 131.

γ = 0 022
Climb rate = 193 ft/min.

Single engine thrust and drag are plotted in Figure 55. The poor single engine performance of the C-119 emphasizes the advantage of the thrust diverter. However, its use to back up the single-engine failure case should allow for better power matching in most aircraft designs.

3. Landing Distance

Landing distance will be principally dependent on deceleration. Demonstration of the capability of the air cushion scheme to achieve equivalent braking to wheels in the manner described in Section II.2 is beyond the scope of this program. A specimen landing distance calculation which illustrates performance required from the cushion braking system is as follows. (The method given in Reference 5 is used):

For the calculation, approach speed is taken as 1.3 V_{SO} where V_{SO} is the stalling speed in the landing configuration. A normal flare with nose wheel lowered at 95 knots is assumed. Also normal reverse thrust application from 90 to 150 knots with brake application from 60 knots to rest will be compared with full reverse thrust to bring the aircraft to rest without brakes in the air cushion case. This shows the importance of cushion braking. Power off approach at 60,000 lb is first considered:

$C_{L_{max}} = 1.76 \quad (T_c = 0$, Reference 2)

$q = W/SC_L = 60{,}000/(1447 \times 1.76)$

$= 23.5 \text{ lb/ft}^2$

$V_{SO} = 140.5 \text{ ft/sec} = 83.3 \text{ kt}$

$1.3\ V_{SO} = 183 \text{ ft/sec} = 108.4 \text{ kt}$

		Wheels	Air Cushion
Takeoff configuration drag from Figure 54	lb	8200	8800
Incremental landing flap drag, ($\Delta C_D = 0.026$)	lb	1490	1490
Total drag,	lb	9690	10,290
D/W		0.1615	0.171
Glide Path - deg.		9.26	9.8

For this high weight case, it will be assumed that the approach is made with power on at 20% thrust to avoid the above steep approach and that slightly more power is used in the air cushion case to give the same approach angle. Approach speed will be somewhat reduced because of the slipstream lift of the flap. At $T_c \approx 0.13$,

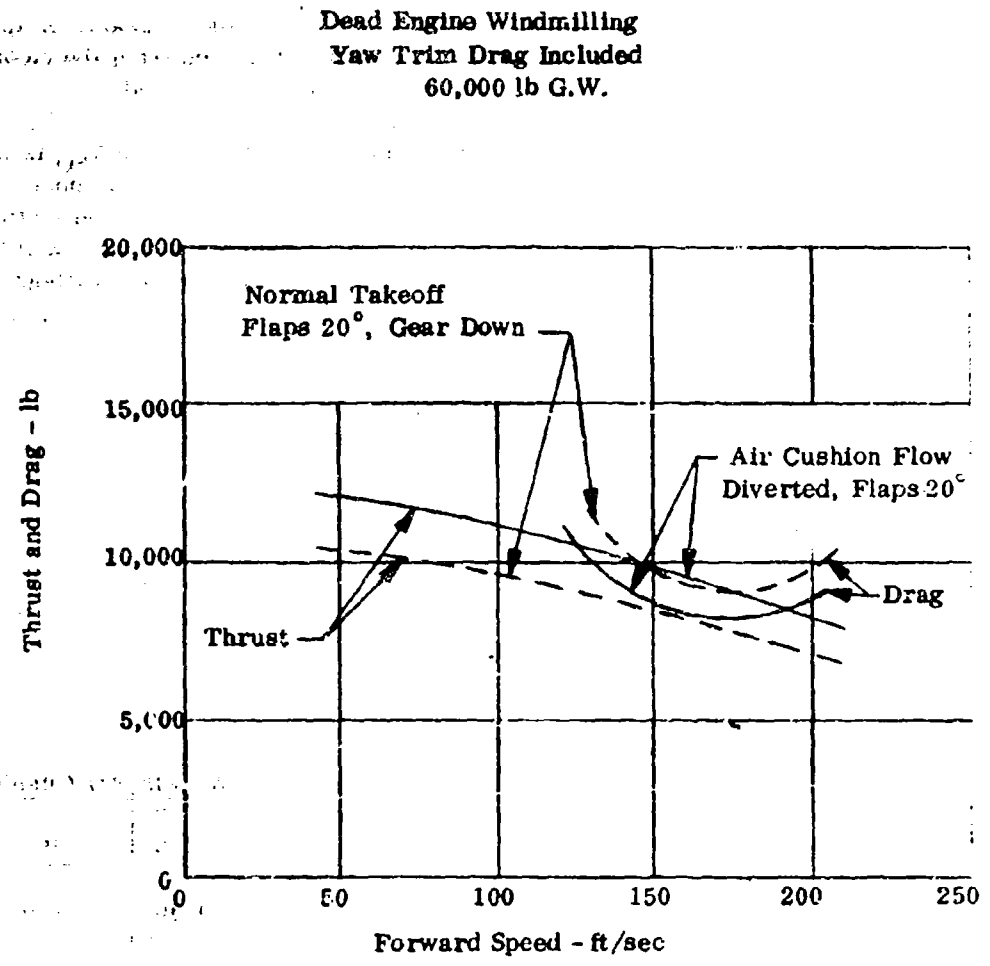

Figure 55. C-119 Single-Engine Performance

$C_{L_{max}} = 1.93$

$1.3\ V_{SO} = 108.4 \times \sqrt{1.76/1.93} = 103.8$ knots

Takeoff drag from Figure 54 ,	lb	8000	8900
Landing flap drag ,	lb	1360	1360
Total drag		9360	9360
20% Thrust (See Figure 54) ,	lb	3100	3100
D-T ,	lb	6260	6260
(D-T)/W		0.104	
Approach angle, deg.		6.0	

Airborne distance is calculated using the method of Reference 5 Sht EG 6/3.

$$h_f = \frac{0.799 \times 103.8^2 \times (0.104)^2}{2}$$

$= 46.6$ ft

The flare is started below the 50 foot screen height. Hence,

$$s_a = 0.799 \times 103.8^2 \times 0.104 + \frac{50-46.6}{0.104}$$

$= 895 + 33$

$= 928$ ft

Also,

$$V_T = \sqrt{103.8^2 - (0.104 \times 928 - 50)\ 22.6}$$

$= 98.5$ knots

Forward thrust is cut off at touchdown.

Ground roll distance is considered in sectors. (Reference 5 Sht EG 6/4)

		Wheels	Air Cushion
(I) Touchdown to level off at 95 kt	C_L	1.32	1.32
	C_{D_I}	0.096	0.096
	C_{D_o}	0.051	0.051
	C_D	0.147	0.147
Average q = 32 lb/ft^2			
Aerodynamic drag C_D Sq ,	lb	6800	6800
Momentum drag (Figure 37) ,	lb	-	695
	D, lb	6800	7495
$s = \frac{V_2^2 - V_1^2}{2g} \cdot \frac{W}{D}$,	ft	260	240
(II) 95 kt to 90 kt)	C_L	0.625	
at $\alpha_{TL} = 0$ $T_c = 0$)	C_{D_I}	0.0219	0.0219
Bag profile reduced 50%)	C_{D_o}	0.051	0.042
on ground)			
	C_D	0.073	0.064
Aerodynamic drag ,	lb	3060	2690
Momentum drag ,		-	662
Rolling friction μR (R = 35,700 lb) ,	lb	840	
	D, lb	3900	3352
	s, ft	630	730
(III) 90 kt to 60 kt: At 80 kt,			
Aerodynamic drag* ,	lb	1670	1390
Momentum drag ,	lb		537
Rolling friction (R = 50,000)* ,	lb	1250	-
Reverse thrust (Figure 59) ,	lb	14,700	14,700
	D-T, lb	17,620	16,627
$s = V_2^2 - V_1^2 \cdot \frac{W}{D-T}$,	ft	670	720

* Lift and drag decrements $\Delta C_L = 0.3, \Delta C_D = 0.02$ for reverse thrust are assumed.

			Wheels	Air Cushion Braked	Air Cushion Unbraked
(iv) 60 kt to 50 kt:					
At 57 kt,					
Aerodynamic drag,		lb	840	700	700
Momentum drag		lb	-	410	410
Braking force (μ 0.4)		lb	22,100	22,100	-
Reverse thrust		lb	12,300	12,300	12,300
	D-T	lb	35,240	35,510	13,410
	s	ft	90	90	240
(v) 50 kt to rest					
At 35 kt					
Aerodynamic drag		lb	440	380	260
Momentum drag		lb	-	250	250
Braking force			22,500	22,500	-
Reverse thrust			-	-	10,000
	D-T	lb	22,940	23,130	10,510
	s	ft	290	290	640
Total ground roll distance		ft	1,940	2,070	2,570
Airborne distances		ft	928	928	928
Total distance from 50 ft		ft	2,868	2,998	3,498
Energy absorption distribution:					
Aerodynamic drag Airborne			5.80	5.80	5.80
ft-lb x 10^{-6}	(i)		1.77	1.63	1.63
	(ii)		1.93	1.97	1.97
	(iii)		1.12	1.00	1.00
	(iv)		0.08	0.06	0.17
	(v)		0.13	0.11	0.17
Total			10.83	10.57	10.74
Momentum drag	(i)		-	0.17	0.17
	(ii)		-	0.48	0.48
	(iii)		-	0.39	0.39
	(iv)		-	0.04	0.10
	(v)		-	0.07	0.16
Total			0	1.15	1.30
Wheel and braking drag					
	(ii)		0.53	-	-
	(iii)		0.84	-	-
	(iv)		1.99	1.59	-
	(v)		6.53	6.52	-
Total			9.89	8.52	0

		Wheels	Air Cushion Braked	Air Cushion Unbraked
Reverse thrust	(iii)	9.85	10.59	10.59
	(iv)	1.11	1.11	2.96
	(v)	-	-	6.40
Total		10.96	11.70	19.95
Total ft - lb x 10^{-6}		31.68	31.94	31.99

Energy of aircraft at approach speed, at screen:

$$h \times W + \frac{WV^2}{2g} = 50{,}000 \left(\frac{103.8^2 \times 2.852}{64.4} + 50\right) = 31.65 \times 10^6$$

Distance is increased from about 3000 to 3500 feet when reverse thrust is used as a substitute for braking. In this case reverse thrust (which appears to be very effective on the C-119)absorbs about 2/3 of the total energy.

4. Overwater Takeoff

The central factor in overwater takeoff is the wave drag at hump speed. This wave is caused by the vehicle. As soon as it can climb on to it wave drag decreases rapidly (similarly to planing boats). It is not necessary in theory for the vehicle to touch the water, the wave being caused by movement of the water depression. Depth of depression is displacement, or cushion pressure divided by water density. Wave drags, speeds and displacements are calculated for contrasting configurations Nos. 1 and 3 as follows: (See Reference 6 Figure D-2)

$$\frac{D_W}{W} = \frac{4\, C_w\, W}{S \times 1 \times \rho\, W}$$

Configuration		1	3
Cushion area S_c ft^2	Main	360.5	166.3
	Nose	-	20.8
Cushion length l ft	Main	33.9	16.9
	Nose	-	5.15
Load, lb (Section II.3.d(2))	Main	60,000	53,450
	Nose	-	6,550
Cushion Pressure lb/ft^2	Main	166.5	321
	Nose	-	315

		1	3
Displacement, inches		31.9	52
C_W =	Main	0.48	0.65
	Nose	-	0.75
D_w, lb	Main	9,040	42,000
	Nose	-	19,200
	Total	9,040	61,200
D_w/W		0.1505	1.02
V_h, ft/sec		23.5	14

The wave causing the drag is driven up before the bow of the vehicle. The theory is invalid if this bow wave is breaking. The wave will "break", i.e., tumble over at its crest and form a "white-cap" if it becomes very steep. For configuration 3, the calculated wave drag is probably very pessimistic since a D_w/W in the order of 0.2 will cause a sufficiently steep wave for breaking. However, in the case of the short cushion it is extremely unlikely that with a displacement of nearly 4 1/2 ft, and such an enormous calculated drag, that any overwater capability is available.

5. Cross-Wind Landing Profile

The air cushion landing gear has no side load capability. It behaves like a freely castering wheel system at all times. Thus, it is possible to make takeoffs and landings without the necessity for heading along the track.

In cross wind takeoff at maximum thrust any tendency to drift sideways off the track is easily countered by yawing through a small angle to provide the necessary component from the thrust.

Cross wind landings can be made approaching with the wings level and without kicking for yaw just before touchdown. However, during the landing rollout down to taxi speed, the sideways drift tendency is less obviously controlled and use of forward thrust is not acceptable. Reverse thrust is available, however and the following is a natural control sequence for use in cross wind landing rollout:

(a) Touchdown heading into relative wind. (Yawed off the track, nose toward the direction from which the wind is coming). After touchdown increase this yaw angle off track to provide body side force balancing decelerating aerodynamic drag components normal to track, preparatory to reverse thrust application.

(b) Yaw out of wind to head toward track (possibly by using cushion brakes) continuing the yaw to head off track away from the wind as reverse thrust is applied. Reverse thrust component then balances body sideload due to sideslip as well as decelerating drag component.

The forces involved are illustrated in the diagrams in Figure 56 (a) and (b). Unfortunately, no side load due to sideslip data for the C-119 is available. Variations in axial and lateral body forces must therefore be estimated. Figure 57 reproduces some typical ACV force variations with sideslip angle. This type of variation is assumed in the present instance, the lateral force being assumed to reach a coefficient C_Y of 1.0 at 90° based on body side area* (corresponding to the value used in Section II.5.a (3) (b) and the axial force decaying with angle from the total level attitude C_{D_O} in the landing configuration. The momentum drag will be assumed to vary with V^2 for simplicity, introducing a very small error. This C_D is the same as that used in the take-off calculation, plus the incremental drag for landing flap:

$C_D = D/Sq$	=	2523/(1447 x 13.65)
	=	0.128
ΔC_D flap	=	0.026
		0.154

The assumed coefficients are plotted in Figure 58 based on wing area. (Body side area/wing area = 470/1447 = 0.325).

Maximum reverse thrust is given in Reference 2 Figure 129. It is plotted versus speed as a coefficient referred to wing area in Figure 59.

In Figure 56

$$X = C_x Sq + T_R$$

$$Y = C_y Sq$$

Resolving laterally and reducing to coefficients

$$(C_x + C_T) \sin \psi = C_y \cos \psi$$

Also $$V_W/V_G = \tan (\psi - \beta)$$

$$V_W/V = \sin (\psi - \beta)$$

Values of ψ and β were obtained by solving these equations for a range of ground speeds and the results are plotted in Figure 60 as yaw angle against speed. Relative wind heading is also shown to illustrate sideslip angle, the difference between this and the aircraft heading. After release of reverse thrust and brakes for taxi the aircraft is turned into wind and forward thrust applied for control. To remain stationary without brakes on it is of course necessary to head into wind and apply some thrust.

* It is assumed that the aircraft less tail has neutral directional stability. Therefore, the total tail load is zero for all sideslip angles.

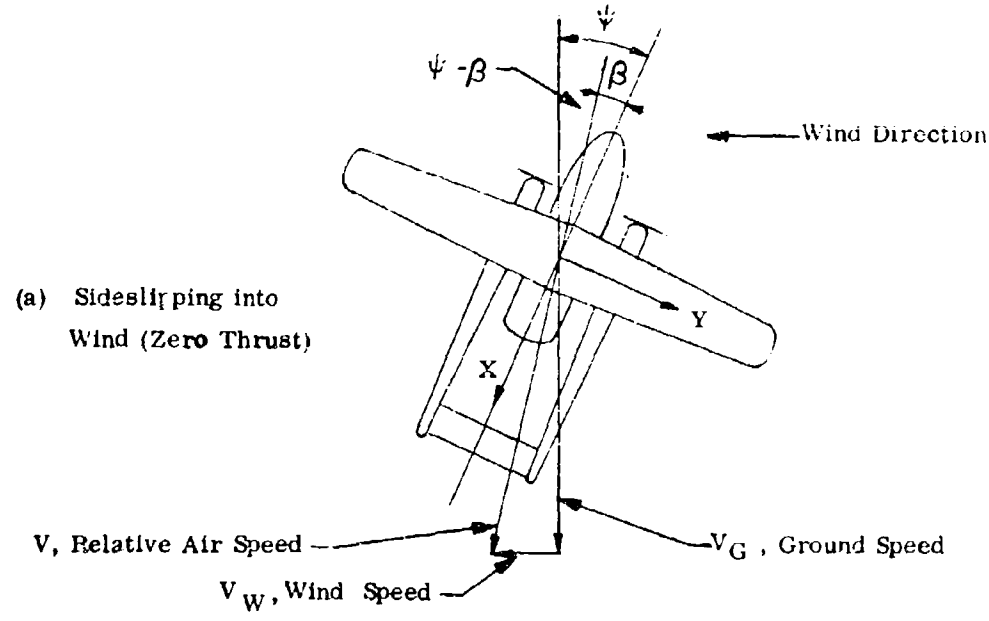

(a) Sideslipping into Wind (Zero Thrust)

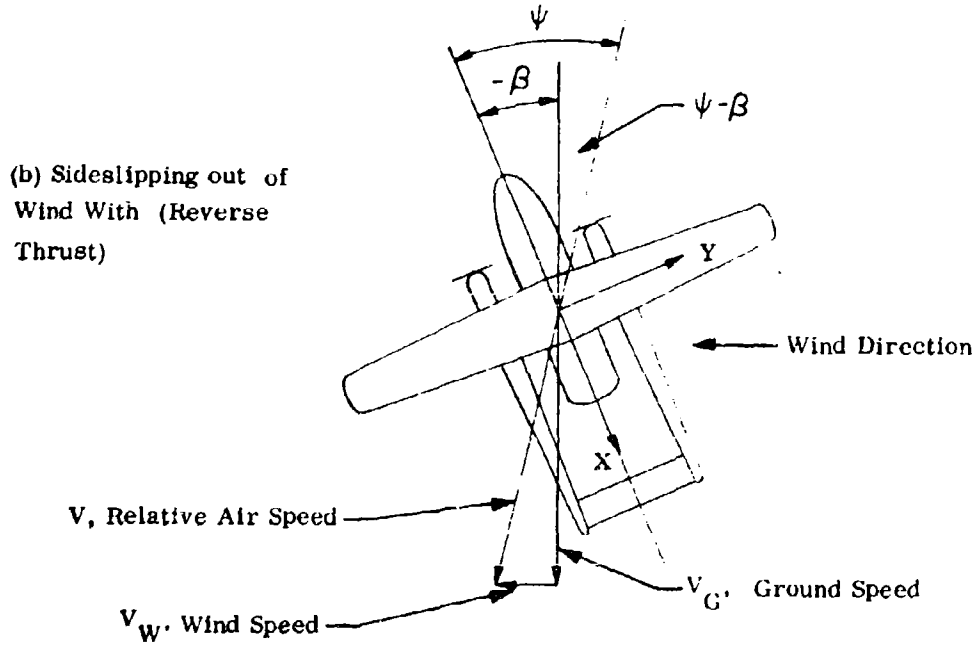

(b) Sideslipping out of Wind With (Reverse Thrust)

Figure 56. Ground Roll Attitude

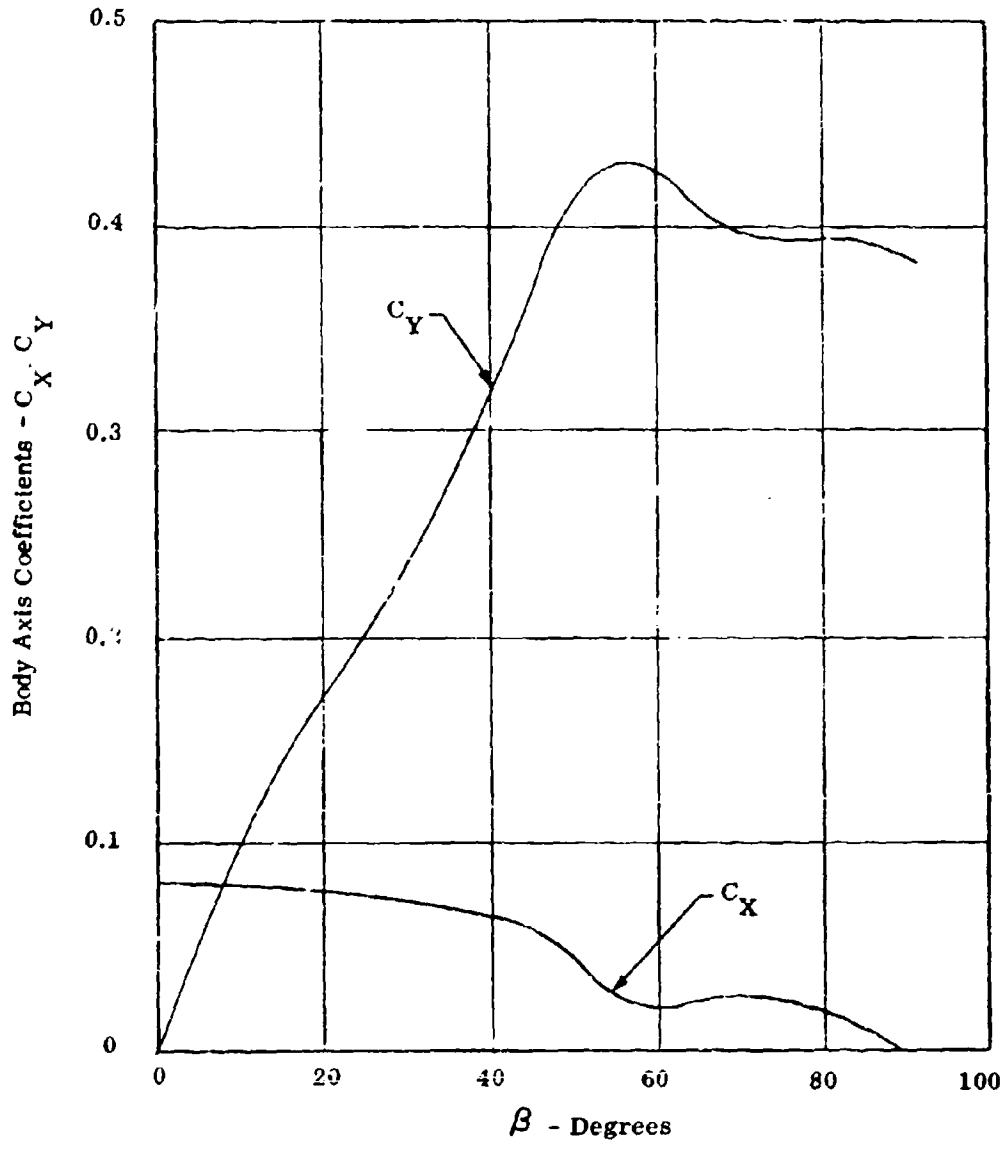

Figure 57. Typical ACV Sideslip Data

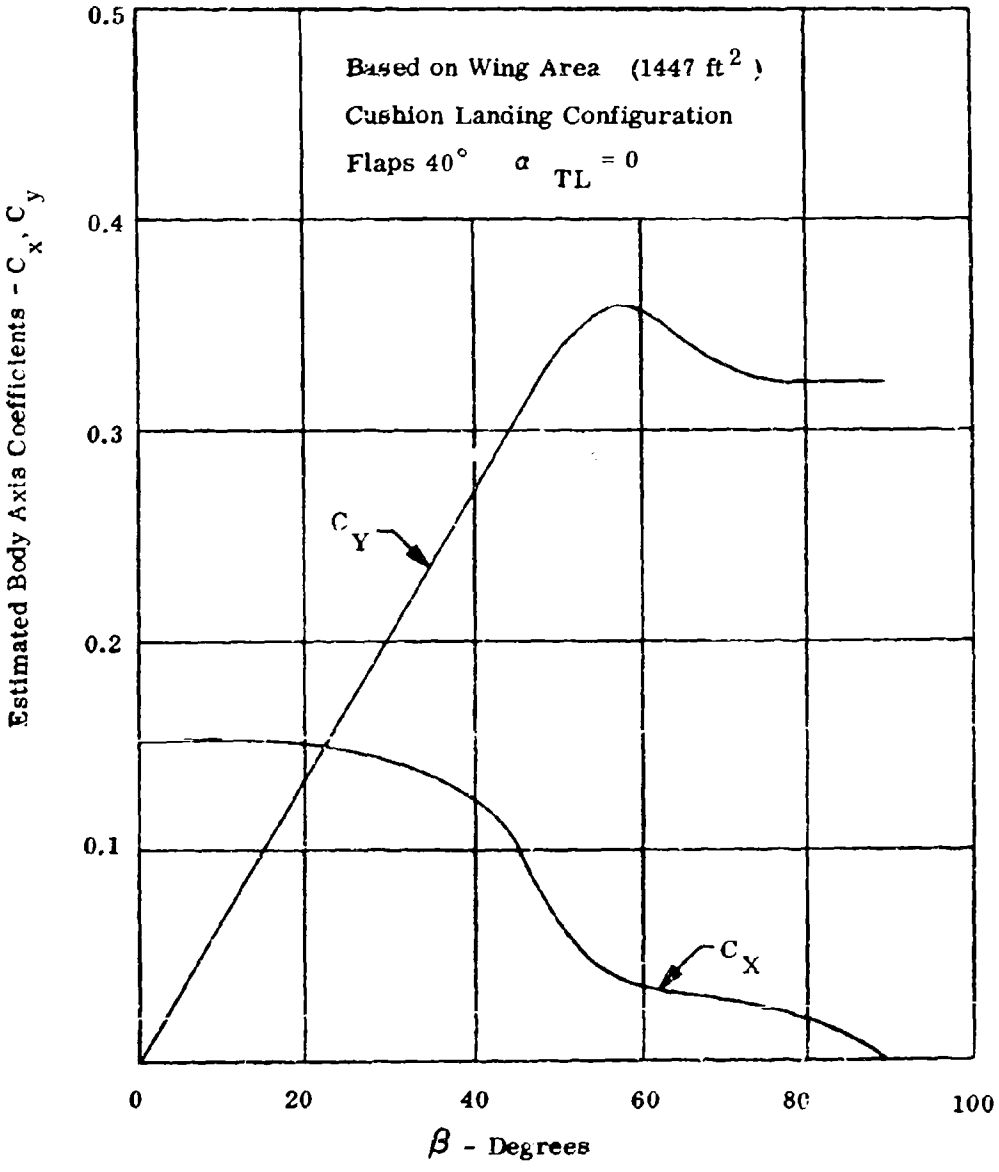

Figure 58. C-119 Sideslip Coefficients

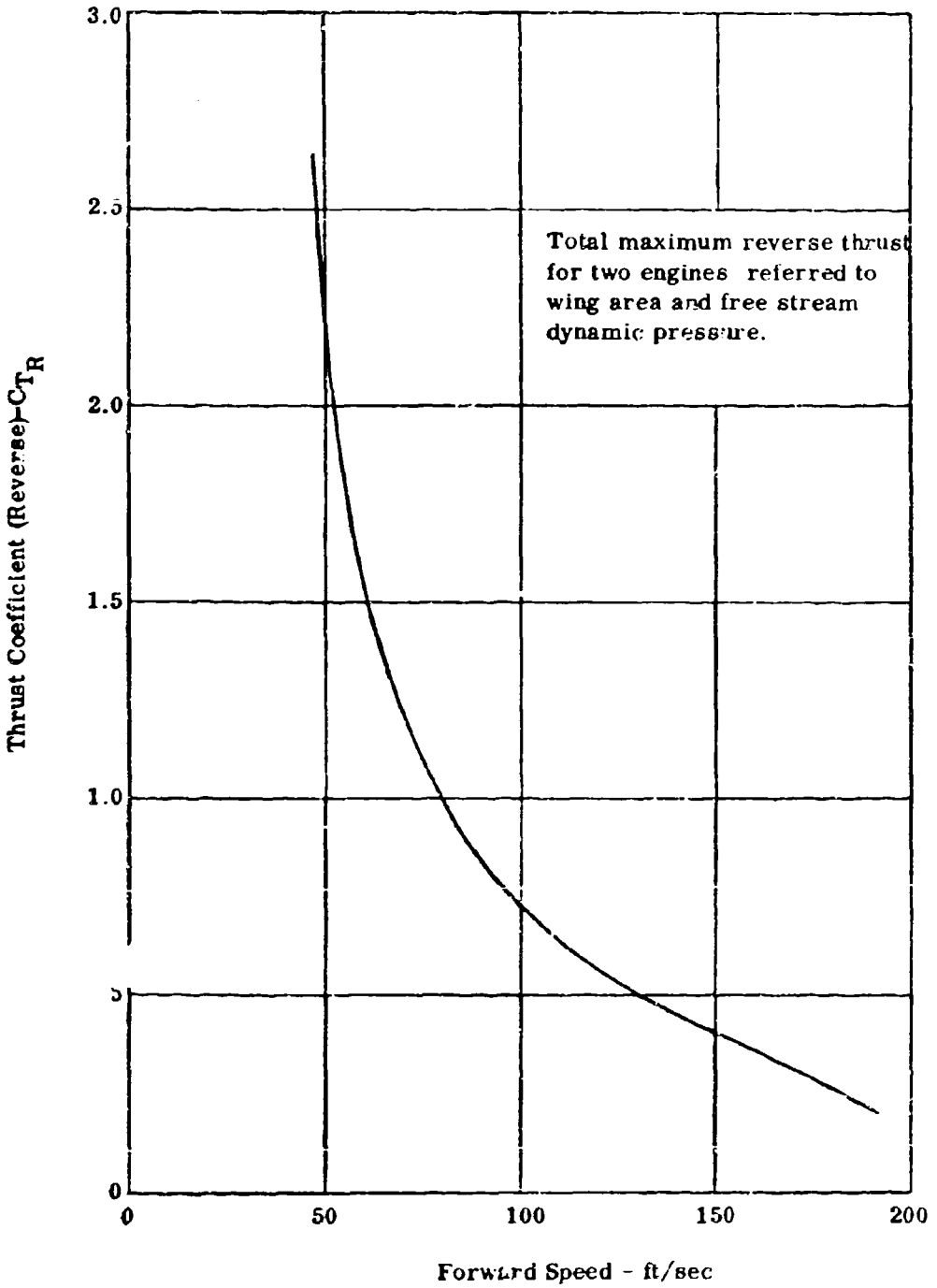

Figure 59. C-119 Reverse Thrust Coefficient

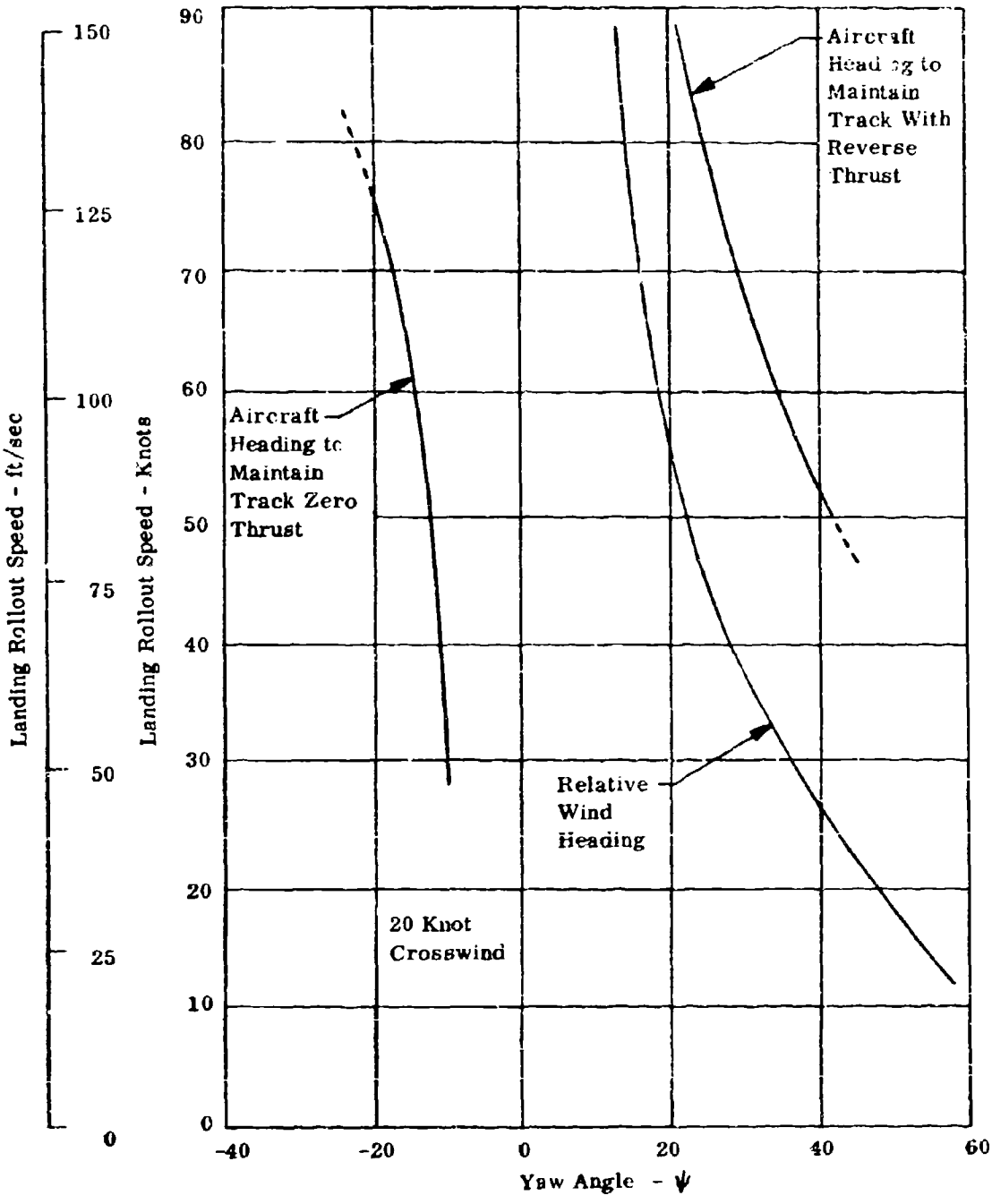

Figure 60. Crosswind Landing Yaw Angles

It is expected that cushion braking will be designed to provide some directional stability. It will also be noted that brakes do not provide side force.

Other means of control, such as the application of cushion momentum to provide side force either directly or by rolling the aircraft slightly and the influence of aerodynamic wing lift due to roll have not been studied. The natural tendency is to roll into wind, bringing these forces into play.

III. WIND TUNNEL MODEL TESTS AND ANALYSIS

A. MODEL DESCRIPTION

Figure 61 is an assembly drawing of the wind tunnel model. The model itself is made of fiberglass and wood; the wing, flaps, each tail boom and fin, the horizontal stabilizer, elevator and fuselage being separate components.

The fuselage is made in two pieces, an upper and lower fiberglass shell which nest together. The air cushion trunk is mounted to the lower shell which is easily removable as a unit. An air plenum chamber is mounted in the upper shell, sealing against the lower shell on assembly. This plenum has a hollow ball joint mounted at the top forming an air seal. The male portion is pinned to the female forming a pitch pivot. A two-inch inside diameter ball bushing is fixed inside the male portion and through this the hollow mounting shaft slides so that the model is free to rise and fall. The mounting shaft is fixed at its top end to a six-component strain gage balance on the end of the tunnel sting. High pressure air is piped to the model from an external source in a 0.5 inch steel line mounted beneath the sting. This pipe is coiled about a longitudinal axis so as not to introduce additional stiffness into the drag balance. It is then connected across the balance into the mounting shaft with a rigid connection. The mounting shaft has a cap on its lower end which incorporates radial holes feeding air to the model plenum. The cap also serves as a bottom stop so that the model can be raised from the ground (air off) by elevating the sting. The top stop, against which the model rests when the lift is greater than the weight, is a pin through the mounting shaft.

A 24-volt electric motor is mounted forward inside the fuselage, and control wires run past the air plenum out through holes in the rear of the upper shell to connect to lugs above and below the elevator. This provides remote control of elevator position.

Rotary potentiometers are fitted to the pitch pivot and elevator drive motor shaft in order to measure angle of attack and elevator angle. A 10-inch linear potentiometer is clamped to the mounting shaft for a record of height. Motor control and potentiometer wiring as well as trunk and cushion pressure tap tubing are led out through the upper shell, fixed to the mounting shaft fairing and then looped across the balance inside the sting fairing.

Two lower fuselage shells were available for the tests and are interchangeable. An elastic trunk was attached to the first configuration and the other three configurations which were all inelastic were attached to the other one. It is shown disassembled from the model in Figure 62. It has the basic inelastic configuration attached.

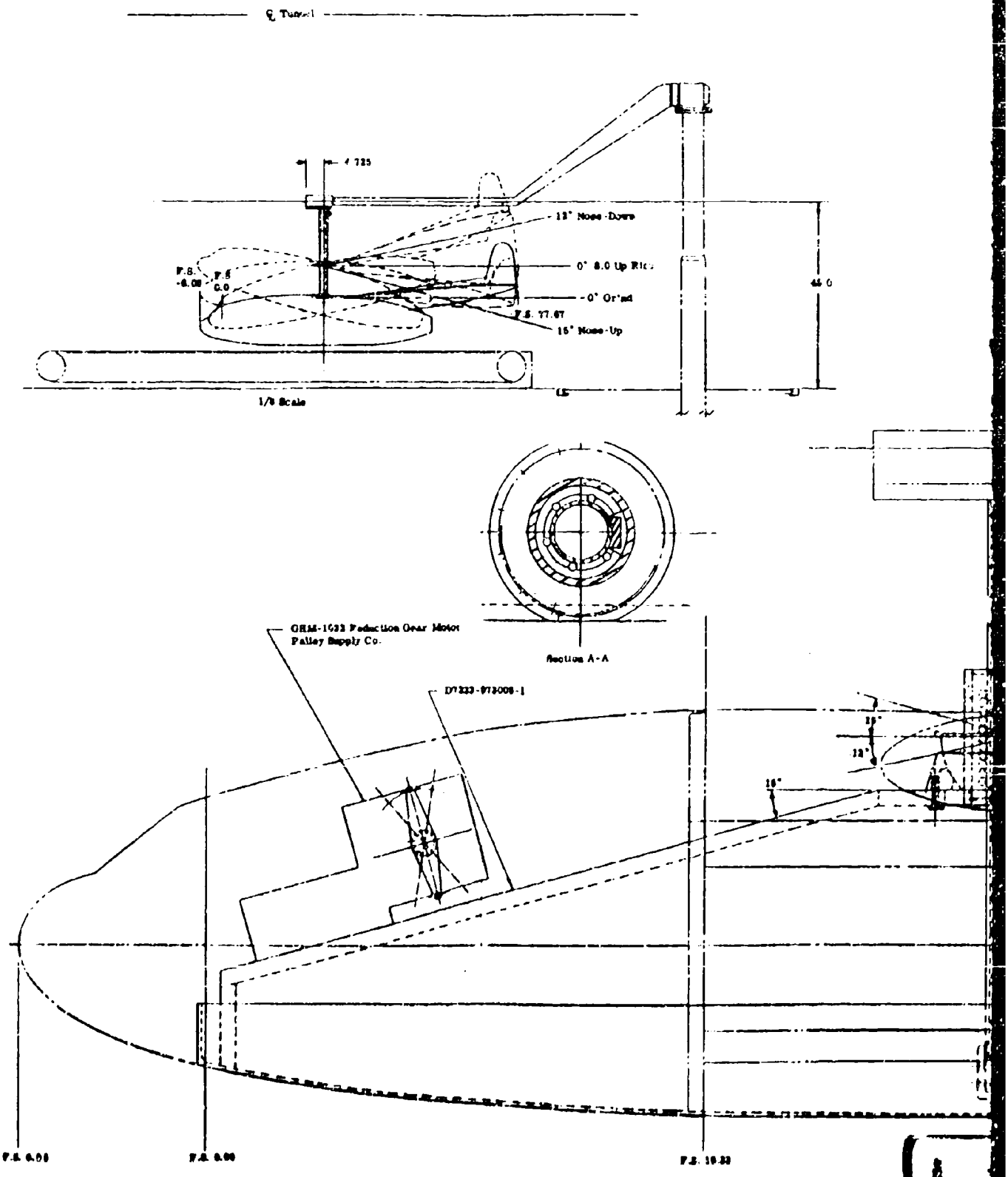

Figure 61. Wind Tunnel Model Assembly

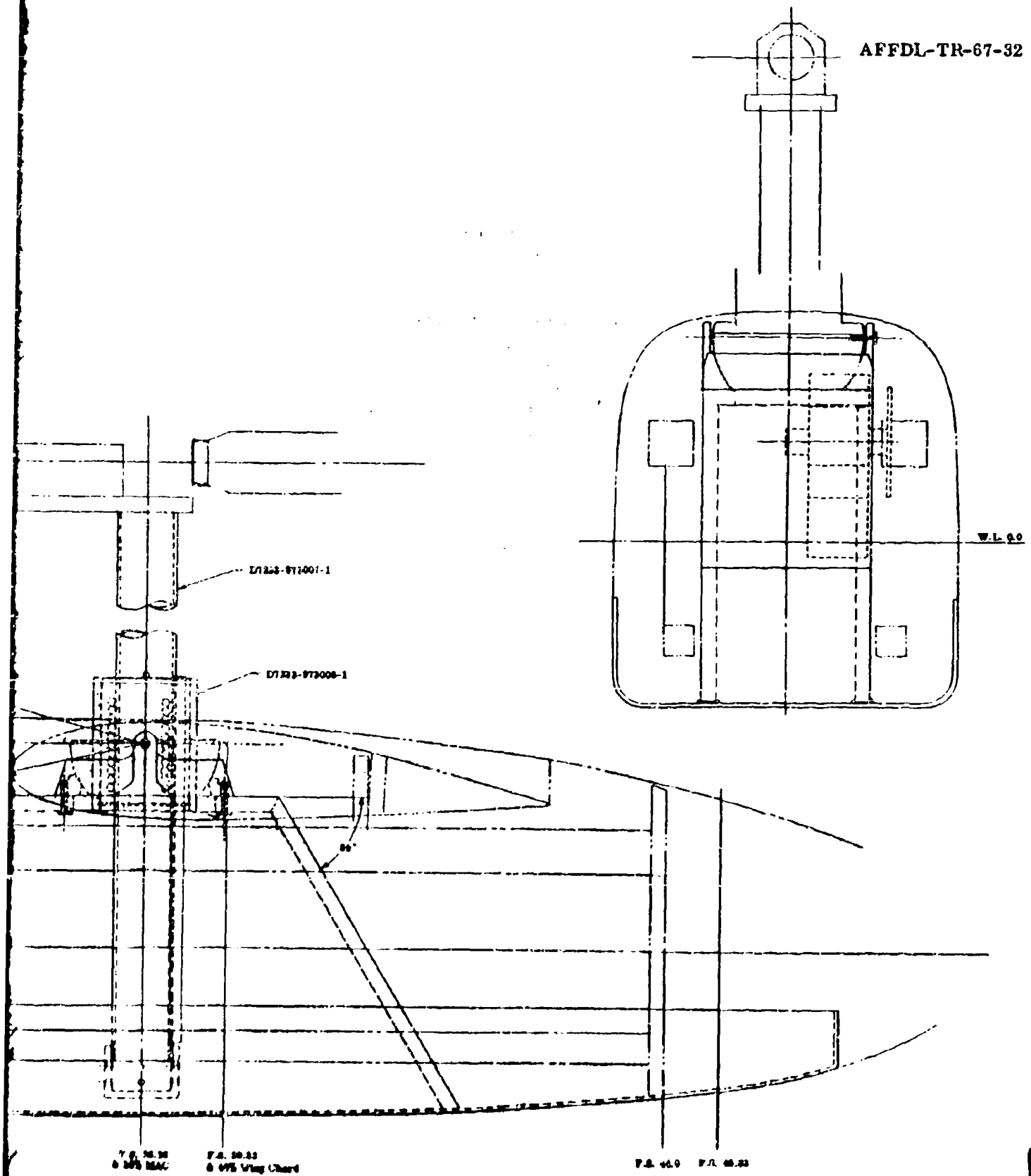
W.L. 0.0
86°

Figure 62. Tunnel Model with Lower Shell Disassembled

B. TRUNK CONFIGURATIONS

1. Elastic Trunk

The elastic trunk and the first inelastic trunk simulated the basic configurations. The elastic trunk was made from a single ply material, rubber/stretch-nylon. The distributed jet was introduced by stitching closely spaced holes with a blunt needle. Because of the small scale and the material available it was not possible to simulate the trunk pressure. The air flow was small.

2. Inelastic Basic Trunk

The inelastic basic trunk was made from a lightweight nylon/hypalon. Using a plaster mold of the inflated shape, a pattern of pieces was cut from the flat sheet and bonded to each other on the mold. The jet pattern was then introduced by hand, using a hole punch. Figure 63 is a photograph of this configuration in the tunnel. Seven rows of jet holes were cut using 1/8 inch diameter spaced apart 3/8 inch. At the ends the spacing was maintained on the ground tangent. This hole pattern provided a gross nozzle area sufficient to simulate the T58 auxiliary power scheme flow using 45° jets as follows:

Net full scale area	=	7.0 ft^2
Discharge coefficient (using average pressure ratio $P_{j_{abs}}/p_{c_{abs}}$ and $P_{j_{abs}}/p_{o_{abs}}$)	=	0.62
Jet angle correction factor	=	1.707
Gross full scale nozzle area	=	7.0 x 1.707/0.62 = 19.25 ft^2
Gross model scale nozzle area	=	19.25/144 ft^2
	=	19.25 $in.^2$

Therefore, 1580 1/8 inch holes are required.

Air flow was measured for the tunnel test. Air flow rather than area is the factor of importance.

Gross full scale air flow = 3250 x 1.707 = 5550 ft^3/sec

Model scale air flow will be greater than the similarity scaling (to the power of 2.5) because the model is much heavier than the similarity weight. Hence, air flow is obtained from model scale p_c using

$$\frac{Q}{g \times c}\sqrt{\frac{\rho}{2p_c}} = 1.22, \text{ for } p_c/P_j = 0.5$$

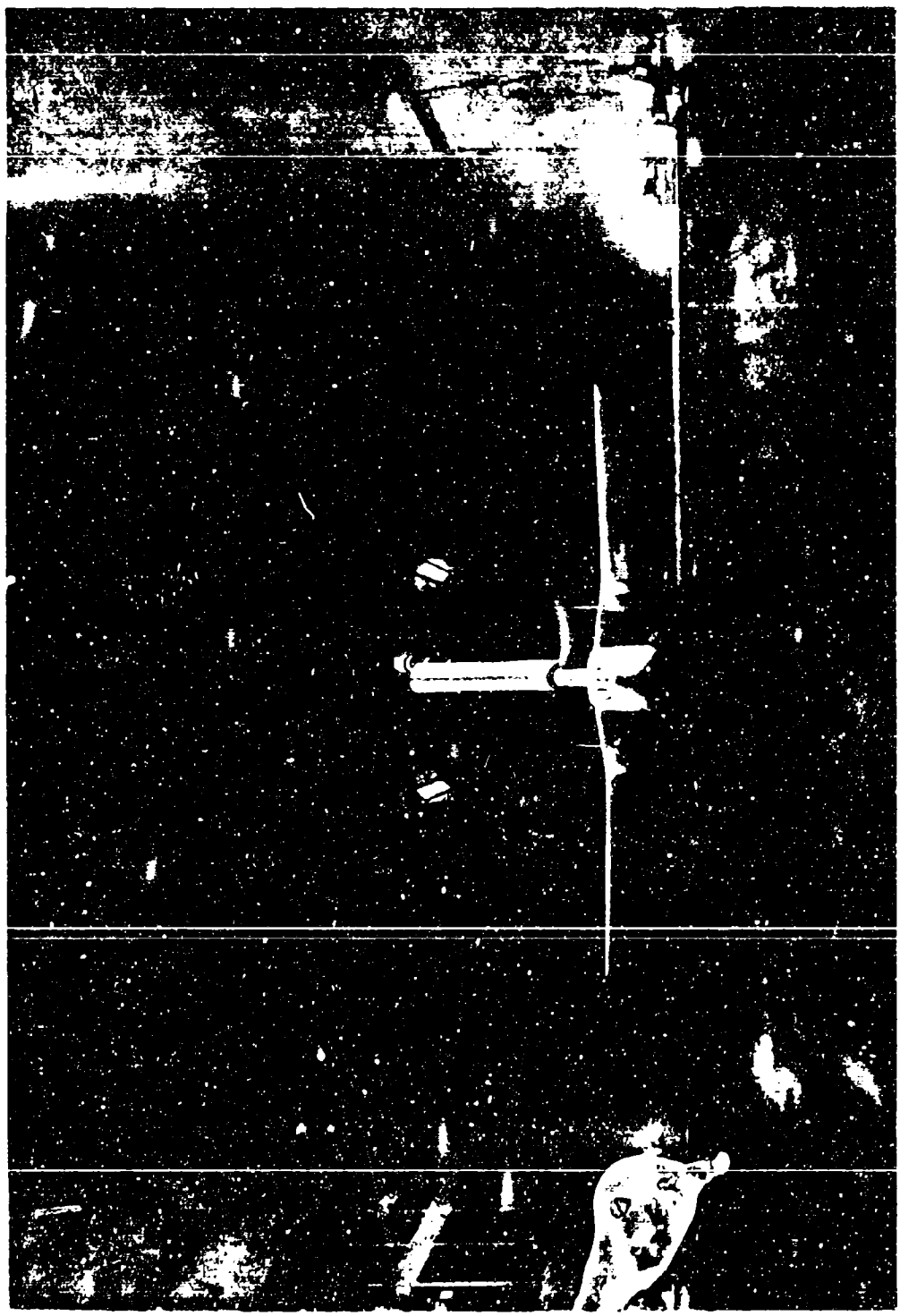

Figure 63. 1/12 Scale Model in Wind Tunnel

In this case, the nozzle area is the flow area and discharge coefficient is not included. Therefore

$$Q = 1.22 \times \frac{7.0 \times 1.707}{144} \times 29 \sqrt{p_c}$$

for a model weight of 95 pounds:

$$p_c = \frac{95 \times 144}{360.5} = 38 \text{ lb/ft}^2$$

Hence $Q = 18.05 \text{ ft}^3/\text{sec}$

$= 1.38 \text{ lb/sec}$

At $p_c/P_j = 0.5$ the total model air flow in the tunnel was found to be slightly in excess of 1.5 lb/sec. Unfortunately, the leak flow was considerable, both through the ball joint and beneath the model plenum so that air flow could not be determined accurately. In runs 2, 3 and 11 total air flow was reduced to approximately 1.25 lb/sec. Little difference in performance could be observed.

3. Half Length Cushion with Nose Plenum

The half-length main cushion configuration was made in a similar fashion. The same p_c/P_j is required and hence the same nondimensional flow factor applies. This can be written, for effective gap g, as

$$g = \frac{Q}{1.22c} \sqrt{\frac{\rho}{2 p_c}} = 0.0283 \frac{Q}{c\sqrt{p_c}}$$

Comparing the two configurations from Section II-C and using the lower jet height for convenience,

	Full Length	Half Length
Q	1780	1800
p_c	166.5	321
c	80.8	46.9
$c\sqrt{p_c}$	1042	840
$Q/c\sqrt{p_c}$	1.7	2.14
g	0.57 in.	0.72 in.

Thus a 25% increase in the nozzle area per foot is required. The hole size was kept the same and the spacing reduced slightly to accomplish this.

The nose plenum was made from a sheet of the same material. A cone angle of 6° was found satisfactory. The plenum is rather tall. Initially this gave some trouble since it could not be relied upon to erect. This was overcome by introducing a plate beneath the plenum supply hole to spread the flow radially as shown below:

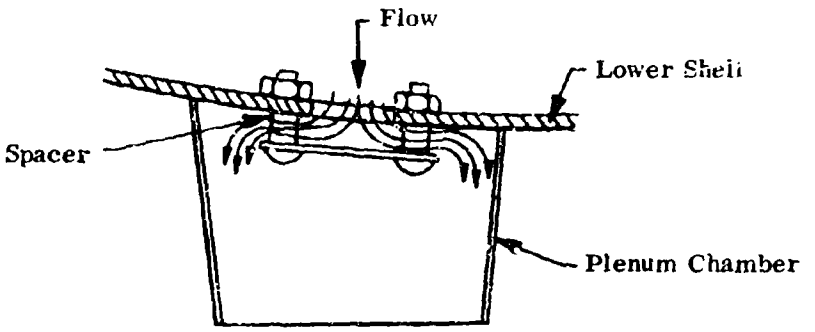

The depth of the spacers was calculated to pass the required flow assuming $P_j = 1.2 p_c$.

4. Three-Plenum Configuration

In this configuration the same nose plenum was retained but the main cushion was provided by a pair of circular plenum chambers, similarly constructed but of maximum diameter to fit beneath the fuselage. Air supply ports into the three inelastic configurations were arranged as four slots of area 4.25 $in.^2$ each, and a hole for the nose plenum feed was blanked using the spreader plate. The slots were positioned to provide a common main trunk air supply for the other three configurations (Figure 64). Thus, in the case of the three-plenum configuration, relative air flow between the main and nose plenums is controlled by the spacer depth at the front. This depth was not changed for this configuration test.

C. STATIC PITCH AND ROLL STIFFNESS TESTS

All configurations were functioned with the model base floating free on a platform, at the appropriate weight, balance and trunk pressure. Static pitch and roll stiffness was observed and behavior compared. The elastic trunk pressure could not be maintained at the proper level because the material is too stiff for inflation at this level. It was inflated to the proper size, which required a trunk pressure of 3.5 $lb/in.^2$. Thus, at the model p_c of 38 lb/ft^2, p_c/P_j was 0.075, which is a very stiff bag. It was very stable in pitch and roll and well damped in roll. Pitch damping was poor, though to be due to flow attachment at the front or rear tending to excite the model.

Static stiffness measurements were taken from the basic configuration with the inelastic trunk. This configuration was also satisfactory, although the pitch damping was still rather marginal. The variation of roll stiffness with trunk pressure is very noticeable. With a very soft bag the roll oscillation frequency is much reduced and the model behavior could be called "sloshy". For this reason stiffness measurements

The nose plenum was made from a sheet of the same material. A cone angle of 6° was found satisfactory. The plenum is rather tall. Initially this gave some trouble since it could not be relied upon to erect. This was overcome by introducing a plate beneath the plenum supply hole to spread the flow radially as shown below:

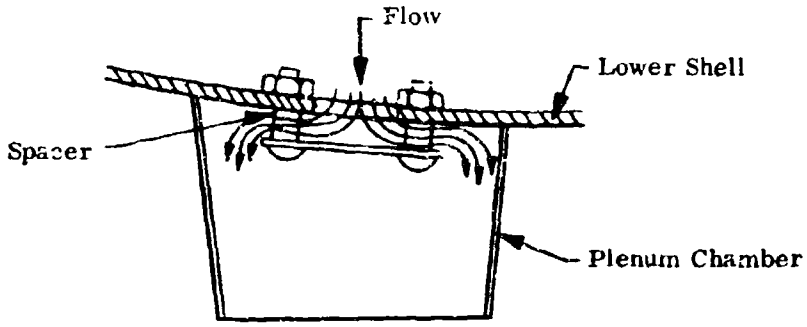

The depth of the spacers was calculated to pass the required flow assuming $P_j = 1.2\,p_c$.

4. Three-Plenum Configuration

In this configuration the same nose plenum was retained but the main cushion was provided by a pair of circular plenum chambers, similarly constructed but of maximum diameter to fit beneath the fuselage. Air supply ports into the three inelastic configurations were arranged as four slots of area 4.25 in.^{2} each, and a hole for the nose plenum feed was blanked using the spreader plate. The slots were positioned to provide a common main trunk air supply for the other three configurations (Figure 64). Thus, in the case of the three-plenum configuration, relative air flow between the main and nose plenums is controlled by the spacer depth at the front. This depth was not changed for this configuration test.

C. STATIC PITCH AND ROLL STIFFNESS TESTS

All configurations were functioned with the model base floating free on a platform, at the appropriate weight, balance and trunk pressure. Static pitch and roll stiffness was observed and behavior compared. The elastic trunk pressure could not be maintained at the proper level because the material is too stiff for inflation at this level. It was inflated to the proper size, which required a trunk pressure of 3.5 lb/in.^{2}. Thus, at the model p_c of 38 lb/ft^2, p_c/P_j was 0.075, which is a very stiff bag. It was very stable in pitch and roll and well damped in roll. Pitch damping was poor, though to be due to flow attachment at the front or rear tending to excite the model.

Static stiffness measurements were taken from the basic configuration with the inelastic trunk. This configuration was also satisfactory, although the pitch damping was still rather marginal. The variation of roll stiffness with trunk pressure is very noticeable. With a very soft bag the roll oscillation frequency is much reduced and the model behavior could be called "sloshy". For this reason stiffness measurements

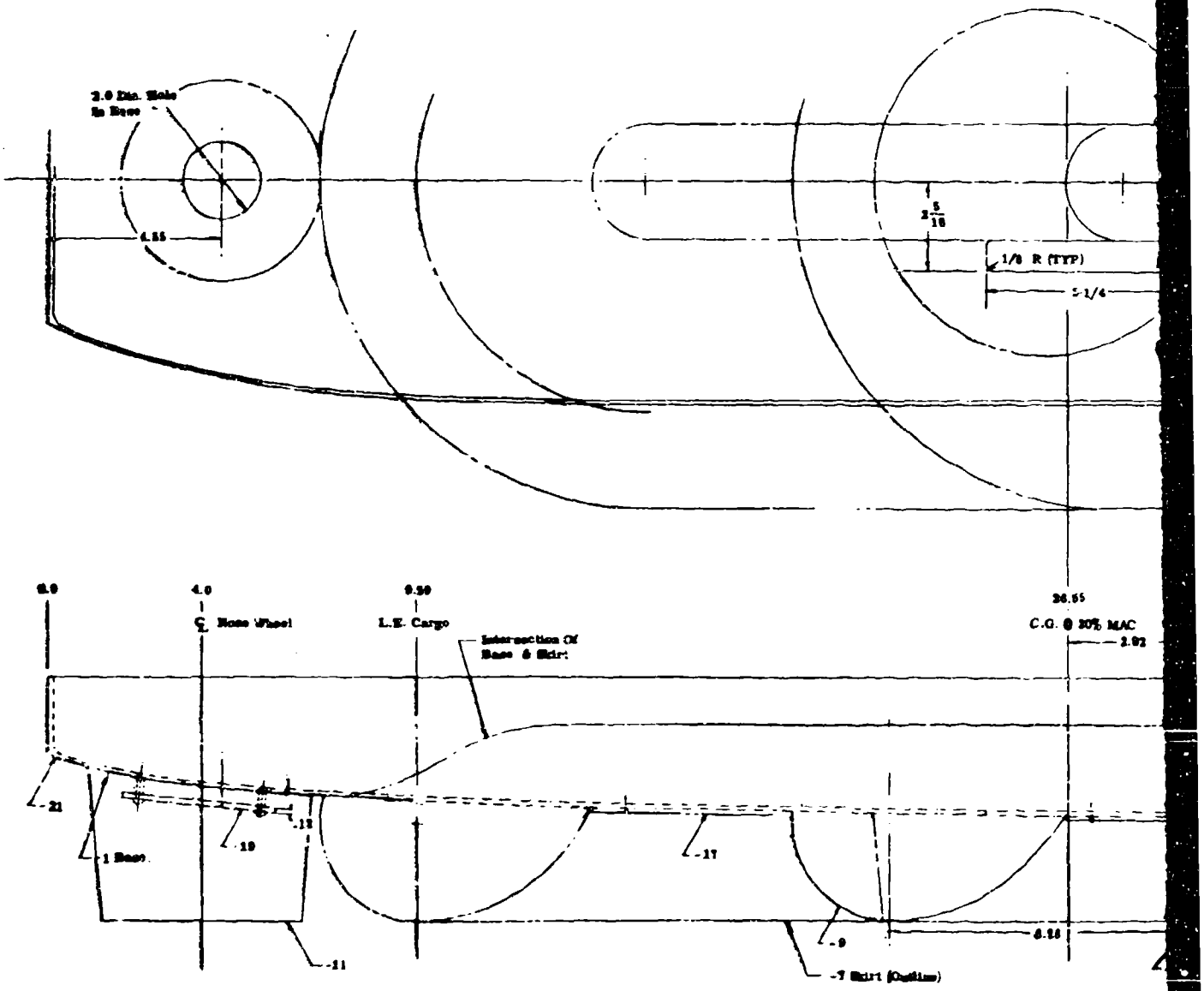

Figure 64. Alternative Trunk Configurations

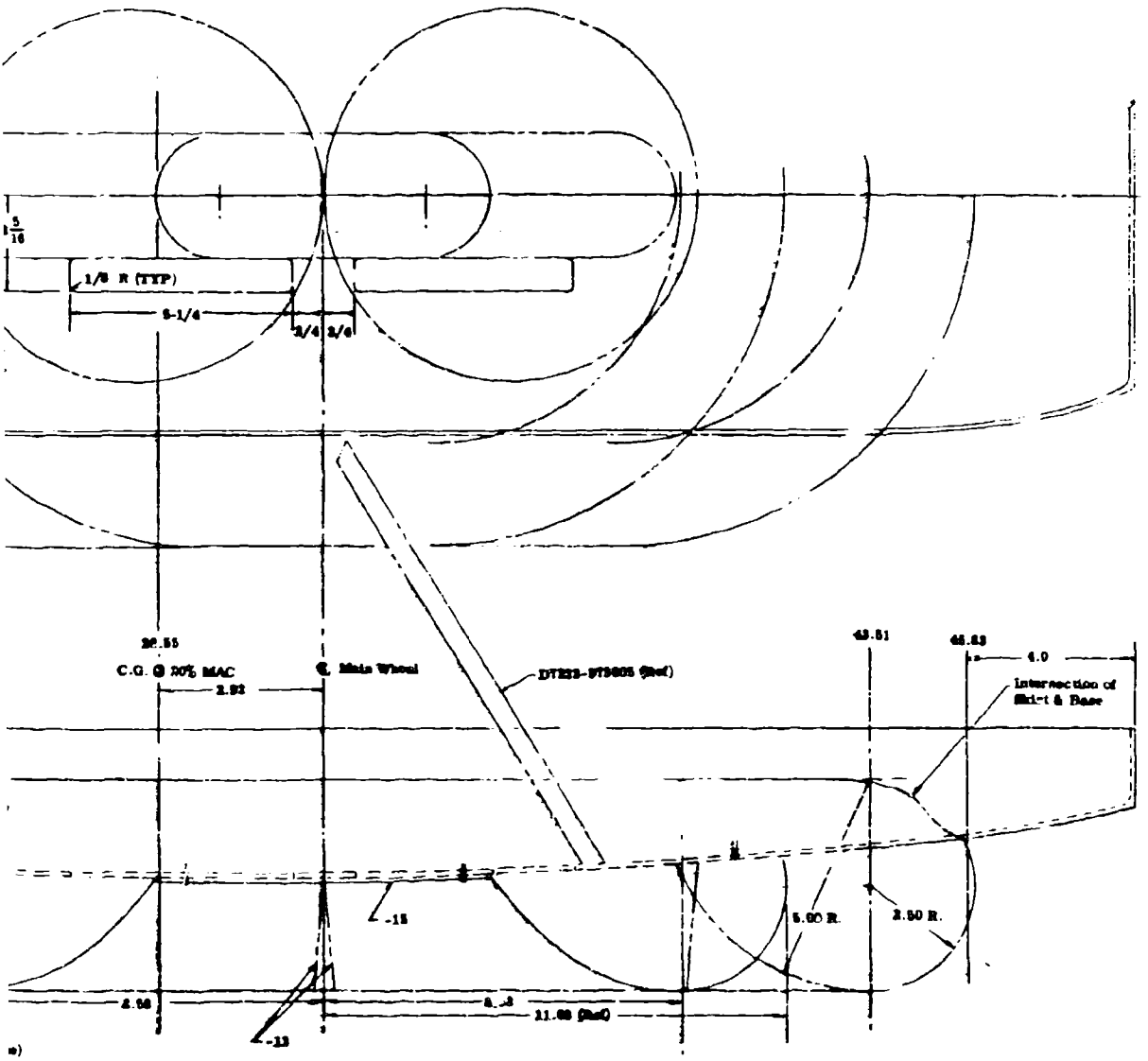
1/8 R (TYP)
5-1/4
3/4
3/4
C.G. @ 20% MAC
2.92
Main Wheel
DT223-975805 (Ref)
43.51
46.83
4.0
Intersection of Skirt & Base
-15
5.00 R.
2.50 R.
2.06
11.00 (Ref)
-13

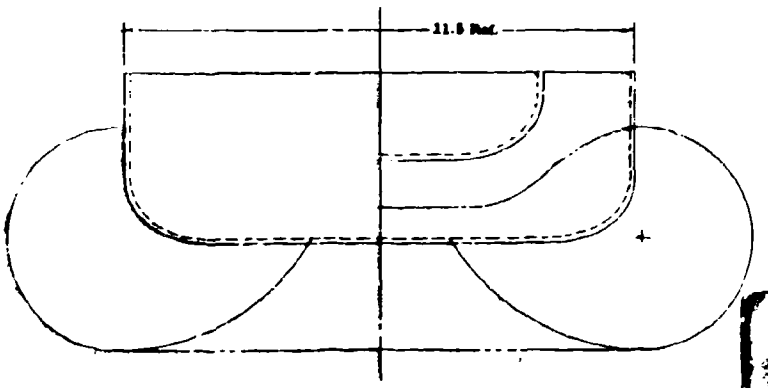
11.5 Ref.

were taken for several values of p_c/P_j. These are shown in Figure 65. There was a tendency for the model to find a different trim point at zero moment on the return curve. These measurements were taken with an overhead flexible supply line and although the stiffness introduced by it was small it could account for the observed hysteresis. The average roll stiffness variation with bag pressure is shown in Figure 41 which plots roll cp_ϕ versus p_c/P_j.

Pitch stiffness measurements were taken at a basic p_c/P_j of 0.5 (i.e., with trunk pressure equal to 76 lb/ft^2) for a model weight of 95 pounds. Direct measurement of cushion pressure confirmed that effective cushion area (model weight divided by cushion pressure) was in fact almost exactly equal to the predicted 360 in.^{2} (360 ft^2 full scale). As far as could be ascertained at this small scale, jet height was 0.20 inch average, (2.45 inch full scale), approximately in line with the predicted value at 50% jet height efficiency allowing for jet angle. For analysis of takeoff rotation stiffness is required as a function of weight. Measurements were therefore also taken with the model weight variable. In practice it is not possible to reduce the weight so a variable upload was applied through the model c.g. A pitch axis pivot was introduced at this point and a teeter-totter lever arrangement was incrementally loaded at its other end.

Evidently pitching moment at small angles can depend importantly on jet height. The simulated nozzle area corresponds to the high power level with an allowance for jet angle. No problems were apparent as a result of this higher power level. However, if pitching moment is found to be larger at lower power level and jet area this will affect rotation. This was therefore checked by blanketing half the nozzle area. The inner two rows and the outer row of nozzle holes were sealed. The jet height was reduced to approximately 1/8 inch at $p_c/P_j = 0.5$. Comparative runs were made at this p_c/P_j. Since the stiffness was found to be substantially unaffected, the variable weight runs were made in this configuration. These results are shown in Figure 66 as full scale pitching moment versus pitch angle. Cross plots of this data are the essential information required for analysis and are shown in Figure 49 (Section II-E).

Qualitative observations were made of the other two configurations. The half-length main cushion is softer in roll and much softer in pitch (as would be expected). The real need for a nose support for such a configuration cannot be decided without further study, including dynamic considerations. Qualitatively, observation of the model indicated that the nose might bob right down to the ground as a result of severe pitch disturbance, such as full cushion braking. The three-plenum configuration was rather unsatisfactory; it was unstable in roll. Without lateral support this leads to awesome dynamic behavior in which the plenums partially collapse and reinflate as roll angle changes and violent random excursions in heave and roll continue. The configuration was tested in the wind tunnel to establish basic feasibility and when fixed in roll, the behavior was quite satisfactory.

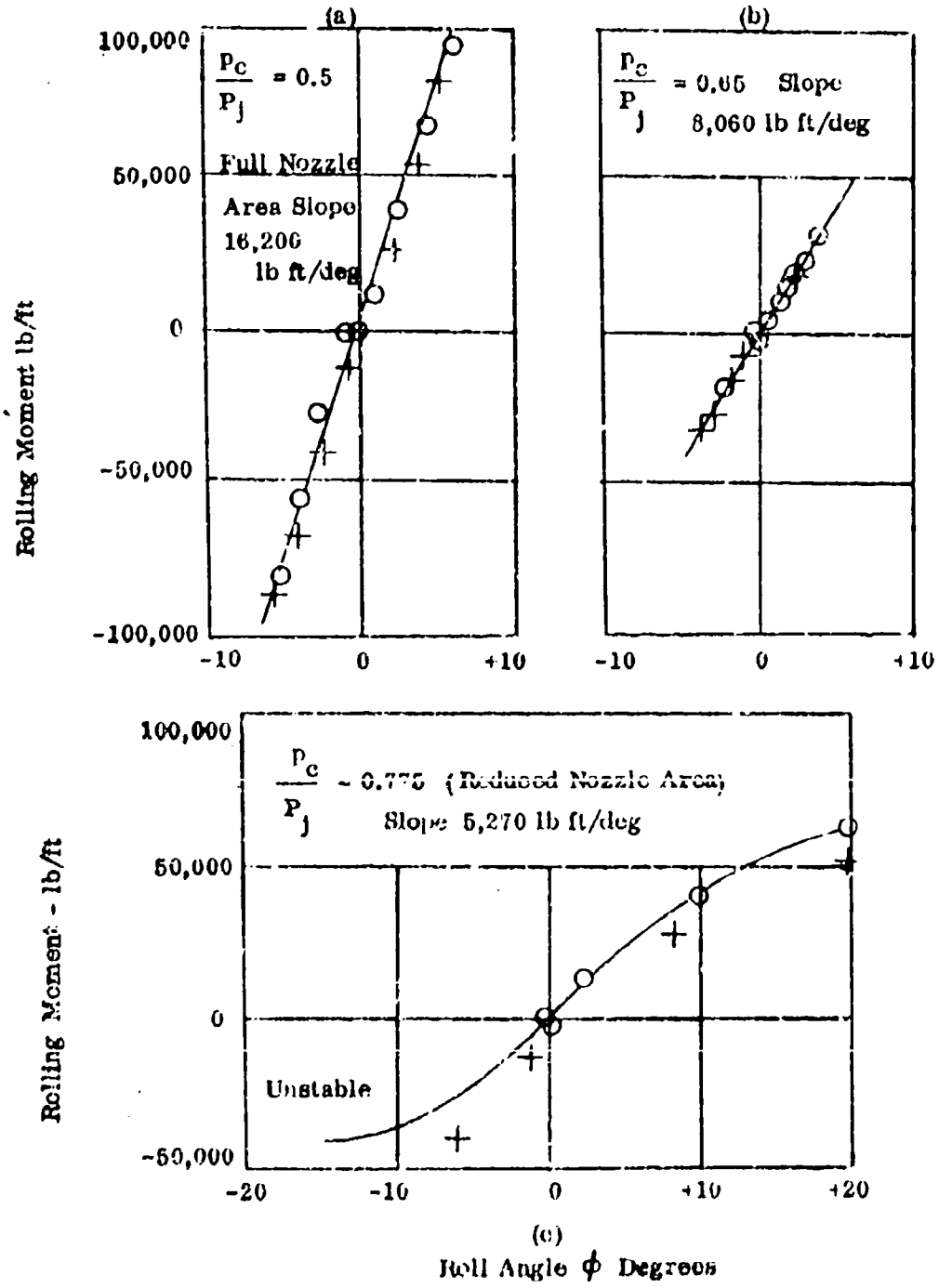

Figure 66. Static Roll Stiffness Measurements

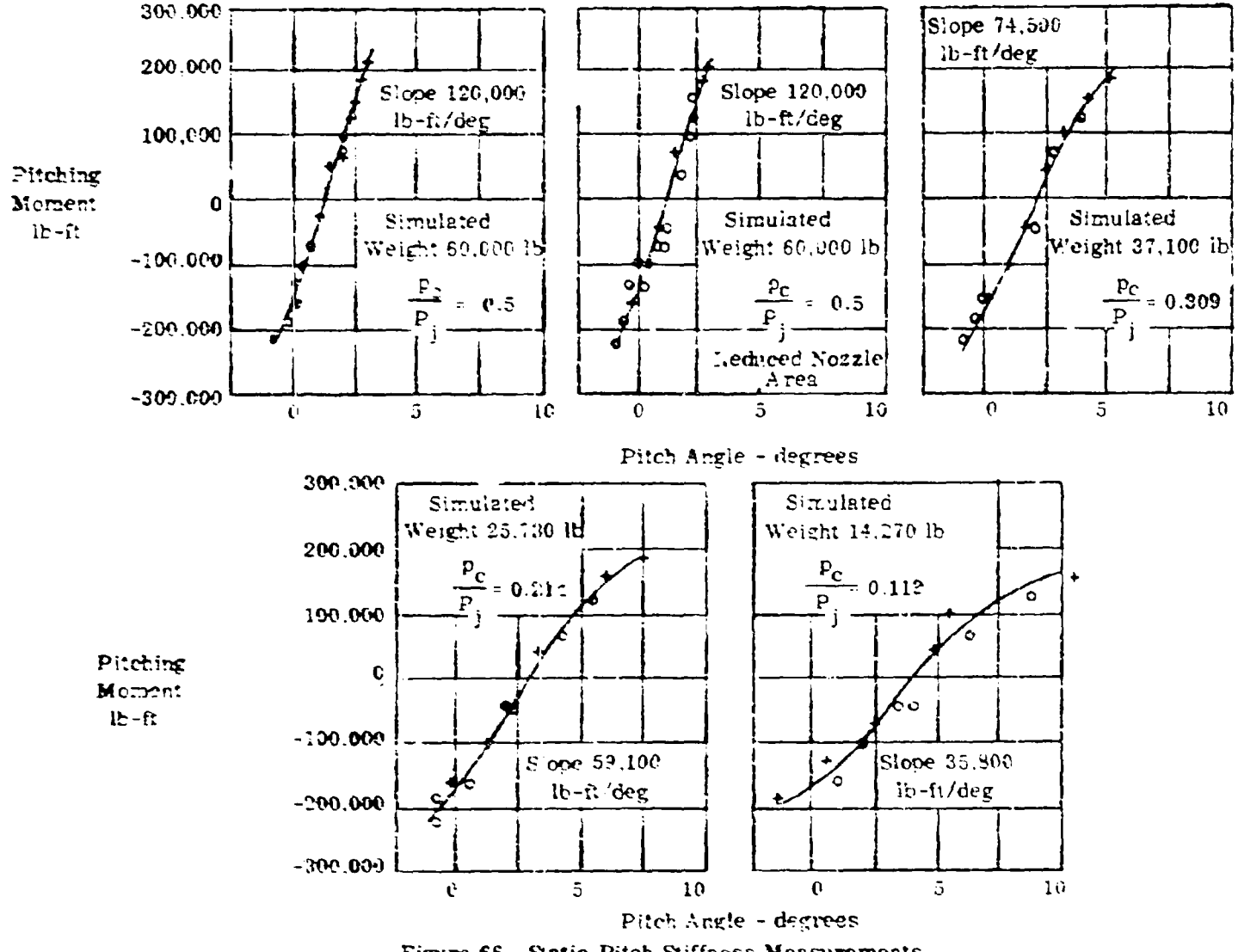

Figure 66. Static Pitch Stiffness Measurements

D. WIND TUNNEL TEST METHOD

Takeoff runs were made at different speeds, for two flap angles and two longitudinal c.g. positions. The basic inelastic trunk was tested for all combinations of flap and c.g. The alternative configurations were compared for selected conditions only in order to conserve tunnel time.

At the start of a run the sting was lowered until the model is resting on the ground belt (Figure 63). There is no lift on the balance then, until the model reaches the up stop, except for friction transmitted through the ball bushing. Model air is turned on, inflating the trunk and lifting the model onto the air cushion. The ground belt is started. As belt speed is increased tunnel air is turned on and belt and tunnel are brought up to the predetermined takeoff speed. Elevator angle is then increased in increments. At each angle as the model rotates and leaves the ground trim measurements are taken, as an average of 10 data points in a one-second time period. Due to unsteadiness in the air flow and friction in the vertical slide, the model experienced random oscillations in pitch and heave. Pitch angle variations of 1 to 2 degrees were estimated.

To land, a nose-up attitude was maintained and tunnel and belt speeds were reduced together. As lift was reduced and aerodynamic lift decreased the model sank back on the ground and the elevator was then moved down to lower the nose in a simulated landing. Instantaneous readings of tunnel velocity as well as other parameters were recorded. The performance was evidently satisfactory and some of the landings were made at large angles of attack involving maximum contact at the rear of the air bag.

E. SIMILARITY CONSIDERATION

1. Geometry

The model pivot is placed at the 20% chord station and is 45 inches (full scale) above the thrust line (see Figure 46). The model is ballasted with nose weights so that the c.g. is either at 20% or 30% MAC, covering the range (Reference 2). The vertical c.g. position on the model corresponds with the lower (or loaded) c.g. positions of the aircraft which are designated 3 and 4. The model did not incorporate means for simulating the high c.g.

Since the model is on a vertical slide it is easily seen that the only load applied to it through the pitch pivot is a thrust equal and opposite to the total drag. The validity of the simulation can best be seen by comparing the tail load with the aircraft on wheels mounted in this way with the tail load in actual takeoff evaluated in Section II-F. Thus (from II-F.3)

$$685\ \Delta L_T = 3320 \times 45 - 16{,}500 \times 18$$

$$\Delta L_T = -252\ \text{lb}$$

decreasing the tail load required for rotation (4,100 lb) by 6% in this case. Evidently if the aircraft is considered at a high c.g. the model is simulating something more difficult since the thrust moment is nose-up on a 9 inch arm while the model moment is nose-down on a 36 inch arm. In this case

$$\Delta L_T = +458 \text{ lb}$$

It is clear that as far as tail load is considered the compromise is acceptable. The model simulation is close to the worst condition.

2. Pressure and Force Relationships

The model is not dynamically similar so that transient motions are not representative. For true dynamic similarity weight varies as scale cubed (60,000 lb = 37 lb 1/12 scale) and moments of inertia must be correct so that mass distribution must be carefully controlled.

To conserve cost and also to increase force level and Reynolds Number, no attempt was made to achieve dynamic similarity. However, this involves no compromise of trim conditions (moments, attitudes and angles) which are in correct relationship.

The criterion for maximum model weight is maximum tunnel q, which is 12 lb/ft^2. A model weight of 95 pounds (forward c.g.) was used, allowing a satisfactory margin, the highest tunnel q used being 10.4 lb/ft^2. The weight of the model is supported either by the air cushion or by the wings. Thus, cushion pressure and wing lift are higher in the same proportion as weight and since lift coefficient depends on angle-of-attack the ratio of cushion pressure, jet pressure etc. to free stream dynamic head is also the same. Thus, the air cushion steady state aerodynamics are unaffected. Angle-of-attack depends on elevator angle independently of scale and thus elevator angle to trim cushion moment as well as aircraft moment is correct.

F. MODEL LIFT AND DRAG CHARACTERISTICS

1. Aerodynamic Lift

The recorded model lift characteristics are shown in Figure 67. These were measured with the wing approximately 50 inches from the ground plane. The wing span is 109.25 inches. As would be expected the stall peaks occur at lower maximum lift coefficient than full scale. However, the indicated lift curve slope is exceedingly low for a wing of aspect ratio 8.5. This discrepancy is hardly reasonable. On the other hand it is quite possible that an error in angle-of-attack is responsible. Angle-of-attack is measured by a rotary potentiometer in the model. This instrument gave trouble in the early runs, lending weight to an assumption of calibration error.

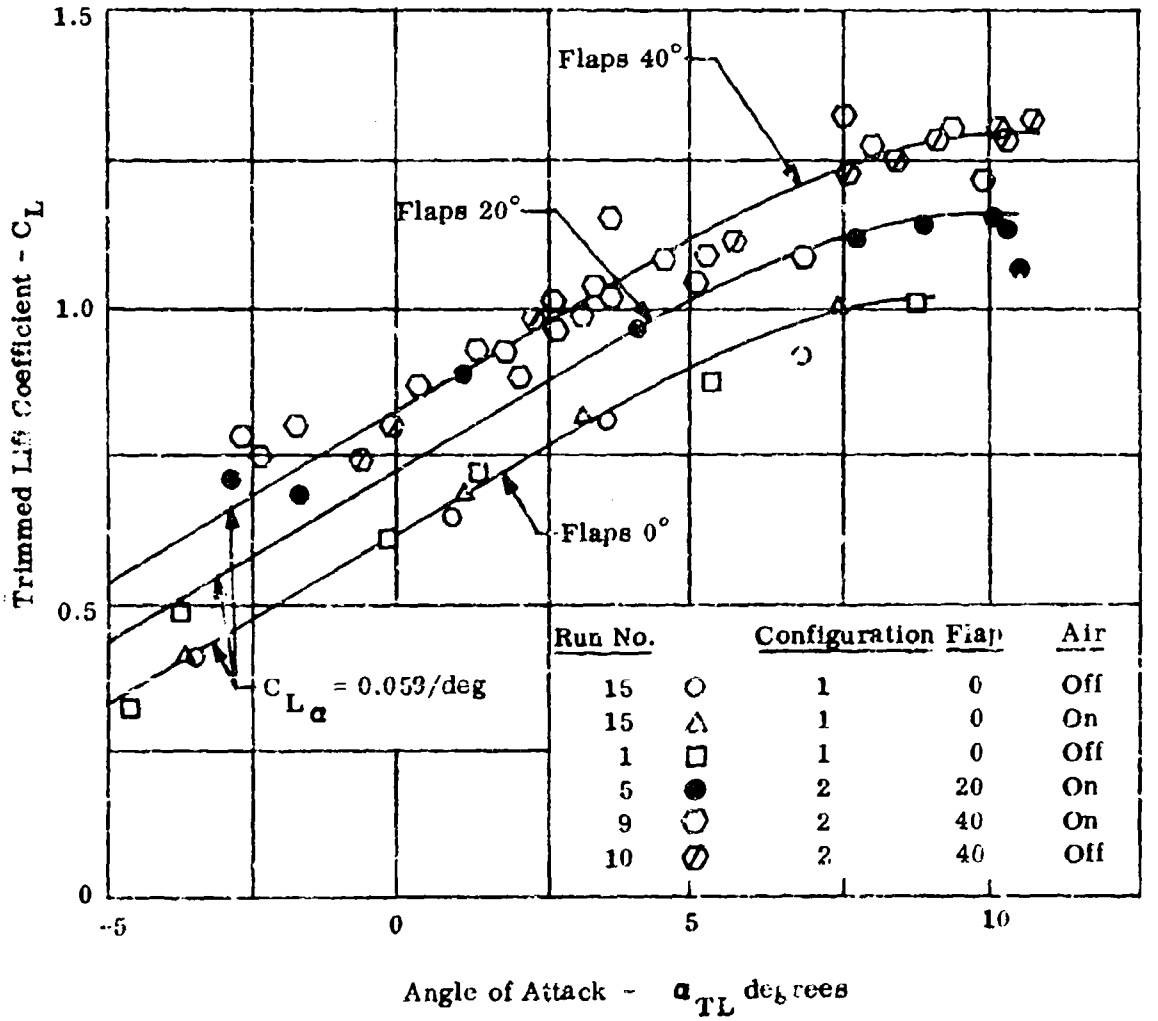

Figure 67. Model Lift Characteristics

Figure 68 is a comparison of lift curves in the takeoff configuration; measured lift is compared with Reference 2 data ($T_c = 0$ and $T_c = 0.64$). A model lift curve adjusted to the same slope as the corresponding full scale value is also shown. Aircraft lift off at maximum power at 1.2 V_{SI} occurs at $C_L = 1.46$ at $\alpha_{TL} = 6.2$ degrees. The model was lifted off closer to its stalling angle (down to 1.06 V_{SI}) but at a lower α_{TL}; about 1° lower according to the recorded data but 2.8° lower if the adjusted data is used.

At worst, this means that takeoff has only been verified at a higher speed than 1.2 V_{SI}; in fact at 130 ft/sec instead of 153 ft/sec. At the higher speed no greater α_{TL} angle than 3.25° would be required for liftoff full scale. The speed itself is satisfactory (see Figure 54). However, it will be shown that a favorable situation with regard to elevator angle to trim exists; furthermore, no significant discontinuity in elevator angle or drag can be discerned. Thus, considered in conjunction with the rotation analysis in Section II-F, it is probable that no problem exists at any practical takeoff speed.

With hindsight it is clear that a more ideal test procedure would have included runs with variable wing to fuselage incidence angle. However, this feature was not incorporated in the model and in fact, due to the method of manufacture, the design washout (1° root to tip) was not realized in practice, so that at $\alpha_{TL} = 0$ the lift coefficient was greater than it should have been (Figure 68).

Figure 69 is a similar comparison of landing lift curves. At 1.15 V_{SO}, final approach C_L is 1.28 which occurs at $\alpha_{TL} = 6.5°$. The model was let down at at least this high an angle on occasion in configurations 1 or 2. (Full length main cushion.) This can be seen from the movie records that were made.

2. Air Cushion Momentum Lift

In run 13 cushion $p_c/P_1 = 0.5$ was set up with tunnel air and belt both off. The sting was then raised in small increments, increasing ground clearance; and cushion lift was recorded. This data is shown in Figure 70. The lift to jet height variation found is compared with the theoretical variation taken from Figure 26 using the estimated static jet height of 2.60 inches as a starting point. Gross cushion momentum was calculated to be approximately 10 pounds. No lift at all was observed in free air, the suction generated in the air cushion cavity and on the trunk surface amongst the jet nozzles being sufficient to cancel this. At a critical height between 20 and 30 inches full scale there was actually some suck down. This is thought to be unlikely to persist with forward speed, but in the static condition is apparently worth about 8000 lb F.S.

3. Drag in Takeoff and Landing

Small differences in measured drag at this scale and Reynolds Number are considered dubious. Comparisons between successive runs or coefficients determined from test at different q values are therefore avoided.

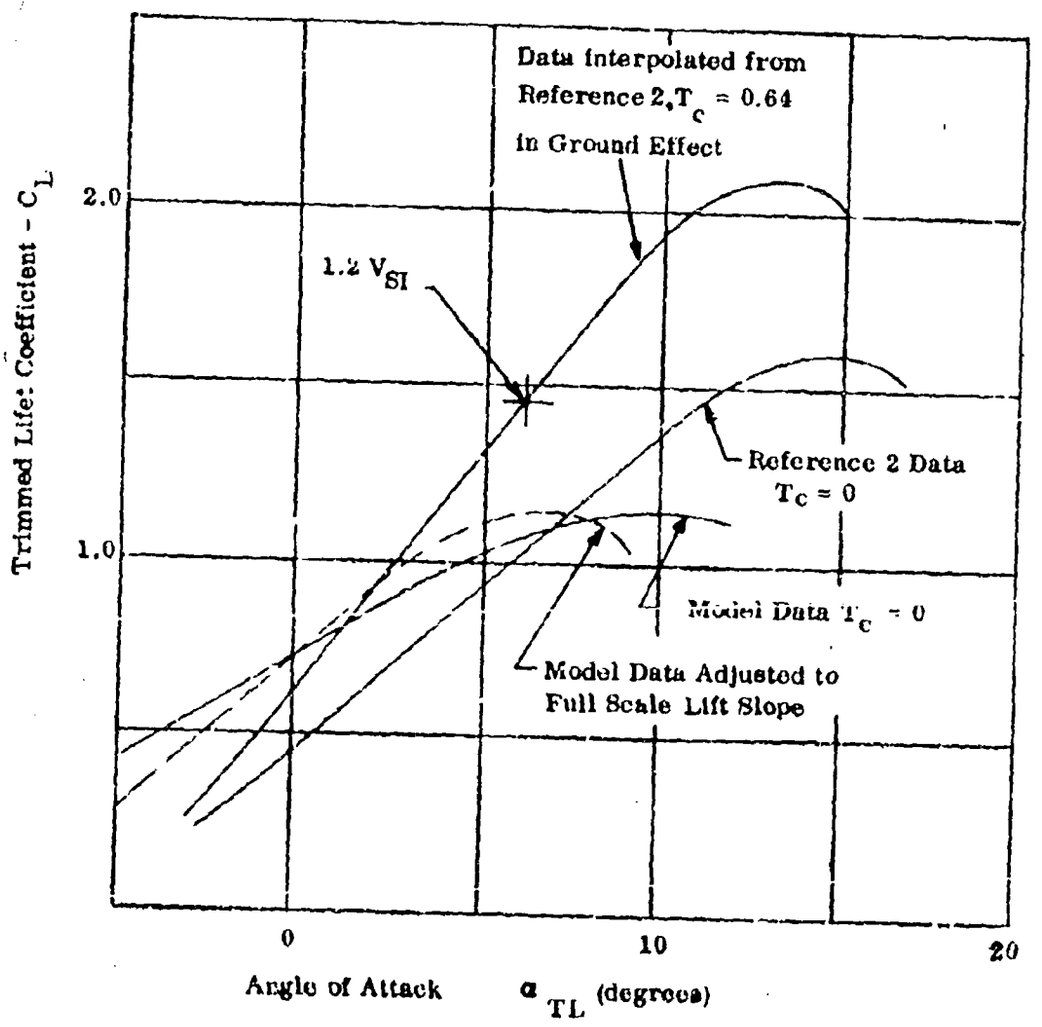

Figure 68. Comparison of Takeoff Attitudes

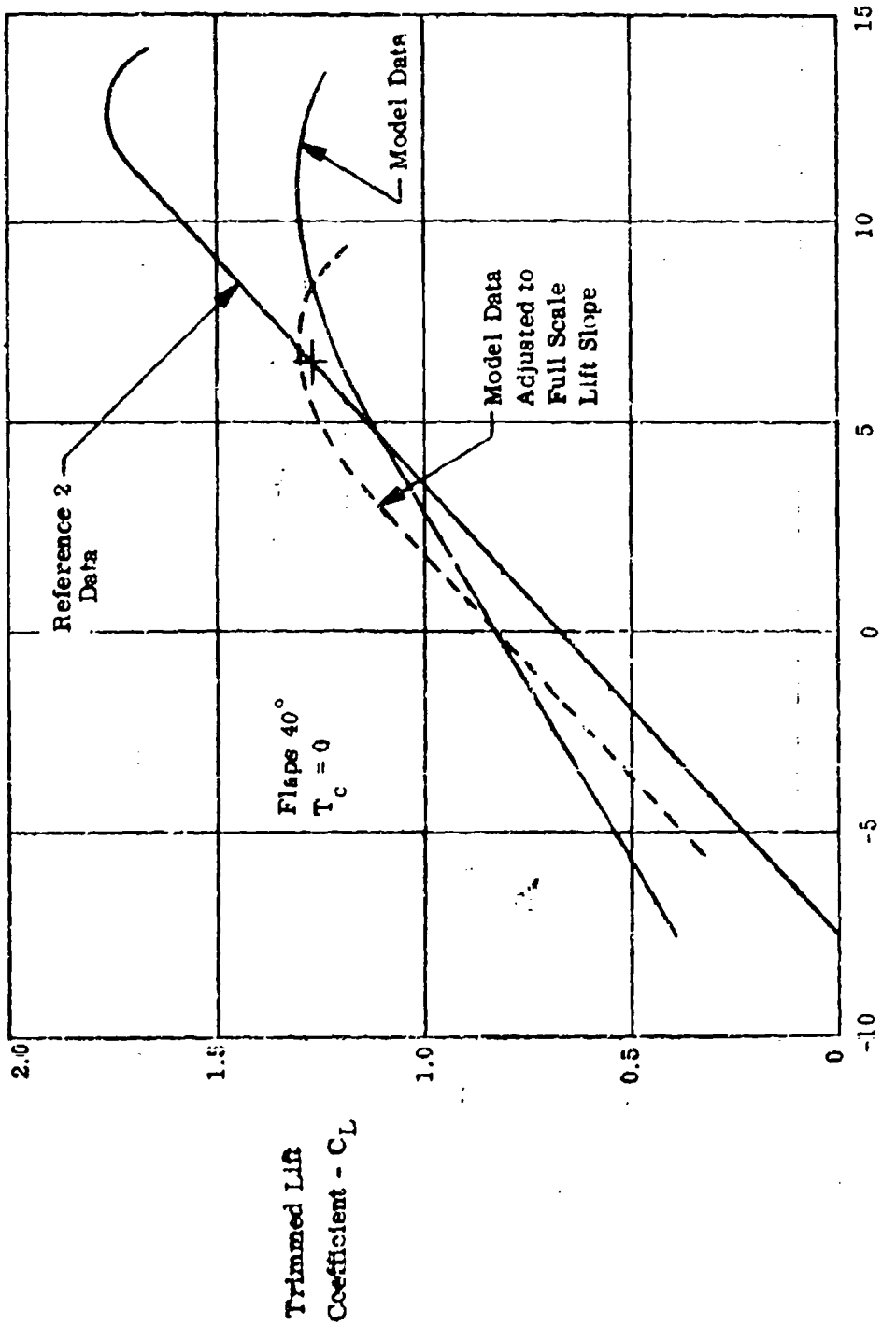

Figure 69. Landing Attitudes

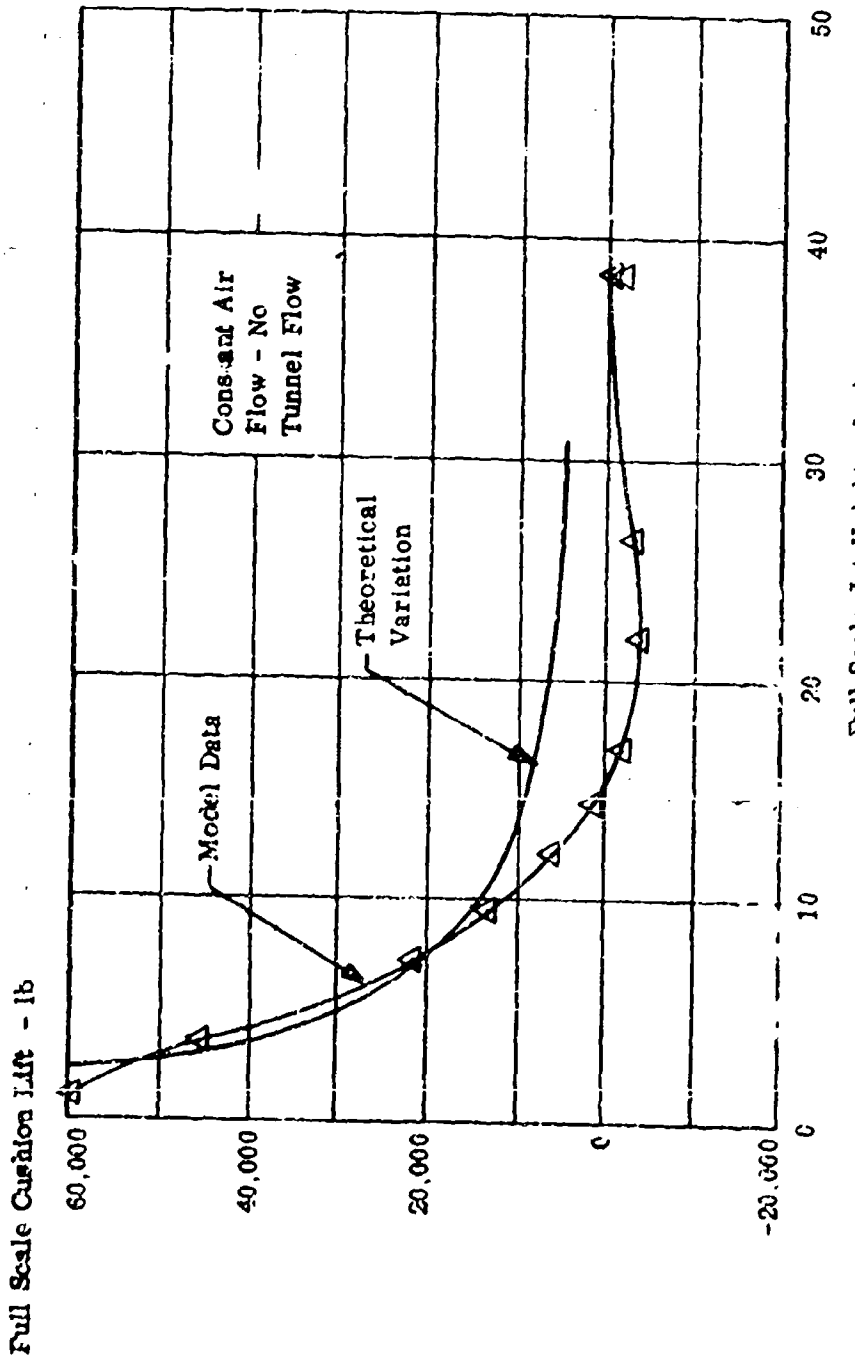

Figure 70. Decay of Cushion Lift with Jet Height

The drag in the takeoff ground roll was determined from a run with q variable in configuration 2 (Run 12). This data is shown in Figure 71 as a plot of C_D versus Reynolds number. A smooth variation of C_D with q was found, the coefficient decreasing as q increased. The reduction in drag coefficient was greater than would be expected from Reynolds number variation. In Figure 71 the data is compared with values determined from Reference 2. A typical Reynolds number variation is drawn through these latter values.

The variation of drag through the takeoff rotation is typically illustrated by Figure 72. The position marked "free from ground" is drawn between two points having jet heights of 0.6 and 4.5 inches at the longitudinal c.g. position. The absence of any drag discontinuity due to bag drag at any angle-of-attack is notable. In the first instance the ground belt was brought up to speed before the tunnel air was turned on. No drag at all could be detected in configuration No. 2. It is evident that this zero friction condition was maintained through the takeoff rotation, duplicating the "air-lubrication" found in static tests.

However, in the case of configuration No. 1, the elastic trunk, a friction drag due to contact did occur. The force level was again carefully observed as the belt was started and was found to be three pounds. It was invariant with belt speed but decreases with tunnel speed as would be expected. This is a friction coefficient, μ , of about 0.03. A takeoff and landing including a high angle approach was successfully done. Subsequent inspection of the trunk showed some wear in three local areas; on either side at the rear and on one side in the center. This was due to imperfect "tailoring" of the trunk and the failure of the tiny jets to maintain air lubrication against the belt porosity.

4. Free Air Drag of Inflated Air Cushion

A continuous run at tunnel q = 10.3 lb/ft^2 was made to determine the drag increment of the inflated air cushion. Air to the cushion was turned off midway through the run to deflate the elastic trunk. This is shown in Figure 73. A drag increment of the same magnitude as the wheel gear is indicated. A wheel gear drag coefficient increment of 0.0173 is quoted in Reference 2.

G. MODEL PITCHING TRIM

1. Ground Effect Pitching Moment

The most significant feature of model behavior found in the tests was its stable height behavior. It was easily trimmed to ride in the middle of the vertical slide, balanced by the total ground effect. For this stable behavior the slope of the curve of height versus lift (or trimmed angle-of-attack) must be negative, elevator angle fixed. The effect is well shown by the data of Run 11 shown in Figure 74 in which the model was landed with elevator angle fixed, reducing tunnel q. As the aircraft approaches the ground, angle-of-attack initially increases. The three upper points are part of a curve having the above negative slope. Clearly this characteristics produces

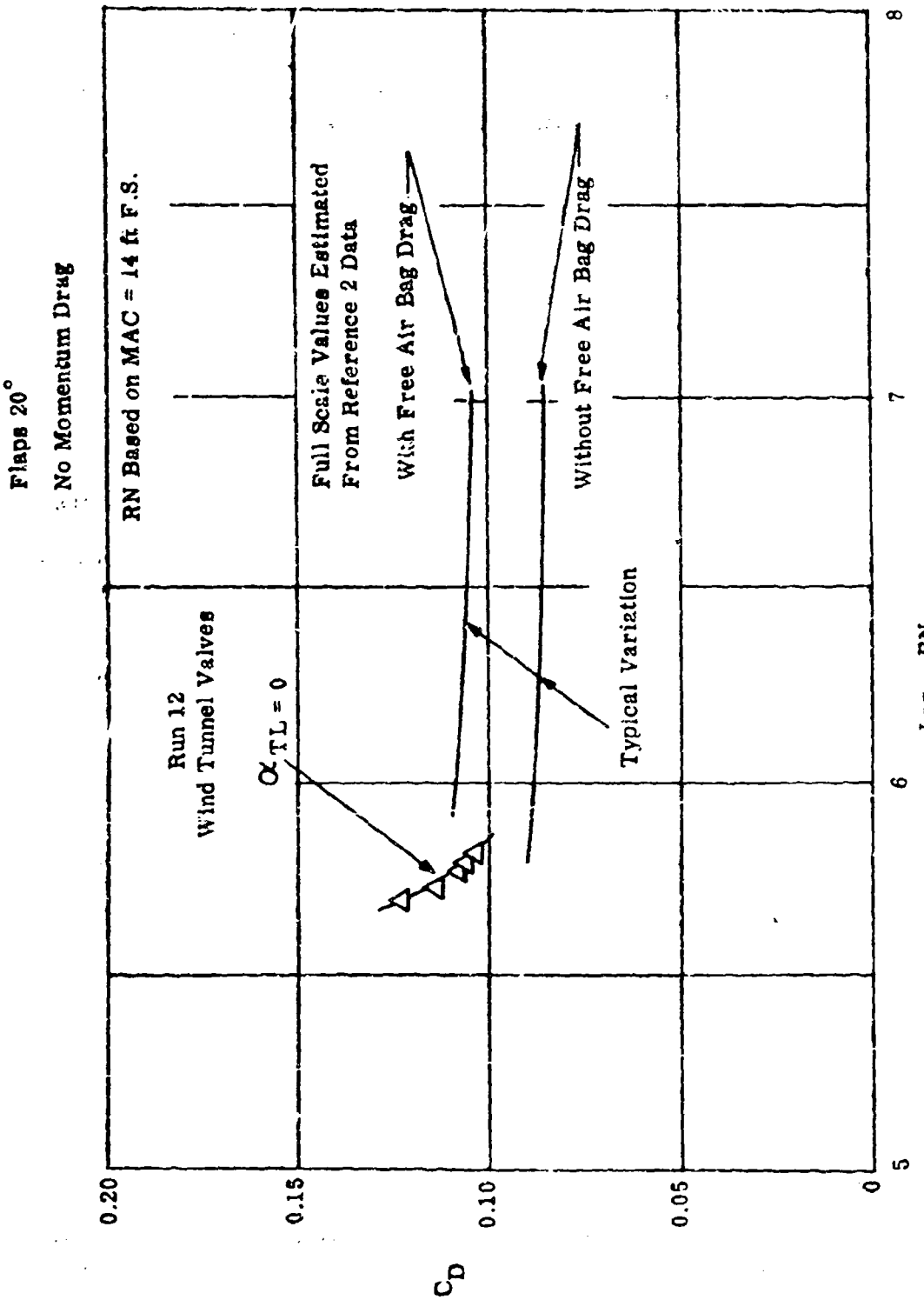

Figure 72. Drag in Ground Roll

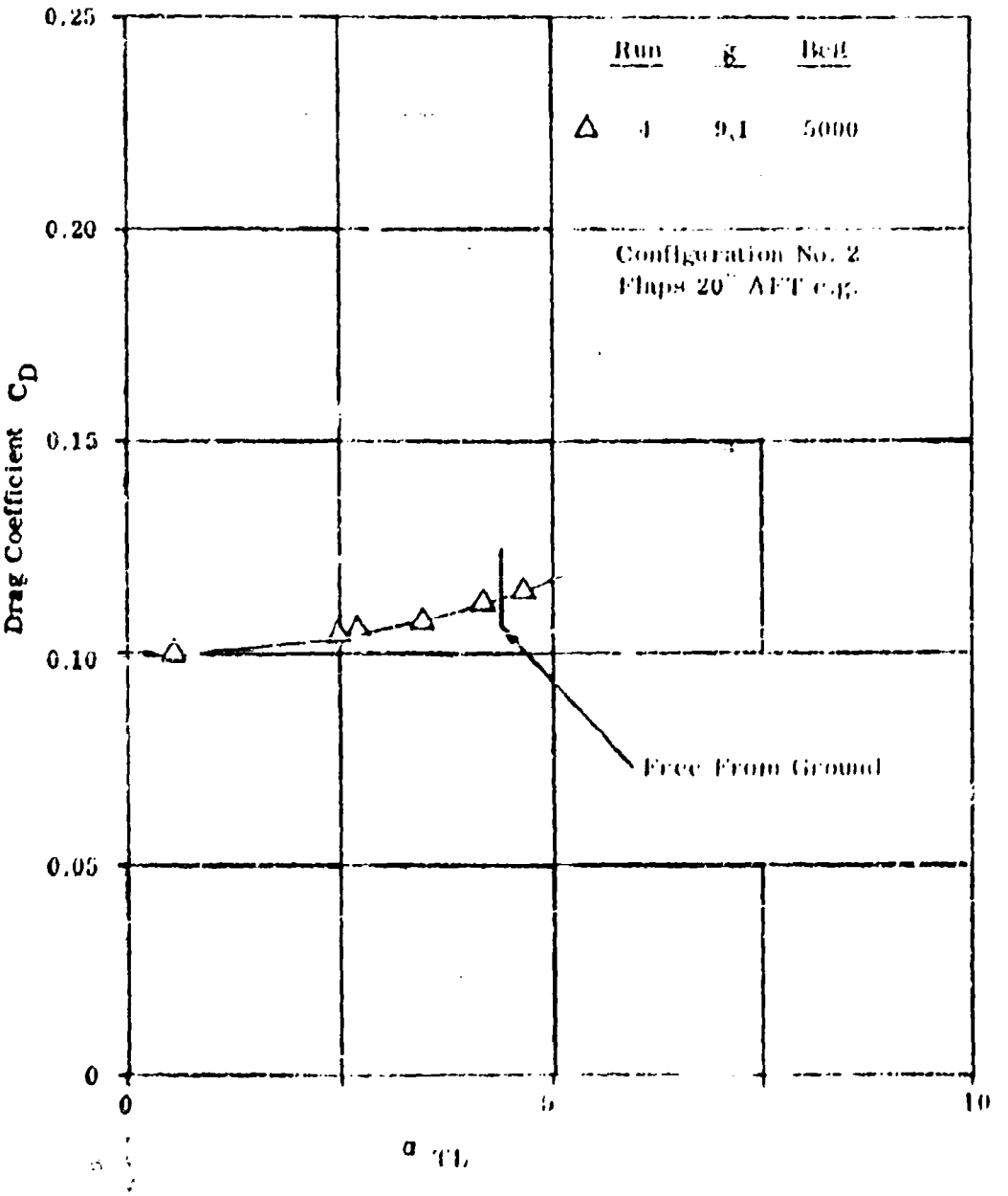

Figure 72. Drag In Takeoff Rotation

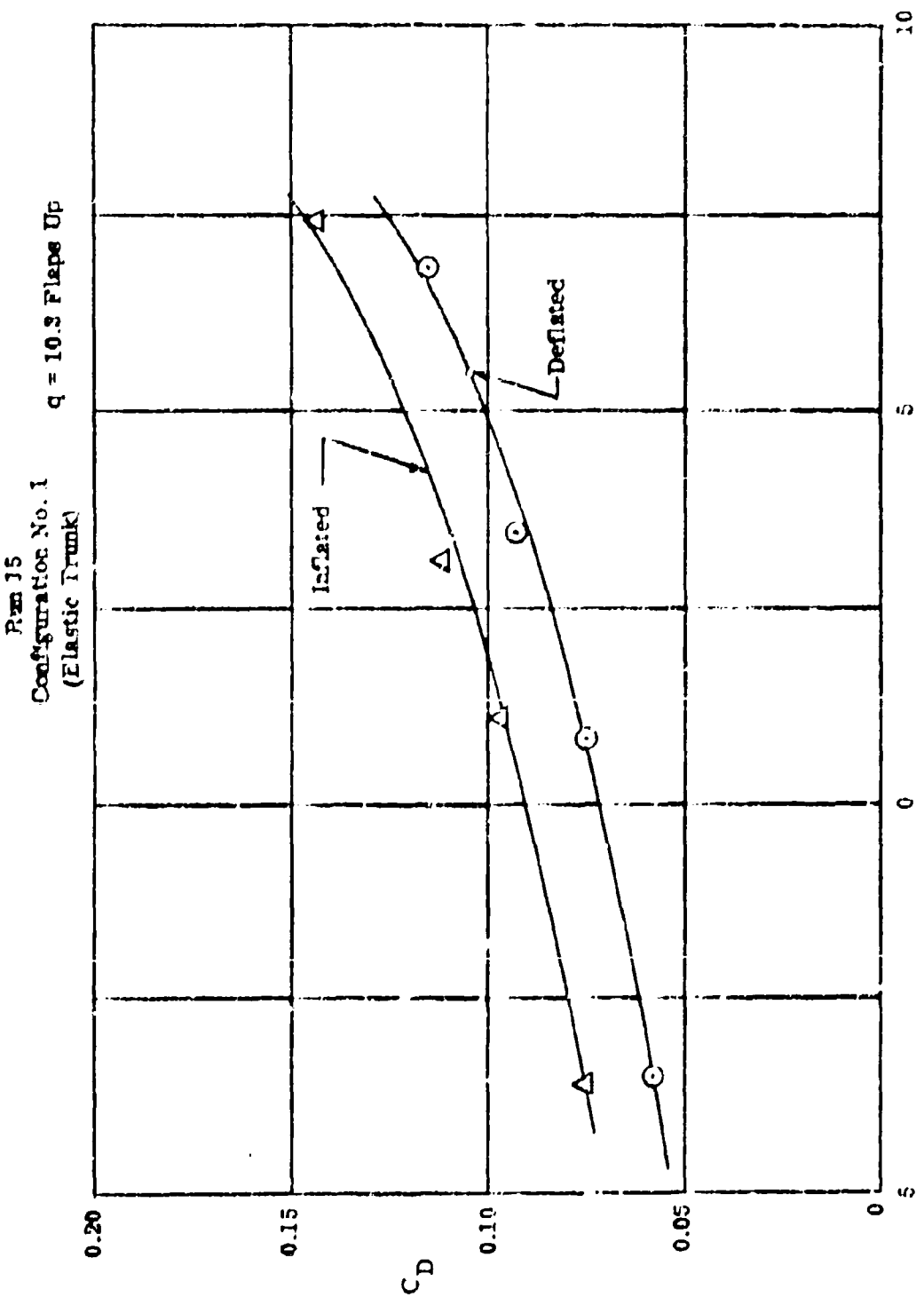

Figure 73 Drag Due to Bag Inflation

Configuration No. 2 Flaps 40°

Aft. c.g. Data from Run 11.

Constant Lift, Constant δ_e = 7°

Variable q, Variable Belt Speed

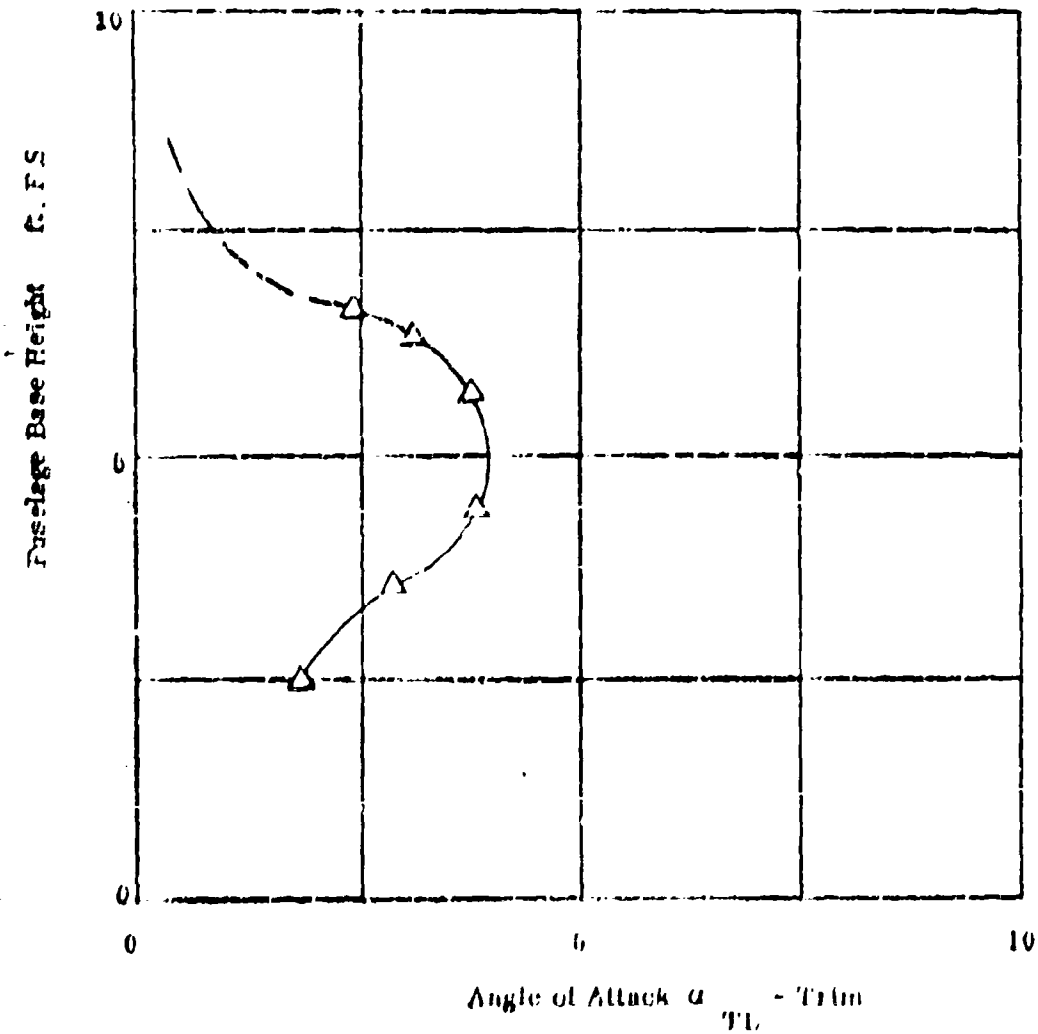

Figure 74. Pitch Change in Landing

an automatic flare-out in landing, followed by a nose-down pitch as the rear of cushion makes contact. This could be observed in the tunnel.

2. Elevator Angle to Trim

a. Comparison of Takeoff with Free Air (Out of Ground Effect)

An increased nose-up moment as the ground is approached indicates that less up-elevator will be required at lift-off and beyond than in free air. At the same time close to the ground the elevator becomes less effective in causing pitch change. These effects are well illustrated by Figure 75 which shows how the curvature of the elevator to trim versus α_{TL} curve is opposite to free air near the ground, in the region near $\alpha_{TL} = 0$. In this figure elevator to trim flaps 20° is less than to trim to the same α_{TL} flaps up in free air for all values. The free air run was made approximately 36 inches from the ground whereas in the takeoff run the model reached a maximum base height of 8-3/4 inches.

b. Elevator Angle to Trim in Free Air

Elevator angle to trim shown in Figure 75 is repeated in Figure 76 for comparison with deflated bag trim and aircraft data from Reference 2. The inflated bag pitching moment is seen to require up to 2-1/2 degrees additional up-elevator to trim. The Reference 2 data shows generally much less elevator angle required. This is because of an error in model manufacture which resulted in the tailplane incidence being set at 2.3 degrees positive to the thrust line instead of 1.5 degrees negative Thus all elevator angles determined in the tests are 5 to 10 degrees larger in the up (-ve) sense than are really required. Despite this the required elevator angles do not approach the maximum available δ_e which is -24°.

3. Elevator Angles to Takeoff

Takeoff profiles are compared in Figures 77 and 78. Figure 77 gives elevator angles versus base height for the two basic configurations - elastic and inelastic. Satisfactory agreement is shown. Figure 78 compares the 1/2 length cushion with the basic version and indicates the expected lower elevator angle required.

4. Elevator Power

Finally Figure 79 plots pitching moment coefficient versus elevator angle from runs at four q levels and elevator angles with the model fixed in pitch. The elevator angle to trim to $C_m = 0$ has no significance because the pitching moment contains a large drag moment due to the offset of the model below the balance center. The slope $C_{m\delta_e}$ of 0.01765 per degree is in reasonable agreement with Reference 2 data from which a value of 0.019 per degree is derived.

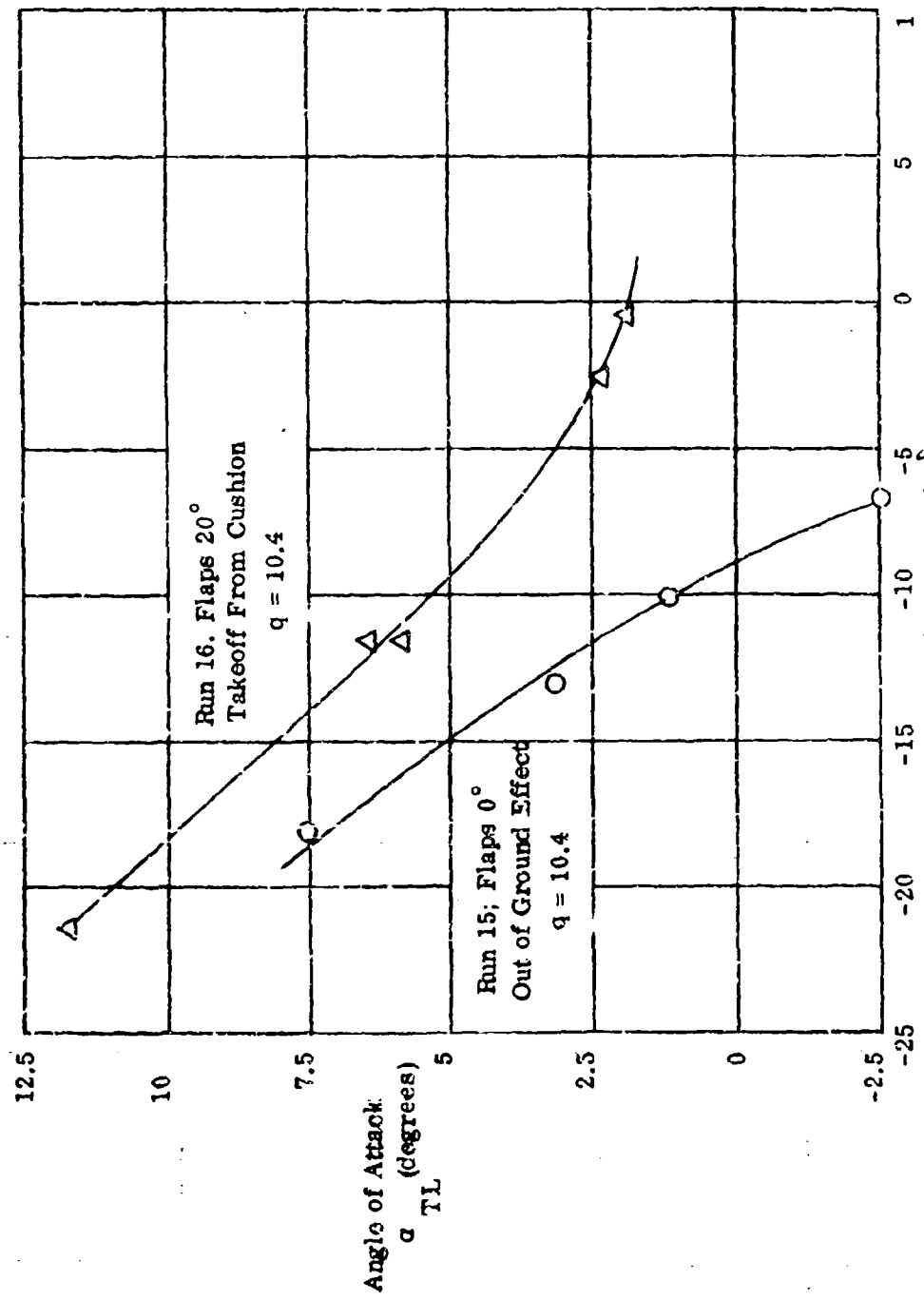

Figure 75. Comparison of Trim Angles

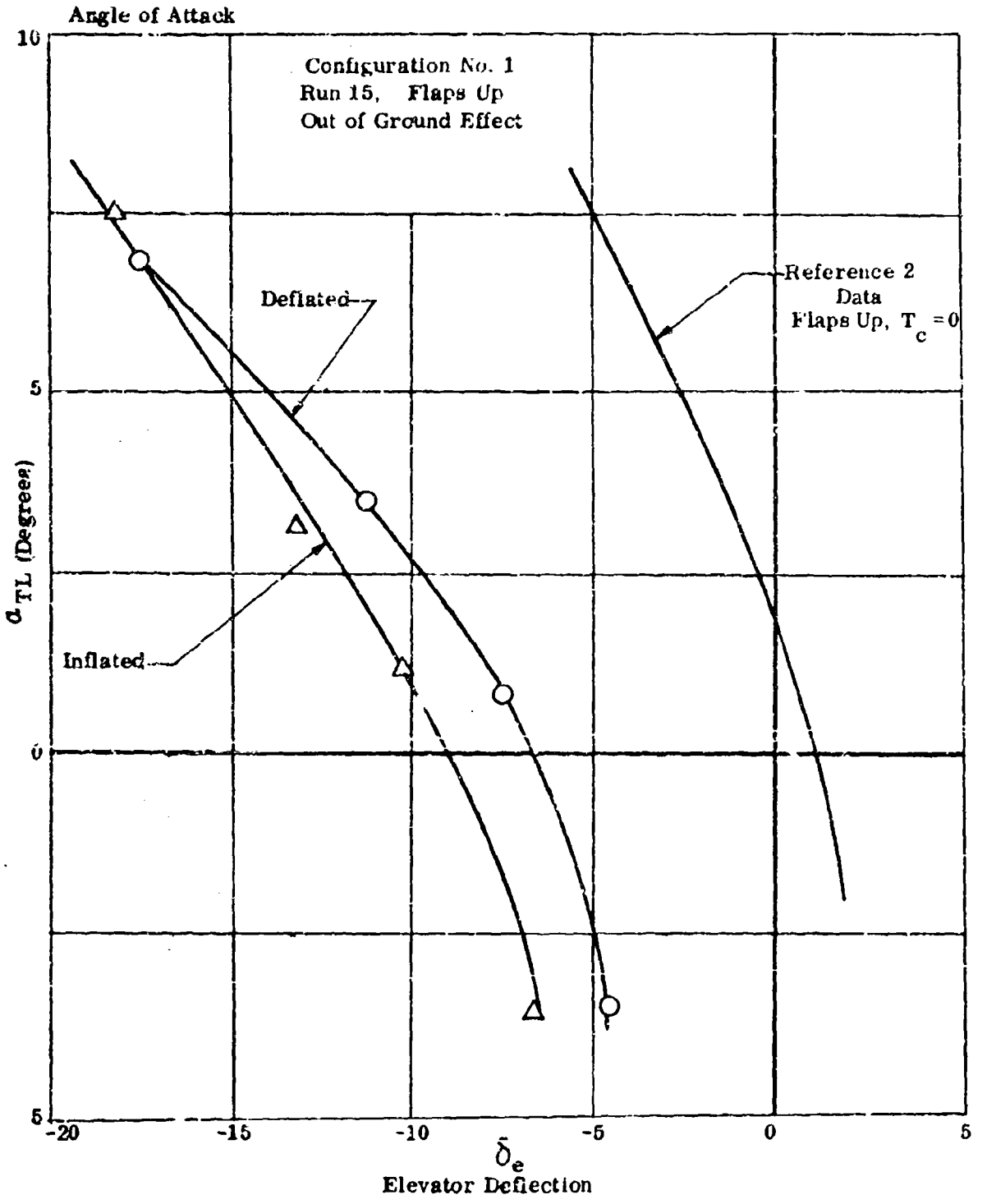

Figure 76. Elevator to Trim in Free Air

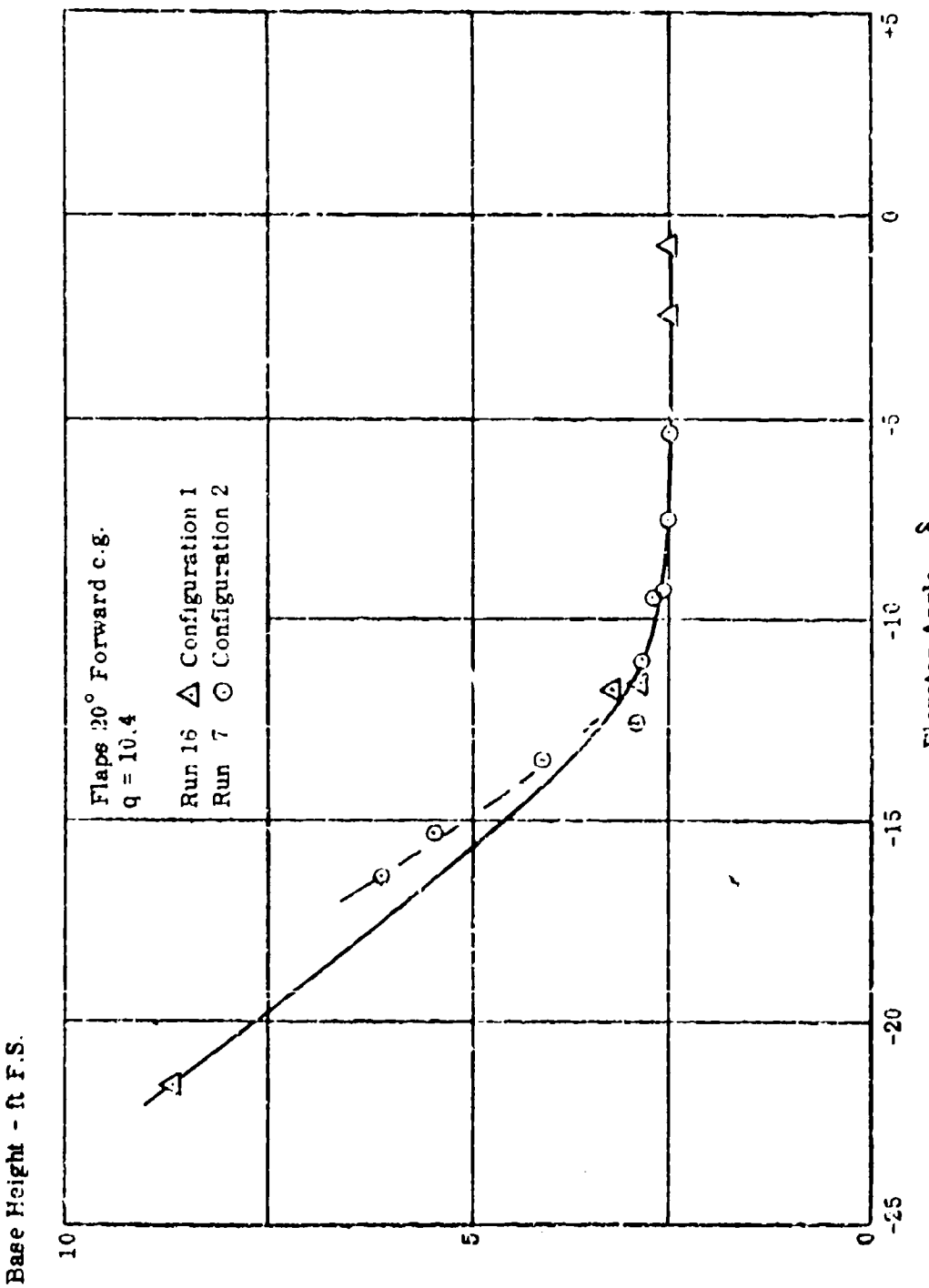

Figure 77. Liftoff Comparison Basic Configuration

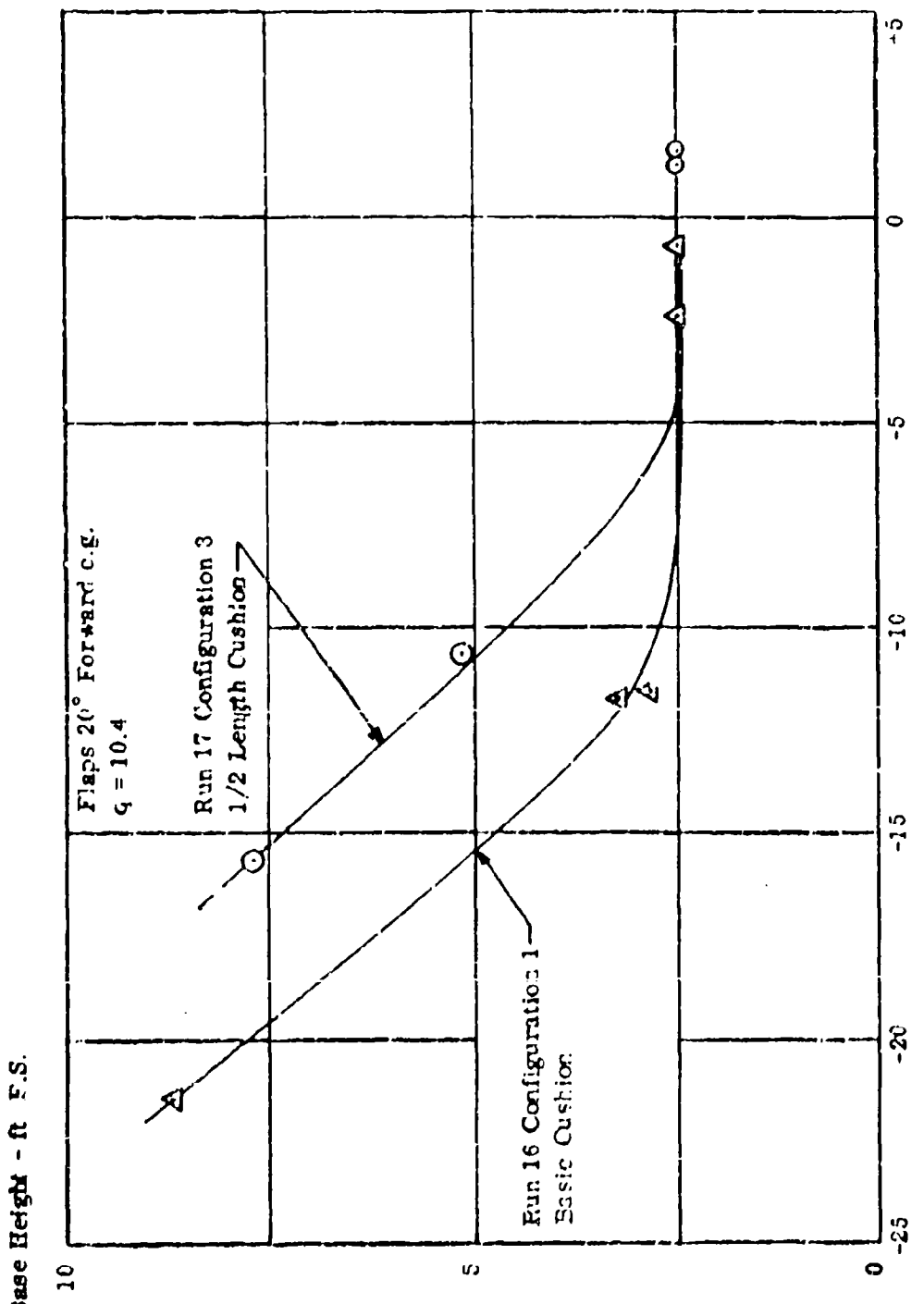

Figure 75. Liftoff Comparison Alternative Configuration

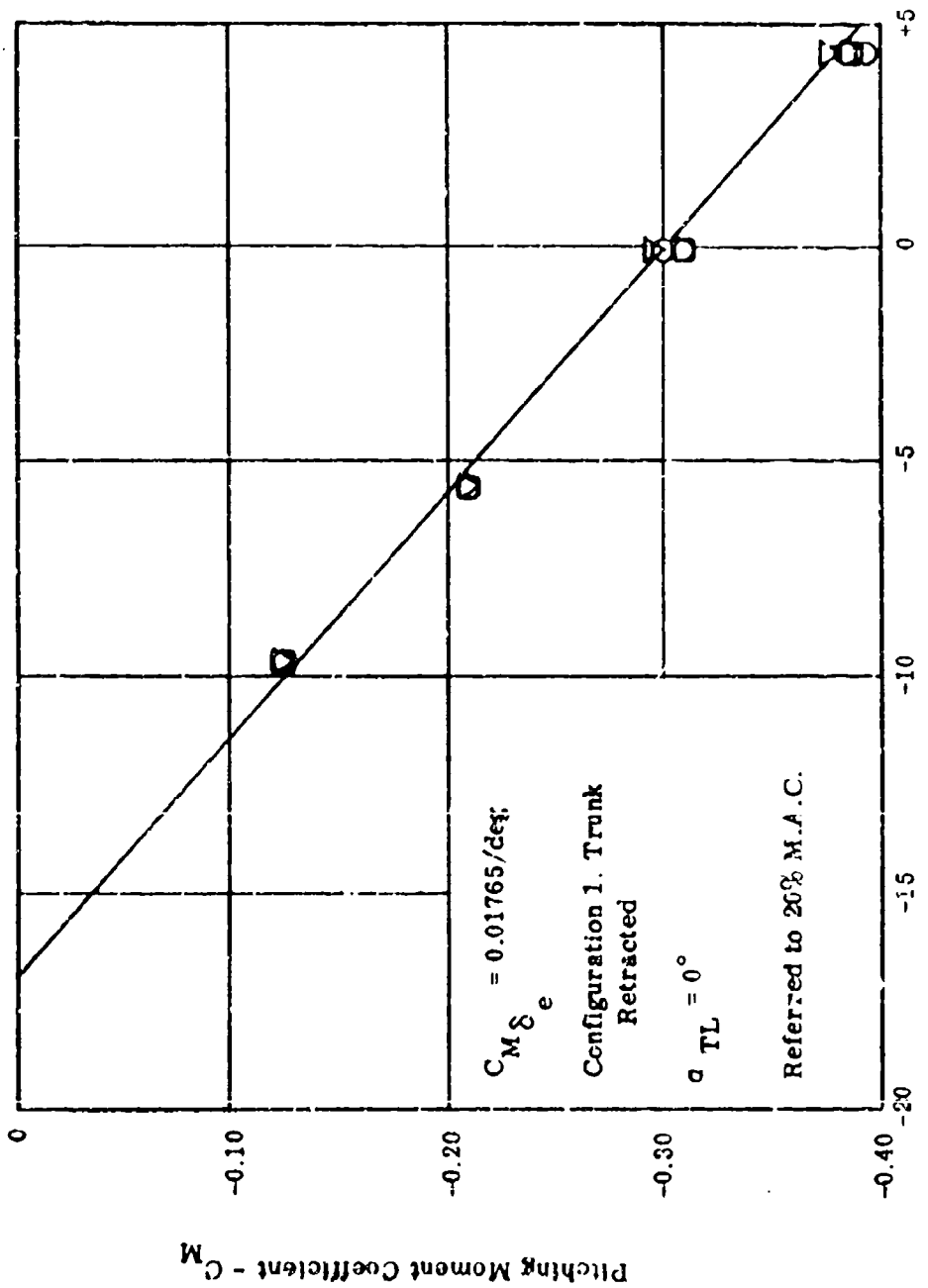

Figure 79. Elevator Power

IV. WIG FLOAT MODEL TESTS AND ANALYSIS

A. MODEL AND RIG DESCRIPTION

Figure 80 is an assembly drawing of the wing float model. The model base consists of a fiberglass shell with plywood ribs to which the rubber trunk sheet is attached. The box cross-section is constant along its length and flat on the bottom. In plan, the ends are radiused to match the trunk design. The trunk attachment is 11 inches up the side-walls from the base in the center at the outside. The trunk is a single sheet of two-ply nylon stretch fabric with a natural rubber core and neoprene coating. The trunk is perforated around the area of ground contact. Two patterns were tested; a basic pattern, and one with approximately 200 additional 5/16 inch diameter holes distributed mainly around the ends. The trunk is mounted on the base with the stretch axis arranged transversely. The center restraint is a thick light alloy plate with radiused ends attached on the outside of the trunk sheet by three through-bolts. The model is powered by a backward-curved centrifugal fan of welded aluminum construction. The maximum speed of the fan is 9,820 rpm. The fan is driven by a hydraulic motor through pulleys and vee belts. The reduction ratio is 3.22:1, giving a maximum motor speed of 3050 rpm. The fan unit is mounted on a welded aluminum transition duct which bifurcates the flow into two rectangular trunk entry ports, one on each side of the bottom plate.

The unit is mounted on the end of the whirling arm by parallel links. These links allow freedom to move vertically but provide restraint in pitch, yaw, roll, and the radial direction. The whirling arm, which has a 15-foot radius, is driven by a tyred wheel powered by an hydraulic motor. The hydraulic motors driving the fan and wheel have a common supply which is controlled remotely, and fed via swivel joints at the center of the arm. The hydraulic motor driving the fan is connected to the arm with flexible hoses, supported on the parallel links. An electrically operated isolating valve controls the power delivered to the drive wheel and hence the speed. The model and rig are shown in Figures 6 and 7.

B. TEST OUTLINE

The static characteristics of the model were found by varying the weight of the rig and fan speed, and measuring the height and pressures obtained in the trunk (p_j) and the cushion (p_c). Two types of dynamic tests were run. The first, a qualitative test, was to evaluate the performance of the trunk at forward speed. The rig was driven over a series of obstacles at a range of speeds. The second series of dynamic tests was to evaluate the effects of vertical motion. For these tests the model was released from preset heights and continuous records taken of height, pressure, and vertical acceleration. These tests were conducted for a range of heights (and hence sink rates), weights, fan speeds, and the two jet patterns.

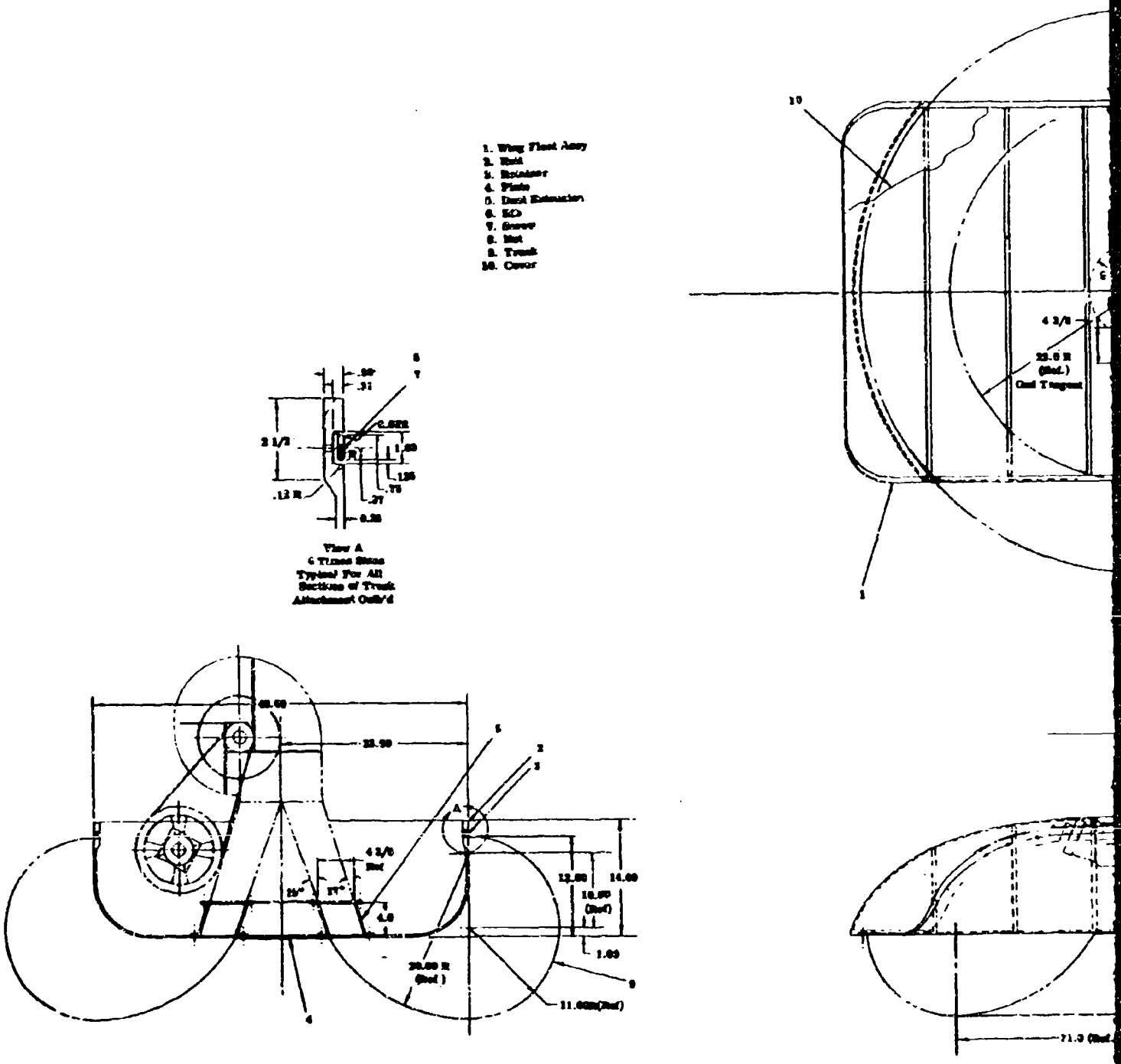

Figure 80. Drawing of Wind Float Model

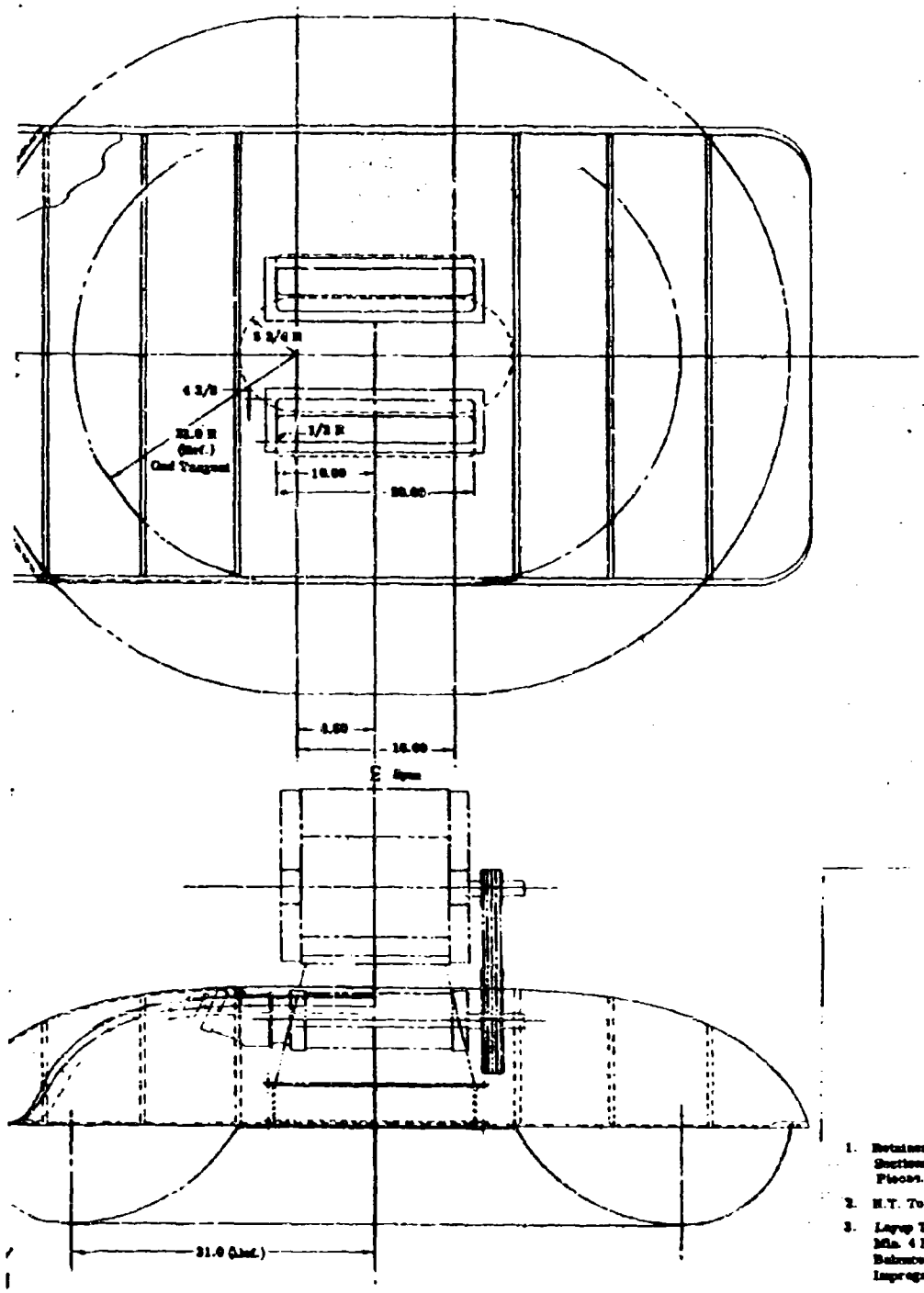

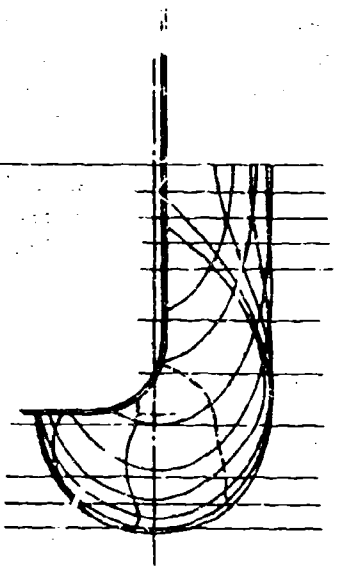

Trunk Section
Ragg Ref. Only

Notes

1. Container May Be Made Of Separate Sections. (Ex. Bottom Ends, Two Side Pieces.)
2. H.T. To T4 Cond. After Forming
3. Layup To Approx. .35 Thickness Min. 4 Layers J.P. Stevens 1581 Cloth Balance J.P. Stevens 20 Oz. Mats Impregnate With Ren 1710 Resin

C. TEST RESULTS AND ANALYSIS

1. Static Inflation Characteristics

The variation of inflation and cushion pressures are shown for a range of motor speeds in Figure 81. Measurements were taken at three rig weights. Figure 82 is a similar plot for the second configuration at a representative scale weight. The model is to a nominal 1/3 scale, but of reduced length. The corresponding values of the main parameters are tabulated in Figure 83.

2. Powering

An assessment of the power level simulated for the full scale landing gear may be made using the above scale factors and the hydraulic motor performance curves shown in Figure 84. Hydraulic input pressure was recorded for a range of rpm. Since the motor is a fixed displacement type (constant flow), the power absorbed at constant rpm varies with pressure. Assuming that the motor efficiency does not vary with pressure the output power line for 3000 psi may be factored by the measured hydraulic pressure drop across the motor divided by 3000 to find the fan input power. The input power absorbed by the model fan determined in this way is shown in Figure 84.

In initial calibrations of fan flow and pressure the model fan efficiency was determined to be approximately 0.65, well below a realistic full scale value In order to relate the input power to the full scale brake horsepower required to produce equivalent performance in the model configuration (without slant jets), the model input power is factored by 0.65/0.85. Test conditions are thus related to full scale brake horsepower as follows, using the relationships in Figure 83.

		Configuration 1	Configuration 2
Operating rpm		2800	2950
Model fan input power		19.25	24
Factored power	bhp	14.7	18.35
Full Scale Power	bhp	1280	1590
Nozzle area	$in.^2$	81.5	96.9

3. Static Heave Stiffness

Static heave stiffness was measured by loading the model to a maximum practical weight of 1300 pounds (850 pounds in shot bags). The results of this test are shown in Figure 85.

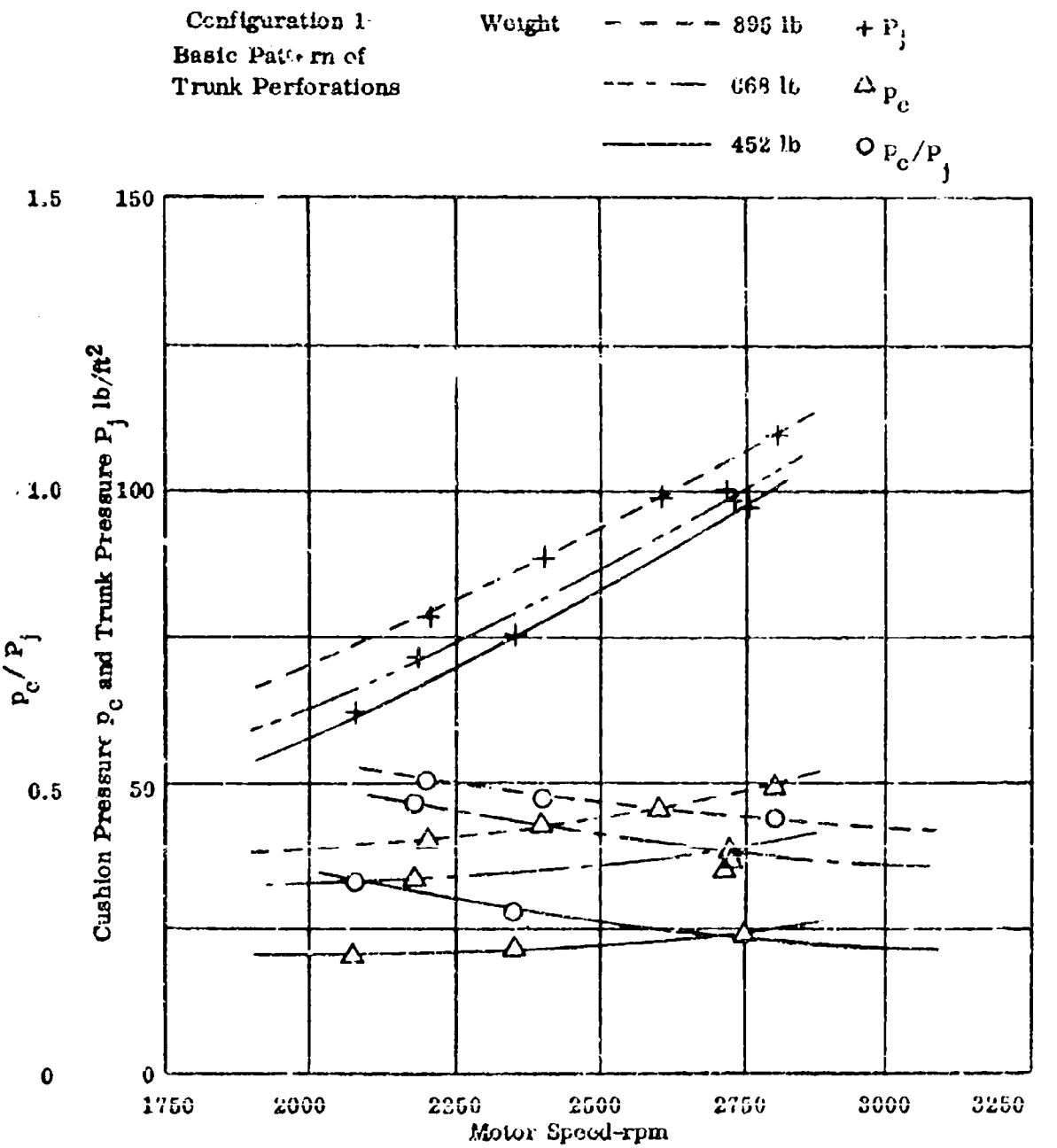

Figure 81. Inflation Characteristics - Initial Jet Pattern

Configuration No. 2
Modified Pattern of Trunk Perforations

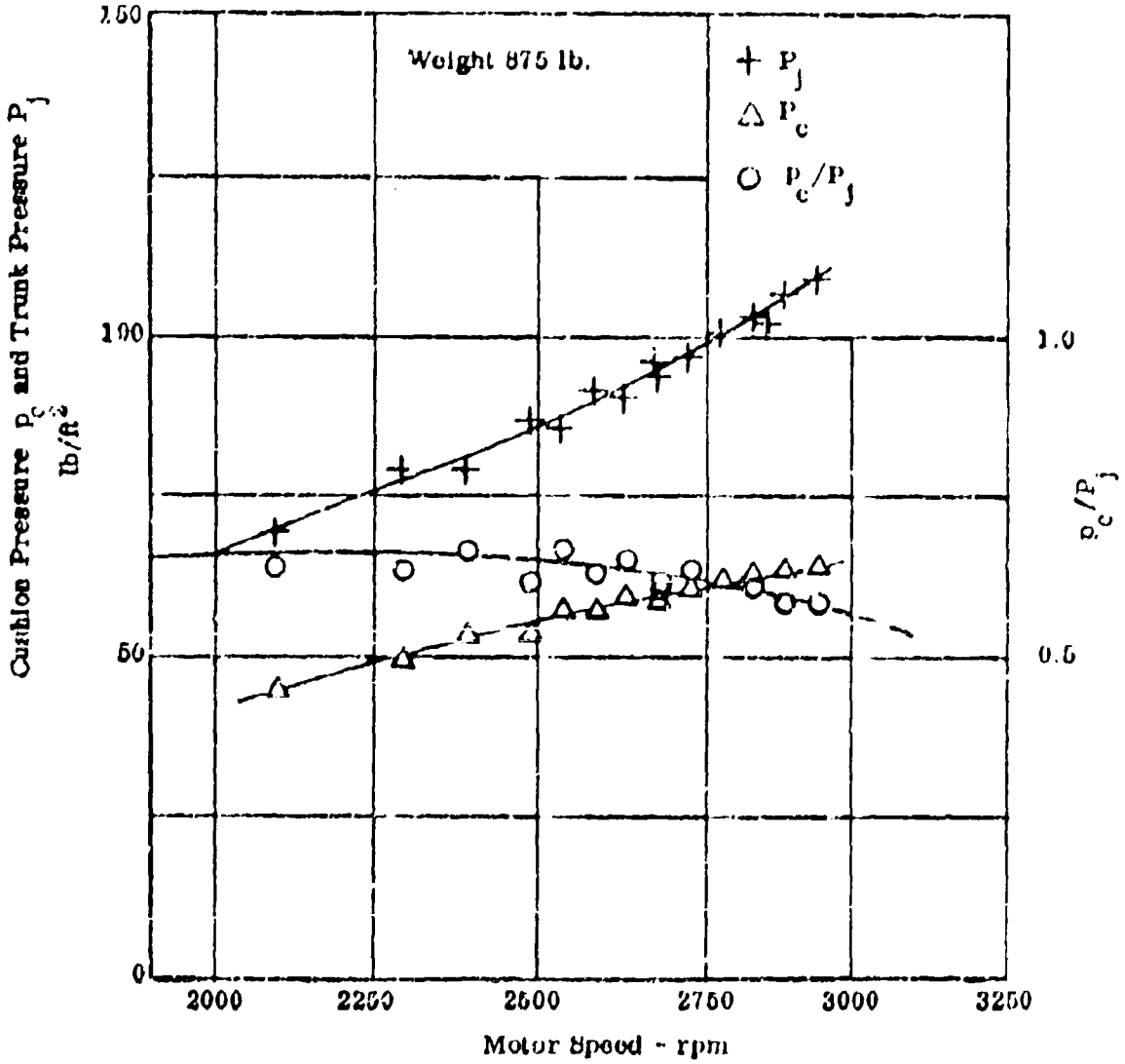

Figure 82. Inflation Characteristics - Fuel Jet Pattern

Parameter	Nominal Scale	Model	Full Scale	Actual Scale
Cushion Pressure	1/3	55.6 psf	167 psf	1/3
Trunk Pressure	1/3	111 psf	333 psf	1/3
Pressure Ratio	1/1	0.5	0.5	1/1
Weight	1/27	895 lb	60,000 lb	1/67
Cushion Area	1/9	16.1 ft^2	360 ft^2	1/22.3
Perimeter	1/3	14.4 ft	80.8 ft	1/5.6
Width	1/3	46 in.	138 in.	1/3
Length	1/3	69.4 in.	404 in.	1/6.7
Power	1/40.7	14.7 hp	1280 hp	1/87

The nominal scale factor refers to geometric similarity to the full scale cushion in all respects. To obtain the power scale factor, the nominal scale factor of $(1/3)^{3.5}$ was factored by the ratio of perimeter scale factors, this being the only quantity affecting power that did not correspond to the nominal scale factor.

Figure 83. Scaling Factors

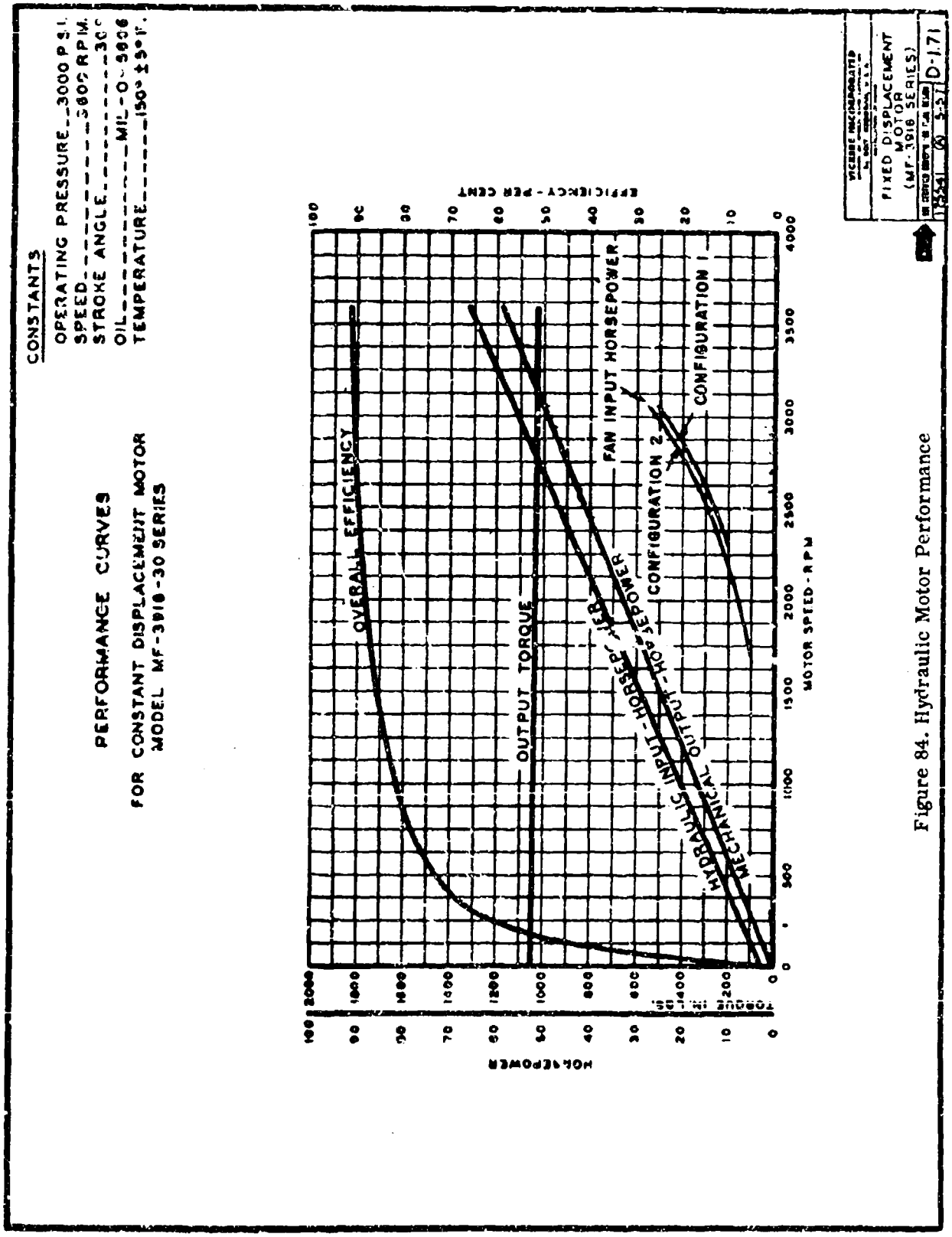

Figure 84. Hydraulic Motor Performance

Configuration No. 2
Motor Speed 2,950 rpm

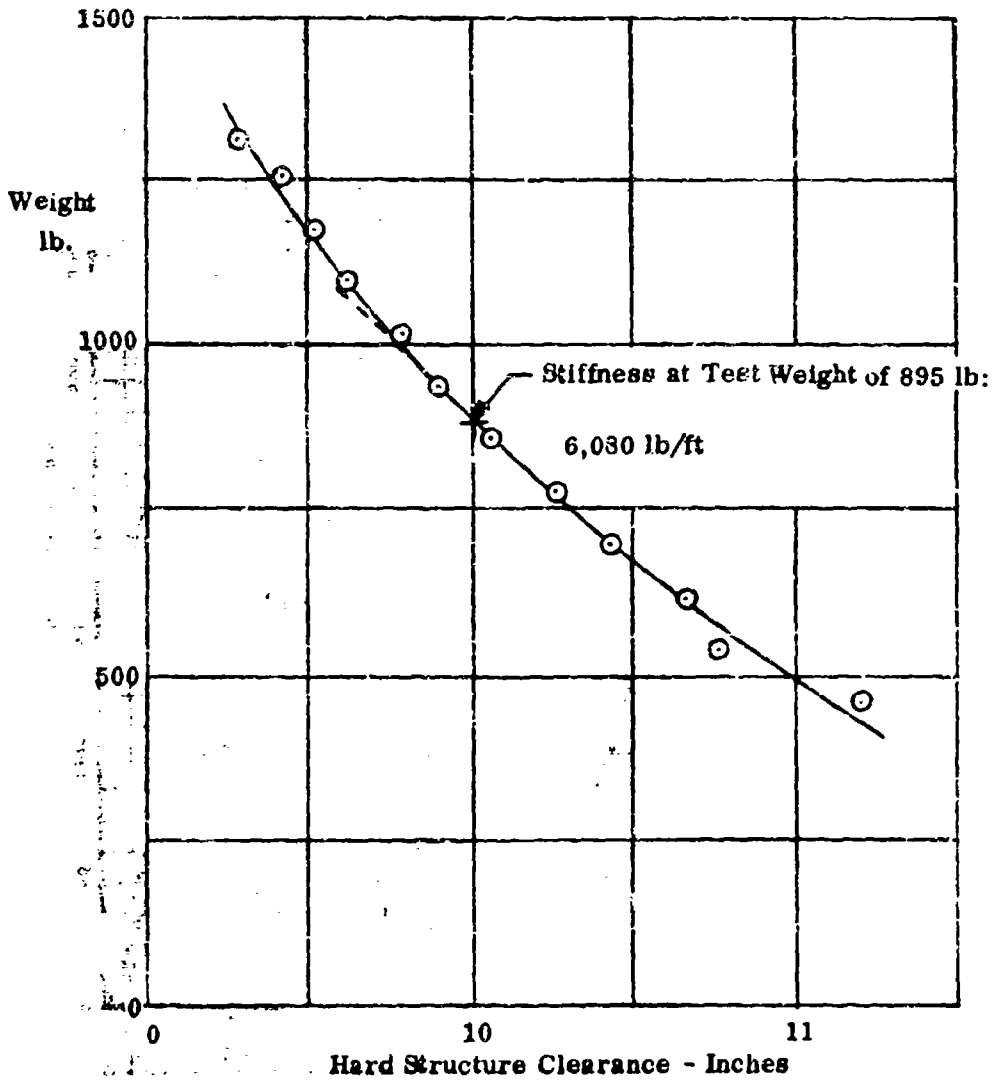

Figure 85. Heave Stiffness Measurement

4. Whirling Tests

The rig was driven at a range of speeds up to approximately 25 ft/sec over a series of obstacles generally without contacting the hard structure. The obstacles included:

(1) Hard conical mounds 5.5 and 7.5 inches high and two and three feet in diameter, respectively. These were arranged in various patterns relative to the path of the model (Figure 86). The object of these obstacles was to investigate the trunk response to abrupt surface undulations.

(2) A soft foam pad, nine inches thick, preceded and followed by gradual wooden ramps. This represents a very soft terrain such as mud or bog (Figure 87).

(3) A two-inch thick fiber mat to simulate a coarse grass surface. Some of the hard mounds were also positioned beneath the mat to resemble bumpy ground (Figure 88). The fiber mat is a surface of large leak capacity and at the same time high friction coefficient. It can therefore be expected to reduce cushion pressure and cause drag.

(4) Transverse bars 2.5 inches by 4 inches and 3.5 inches by 4 inches. This wall type obstacle provides for the maximum trunk impact, at the front.

(5) A three inch by three inch transverse channel.

The remainder of the circuit between the obstacles is smooth sealed concrete.

The majority of these tests were conducted at a model weight of 895 pounds, a fan motor speed of 2,950 rpm, and with the second hole pattern. Both closeup photographs from a camera rotating with the arm and distant shots were taken. The model negotiates all the obstacles satisfactorily with no noticeable deceleration except at very low speeds. Some pitching occurs in response to the obstructions, particularly the higher wall. The model could become hung up on this wall if stopped on it and would require considerable force to move; in the order of a D/W = 0.25 to 0.3. At about five ft/sec it would cross satisfactorily with drive wheel on and providing T/W = 0.08.

A D/W of approximately 0.01 was experienced over the concrete surface. It is notable that the trunk inflated shape was imperfect, due to the material being substantially below full stretch for the two-ply used at $p_c/P_j = 0.5$.

D/W was also measured statically on the mat, in both jet pattern configurations at 2750 rpm. In the first, a value of approximately 0.1 was found; in the second, approximately 0.075. The reduction was caused by the increased flow tending to overcome the mat porosity.

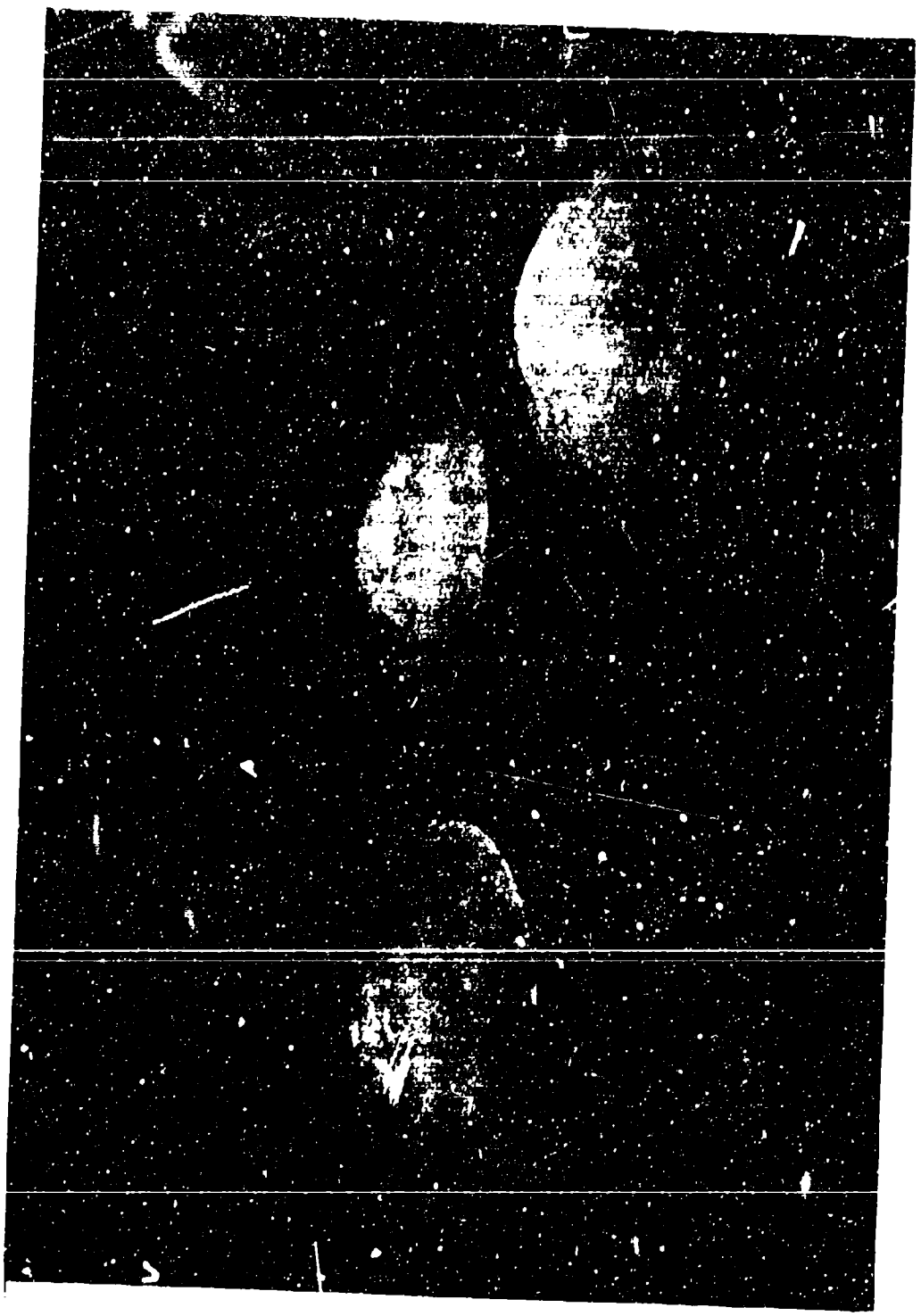

Figure 86. Mound Obstacles

Figure 87. Soft Surface and Ramps

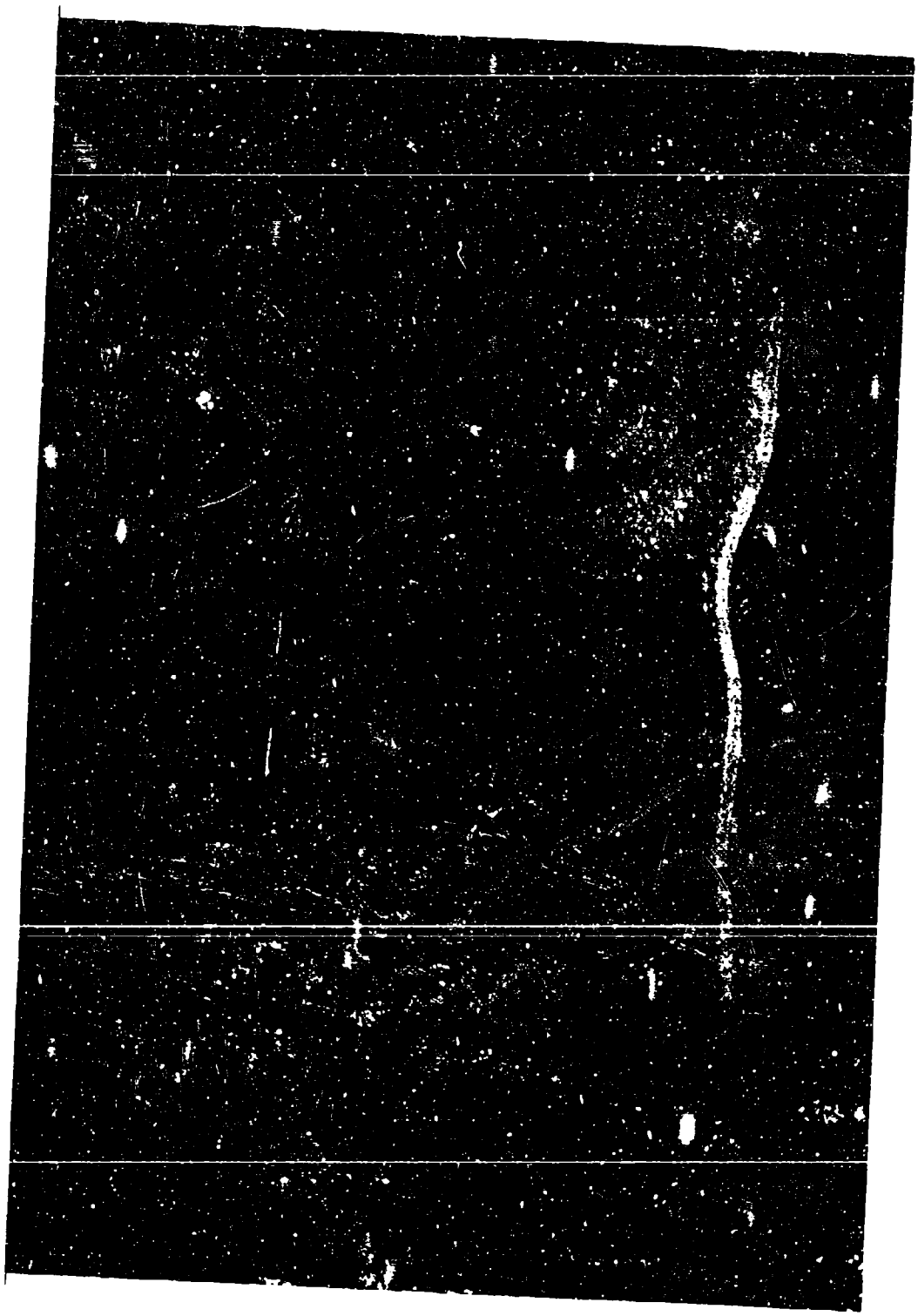

Figure 88. Fiber Mat with Bumps

In relation to these measurements it is important to state that the imperfect hole pattern on this model led to considerable flow wastage. Far too much flow was exhausted outside the ground tangent.

On one occasion, at speed, the pitching of the model coming off the mat (with bumps placed centrally) was such as to cause the nose to dip to the maximum just as the model reached the large cone. The front of the model base collided with the top of the cone cutting a five inch gash in the trunk which opened to an oval hole. Model performance was not significantly affected and the damage was not observed until another circuit had been completed.

5. Drop Tests

For drop tests, the model was mounted on long links on the end of the arm, hoisted above the ground to a given height with the fan running. It was released from successively increasing heights by a quick release hook and cable. The equipment is shown in Figure 89.

Preliminary tests were first conducted for three weights as shown in the following tabulation. During this initial series, no hard structure contact occurred and behavior was satisfactory.

Model Weight (lb)	Fan (rpm)	Cushion Pressure p_c (lb/ft^2)	Trunk Pressure p_j (lb/ft^2)	p_c/p_j	Release Height (in.)
452	2750	25	98	0.255	15.3
452	2350	21.4	75	0.285	21.7
452	2075	20.3	61.4	0.330	25.5
668	2180	33.3	70.8	0.471	18.5
668	2725	38.0	99.2	0.382	25.5
668	2725	38.5	99.0	0.390	32.2
895	2770	51.5	105.5	0.487	18.3

Instrumentation was then added. Recordings were taken of drops from three heights at 895 lb weight and 2770 fan rpm (Figure 90). The value of peak vertical acceleration against hard structure clearance at release is plotted in Figure 91. The values of minimum hard structure clearance and maximum sink rate against release height are shown in Figures 92 and 93, respectively. These data apply to the initial jet pattern configuration. Similar tests and plots were made with the model after modification of the trunk and are shown in Figures 94 and 95. Further analysis of one of the drop tests in this series is shown in Figure 96. The lift on the model (vertical acceleration times weight) is plotted against the hard structure clearance or base height of the model. The area beneath the curves is a measure of the work done or energy absorbed by the trunk/cushion system. The static lift against height curve is also plotted on this same figure, the difference between the two curves denoting the rate dependent lift or damping force of the system. It can be seen in Figure

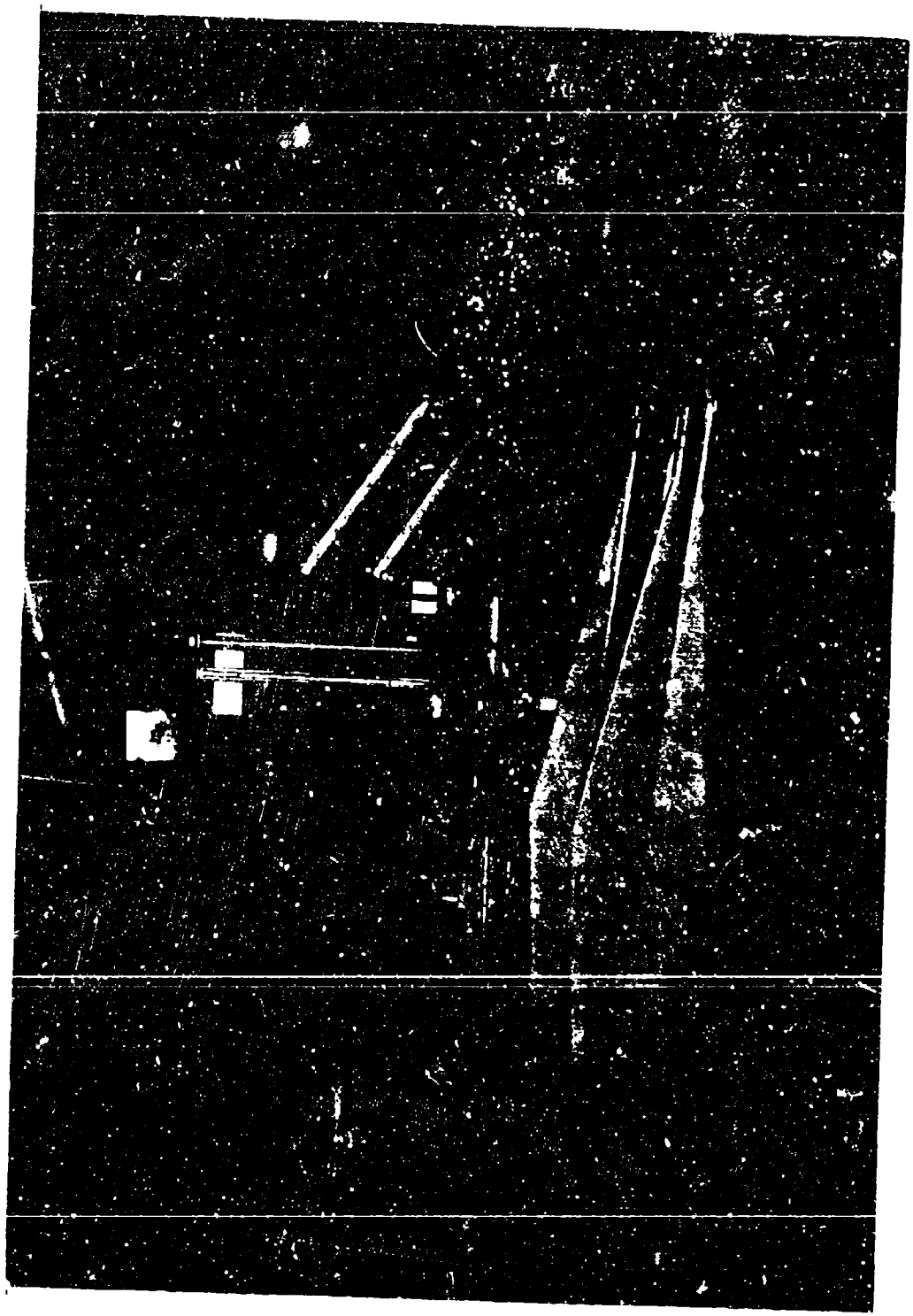

Figure 89. Drop Test Equipment

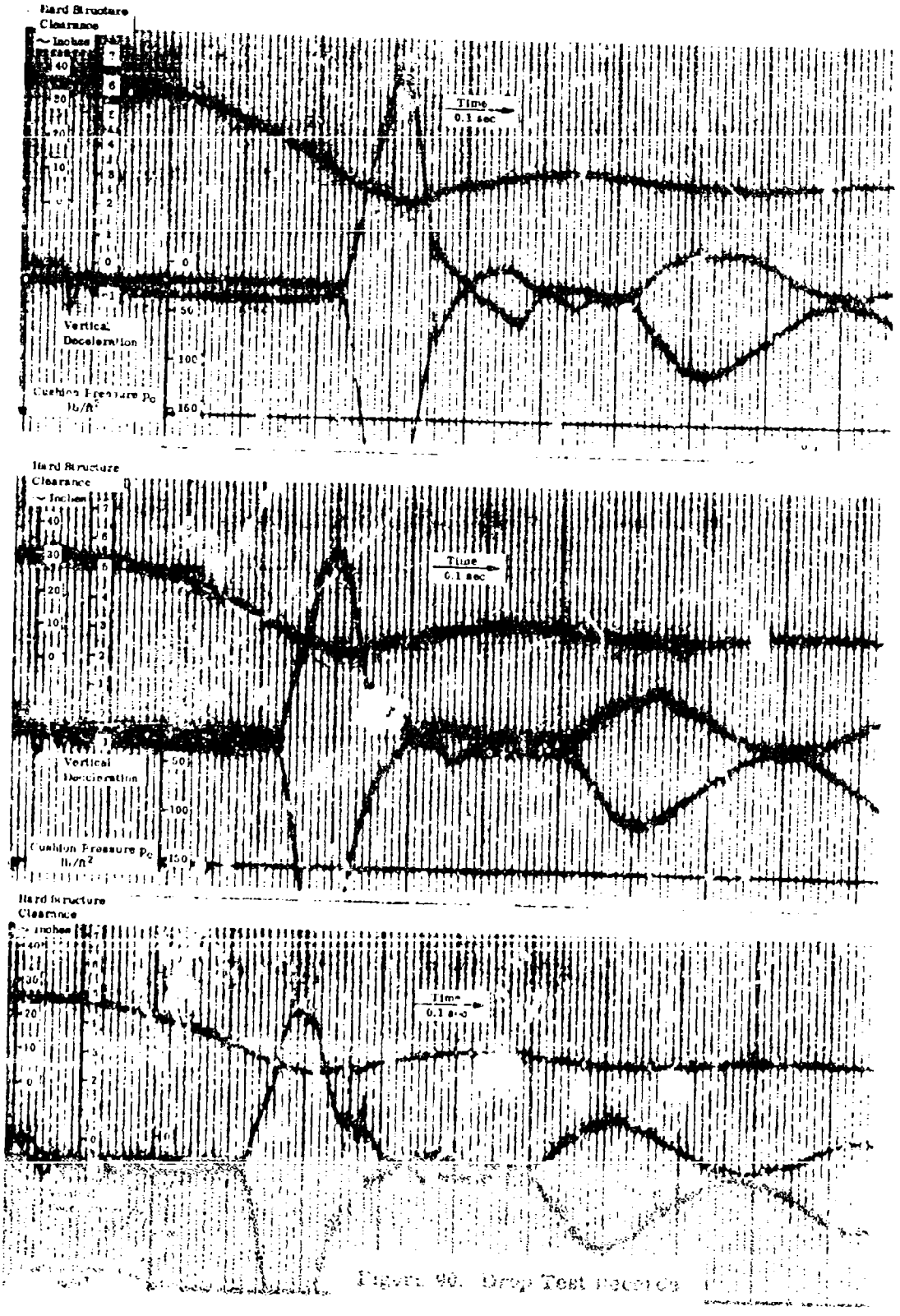

Figure 90. Drop Test Record

Hard Structure Clearance
at Release

Weight 895 lb

Motor Speed 2770 rpm

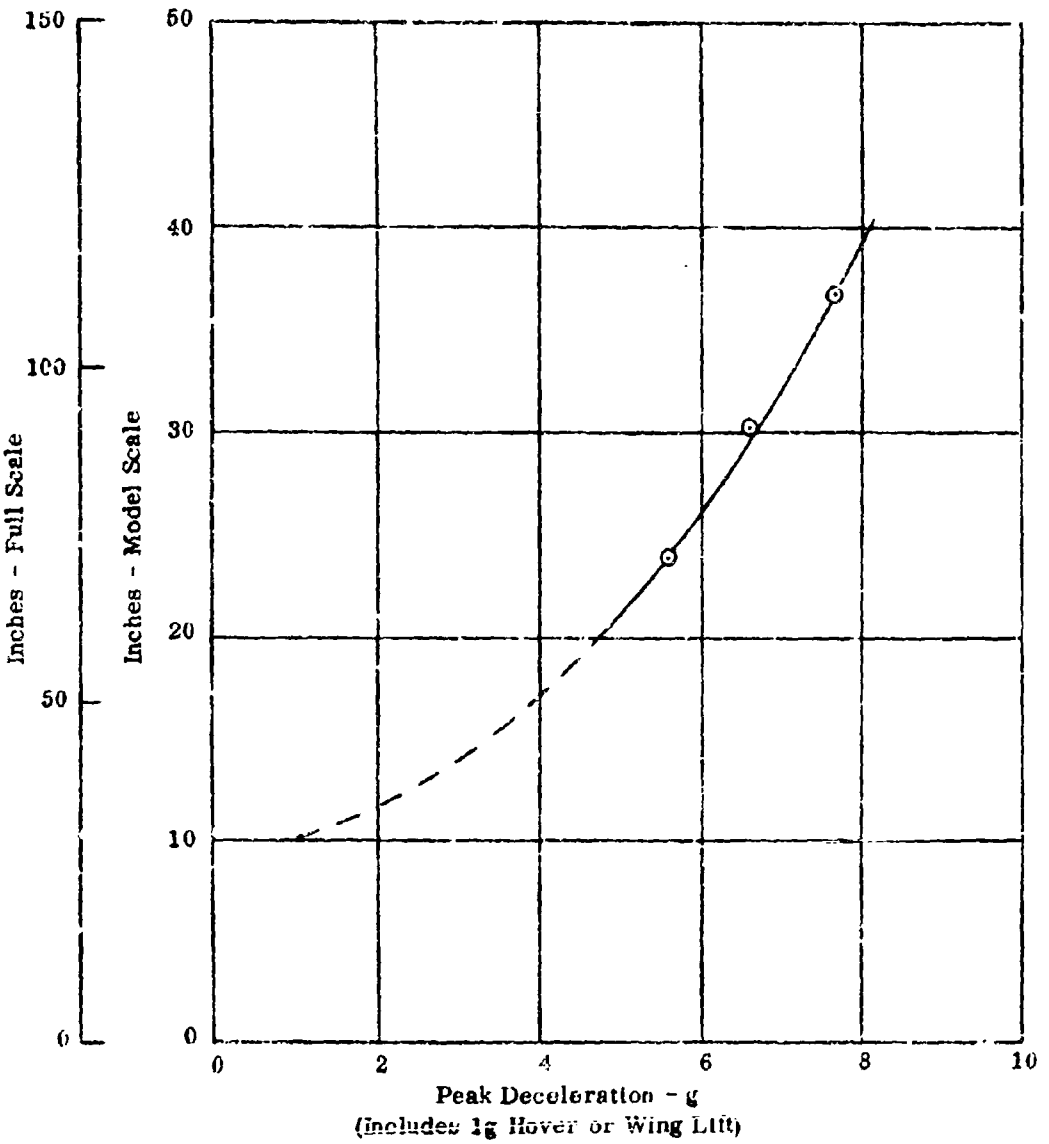

Figure 91. Decelerations - Conguration No. 1

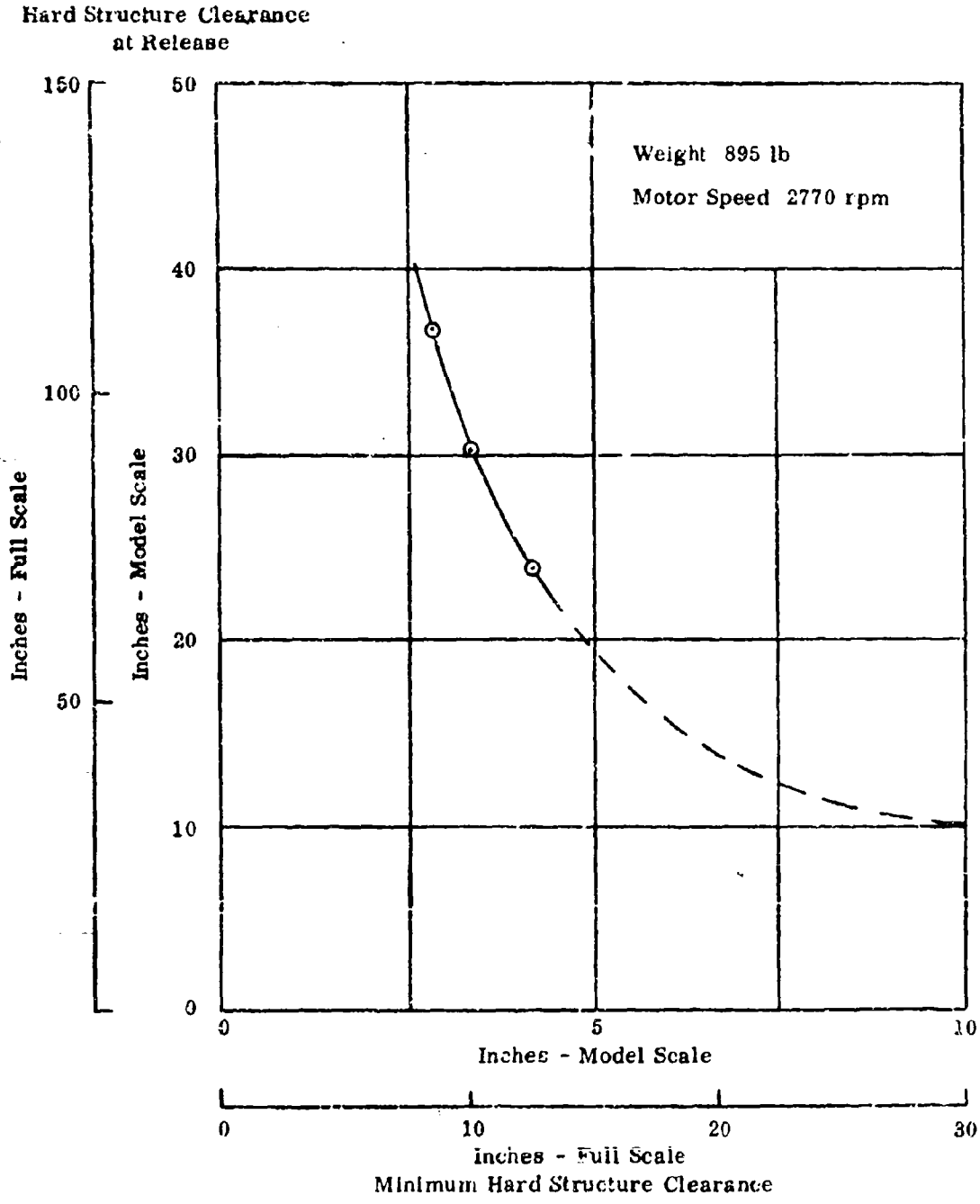

Figure 92. Clearances - Configuration 1

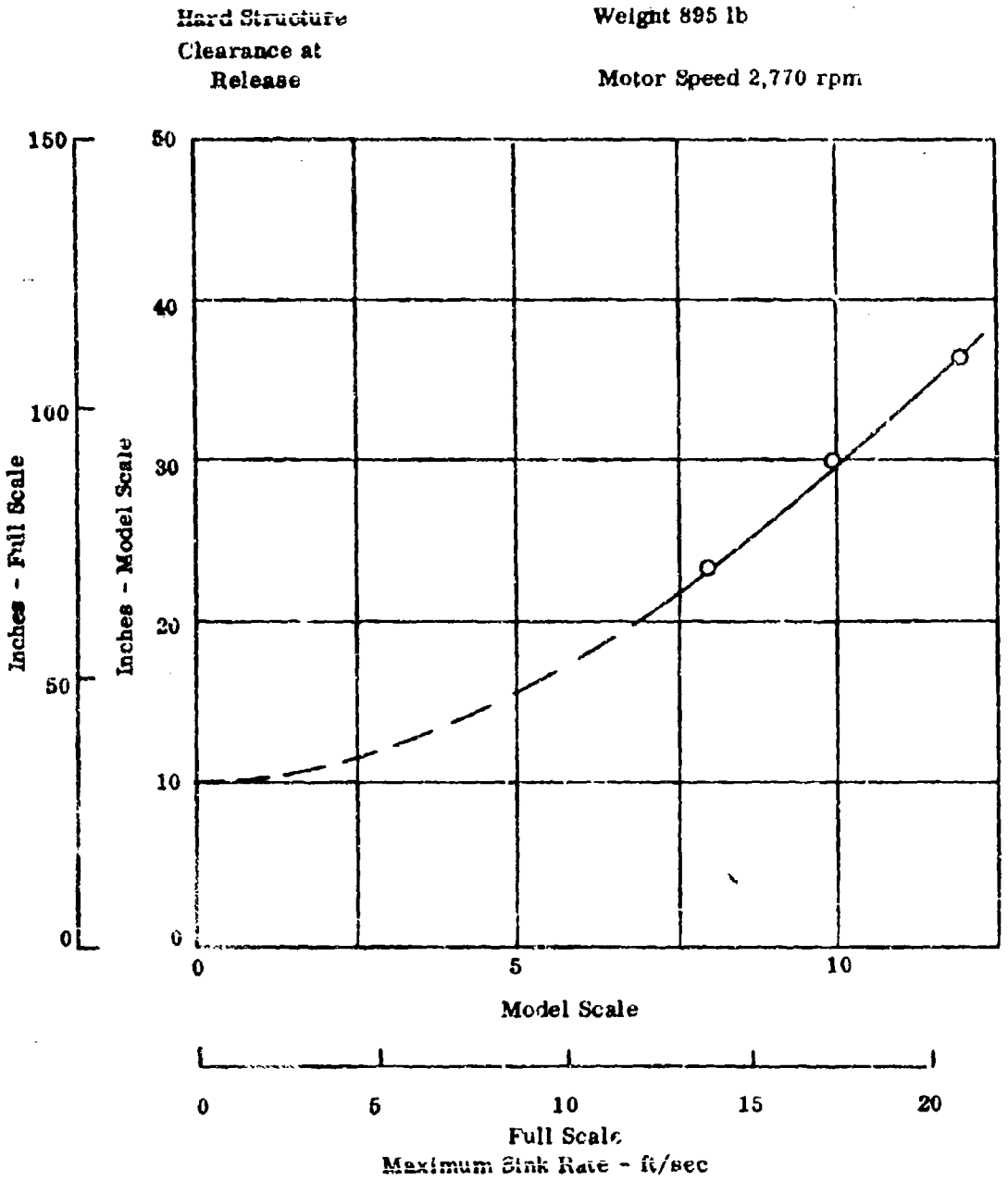

Figure 93. Sink Rates

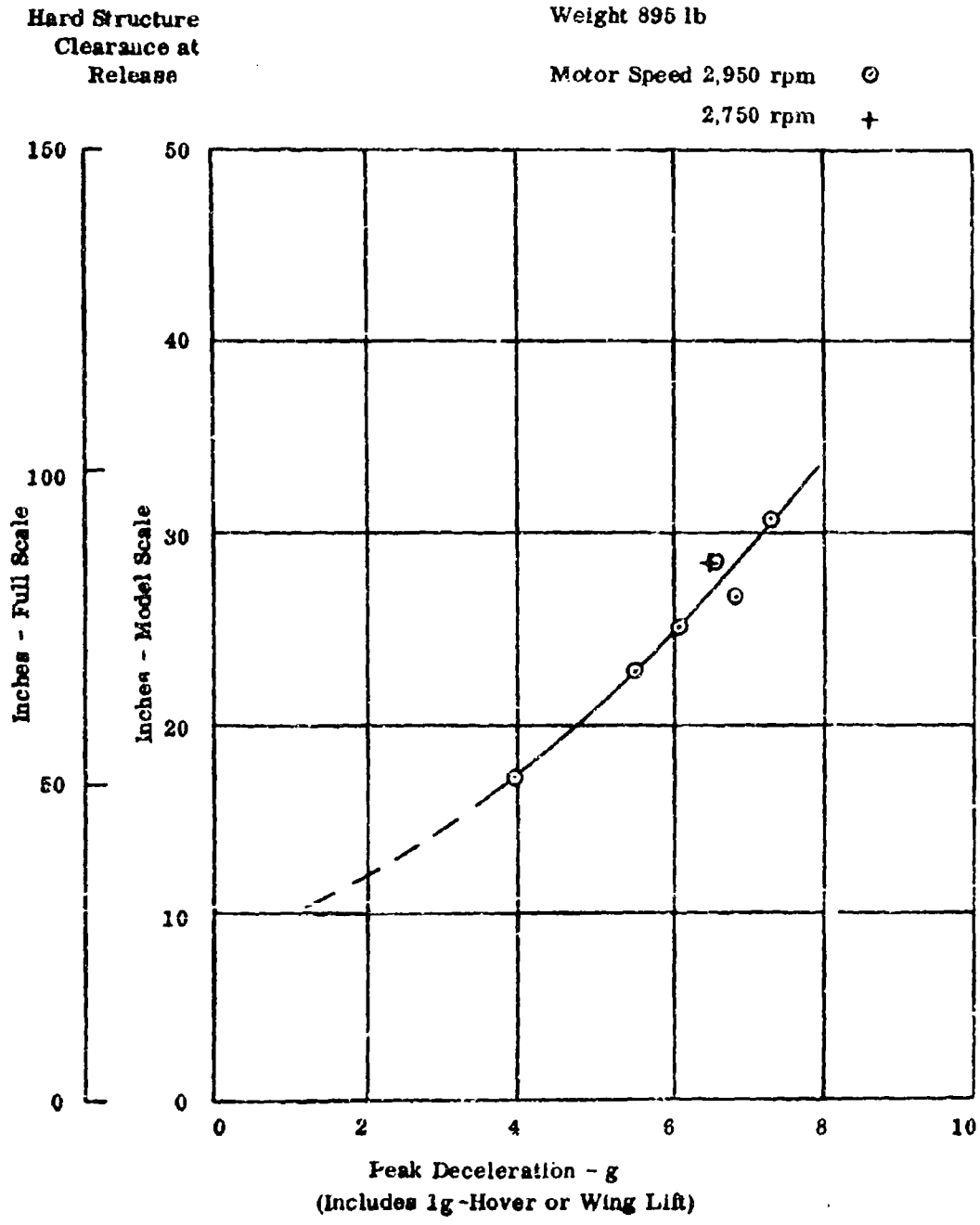

Figure 94. Decelerations - Configuration No. 2

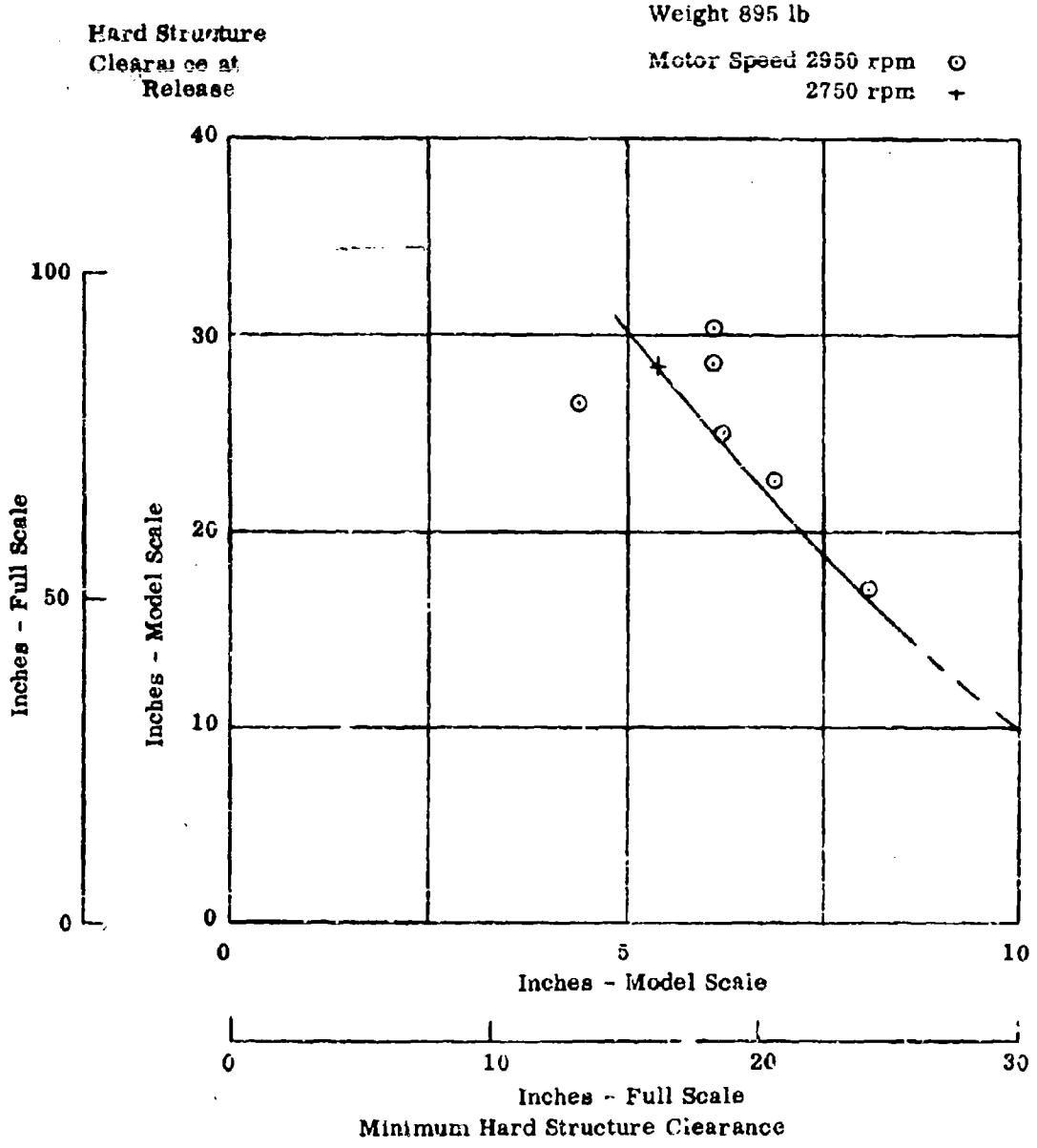

Figure 95. Clearance – Configuration No. 2

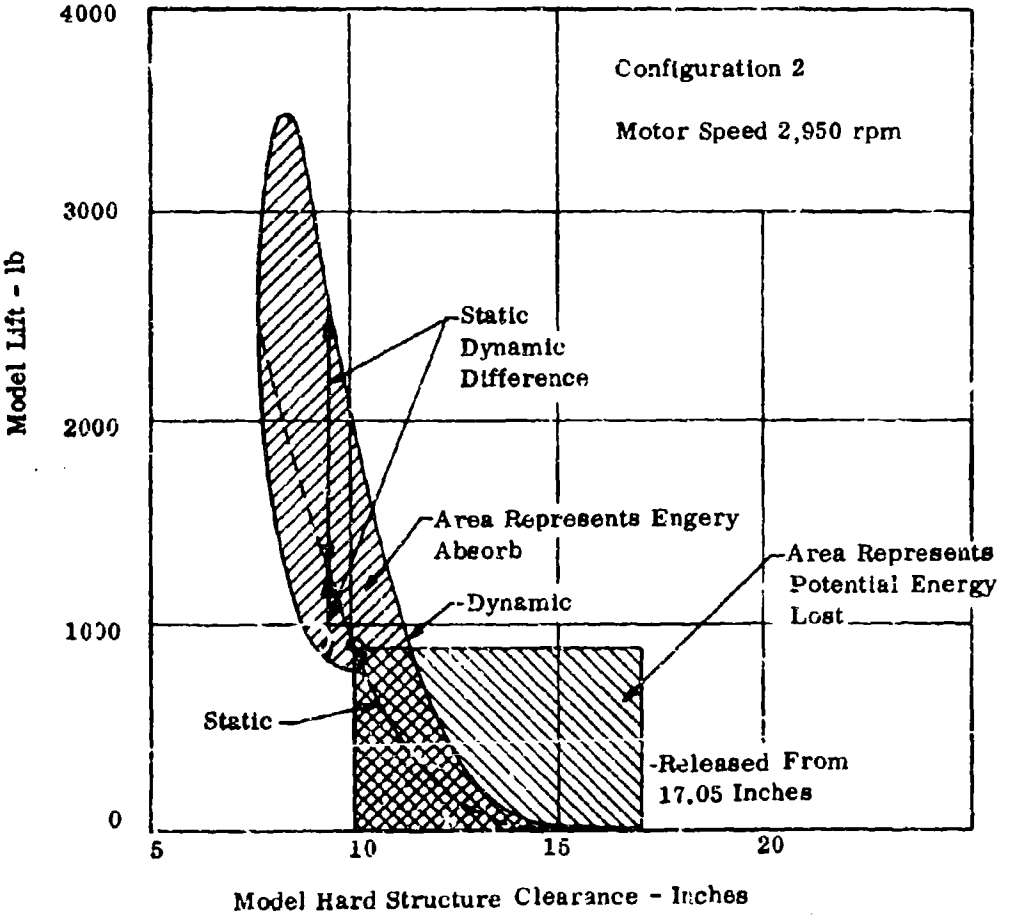

Figure 96. Energy Absorption Breakdown

97 that the damping force is not proportional to vertical velocity; i.e., the damping is not a linear function of height. The ideal value of damping is one that is equivalent to the critical damping of a linear system, this is where the motion would be non-oscillatory, or the aircraft would not bounce in a hard landing. For a linear system, the damping is critical if:

$$c = \sqrt{\frac{k.W}{g}}$$

where c is the damping in lb/ft/sec
k is the stiffness in lb/ft
W is the weight in lb
g is gravity; i.e., 32.2 ft/sec^2

From the static stiffness curve of Figure 85:

$k = 6{,}080$ lb/ft, when $W = 895$ lb

Therefore,

$$c = \sqrt{\frac{6{,}080 \times 698}{32.2}} = 411 \text{ lb/ft/sec}$$

This critical value of damping is shown in Figure 97, where it can be seen to be of the same order as that measured during the drop tests. The trace recording of vertical motion shown in Figure 90 also shows that there is only a small overshoot from the static equilibrium condition, allowing considerable reserve before contact of the hard structure, and only a small residual oscillation.

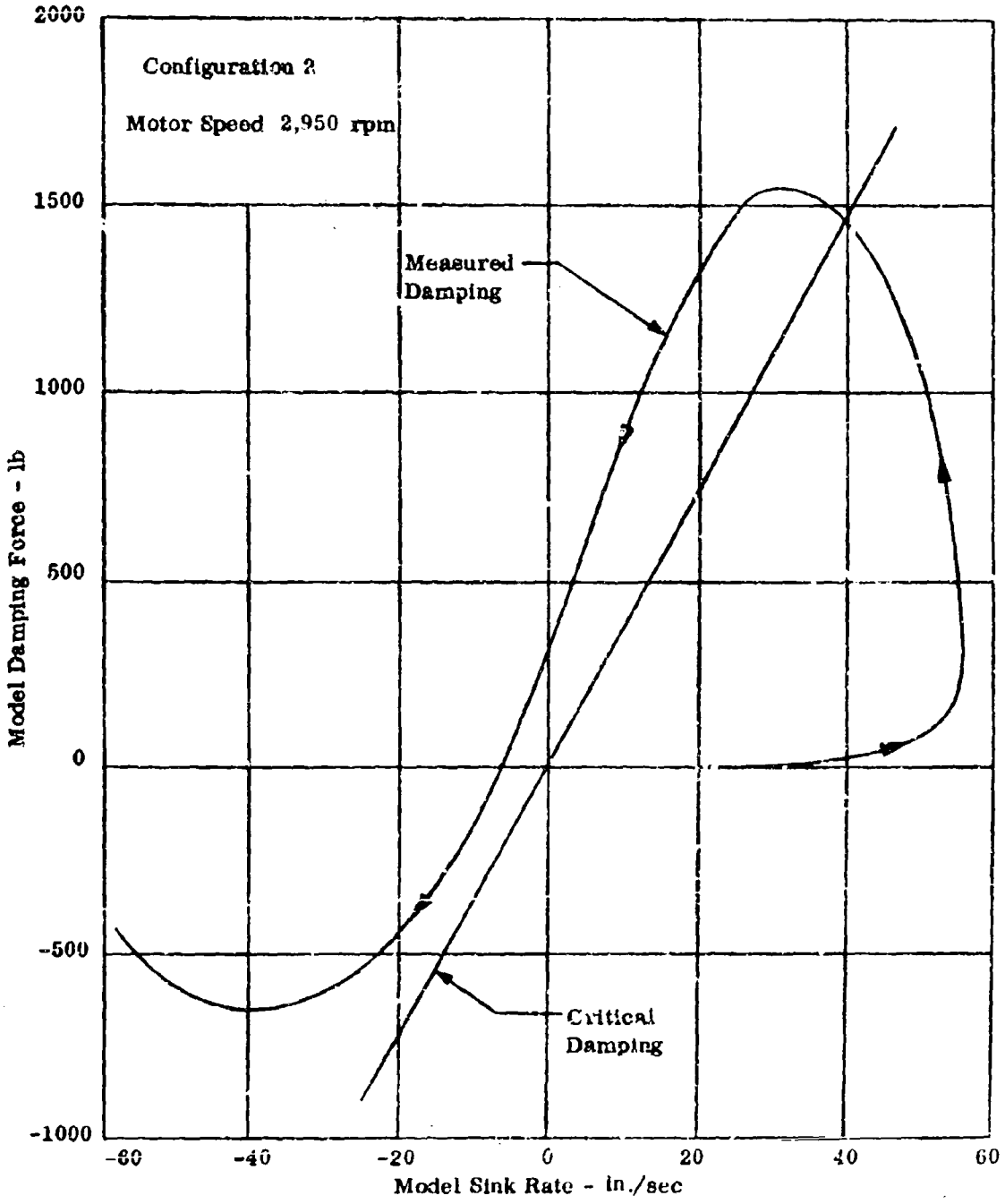

Figure 97. Critical Damping Comparison

V. CONCLUSIONS

The following conclusions are drawn from the preceding work, summarizing the development status of the air cushion landing gear:

(1) Basic system feasibility is established. It has been shown that a flexible retractable structure can be fitted to an aircraft and powered to form an air cushion. With the air cushion the aircraft will be friction free over a smooth surface and using an acceptably low power level it will traverse soft surfaces and considerable obstacles with low drag. It has also been shown that an aircraft can be taken off and landed from this air cushion in the normal manner. No compromise of normal controls is required, and the C-119 is a suitable test aircraft. It has been shown that the air cushion is a soft landing system, capable of absorbing a very high sink rate without excessive g and with excellent damping.

(2) Suitable methods for the design construction and assembly of a full scale trunk system have been determined. The powering system has been investigated and presents no problems in a test installation.

(3) Design of a cushion braking and control system appears straightforward but the required system has not been developed and no firm data on its characteristics is established. Similarly, the relationship between terrain performance and power is not established.

(4) It appears that amphibious performance can be provided but capability over water has not been established.

(5) System total weight is competitive with wheel gear.

The advantages claimed for the system have not been diminished by the investigation.

REFERENCES

1. The Theory of Plates and Shells Timoshenko

2. Report No. R110-031 C-119 Simulator Data
Fairchild Aircraft
Hagerstown, Md.

3. NACA TN 3916 Systematic Two Dimensional Cascade
Tests at NACA 65 Series Compressor Blades at Low Speeds
L. Joseph Herrig, James L. Emery
and John R. Erwin. February 1957

4. Handbook of Instructions for Aeronautical Designers (HIAD) Vol. 1, part B, Chap. 3

5. Royal Aeronautical Society Data Sheets, Performance

6. David Taylor Model Basin Report 2121D, Some Design Principles of Ground Effect Machines, Section D - Drag, Harvey R. Chaplin and Allen G. Ford

Unclassified
Security Classification

DOCUMENT CONTROL DATA - R&D

(Security classification of title, body of abstract and indexing annotation must be entered when the overall report is classified)

1. ORIGINATING ACTIVITY (Corporate author)	2a. REPORT SECURITY CLASSIFICATION
Bell Aerosystems Company P.O. Box 1, Buffalo 5, N.Y.	Unclassified 2b. GROUP

3. REPORT TITLE

AIR CUSHION LANDING GEAR FEASIBILITY STUDY

4. DESCRIPTIVE NOTES (Type of report and inclusive dates)

Final Technical Report Feb. 1966 to March 1967

5. AUTHOR(S) (Last name, first name, initial)

T. Desmond Earl

6. REPORT DATE	7a. TOTAL NO. OF PAGES	7b. NO. OF REFS
March 1967	173	6

8a. CONTRACT OR GRANT NO.	9a. ORIGINATOR'S REPORT NUMBER(S)
AF33(615) 3296 b. PROJECT NO.	AFFDL-TR-67-32
c.	9b. OTHER REPORT NO(S) (Any other numbers that may be assigned this report)
d.	D7233-945001

10. AVAILABILITY/LIMITATION NOTICES This document is subject to special export controls and each transmittal to foreign governments or foreign nationals may be made only with prior approval of AF Flight Dynamics Laboratory (FDFM), WPAFB, Ohio 45433.

11. SUPPLEMENTARY NOTES	12. SPONSORING MILITARY ACTIVITY
	USAF AFFDL Wright Patterson AFB Dayton, Ohio

13. ABSTRACT

The report describes the air cushion landing gear system concept. The objective is to provide an improved tolerance to the takeoff and landing maneuver and environment with no compromise of flight performance. The study considers test application to a C-119 aircraft, alternative configurations are considered and a single main cushion beneath the fuselage is recommended. Analysis of takeoff and landing wind tunnel model tests conducted over a moving ground and of a large scale elastic trunk model is included. It is concluded that system basic feasibility is established.

DD FORM 1 JAN 64 1473

Unclassified
Security Classification

Unclassified

Security Classification

14 KEY WORDS	LINK A		LINK B		LINK C	
	ROLE	WT	ROLE	WT	ROLE	WT

INSTRUCTIONS

1. ORIGINATING ACTIVITY: Enter the name and address of the contractor, subcontractor, grantee, Department of Defense activity or other organization *(corporate author)* issuing the report.

2a. REPORT SECURITY CLASSIFICATION: Enter the overall security classification of the report. Indicate whether "Restricted Data" is included. Marking is to be in accordance with appropriate security regulations.

2b. GROUP: Automatic downgrading is specified in DoD Directive 5200.10 and Armed Forces Industrial Manual. Enter the group number. Also, when applicable, show that optional markings have been used for Group 3 and Group 4 as authorized.

3. REPORT TITLE: Enter the complete report title in all capital letters. Titles in all cases should be unclassified. If a meaningful title cannot be selected without classification, show title classification in all capitals in parenthesis immediately following the title.

4. DESCRIPTIVE NOTES: If appropriate, enter the type of report, e.g., interim, progress, summary, annual, or final. Give the inclusive dates when a specific reporting period is covered.

5. AUTHOR(S): Enter the name(s) of author(s) as shown on or in the report. Enter last name, first name, middle initial. If military, show rank and branch of service. The name of the principal author is an absolute minimum requirement.

6. REPORT DATE: Enter the date of the report as day, month, year, or month, year. If more than one date appears on the report, use date of publication.

7a. TOTAL NUMBER OF PAGES: The total page count should follow normal pagination procedures, i.e., enter the number of pages containing information.

7b. NUMBER OF REFERENCES: Enter the total number of references cited in the report.

8a. CONTRACT OR GRANT NUMBER: If appropriate, enter the applicable number of the contract or grant under which the report was written.

8b, 8c, & 8d. PROJECT NUMBER: Enter the appropriate military department identification, such as project number, subproject number, system numbers, task number, etc.

9a. ORIGINATOR'S REPORT NUMBER(S): Enter the official report number by which the document will be identified and controlled by the originating activity. This number must be unique to this report.

9b. OTHER REPORT NUMBER(S): If the report has been assigned any other report numbers *(either by the originator or by the sponsor)*, also enter this number(s).

10. AVAILABILITY/LIMITATION NOTICES: Enter any limitations on further dissemination of the report, other than those imposed by security classification, using standard statements such as:

(1) "Qualified requesters may obtain copies of this report from DDC."

(2) "Foreign announcement and dissemination of this report by DDC is not authorized."

(3) "U. S. Government agencies may obtain copies of this report directly from DDC. Other qualified DDC users shall request through

_____."

(4) "U. S. military agencies may obtain copies of this report directly from DDC. Other qualified users shall request through

_____."

(5) "All distribution of this report is controlled. Qualified DDC users shall request through

_____."

If the report has been furnished to the Office of Technical Services, Department of Commerce, for sale to the public, indicate this fact and enter the price, if known.

11. SUPPLEMENTARY NOTES: Use for additional explanatory notes.

12. SPONSORING MILITARY ACTIVITY: Enter the name of the departmental project office or laboratory sponsoring *(paying for)* the research and development. Include address.

13. ABSTRACT: Enter an abstract giving a brief and factual summary of the document indicative of the report, even though it may also appear elsewhere in the body of the technical report. If additional space is required, a continuation sheet shall be attached.

It is highly desirable that the abstract of classified reports be unclassified. Each paragraph of the abstract shall end with an indication of the military security classification of the information in the paragraph, represented as *(TS), (S), (C), or (U)*

There is no limitation on the length of the abstract. However, the suggested length is from 150 to 225 words.

14. KEY WORDS: Key words are technically meaningful terms or short phrases that characterize a report and may be used as index entries for cataloging the report. Key words must be selected so that no security classification is required. Identifiers, such as equipment model designation, trade name, military project code name, geographic location, may be used as key words but will be followed by an indication of technical context. The assignment of links, rules, and weights is optional.

Unclassified

Security Classification